

**Second order QCD corrections
to deep inelastic processes**

Ellen Zijlstra



Second order QCD corrections to deep inelastic processes

Second order QCD corrections
to deep inelastic processes

Second order QCD corrections to deep inelastic processes

Proefschrift

ter verkrijging van de graad van Doctor
aan de Rijksuniversiteit te Leiden, op gezag
van de Rector Magnificus Dr. L. Leertouwer,
hoogleraar in de faculteit der Godgeleerdheid,
volgens besluit van het College van Dekanen
te verdedigen op woensdag 8 september 1993
te klokke 16.15 uur

door

Ellen Bertina Zijlstra

geboren te Assen op 30 oktober 1967

Promotiecommissie:

- | | |
|----------------|----------------------------|
| Promotor: | Prof.dr. F.A. Berends |
| Co-promotor: | Dr. W.L.G.A.M. van Neerven |
| Overige leden: | Prof.dr. P.J. van Baal |
| | Prof.dr. J.J. Engelen |
| | Prof.dr. H.J. Habing |
| | Prof.dr. J. Smith |

Contents

1	Introduction	1
1.1	The strong interaction and QCD	1
1.2	Experiments and QCD	2
1.3	Perturbative QCD	3
	References to chapter 1	5
2	Higher order QCD calculations	7
2.1	Introduction	7
2.2	The naive parton model	11
2.3	The QCD improved parton model	15
2.4	Mass factorization	18
2.5	Calculable quantities in perturbative QCD	20
2.6	Phase space integrals	22
	Appendix	26
2A	The kinematics of the DIS process	26
	References to chapter 2	29
3	The structure functions F_2 and F_L	31
3.1	Introduction	31
3.2	The calculation of the coefficient functions	34
3.2.1	The first order results	36
3.2.2	Diagrams contributing at second order	39
3.2.3	Mass factorization in the $\overline{\text{MS}}$ scheme	45
3.2.4	Mass factorization in the DIS scheme	49
3.2.5	Checks on our results	52
3.2.6	The omission of the third order anomalous dimension	54

3.3	Results	58
3.3.1	Results for F_2	59
3.3.2	Results for F_L	66
3.3.3	Conclusions	74
	Appendices	74
3A	Phase space integrals	74
3B	The DIS coefficient functions in the $\overline{\text{MS}}$ and DIS scheme	76
3B.1	Order α_s^2 corrected coefficient functions in the $\overline{\text{MS}}$ scheme	76
3B.2	Order α_s^2 corrected coefficient functions in the DIS scheme	85
	References to chapter 3	86
4	The Drell-Yan K-factor in the $\overline{\text{MS}}$ and DIS scheme	91
4.1	Introduction	91
4.2	The order α_s^2 correction to the DY process	93
4.2.1	Diagrams contributing at second order	95
4.2.2	Mass factorization in the DIS scheme	97
4.3	Total cross sections for W- and Z-production	105
4.3.1	The size of the corrections	108
4.3.2	Dependence on the parton density parametrization	113
4.3.3	The omission of the third order anomalous dimension	116
4.3.4	Scale dependence	120
4.3.5	Comparison with experiment	124
4.3.6	Conclusions	126
	Appendix	127
4A	Drell-Yan coefficient functions	128
	References to chapter 4	142
5	The structure function F_3	145
5.1	Introduction	145
5.2	The calculation of the second order coefficient function	146
5.2.1	The regularization of γ_5 in n dimensions	147
5.2.2	Results for the coefficient functions	150
5.3	Results for F_3	152

References to chapter 5	156
6 The polarized structure function G_1	158
6.1 Introduction	158
6.2 Kinematics	160
6.3 The calculation of the order α_s^2 corrections	161
6.4 Results	166
6.4.1 Preliminaries	167
6.4.2 Plots of $G_1(x, Q^2)$	173
6.4.3 Conclusions	181
Appendix	183
6A The polarized DIS coefficient functions in the $\overline{\text{MS}}$ scheme	183
References to chapter 6	188
Samenvatting	191
Curriculum vitae	194
List of publications	195

Introduction	1
1. The purpose of the study	1
2. The scope of the study	2
3. The methodology	3
4. The results	4
5. The conclusions	5
6. The implications	6
7. The limitations	7
8. The future research	8
9. The references	9
10. The appendix	10
11. The bibliography	11
12. The index	12
13. The glossary	13
14. The list of figures	14
15. The list of tables	15
16. The list of abbreviations	16
17. The list of symbols	17
18. The list of units	18
19. The list of acronyms	19
20. The list of initialisms	20
21. The list of contractions	21
22. The list of colloquialisms	22
23. The list of idioms	23
24. The list of proverbs	24
25. The list of sayings	25
26. The list of maxims	26
27. The list of aphorisms	27
28. The list of epigrams	28
29. The list of epigrams	29
30. The list of epigrams	30

Chapter 1

Introduction

1.1 The strong interaction and QCD

There are four fundamental forces in nature: the gravitational, electromagnetic, weak and strong force. In modern physics each fundamental force is described in the framework of a field theory possessing a local symmetry. This means the Lagrangian of the theory is invariant under space and time dependent transformations of the fields. To establish a local symmetry it is necessary to introduce gauge fields, which represent particles that couple to the matter fields already present in the Lagrangian. This changes the equations of motion of the matter fields. By the principle of covariantization of derivatives we get an interaction term in the Lagrangian, multiplied by an arbitrary coupling constant. In general this coupling constant characterizes the strength of the force.

From the four fundamental forces, it is the strong force we are interested in in this thesis. It determines the behaviour of hadrons in highly energetic collisions with leptons or other hadrons, which will be our subject of investigation. The gauge field theory describing the strong force is Quantum Chromo Dynamics (QCD) [1]. In QCD the quarks, of which the hadrons are made up, interact through the exchange of gluons. The quarks are spin-1/2 particles and the gluons, with a spin equal to 1, belong to the class of Yang-Mills fields [2]. They share with the quarks a quantum number called color. Originally this additional degree of freedom was introduced to explain the hadron spectrum in the constituent quark model of Gell-Mann [3]. It seemed that hadrons contained quarks which were in the same quantum state, which would violate the Pauli exclusion principle for fermions. However, the Pauli principle can be rescued by antisymmetrizing the quark wave-function with respect to the color label, which takes on the 'values' red, green and blue [4, 5]. Experimental evidence

for the existence of three colors came from the lifetime of a neutral pion and the R -factor defined in e^+e^- annihilation [5].

The QCD Lagrangian is invariant under local $SU(3)$ transformations which change the color of the quarks and gluons. The hypothesis is that physical particles are colorless. This explains why the existing hadrons are made up of either three quarks (baryons) or a quark-antiquark pair (mesons) [5]. The local $SU(3)$ color symmetry is an exact symmetry, so the quark masses must be color independent. They do however depend on the flavor quantum number: the up, down, strange, charm, bottom and top quarks all have different masses. Where these mass differences come from is not known.

1.2 Experiments and QCD

One of the achievements of QCD is that it yields an improvement of Feynman's parton model [6]. In this model hadrons are composite particles made up of partons, which were identified later on with quarks and gluons. The parton model tried to explain the results of the deep inelastic electron-proton scattering experiments¹ done at SLAC in 1968 [7], for a review see [8]. In these experiments one observed that the dynamics of deep inelastic scattering is independent of the interaction scale, which equals the four-momentum squared of the virtual photon exchanged between the electron and the proton. This phenomenon is called scaling [9]. The parton model could explain this by assuming that the partons are free point-particles and that deep inelastic electron-hadron scattering is the incoherent sum of electron-parton scatterings. To be more specific, the hadronic cross-section is equal to the incoherent sum of partonic cross-sections weighted by parton distribution functions (also called parton densities) $f_i^H(y)$. They give the probability of finding in hadron H a parton 'i' carrying a momentum fraction y of its parent hadron. The quantity y is usually called the scaling variable.

However, later experiments at Fermilab and CERN, with better statistics, showed a slight breaking of scaling [10]. This could be understood in the context of QCD, where quarks are no longer considered to be free, but instead couple to gluons. However the effective strong coupling constant α_s vanishes logarithmically for increasing energies, a unique feature of non-abelian gauge theories like QCD. At sufficiently high energies the quarks behave as if they are free, a property called asymptotic freedom [11]. For this reason only a minor deviation of scaling is measured. For small values

¹The physicists responsible for this experiment were awarded the 1990 Nobel prize for physics.

of the energy, so at a large distance scale, the self-interactions of quarks and gluons cause α_s to rise to infinity. This could explain another experimental fact: free quarks have never been observed. (This property is called confinement.) It also implies that in the low-energy range α_s grows too large to make a convergent expansion in it around the free field theory, a method named perturbative QCD. In this region non-perturbative techniques [12] have to be used, which will not be discussed in this thesis.

In deep inelastic electron-hadron scattering (DIS) the parton model is the lowest order term of the QCD perturbation series. S.D. Drell and T.M. Yan constructed an analogue of the parton model for another process involving hadrons, namely massive lepton-pair production in hadron-hadron scattering [13]. This is generally called the Drell-Yan process (DY). The lepton-pair is produced by the decay of a virtual vector-boson (photon, W^\pm - or Z -particle). According to the Drell-Yan model the vector-boson is created by the annihilation of a parton from one hadron with an antiparton from the other hadron. The DY model also predicts scaling. One could expect a QCD induced breaking of scaling here too, but the Drell-Yan experiments that have been carried out so far were not accurate enough to observe this. However, the theoretical prediction for the DY cross-section that was made by the DY model had to be multiplied by a large normalization constant, the so-called K -factor, to fit the experimental data [14]. This is due to the omission of higher order QCD corrections.

1.3 Perturbative QCD

It is clear that QCD is a model for the strong interaction which is theoretically attractive, because it has the same general structure as the theories for the other three fundamental forces, and experimentally successful, in the sense that its global predictions are not contradicted by experiments. Unfortunately it requires a lot of work to obtain precise theoretical predictions that can be compared with the results of the experiments. We will give an overview of some calculations done in perturbative QCD and mention the difficulties and uncertainties in the calculations.

Both for DIS and for DY the first order QCD corrections were calculated already 15 years ago. To simplify the calculations quarks are taken to be massless. Together with the fact that gluons are massless, this gives rise to the appearance of mass singularities, also called collinear divergences, in the expressions for the partonic cross-sections. One can get rid of these singularities by absorbing them into the

parton densities [15]. This is a renormalization procedure called mass factorization (QCD is a renormalizable theory [16]). Since the parton densities play a role in both the parton model and the DY model, the DIS and DY partonic cross-sections should yield the same mass singularities, if one wants the renormalized parton densities to be process-independent. At first order this turned out to be indeed the case.

After removing the mass singularities from the partonic cross-section by means of mass factorization, one was able to determine the first order QCD corrections to the DY- and DIS cross-sections [17]. The corrections could more or less explain the scaling violations found in DIS and the large K -factor in DY. However, the large size of the first order corrections is alarming. For low energies it can partially be explained by the increasing coupling constant, but the first order corrections remain large in the high energy region. This raises the question whether the perturbation series is convergent. It is hard to judge this when having only the first order terms at ones disposal, although some authors have tried to estimate higher order terms by an exponentiation of the first order corrections (known as resummation techniques [18, 19]). Another point of concern is the strong dependence of the first order corrections on the energy scale at which the mass factorization is performed, which makes the results somewhat arbitrary. This is due to the truncation of the perturbation series and can only be reduced by including higher order corrections.

So one felt the need for the computation of at least the second order QCD corrections. Another motivation for more precise calculations was the progress in experimental high energy physics. Colliders provide us with an increasing amount of high-precision data covering various strong interaction processes. When experiments become more accurate, one needs better theoretical predictions with which to compare the data. In 1989 a first start with this was made in [20, 21], where part of the second order corrections to DY and DIS has been calculated. Here the so-called soft gluon limit was taken, which amounts to keeping only those contributions that are singular in the limit $y \rightarrow 1$, where y is the earlier mentioned scaling variable. It means the gluons have a very low energy. This not only simplifies the calculations but also reduces the number of parton processes that have to be taken into account. In the case of DY it was suspected that the soft gluon contributions dominate the cross-section. In 1991 the calculation of the second order contributions to DY was completed in [22]–[24], where the hard gluon part has been calculated. Notice the large time span between the performing of the first- and second order calculations! It is an indication of the complexity of second order QCD computations.

This thesis aims at completing the calculation of the second order QCD contri-

butions to DIS. We will explain in detail how the work was done and also present many graphs and tables to illustrate the consequences of including second order QCD corrections for the analysis of several collider experiments.

References

- [1] H. Fritsch, M. Gell-Mann and H. Leutwyler, Phys. Lett. B74 (1973) 365
- [2] C.N. Yang and R.L. Mills, Phys. Rev. 96 (1954), 191
- [3] M. Gell-Mann, Phys. Lett. 8 (1964), 214; G. Zweig, CERN reports TH-401 and TH-412
- [4] G.W. Greenberg, Phys. Rev. Lett. 13 (1964), 598
- [5] H. Fritsch and M. Gell-Mann, Proc. 16th Int. Conf. on High Energy Physics, Chicago-Batavia, 1972, vol. 2, p. 135; M. Gell-Mann, Acta Phys. Austr. Suppl. 9 (1972), 733
- [6] R.P. Feynman, Phys. Rev. Lett. 23 (1969), 1415
- [7] D.H. Coward et al., Phys. Rev. Lett. 20 (1968), 292; E.D. Bloom et al., Phys. Rev. Lett. 23 (1969), 930; M. Breidenbach et al., Phys. Rev. Lett. 23 (1969), 935
- [8] R.E. Taylor, Rev. Mod. Phys. 63 (1991), 573; H.W. Kendall, Rev. Mod. Phys. 63 (1991), 597; J.I. Friedman, Rev. Mod. Phys. 63 (1991), 615
- [9] J.D. Bjorken, Phys. Rev. 179 (1969), 1547
- [10] R.E. Taylor, Proceedings of the International Symposium on Lepton and Photon Interactions at High Energies, Stanford 1975
- [11] H.D. Politzer, Phys. Rev. Lett. 30 (1973), 1346; D.J. Gross and F. Wilczek, Phys. Rev. Lett. 30 (1973), 1343; S. Coleman and D.J. Gross, Phys. Rev. Lett. 31 (1973), 851
- [12] K.G. Wilson, Phys. Rev. D10 (1974), 2445; J.M. Drouffe and C. Itzykson, Phys. Rep. 38C (1978), 133; A. Hasenfratz and P. Hasenfratz, Ann. Rev. Nucl. Part. Sci. 35 (1985), 559

- [13] S.D. Drell and T.M. Yan, Phys. Rev. Lett. **25** (1970), 316; Ann. Phys. **66** (1971), 578
- [14] J. Badier et al., Phys. Lett. **89B** (1979), 145; R. Barate et al., Phys. Rev. Lett. **43** (1979), 1541
- [15] H.D. Politzer, Nucl. Phys. **B129** (1977), 301
- [16] G. 't Hooft, Nucl. Phys. **B33** (1971) 173
- [17] J. Kubar-André and F.E. Paige, Phys. Rev. **D19** (1979), 221; G. Altarelli, R.K. Ellis and G. Martinelli, Nucl. Phys. **B157** (1979), 461; B. Humpert and W.L. van Neerven, Nucl. Phys. **B184** (1981), 225; G. Parisi, Phys. Lett. **90B** (1980), 295
- [18] G. Parisi, Phys. Lett. **B90** (1980) 295; G. Sterman, Nucl. Phys. **281** (1987) 319.
- [19] D. Appel, P. Mackenzie and G. Sterman, Nucl. Phys. **B309** (1988) 259; S. Catani and L. Trentadue, Nucl. Phys. **B327** (1989) 323; *ibid.* **B353** (1991) 183; E. Laenen, J. Smith and W.L. van Neerven, Nucl. Phys. **B369** (1992) 543
- [20] T. Matsuura, S.C. van der Marck and W.L. van Neerven, Phys. Lett. **B211** (1988) 171; Nucl. Phys. **B319** (1989) 570.
- [21] T. Matsuura, Ph.D. thesis, University of Leiden, The Netherlands (1989).
- [22] T. Matsuura, R. Hamberg and W.L. van Neerven, Nucl. Phys. **B345** (1990) 331.
- [23] R. Hamberg, W.L. van Neerven and T. Matsuura, Nucl. Phys. **B359** (1991) 343.
- [24] R. Hamberg, Ph.D. thesis, University of Leiden, The Netherlands (1991).

Chapter 2

Higher order QCD calculations

2.1 Introduction

In this chapter we will outline the procedure for calculating higher order QCD contributions to the theoretical cross-sections of deep inelastic scattering (DIS) and the Drell-Yan process (DY). The emphasis will be on DIS calculations.

Before going into the details of deep inelastic scattering, we will define some of the relevant quantities of DIS and DY. In figure 2.1 we have depicted the deep inelastic scattering process

$$\ell_1 + H \rightarrow \ell_2 + 'X' , \quad (2.1.1)$$

where the interaction is mediated by one of the vector bosons of the standard model ($V = \gamma, W^\pm$ or Z). The incoming lepton is denoted by ℓ_1 , the incoming hadron by H , the scattered lepton by ℓ_2 and the remnants of the broken up hadron by ' X ', which can contain any combination of hadronic states that is allowed by conservation of quantum numbers.

As shown in the figure, q represents the momentum of the vector boson, while k_i , p and p_X denote the momenta of ℓ_i , H and X , respectively. The mass of the hadron is M . The measurable quantities in the process are p , q and M . For convenience these three quantities are recombined into three other variables, which will be frequently used.

$$Q^2 = -q^2 , \quad (2.1.2)$$

$$\nu = \frac{p \cdot q}{M} \quad (2.1.3)$$

and

$$x = -\frac{q^2}{2p \cdot q} , \quad (2.1.4)$$

where ν and x represent the energy transfer to the hadron in its rest frame and the DIS scaling variable, respectively. The ultimate purpose will be the calculation of the DIS differential cross section. Because the outgoing hadronic states are not measured separately (only the outgoing lepton is detected), we have to consider an inclusive cross-section, i.e. we sum over the final state quantum numbers. Furthermore we consider for the moment unpolarized cross-sections and average over all possible initial state spins. Polarized deep inelastic scattering will be discussed in chapter 6.

The deep inelastic scattering process can be split in two parts:

- a. A leptonic part, consisting of the emission of a vector boson by the lepton,
- b. A hadronic part, consisting of the subsequent vector boson-hadron scattering.

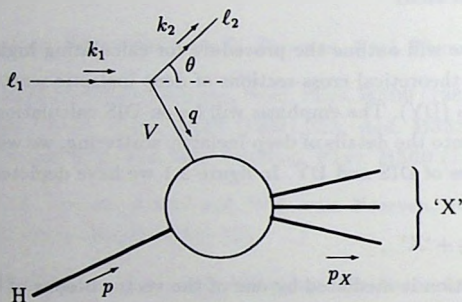


Fig. 2.1. The kinematics of the DIS process.

The inclusive DIS differential cross-section is proportional to the product of the leptonic and hadronic tensors, which are indicated by $L_{\mu\nu}$ and $W_{\mu\nu}$, respectively. In the case of a charged current process where $V = W$, the cross section becomes

$$\frac{d^2\sigma}{dQ^2 d\nu} = \frac{g^4}{2^{10}\pi(q^2 - M_V^2)^2 E_1^2 M} L^{\mu\nu} W_{\mu\nu}, \quad (2.1.5)$$

where E_1 is the energy of the incoming lepton in the rest frame of the hadron, M_V is the mass of the vector boson and g is the electroweak coupling constant. Because leptons are generally assumed to be point-particles, the leptonic part is easy to compute (neglecting electroweak radiative corrections). Using standard Feynman rules one obtains for the leptonic tensor in lowest order of electroweak theory

$$L^{\mu\nu} = 4(v^2 + a^2) [k_1^\mu k_2^\nu + k_1^\nu k_2^\mu - g^{\mu\nu} k_1 \cdot k_2] - 8ivae^{\mu\nu\sigma\lambda} k_{1\sigma} k_{2\lambda}, \quad (2.1.6)$$

where the lepton masses are neglected and v and a denote the vector- and axial parts of the vector boson coupling to the lepton pair, which can be found in [1]. Further we use the convention $\varepsilon^{0123} = 1$. The last term of (2.1.6) is absent in purely electromagnetic processes due to parity conservation.

The computation of the contribution of the hadronic part of the process is less straightforward, because the hadron is a composite particle instead of a point-particle. This means that without further investigation one cannot say much about the hadronic tensor $W_{\mu\nu}$, except that one can write down the most general formula for it in terms of the four-momenta occurring in the process. By imposing constraints on $W_{\mu\nu}$, like Lorentz invariance and time reversal invariance, and neglecting terms proportional to the lepton masses, some of the possible Lorentz structures are ruled out. The left-over Lorentz structures are parametrized by dimensionless coefficients F_i . This yields

$$\begin{aligned} W_{\mu\nu}(x, Q^2) = & - \left(g_{\mu\nu} - \frac{q_\mu q_\nu}{q^2} \right) F_1(x, Q^2) + \\ & + \left(p_\mu - \frac{p \cdot q}{q^2} q_\mu \right) \left(p_\nu - \frac{p \cdot q}{q^2} q_\nu \right) \frac{1}{p \cdot q} F_2(x, Q^2) + \\ & - \frac{1}{2} i \varepsilon_{\mu\nu\sigma\lambda} p^\sigma q^\lambda \frac{1}{p \cdot q} F_3(x, Q^2) , \end{aligned} \quad (2.1.7)$$

provided we assume that the hadronic (weak) current is conserved at high energies. The coefficients F_i in (2.1.7), which are yet to be determined, are called DIS hadron structure functions. This decomposition of the hadronic tensor enables us to express the differential cross section of the DIS process in terms of the F_i . It reads

$$\begin{aligned} \frac{d^2\sigma}{dQ^2 d\nu} = & \frac{g^4}{2^8 \pi (q^2 - M_V^2)^2} \frac{E_2}{E_1 M} \left((v^2 + a^2) \left(2F_1 \sin^2 \frac{\theta}{2} + \frac{M}{\nu} F_2 \cos^2 \frac{\theta}{2} \right) \right. \\ & \left. + 2va \frac{E_1 + E_2}{\nu} F_3 \sin^2 \frac{\theta}{2} \right) , \end{aligned} \quad (2.1.8)$$

where E_1 and E_2 are the energies of the incoming- and outgoing leptons in the rest frame of the hadron and θ is the lepton scattering angle (see fig. 2.1), which satisfies

$$Q^2 = 4E_1 E_2 \sin^2 \left(\frac{1}{2} \theta \right) . \quad (2.1.9)$$

In the case of a purely electromagnetic process, $F_3 = 0$ due to parity conservation and one can use in (2.1.5) and (2.1.8)

$$M_V = M_\gamma = 0 , \quad v = 1 , \quad a = 0 , \quad g^4 = 2^{10} \pi^2 \alpha , \quad (2.1.10)$$

where $\alpha = e^2/4\pi$ is the fine structure constant.

We will now switch to the description of the Drell-Yan process, i.e. massive lepton pair production in hadronic collisions, proceeding through the following reaction

$$H_1 + H_2 \rightarrow V + 'X'$$

$$\quad \quad \quad \downarrow$$

$$\quad \quad \quad \ell_1 + \ell_2,$$
(2.1.11)

where V is a vector boson, which subsequently decays into a lepton pair (ℓ_1, ℓ_2) . The process is depicted in fig. 2.2. The symbol 'X' again denotes any inclusive final

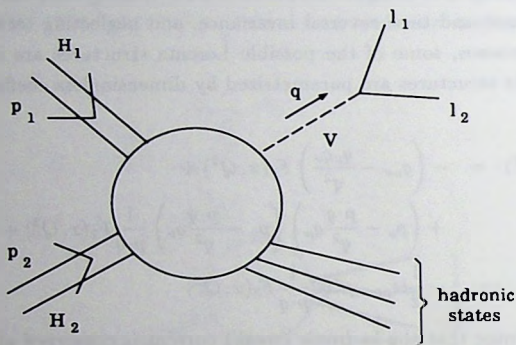


Fig. 2.2. The kinematics of the Drell-Yan process.

hadronic state allowed by conservation of quantum numbers. The colour averaged inclusive cross section is given by

$$\frac{d\sigma^V}{dQ^2} = x \frac{d\sigma_{\text{point}}^V}{dQ^2} W_V(x, Q^2),$$
(2.1.12)

where

$$x = \frac{Q^2}{S}, \quad S = (p_1 + p_2)^2,$$
(2.1.13)

with p_1 and p_2 denoting the momenta of the two incoming hadrons. The quantity $\frac{d\sigma_{\text{point}}^V}{dQ^2}$ is the pointlike DY cross section (the cross section that we would have if the hadrons were point-particles), which can be found in appendix A of [2]. The variables \sqrt{S} and $\sqrt{Q^2}$ stand for the C.M. energy of the incoming hadrons H_1 , H_2 and the invariant mass of the lepton pair, respectively. $W_V(x, Q^2)$ represents the DY

hadron structure function, indicating the deviation from pointlike behaviour. For its calculation more work needs to be done.

To make a theoretical prediction for the structure functions of both DIS and DY, we need a model for the composition of hadrons. In the subsequent sections we will describe how the hadron structure functions $W_V(x, Q^2)$ and $F_2(x, Q^2)$ can be determined using the QCD improved parton model.

2.2 The naive parton model

The naive parton model [3] gives a description of the composite structure of hadrons as probed in highly energetic collisions. Its assumptions are:

1. All hadrons consist of partons (which can be identified with the quarks; later the denomination partons will be used as the collective name of both quarks and gluons.)
2. The partons are free point-particles, they do not interact with each other. They only interact with leptons, via the exchange of vector bosons of the standard weak model.
3. Deep inelastic collisions involving hadrons are determined by collisions involving partons. E.g. the cross-section of photon-hadron scattering is the incoherent sum of elastic photon-parton scatterings and the cross-section of hadron-(anti)hadron scattering is the incoherent sum of parton-(anti)parton annihilations.

The idea is shown in fig. 2.3 (taken from [4]). In order to compute the hadron structure functions which are necessary to make a theoretical prediction for DIS and DY cross-sections, the rather simple concepts of the parton model need to be incorporated in the calculation. For DIS this can be done in three steps:

Step 1 : Define the parton density¹ $\hat{f}_i^H(y)$ of a parton of type i with momentum \hat{p} inside a hadron H with momentum p . The variable y denotes the momentum fraction carried by the parton 'i' with respect to the momentum of its parent hadron, which

¹We will mostly use hatted symbols to denote parton level quantities. However in the case of the parton density the hat indicates that it is an unrenormalized or 'bare' quantity, without physical meaning. Although in the naive parton model the parton density does have a physical interpretation, we use the hat here in consideration of later sections, where the story continues.

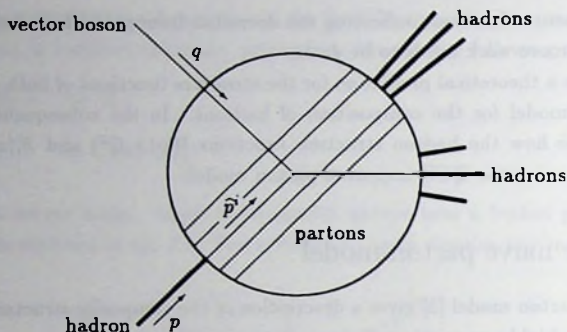


Fig. 2.3. The parton picture of deep inelastic scattering.

is supposed to have the same direction: $\hat{p}_\mu = yp_\mu$, where $0 \leq y \leq 1$.

Step 2 : Define the DIS scaling variable at the parton level

$$z = \frac{-q^2}{2\hat{p} \cdot q} . \quad (2.2.1)$$

This is the analogue of the hadron scaling variable x , which is related to z by $x = yz$.

Step 3 : Introduce parton structure functions \hat{F}_1^i , \hat{F}_2^i and \hat{F}_3^i , which mathematically play exactly the same role as the hadron structure functions, namely parametrization of a tensor $\hat{W}_{\mu\nu}$, which shows up if we write the cross-section of the parton process

$$\text{parton } i + V \rightarrow \text{some multi-parton state} \quad (2.2.2)$$

as

$$\frac{d^2\hat{\sigma}^i}{dQ^2 d\nu}(z, Q^2) \propto L^{\mu\nu} \hat{W}_{\mu\nu}^i . \quad (2.2.3)$$

For the precise definition of $\hat{W}_{\mu\nu}^i$, see (2.6.4). However, physically \hat{F}_k^i must mean something else than F_k , because unlike hadrons, partons are point-particles, as stated by the second assumption of the parton model. We will use that assumption later.

For the Drell-Yan process three equivalent steps need to be taken [5]:

Step 1 : Same as step 1 for DIS.

Step 2 : Define the DY scaling variable at the parton level

$$z = \frac{Q^2}{(\hat{p}_1 + \hat{p}_2)^2} , \quad (2.2.4)$$

where \hat{p}_1 and \hat{p}_2 denote the momenta of the incoming partons belonging to the two colliding hadrons. If y_1 and y_2 denote their momentum fractions with respect to the momenta of the respective parent hadrons, we have the relation $x = y_1 y_2 z$. Note that we indicate the DIS and DY scaling variables by the same symbols, although mathematically they have different meanings. This should not cause confusion, as we will always make a clear distinction between the discussion of DIS and DY.

Step 3 : Define

$$\hat{\sigma}_{ij}(z, Q^2) , \quad (2.2.5)$$

the cross section of the process

$$\text{parton } i + \text{parton } j \rightarrow V + \text{some multi-parton state} . \quad (2.2.6)$$

Then a parton DY 'structure function' \hat{W}^{ij} can be introduced in the same way as the hadron DY structure function by

$$\frac{d\hat{\sigma}^{ij}}{dQ^2} = z \left(\frac{d\sigma}{dQ^2} \right)_{\text{point}} \hat{W}^{ij}(z, Q^2) . \quad (2.2.7)$$

Now we are able to make both for DIS and for DY a connection between the process at the parton level and the process at the hadron level, that is, we can express the hadron structure functions in the parton structure functions. According to the parton model we obtain for DIS

$$F_j(x, Q^2) = \sum_i e_i^2 \int_0^1 dy \int_0^1 dz \delta(x - yz) \hat{f}_i(y) \hat{F}_j^i(z, Q^2) , \quad (2.2.8)$$

where we integrate over all possible momentum fractions of the partons and sum over all possible parton types. The parton structure functions $\hat{F}_j^i(x, Q^2)$ are weighted by the parton density $\hat{f}_i(y)$. The delta-function implements the constraint $x = yz$ and e_i denotes the parton charge. Eq. (2.2.8) plays a key-role in the description of deep inelastic lepton-hadron scattering and we will refer to it as the DIS master equation. The DY master equation is very similar:

$$W(x, Q^2) = \sum_{i,j} e_i e_j \int_0^1 dy_1 \int_0^1 dy_2 \int_0^1 dz \delta(x - y_1 y_2 z) \hat{f}_i(y_1) \hat{f}_j(y_2) \hat{W}^{ij}(z, Q^2) . \quad (2.2.9)$$

From now on we suppress the parton charges e_i . These master equations can be written in a short-hand notation as

$$F_j(x, Q^2) = \hat{f}_i(y) \otimes \hat{F}_j^i(z, Q^2) , \quad (2.2.10)$$

$$W(x, Q^2) = \hat{f}_i(y_1) \otimes \hat{f}_j(y_2) \otimes \hat{W}^{ij}(z, Q^2) , \quad (2.2.11)$$

where the convolution symbol \otimes is defined by

$$(f \otimes g)(x) = \int_0^1 dx_1 \int_0^1 dx_2 \delta(x - x_1 x_2) f(x_1) g(x_2) . \quad (2.2.12)$$

Further repeated indices are summed over.

It may seem that we did not gain much by the construction of the master equations: we only shifted our attention from the hadron structure functions to the obscure concept of parton structure functions. However, we can now use the assumption of the naive parton model that the partons are non-interacting point particles, which implies that

$$\hat{F}_2^i(z, Q^2) = \delta(1 - z) \Rightarrow F_2(x, Q^2) = \hat{f}_i(x) , \quad (2.2.13)$$

$$\hat{W}^{ij}(z, Q^2) = \delta(1 - z) \Rightarrow W(x, Q^2) = \hat{f}_i(y_1) \otimes \hat{f}_j(y_2) . \quad (2.2.14)$$

(We take as an example pure electromagnetism and limit ourselves to F_2 .) The right-hand sides of (2.2.13) and (2.2.14) do not contain any Q^2 -dependence. This implies that if one believes the assumption of the naive parton model that at the parton level we only have to deal with simple Compton scatterings of free, point-like particles (or an annihilation process in the case of DY), the hadron structure functions for DY and DIS should be independent of Q^2 . This property is called scaling [6], and this prediction of the naive parton model was confirmed (within the error bars) by the first measurements of DIS [7] and DY [8, 9] cross-sections .

However, later DIS experiments with higher accuracy showed a slight breaking of scaling [10]. So apparently the naive parton model just described is a bit too simple to give a satisfactory description of high energy strong interaction processes. As discussed in chapter 1, Quantum Chromo Dynamics (QCD) would be a better candidate for this. Still we would like to preserve some of the attractive features of the naive parton model, which has the advantage that it is intuitively appealing. This is achieved in the so-called QCD improved parton model, which will be discussed in the next section. It will give rise to Q^2 -dependent corrections to the parton structure functions.

2.3 The QCD improved parton model

In the previous section we have seen that the naive parton model establishes a link between the processes at the hadron level and the parton subprocesses in an elegant way, but fails in giving an explanation for the observed breaking of scaling in DIS experiments. With the advent of QCD it was possible to identify the partons with the quarks and gluons. However, there is one essential difference: unlike the partons of the naive parton model, the quarks are not free particles, because they couple to the gluons. The strong coupling constant α_s decreases with growing energies, so only at very high energy the quarks do become more or less free and we are allowed to a) make a perturbative expansion in α_s , around the free field theory (which equals the naive parton model), and b) maintain the incoherence assumption of the naive parton model, according to which a photon-parton collision proceeds unaffected by the neighbourhood of other partons. At low energy however, the quarks are in tightly bound states and the quark-photon scattering becomes coherent. In that region perturbative QCD is no longer valid.

In this section we will discuss DIS and DY calculations in perturbative QCD. The parton subprocesses can be calculated using QCD Feynman rules. The processes contributing to DIS and DY up to order α_s^2 , are listed in table 2.1 and 2.2.

Note that the zeroth order DIS and DY processes correspond to the DIS and DY processes of the naive parton model, giving parton structure functions that are proportional to delta functions (see (2.2.13) and (2.2.14)). All higher order QCD contributions to the cross-section will be added to the parton structure functions \hat{F} and \hat{W} . This means we do not have to change our master equations but instead change the contents of \hat{F} and \hat{W} , which is the reason why they are useful quantities, even though they have nothing to do with any 'structure' of the partons as their name may suggest.

The calculation of higher order corrections to parton structure functions involves many complicated phase space and loop integrals, because we have to integrate over the outgoing momenta (we consider inclusive processes). As most of these integrals are divergent, one should introduce a regulator to display the singularities in a convenient way. We have chosen the dimensional regularization method [11], i.e. we perform our calculations in $n = 4 + \epsilon$ instead of 4 dimensions. The singularities, appearing in the integrals, will manifest themselves as $\epsilon^{-\ell}$ terms (where ℓ is a positive integer). These poles can be classified according to their origin. We distinguish three types:

figure	DIS subprocesses	
3.1	$\alpha_s^0: V + q(\bar{q}) \rightarrow q(\bar{q})$	
3.2	$\alpha_s^1: V + q(\bar{q}) \rightarrow q(\bar{q})$	(one loop correction)
3.3	$V + q(\bar{q}) \rightarrow q(\bar{q}) + g$	
3.3	$V + g \rightarrow q + \bar{q}$	
3.4	$\alpha_s^2: V + q(\bar{q}) \rightarrow q(\bar{q})$	(two loop correction)
3.5	$V + q(\bar{q}) \rightarrow q(\bar{q}) + g$	(one loop correction)
3.6	$V + q(\bar{q}) \rightarrow q(\bar{q}) + g + g$	
3.7	$V + q(\bar{q}) \rightarrow q(\bar{q}) + q(\bar{q}) + \bar{q}(q)$	
3.5	$V + g \rightarrow q + \bar{q}$	(one loop correction)
3.6	$V + g \rightarrow q + \bar{q} + g$	

Table 2.1. List of deep inelastic lepton-parton subprocesses up to $\mathcal{O}(\alpha_s^2)$.

Type 1 : Ultraviolet divergences :

Ultraviolet singularities show up in loop integrals where the loop momentum k goes to infinity, $|k| \rightarrow \infty$. They are removed by coupling constant renormalization.

Type 2 : Infrared divergences :

This type of divergence is encountered in both loop- and phase space integrals. They are found in the low energy region where the integration momentum goes to zero. According to the Bloch-Nordsieck theorem [12], these singularities have to cancel between the virtual processes (with gluons in the loop) and the bremsstrahlung processes (with gluons in the final state).

Type 3 : Mass singularities :

figure	DY subprocesses		
4.1	$\alpha_s^0:$	$q + \bar{q} \rightarrow V$	
4.2	$\alpha_s^1:$	$q + \bar{q} \rightarrow V$	(one loop correction)
4.3		$q + \bar{q} \rightarrow V + g$	
4.3		$q(\bar{q}) + g \rightarrow V + q(\bar{q})$	
4.4	$\alpha_s^2:$	$q + \bar{q} \rightarrow V$	(two loop correction)
4.5		$q + \bar{q} \rightarrow V + g$	(one loop correction)
4.6		$q + \bar{q} \rightarrow V + g + g$	
4.5		$q(\bar{q}) + g \rightarrow V + q(\bar{q})$	(one loop correction)
4.6		$q(\bar{q}) + g \rightarrow V + q(\bar{q}) + g$	
4.7, 4.8		$q + \bar{q} \rightarrow V + q + \bar{q}$	
4.8, 4.9		$q(\bar{q}) + q(\bar{q}) \rightarrow V + q(\bar{q}) + q(\bar{q})$	
4.6		$g + g \rightarrow V + q + \bar{q}$	

Table 2.2. List of Drell-Yan parton subprocesses up to $\mathcal{O}(\alpha_s^2)$.

These divergences are sometimes called collinear divergences because they arise when the momenta of two massless particles become parallel. (To simplify the calculations, we take both gluons and quarks massless.)

In that case a propagator $[(p - k)^2]^{-1}$ can be expressed by

$$(p - k)^2 = -2|\vec{p}||\vec{k}|(1 - \cos \theta) \xrightarrow{\theta \rightarrow 0} -|\vec{p}||\vec{k}|\theta^2, \quad (2.3.1)$$

which gives rise to a singularity in both phase space and loop integrals. We can distinguish two subtypes of mass singularities:

Subtype 3a : Final state mass singularities

In this case the integration momentum becomes parallel to the momentum of a final

state particle. According to the theorem of Kinoshita, Lee and Nauenberg [13] (see also [14]), the final state mass singularities cancel, because we are considering a final state inclusive process, where one sums over all degenerate (= experimentally indistinguishable) final states.

Subtype 3b : Initial state mass singularities

Here the integration momentum becomes parallel to the momentum of an initial state particle. It is not possible to get rid of the initial state mass singularities in a trivial way.

It is clear that one does not have to do much work to remove the poles of type 1 to 3a, but the initial state mass singularities remain present in the parton structure functions. Because the hadron structure functions are physical quantities which should be finite, the initial state mass singularities must be disposed of, one way or another. How this is achieved will be discussed in the next section.

2.4 Mass factorization

Due to the initial state mass singularities arising from higher order QCD contributions, the parton structure functions $\hat{F}_j(z, Q^2, \epsilon)$ and $\hat{W}(z, Q^2, \epsilon)$ contain poles in ϵ . We will remove these singularities by using *mass factorization* [15]. This is a renormalization procedure which amounts to factorizing the mass singularities out of the parton structure functions and absorbing them into the bare parton densities. Because we would like the renormalized parton densities to be process independent, the mass singularities must be universal. For example, they are the same for DY and DIS.

We will explain mass factorization by considering the DIS master equation for F_2 (2.2.10). Suppose we have performed a higher order QCD calculation. Infrared divergences and final state mass singularities have vanished, but ultraviolet divergences and initial state mass singularities are still left. We add the result to the DIS parton structure function, which then becomes dependent on Q^2 , ϵ and on μ , an arbitrary mass scale which is an artefact of dimensional regularization. We now have

$$F_2(Q^2) = \hat{f}_i \otimes \hat{F}_2^i(\alpha_s, \frac{Q^2}{\mu^2}, \epsilon) , \quad (2.4.1)$$

where ϵ denotes both initial state mass singularities and ultraviolet divergences. The summation index i labels the parton types (quark (q), antiquark (\bar{q}) and gluon (g)).

We remove the ultraviolet divergences by renormalization of the bare strong coupling constant α_s , which we perform at a renormalization scale R . We denote the renormalized, running coupling constant by $\alpha_s(R^2)$. This yields

$$F_2(Q^2) = \hat{f}_i \otimes \hat{F}_2^i(\alpha_s(R^2), \frac{Q^2}{\mu^2}, \frac{R^2}{\mu^2}, \epsilon) . \quad (2.4.2)$$

Now ϵ stands for the initial state mass singularities only. The next step is to separate the pole part of \hat{F}_2^i from the non-pole part. The part containing poles is called the transition function Γ_{ik} ($i, k = q, \bar{q}, g$), which is process independent. The residues of the pole terms $1/\epsilon^\ell$ ($\ell = 0, 1, 2, \dots$) in Γ_{ik} are given by the so-called Altarelli-Parisi splitting functions [16]. The finite part is called the (Wilson) coefficient function C_k [17]. The separation takes place at a mass factorization scale M .

$$F_2(Q^2) = \hat{f}_i \otimes \Gamma_{ik, \text{scheme}}(\alpha_s(R^2), \frac{M^2}{\mu^2}, \frac{M^2}{R^2}, \epsilon) \quad (2.4.3)$$

$$\otimes C_{2,k, \text{scheme}}(\alpha_s(R^2), \frac{Q^2}{M^2}, \frac{M^2}{R^2}) . \quad (2.4.4)$$

We have different schemes for separating the pole terms from the non-pole terms, because it is arbitrary what one factorizes into Γ_{ik} , as long as Γ_{ik} contains at least the pole terms. In the literature one has chosen the following two mass factorization schemes:

The $\overline{\text{MS}}$ scheme [18]: This implies only the pole terms of \hat{F}_2^i are absorbed into Γ_{ik} .

The DIS scheme [19]: The complete \hat{F}_2^i is absorbed into Γ_{ik} .

For convenience we choose the arbitrary scales M and R both equal to Q , which yields

$$F_2(Q^2) = \hat{f}_i \otimes \Gamma_{ik, \text{scheme}}(\alpha_s(Q^2), \frac{Q^2}{\mu^2}, \epsilon) \otimes C_{2,k, \text{scheme}}(\alpha_s(Q^2)) \quad (2.4.5)$$

Finally we redefine the parton density:

$$f_{k, \text{scheme}}(\alpha_s(Q^2), Q^2) = \hat{f}_i \otimes \Gamma_{ik, \text{scheme}}(\alpha_s(Q^2), \frac{Q^2}{\mu^2}, \epsilon) , \quad (2.4.6)$$

so that we can write

$$F_2(Q^2) = f_{k, \text{scheme}}(\alpha_s(Q^2), Q^2) \otimes C_{2,k, \text{scheme}}(\alpha_s(Q^2)) . \quad (2.4.7)$$

In contrast to the bare parton density \hat{f} , the renormalized parton density f is finite, but scheme- and scale dependent. How do we know it is finite? It should be finite, because the hadron structure function $F_2(Q^2)$ is directly related to the measurable cross-section and thus cannot contain divergences. Further C_2 is finite by definition. Along the same lines one can argue that f does not depend on μ .

In the DIS scheme we get a simple expression for $F_2(x, Q^2)$, namely

$$F_2(x, Q^2) = \sum_k f_{k, \text{DIS}}(x, \alpha_s(Q^2), Q^2) . \quad (2.4.8)$$

This is the reason why some people prefer the DIS scheme. However, the price one pays is that the expressions for the other hadronic structure functions become more complicated. We should remark that of course one can also define different schemes for the coupling constant renormalization. In this thesis we will always renormalize the coupling constant in the $\overline{\text{MS}}$ scheme.

Having explained mass factorization for DIS, we can perform the mass factorization for DY in one step. Recall that according to the mass factorization theorem Γ_{ik} is process independent, so we can use it for DY as well. The DY master equation (2.2.11) containing QCD corrections is

$$W(Q^2) = \hat{f}_i \otimes \hat{f}_j \otimes \hat{W}^{ij}(\alpha_s, \frac{Q^2}{\mu^2}, \epsilon) . \quad (2.4.9)$$

After mass factorization we have

$$W(Q^2) = f_{i, \text{scheme}}(Q^2) \otimes f_{j, \text{scheme}}(Q^2) \otimes \Delta_{ij, \text{scheme}}(\alpha_s(Q^2)) , \quad (2.4.10)$$

where Δ_{ij} is the finite DY coefficient function, which satisfies

$$\hat{W}^{ij} = \Gamma_{ik, \text{scheme}} \otimes \Gamma_{jl, \text{scheme}} \otimes \Delta_{kl, \text{scheme}} . \quad (2.4.11)$$

In the remainder of this thesis the scheme label will be omitted most of the time, because we will separate the discussions of the DIS- and $\overline{\text{MS}}$ scheme results. We must admit that the explanation of mass factorization is a little bit simplified in the sense that we did not specify what exactly is meant by the summation over parton labels hidden in the equations. We will see later that different parton types mix in the higher order corrected master equations, a fact that was partly ignored here to keep the discussion transparent. Furthermore we suppressed the dependence on the scaling variables. Later we will show explicitly worked out formulas.

The main achievement of this section is the derivation of the equations (2.4.7) and (2.4.10). In the following section we will take a closer look at them.

2.5 Calculable quantities in perturbative QCD

In this section we give an outline of what will be calculated in the chapters hereafter. The starting point of these calculations is given by the mass factorized master equations (2.4.7) and (2.4.10). In these equations the renormalized parton density f_i is

the unknown quantity in which we are interested. The DY and DIS hadron structure functions depend on the same renormalized parton densities, which are universal as stated by the mass factorization theorem. Only the DIS and DY coefficient functions differ and they can be calculated up to order α_s^2 from the subprocesses listed in table 2.1 and 2.2.

The relation between the DY coefficient functions in the DIS and $\overline{\text{MS}}$ scheme, which we denote by Δ_{DIS}^{ij} and Δ_{MS}^{ij} respectively, is given by

$$\Delta_{\text{DIS}}^{ij} = \Delta_{\text{MS}}^{ij} \otimes C_{2,i,\text{MS}}^{-1} \otimes C_{2,j,\text{MS}}^{-1} . \quad (2.5.1)$$

So if one wants to calculate $W(x, Q^2)$ up to second order in the DIS scheme (which will be done in chapter 4), one needs to know the DIS coefficient functions of F_2 up to second order in the $\overline{\text{MS}}$ scheme (which will be calculated in chapter 3). Also the deep inelastic coefficient functions belonging to F_L and F_3 can be calculated both in the $\overline{\text{MS}}$ and in the DIS scheme (see chapter 3 and 5). If we could perform an exact calculation, that is, compute all higher order contributions, we would not have any scheme dependence, because there should be no ambiguity in physical quantities. However, the truncation of the QCD perturbation series introduces both a dependence on the mass factorization scheme and on the mass factorization- and renormalization scale. This will also be subject of investigation.

The deep inelastic structure functions are measured more or less accurately at several colliders, so if one knows the coefficient functions, it is possible to extract the parton densities from the deep inelastic data by means of (2.4.7) and use them as input for the DY mass factorized master equation (2.4.10). Then we can make a theoretical prediction for the DY structure functions (up to second order in the strong coupling constant), which can be compared with the data as a test of second order QCD.

Although the parton densities cannot be calculated in perturbation theory, we can say something about their scale dependence. From the discussion in section 2.4 it is clear that the Q^2 dependence of f_i comes from the scales R and M , which are introduced at the moment of renormalization and mass factorization, respectively. In the original master equation (2.4.1) M is absent, from which we conclude that the M dependence of Γ_{ij} compensates that of C_{2k} . Apparently the scale dependence of Γ_{ij} is closely related to the pole part of \hat{F}_2^i , which is universal. This implies one must also be able to derive both the pole terms and the dependence on the mass factorization scale in other ways. One of these 'other ways' is the operator product expansion [17]. Besides the dependence on M , Γ_{ik} also has an indirect dependence on R , via the

$\alpha_s(R^2)$ dependence. This is given by

$$R \frac{d\alpha_s(R^2)}{dR} = \beta(\alpha_s(R^2)) , \quad (2.5.2)$$

where the well-known β -function (3.2.28) has been calculated up to third order in α_s . Putting both M and R equal to Q , we can write the resulting Q^2 dependence of the transition function Γ_{ik} as

$$Q \frac{d}{dQ} \Gamma_{ik} = -P_{ij} \otimes \Gamma_{jk} , \quad (2.5.3)$$

where P_{ij} denote the so-called AP splitting functions, which are known up to second order in α_s . As Γ_{ij} is contained within f_i , the conclusion is that the Q^2 dependence of the parton densities can be predicted theoretically. We have

$$Q \frac{d}{dQ} f_i \equiv Q \frac{d}{dQ} (\Gamma_{ik} \otimes \hat{f}_k) = (Q \frac{d}{dQ} \Gamma_{ik}) \otimes \hat{f}_k \quad (2.5.4)$$

$$= -P_{ij} \otimes \Gamma_{jk} \otimes \hat{f}_k = -P_{ij} \otimes f_j . \quad (2.5.5)$$

However, to determine the dependence of f_i on the scaling variable x , one needs the coefficient function belonging to the specific structure function considered (F_2 , F_L or F_3), together with measurements of that structure function. Furthermore an additional Q^2 dependence enters the structure function because of the $\alpha_s(Q^2)$ occurring in the perturbation series of the coefficient functions as well as the transition functions.

Summarizing, the theoretical ingredients for the extraction of parton densities from the measurements of deep inelastic structure functions are the splitting functions and the coefficient functions, which both can be computed in QCD perturbation theory. Once the parton densities are known, they can be used to make predictions for the Drell-Yan structure function, which provides us with a consistency check of perturbative QCD. The main goal of this thesis is to calculate the second order QCD corrected DIS coefficient functions of F_2 , F_L and F_3 .

2.6 Phase space integrals

The three particle phase space integrals occurring in the calculation of inclusive $2 \rightarrow 3$ processes, like

$$q(\hat{p}_1) + \bar{q}(\hat{p}_2) \rightarrow g(\hat{p}_3) + g(\hat{p}_4) + V(q) \quad (\text{DY}) , \quad (2.6.1)$$

$$q(\hat{p}_1) + V(q) \rightarrow g(\hat{p}_3) + g(\hat{p}_4) + \bar{q}(\hat{p}_2) \quad (\text{DIS}) , \quad (2.6.2)$$

constitute the biggest stumbling block in the calculation of second order contributions to the DIS and DY coefficient functions. For the calculation of the coefficient functions we need to compute the parton structure functions, which will be mass factorized later by means of the transition functions. In this section we will outline how the integrations over the three outgoing momenta in the parton structure functions are performed. First we need to give some more details of the processes at the parton level.

As already said in section 2.2, the partonic cross-section can be defined similar to the hadronic cross-section as

$$\frac{d^2\hat{\sigma}^i}{dQ^2 d\nu}(z, Q^2) \propto L^{\mu\nu} \widehat{W}_{\mu\nu}^i, \quad (2.6.3)$$

where $\widehat{W}_{\mu\nu}^i$ is defined completely similar to the hadron tensor $W_{\mu\nu}$ (2.1.7), except that it is expressed in terms of the parton structure functions.

$$\begin{aligned} \widehat{W}_{\mu\nu}^i(z, Q^2) = & - \left(g_{\mu\nu} - \frac{q_\mu q_\nu}{q^2} \right) \widehat{F}_1^i(z, Q^2) + \\ & + \left(\widehat{p}_\mu - \frac{\widehat{p} \cdot q}{q^2} q_\mu \right) \left(\widehat{p}_\nu - \frac{\widehat{p} \cdot q}{q^2} q_\nu \right) \frac{1}{\widehat{p} \cdot q} \widehat{F}_2^i(z, Q^2) + \\ & - \frac{1}{2} i \varepsilon_{\mu\nu\sigma\lambda} \widehat{p}^\sigma q^\lambda \frac{1}{\widehat{p} \cdot q} \widehat{F}_3^i(z, Q^2) . \end{aligned} \quad (2.6.4)$$

where $i = q, \bar{q}, g$, the type of the initial state parton. For example, $\widehat{F}_2^i(z, Q^2)$ can be projected out by

$$\widehat{F}_2^i(z, Q^2) = -\frac{1}{4\pi} \left(g^{\mu\nu} + 12 \frac{z^2}{q^2} \widehat{p}^\mu \widehat{p}^\nu \right) \widehat{W}_{\mu\nu}^i(z, Q^2) , \quad (2.6.5)$$

where \widehat{p}^μ is the momentum of the incoming parton of type i and the factor $1/(4\pi)$ is needed to get the right normalization. $\widehat{W}_{\mu\nu}^i(z, Q^2)$ contains the contribution of the parton i subprocesses, averaged over the initial state quantum numbers, summed over the final state quantum numbers and integrated over the outgoing momenta. Because we will regularize the divergences in the integrals in n dimensions, the phase space integration has to be done in n dimensions ($n = 4 + \varepsilon$) as follows.

$$\begin{aligned} \widehat{F}_2^i(z, Q^2, \varepsilon) = & -\frac{1}{4\pi} \frac{1}{1 + \frac{1}{2}\varepsilon} \int dPS^{(3)} \left(g^{\mu\nu} + 12 \frac{z^2}{q^2} (1 + \frac{1}{3}\varepsilon) \widehat{p}^\mu \widehat{p}^\nu \right) \langle M_\mu^i M_\nu^i \rangle_{\mathbf{a}\mathbf{v}} , \end{aligned} \quad (2.6.6)$$

where M_μ^i denotes the amplitude of the parton subprocess, which is obtained by summing the results of all second order Feynman diagrams where a parton of type i

is in the initial state. Further

$$\int dPS^{(3)} = \frac{1}{(2\pi)^{2n-3}} \int d^n \hat{p}_2 \int d^n \hat{p}_3 \int d^n \hat{p}_4 \delta^+(\hat{p}_2^2) \delta^+(\hat{p}_3^2) \delta^+(\hat{p}_4^2) \delta^n(\hat{p}_1 + q - \hat{p}_2 - \hat{p}_3 - \hat{p}_4) . \quad (2.6.7)$$

The partons are taken to be massless.

The 5 momenta can be parametrized in some convenient C.M. frame and expressed in convenient variables x, y, z, θ, χ and ϕ , which are not linearly independent (see appendix A). After applying the projection operator $g^{\mu\nu} + 12z^2/q^2 \hat{p}^\mu \hat{p}^\nu$ on $M_{ij}^{\mu\nu}$ and working out the traces (which we did by using the algebraic manipulation program FORM [25]), the resulting matrix element can be expressed in terms of $P_{ij} = (\hat{p}_i - \hat{p}_j)^2$. It is important to reduce and partial-fraction the matrix element in such a way that no term contains more than two types of P_{ij} that depend on the angular variables θ, χ and ϕ . For this one can use identities following from the symmetry in the outgoing momenta and momentum- and energy conservation.

Now we will outline how one in general can compute the integrals. The majority of the integrals are very similar to each other and can be solved by taking the same steps.

1. The angular integration.

After partial fractioning and reduction every term in the matrix element contains 0, 1 or 2 types of factors out of the 'angular' set

$$\left\{ (1 - \cos \theta) , (1 + \cos \theta) , (1 + \cos \chi \cos \theta + \sin \chi \cos \phi \sin \theta) , \right. \\ \left. (1 - \cos \chi \cos \theta - \sin \chi \cos \phi \sin \theta) \right\} . \quad (2.6.8)$$

The integration over θ and ϕ is always done by expressing the result in a hypergeometric function of the form: $F(a, b, 1 + \frac{1}{2}\epsilon, c(x, y, z))$ [20, 21]. (Note that the remaining candidate variables to integrate over are x, y and z ; the final result will be a function of x .) In the case a and b are both unequal to 0 or to $k\epsilon$, the hypergeometric function is reduced using Kummer relations [20] until a or b is 0 or $k\epsilon$. After this it is possible to expand the hypergeometric function in polylogarithms, as a power series in ϵ . Polylogarithms are integrals that cannot be evaluated analytically. In a second order calculation we need to expand up to di- and trilogarithms ($Li_2(z)$, $Li_3(z)$ and $S_{1,2}(z)$) for which many identities have been derived [21]. If we would want to do a third order calculation, quadrilogarithms would be needed, the mathematics of which is less developed.

In some cases it is not allowed to expand F , because the remaining z -integration (or even both z - and y -integration) has to be done exactly.

2. The z -integration.

After the angular integration one is left with integrals of the form

$$\int_0^1 dy \int_0^1 dz \, k(x, y, z, \epsilon) ,$$

$$\text{where } k(x, y, z, \epsilon) = f(x, y, z, \epsilon) g(x, y, z) h(x, y, z, \epsilon) , \quad (2.6.9)$$

with $f(x, y, z, \epsilon)$ coming from the Jacobian in $\int dPS$, $g(x, y, z)$ from the angular independent \mathcal{M}_i 's left in the expression and $h(x, y, z, \epsilon)$ from the result of the angular integration. With these three ingredients $k(x, y, z, \epsilon)$ can become a very complicated function, with poles in the integration boundaries. These poles will be expressed in inverse powers of ϵ . (Maximum depth ϵ^{-3} , because the maximum number of outgoing momenta is 3 in a second order calculation.) First $k(x, y, z, \epsilon)$ is reduced to simpler functions by partial fractioning. After that large negative powers of z and $1 - z$ are increased by partial integration. Say we are left with something like

$$\int_0^1 dz \, z^{\epsilon-1} f(z) = \int_0^\delta dz \, z^{\epsilon-1} f(z) + \int_\delta^1 dz \, z^{\epsilon-1} f(z) , \quad (2.6.10)$$

with δ a small constant. In the second term we can safely expand z^ϵ in ϵ and the first term we can approximate as

$$\left[\frac{1}{\epsilon} z^\epsilon f(z) \right]_0^\delta \approx \left(\frac{1}{\epsilon} + \ell n \, \delta + \frac{1}{2} \epsilon \ell n^2 \delta \right) f(0) . \quad (2.6.11)$$

Usually derivatives of $f(z)$ yield ϵ in the numerator killing the ϵ in the denominator. Subsequently the expanded second term is evaluated by further partial integration in order to express it in some standard integrals. In the end $\ell n \, \delta$ terms should of course drop out.

This is the method of integration by expansion and it is rather laborious, though straightforward. Less laborious, but also less straightforward, are the cases in which we do not expand the hypergeometric function in $h(x, y, z, \epsilon)$, but instead perform an exact z -integration using identities in [20]. The result of the z -integration again contains polylogarithms, and Riemann zeta-functions.

3. The y -integration.

Basically one can perform the same operations as for the z -integration. Expansion is almost always possible. The final result, a function of the scaling variable x and of

ϵ^{-k} , with $k = 0, 1, 2, 3$, can generally be expressed in polynomials, logarithms, dilogarithms and trilogarithms. After removal of the pole terms by summing all integrals in the matrix element and applying mass factorization and coupling constant renormalization, the remaining part can be evaluated numerically. We also have analytical programs to calculate moments of coefficient functions (for which integration over x is needed).

Most integrals (about 200 each for DIS and DY) can be handled by our FORM program which performs the previously mentioned steps and fills in the standard integrals. The standard integrals of DIS form a subset of those needed for DY. It would be extremely time consuming to calculate matrix elements by hand. However, we did part of the integrals by hand as a check, or because they had a massive propagator in the denominator which makes them hard to program. A non-trivial check is provided by calculating a phase space integral in different kinematical frames or by interchanging an outgoing gluon line with an outgoing quark line, which should not influence the result.

Integrals from the process $2 \rightarrow 2$ (plus one loop) arise after tensor reduction of the matrix element, which we performed according to the Passarino-Veltman method [22]. The tensor reduction as well as the solving of the resulting scalar integrals can easily be programmed. We used the algebraic manipulation programs REDUCE [23], SCHOONSCHIP [24] and FORM [25].

In this chapter we discussed some important concepts like the parton model, the QCD perturbation series, renormalization, mass factorization and the specialized techniques of n -dimensional phase space integrations. The understanding of these concepts is a necessary condition for being able to do higher order QCD calculations. The next chapters will all deal with the calculation of second order QCD contributions. A detailed description of first order QCD calculations in DIS and DY can be found in [26].

Appendix

2A The kinematics of the DIS process

In this appendix we give the set up for the calculation of 2- and 3-particle phase space integrals in DIS. For the kinematics of DY, which is very similar because DY is just

a crossing of DIS, we refer to appendix D of [26].

The 2-particle phase space integrals

For the DIS process

$$V(q) + q(p_1) \rightarrow q(p_2) + g(p_3) \quad (2A.1)$$

the 2-particle phase space is given by

$$\int dPS^{(2)} = \frac{1}{(2\pi)^{n-2}} \int d^n p_2 \int d^n p_3 \delta^+(p_2^2) \delta^+(p_3^2) \delta^n(p_1 + q - p_2 - p_3) \quad (2A.2)$$

(From now on we no longer use hatted symbols to denote the parton momenta.) We parametrize the n -dimensional momenta in the C.M. frame of the incoming particles as follows ($s = (p_1 + q)^2$).

$$p_1 = \frac{s - q^2}{2\sqrt{s}}(1, 0, \dots, 0, 0, 1) \quad (2A.3)$$

$$q = \left(\frac{s + q^2}{2\sqrt{s}}, 0, \dots, 0, 0, -\frac{s - q^2}{2\sqrt{s}} \right) \quad (2A.4)$$

$$p_3 = \frac{1}{2}\sqrt{s}(1, 0, \dots, 0, 0, \cos \theta) \quad (2A.5)$$

This gives

$$\int dPS^{(2)} = 2^{4-2n} \frac{\pi^{1-\frac{1}{2}n}}{\Gamma(\frac{1}{2}n - 1)} s^{\frac{1}{2}n-2} \int_0^\pi d\theta (\sin \theta)^{n-3} \quad (2A.6)$$

where Γ denotes the well-known gamma-function. It turns out to be convenient to use the variables

$$x = \frac{-q^2}{2p_1 \cdot q} = \frac{-q^2}{s - q^2} \quad \text{and} \quad y = \frac{1}{2}(1 + \cos \theta) \quad (2A.7)$$

in terms of which the DI 2-particle phase space integral becomes

$$\int dPS^{(2)} = \frac{2\pi}{(4\pi)^{\frac{1}{2}n}} \frac{(-q^2)^{\frac{1}{2}n-2}}{\Gamma(\frac{1}{2}n - 1)} \left(\frac{1-x}{x} \right)^{\frac{1}{2}n-2} \int_0^1 dy \{y(1-y)\}^{\frac{1}{2}n-2} \quad (2A.8)$$

The 3-particle phase space integrals

We will present the parametrization of the 3-particle phase space integrals in the C.M. frame of the two outgoing gluons. In this frame the integrals are easier to calculate than in the C.M. frame of the incoming particles. For the DIS process

$$V(q) + q(p_1) \rightarrow q(p_2) + g(p_3) + g(p_4) , \quad (2A.9)$$

the 3-particle phase space is defined as

$$\int dPS^{(3)} = \frac{1}{(2\pi)^{2n-3}} \int d^n p_2 \int d^n p_3 \int d^n p_4 \delta^+(p_2^2) \delta^+(p_3^2) \delta^+(p_4^2) \delta^n(p_1 + q - p_2 - p_3 - p_4) . \quad (2A.10)$$

The n -dimensional momenta are parametrized as follows.

$$p_3 = \frac{1}{2} \sqrt{s_{12}} (1, 0, \dots, \sin \phi \sin \theta, \cos \phi \sin \theta, \cos \theta) , \quad (2A.11)$$

$$p_4 = \frac{1}{2} \sqrt{s_{12}} (1, 0, \dots, -\sin \phi \sin \theta, -\cos \phi \sin \theta, -\cos \theta) , \quad (2A.12)$$

$$p_1 = \frac{(s - t - q^2)}{2\sqrt{s_{12}}} (1, 0, \dots, 0, 0, 1) , \quad (2A.13)$$

$$p_2 = \frac{(s - s_{12})}{2\sqrt{s_{12}}} (1, 0, \dots, 0, \sin \psi, \cos \psi) , \quad (2A.14)$$

$$\cos \psi = 1 - \frac{2s_{12}t}{(s - t - q^2)(s - s_{12})} , \quad (2A.15)$$

with $t = 2p_1 \cdot p_2$, $u = 2p_2 \cdot q$, $s = (p_1 + q)^2$ and $s_{12} = s - t - u$. Applying this parametrization to (2A.10), we obtain

$$\int dPS^{(3)} = \frac{1}{(4\pi)^n} \frac{(s - q^2)^{3-n}}{\Gamma(n-3)} \int_0^\pi d\theta \int_0^\pi d\phi (\sin \theta)^{n-3} (\sin \phi)^{n-4} \int_0^{s-q^2} dt \int_{tq^2/s-q^2}^{s-t} du (s_{12})^{\frac{1}{2}n-2} t^{\frac{1}{2}n-2} \{(s - q^2)u - q^2t\}^{\frac{1}{2}n-2} . \quad (2A.16)$$

This result can be rewritten as

$$\int dPS^{(3)} = \frac{1}{(4\pi)^n} \frac{(-q^2)^{n-3}}{\Gamma(n-3)} \left(\frac{1-x}{x}\right)^{n-3} \int_0^\pi d\theta \int_0^\pi d\phi (\sin \theta)^{n-3} (\sin \phi)^{n-4} \int_0^1 dy \int_0^1 dz y^{\frac{1}{2}n-2} (1-y)^{n-3} \{z(1-z)\}^{\frac{1}{2}n-2} , \quad (2A.17)$$

where the variables x , y and z are defined by

$$x = \frac{-q^2}{2p_1 \cdot q} = \frac{-q^2}{s - q^2} , \quad (2A.18)$$

$$u = \{1 - x - y - (1-x)(1-y)z\}(s - q^2) , \quad (2A.19)$$

$$t = y(s - q^2) . \quad (2A.20)$$

References

- [1] J. Blümlein et al., Proceedings of the HERA Workshop, Aachen, October 12-14, 1987, ed. R.P. Peccei, vol. 1, p. 67.
- [2] R. Hanberg, W.L. van Neerven and T. Matsuura, Nucl. Phys. **B359** (1991) 343.
- [3] R.P. Feynman, Phys. Rev. Lett. **23** (1969), 1415; J.D. Bjorken and E. Paschos, Phys. Rev. **185** (1969) 1975; J. Kuti and V. Weiskopf, Phys. Rev. **D14** (1971) 3412.
- [4] R. Hanberg, Ph.D. thesis, University of Leiden, The Netherlands (1991).
- [5] S.D. Drell and T.M. Yan, Phys. Rev. Lett. **25** (1970), 316; Ann. Phys. **66** (1971), 578.
- [6] J.D. Bjorken, Phys. Rev. **179** (1969), 1547.
- [7] W.K.H. Panofsky, Proc. 14th Int. Conf. on High Energy Physics, Vienna, 1968, CERN, Scientific Information Service, p. 23; D.H. Coward et al., Phys. Rev. Lett. **20** (1968).
- [8] J.H. Christenson et al., Phys. Rev. Lett. **25** (1970), 1523; L.M. Ledermann and B.G. Pope, Phys. Lett. **B66** (1977) 486.
- [9] L. Kluberg et al., Phys. Rev. Lett. **27** (1976) 1451; M. Binkley et al., Phys. Rev. Lett. **37** (1976) 571, 578; D.C. Hom et al., Phys. Rev. Lett. **36** (1976) 1236, *ibid.* **37** (1976) 1374.
- [10] R.E. Taylor, Proceedings of the International Symposium on Lepton and Photon Interactions at High Energies, Stanford 1975; Y. Watanabe et al., Phys. Rev. Lett. **35** (1975), 898; C. Chang et al., Phys. Rev. Lett. **35** (1975), 901.
- [11] G. 't Hooft and M. Veltman, Nucl. Phys. **B44** (1972) 189.
- [12] F. Bloch and A. Nordsieck, Phys. Rev. **52** (1937), 54.
- [13] T. Kinoshita, J. Math. Phys. **3** (1962), 650; T.D. Lee and M. Nauenberg, Phys. Rev. **133** (1964), B1549.

- [14] N. Nakanishi, Prog. Theor. Phys. **19** (1958), 159
- [15] H.D. Politzer, Nucl. Phys. **B129** (1977), 301; D. Amati, R. Petronzio and G. Veneziano, Nucl. Phys. **B140** (1978), 54; S.B. Libby and G. Sterman, Phys. Rev. **D18** (1978), 3252, 4737; A.H. Mueller, Phys. Rev. **D18** (1978), 3705; J.C. Collins and G. Sterman, Nucl. Phys. **B185** (1981), 172; J.C. Collins, D.E. Soper and G. Sterman, Nucl. Phys. **B261** (1985), 104; G.T. Bodwin, Phys. Rev. **D31** (1985), 2616
- [16] G. Altarelli and G. Parisi, Nucl. Phys. **B126** (1977), 298; V.N. Gribov and L.N. Lipatov, Sov. J. Nucl. Phys. **15** (1972) 438, 675.
- [17] K.G. Wilson, Cornell Report (1964), unpublished; Phys. Rev. **179** (1969), 1499
- [18] W.A. Bardeen, A.J. Buras, D.W. Duke and T. Muta, Phys. Rev. **D18** (1978) 3998
- [19] G. Altarelli, R.K. Ellis and G. Martinelli, Nucl. Phys. **B143** (1978) 521; (Erratum **B146** (1978) 544)
- [20] Higher transcendental functions, vol. 1, Bateman manuscript, ed. A. Erdély (McGraw-Hill, New York, 1953); I.S. Ghradshteyn and I.M. Ryzhik, Table of integrals, series and products (Academic Press, New York, 1980).
- [21] L. Lewin, Polylogarithms and Associated Functions, North Holland 1983; R. Barbieri, J.A. Mignaco and E. Remiddi, Nuovo Cim. **11A** (1972) 824; A. Devoto and D.W. Duke, Riv. Nuovo Cim. **7**, No. 6 (1984) 1.
- [22] G. Passarino and M. Veltman, Nucl. Phys. **B160** (1979) 151; W.J.P. Beenakker, Ph.D. thesis, University of Leiden, The Netherlands (1989).
- [23] A.C. Hearn, Reduce Users's Manual, The Rand Corporation, Santa Monica, CA, 1985.
- [24] H. Strubbe, Comput. Phys. Comm. **8** (1974) 1.
- [25] J.A.M. Vermaseren, Symbolic manipulation with FORM, published by CAN, Kruislaan 413, 1098 SJ Amsterdam (1991), ISBN 90-74116-01-9.
- [26] T. Matsuura, Ph.D. thesis, University of Leiden, The Netherlands (1989).

Chapter 3

The structure functions F_2 and F_L

3.1 Introduction

Deep inelastic lepton-hadron scattering experiments, started by the SLAC-MIT group [1] at the end of the sixties, opened a new era in the study of strong interaction physics. These experiments revealed that hadrons are composed of pointlike constituents, called partons, which were later on identified as quarks and gluons. In the framework of the parton model [2] the early data could be interpreted by assuming that the scattering process between the lepton and the partons is incoherent. In this way one could explain the apparent scaling behaviour of the hadron structure functions appearing in the deep inelastic cross section. These structure functions also appear in the various sum rules, derived in the context of the parton model, of which the validity was subsequently confirmed by the data.

Considerable progress was made after the advent of Quantum Chromo Dynamics (QCD) [3], a non-Abelian (here $SU(3)$) gauge field theory, which describes the strong interaction between the quarks and gluons inside the hadron. In particular it is supposed to give an explanation for the phenomenon that the quarks and gluons are confined [4] in all existing hadrons. Another important feature of QCD is asymptotic freedom [5] which implies that the renormalization group improved (running) coupling constant $\alpha_s(R^2)$ goes to zero when the renormalization scale R^2 tends to infinity. This allows us to make a perturbative expansion in α_s of many physical quantities showing up in so called hard processes. Here hard means that the kinematical invariants involved get asymptotic whereas their mutual ratios stay fixed. Deep inelastic lepton-hadron scattering, which will be the subject of our study in this chapter, is an example of such a process and it provides us with a beautiful testing ground of the predictions of perturbative QCD. This became immediately apparent after the discovery of the

scale dependence of the hadron structure functions, observed by the second generation of experiments [6], which can be considered as one of the most important successes of the theory. With the advent of HERA (DESY, Hamburg) and the planned electron-proton facility at LEP*LHC (CERN, Geneva) a new generation of experiments will start to test QCD in kinematical regions which were inaccessible so far. Since in these experiments the hadron is represented by the proton we will concentrate on the effect of higher order QCD corrections to the proton structure functions, in particular in the above-mentioned regions.

Deep inelastic lepton-proton scattering is given by the reaction (see fig. 2.1)

$$l_1(k_1) + H(p) \rightarrow l_2(k_2) + "X" , \quad (3.1.1)$$

where l_1 , l_2 denote the in- and outgoing leptons respectively and H stands for the proton. The symbol " X " denotes any inclusive hadronic final state allowed by quantum number conservation laws. In lowest order of the electro-weak coupling constant the reaction proceeds via the exchange of one of the vector bosons of the standard model, i.e. $V = \gamma, Z, W^\pm$ (see fig. 2.1). Since the above process is inclusive with respect to the outgoing hadrons denoted by " X ", only the outgoing lepton is detected. Here we will limit ourselves to $V = \gamma$ and $l_1 = l_2 = e$. In the case of unpolarized deep inelastic scattering the electron-proton cross section can be written as (see also (2.1.8))

$$\frac{d^2\sigma}{dx dy} = \frac{2\pi\alpha^2}{Q^4} S \left[\{1 + (1-y)^2\} F_2(x, Q^2) - y^2 F_L(x, Q^2) \right] . \quad (3.1.2)$$

Here \sqrt{S} denotes the C.M. energy of the electron-proton system. The variables x and y are defined by

$$x = \frac{Q^2}{2p \cdot q} \quad (0 < x < 1) , \quad y = \frac{p \cdot q}{p \cdot k_1} \quad (0 < y < 1) \quad (3.1.3)$$

and q denotes the momentum of the virtual vector boson V (in this case the photon) which is given by

$$q = k_1 - k_2 , \quad Q^2 = -q^2 > 0 . \quad (3.1.4)$$

The deep inelastic proton structure functions appearing in (3.1.2) are represented by $F_i(x, Q^2)$ ($i = 2, L$). There exists a third structure function in the literature, i.e. $F_1(x, Q^2)$ which however depends on the two previous ones. It is given by

$$F_1(x, Q^2) = \frac{1}{2x} (F_2(x, Q^2) - F_L(x, Q^2)) . \quad (3.1.5)$$

In the QCD improved parton model the deep inelastic structure functions can be expressed for an even number of flavours in the following way:

$$F_i(x, Q^2) = x \int_x^1 \frac{dz}{z} \left[\frac{5}{18} \left\{ \Sigma\left(\frac{x}{z}, M^2\right) C_{i,q}^S(z, Q^2/M^2) + G\left(\frac{x}{z}, M^2\right) C_{i,g}(z, Q^2/M^2) \right\} + \frac{1}{6} \Delta\left(\frac{x}{z}, M^2\right) C_{i,q}^{NS}(z, Q^2/M^2) \right] ,$$

$$i = 2, L . \quad (3.1.6)$$

(See also (2.4.7).) Here $G(x, M^2)$ denotes the gluon density and $\Sigma(x, M^2)$, $\Delta(x, M^2)$ stand for the singlet (S) and non-singlet (NS) combinations of the quark densities respectively. The same nomenclature also applies to the deep inelastic scattering (DIS) coefficient functions $C_{i,g}(x, Q^2/M^2)$. All quantities defined above depend both on the mass factorization scale M and on the renormalization scale R . However in (3.1.6) these scales are set to be equal. In the case of four flavours the S and NS parton densities become equal to

$$\Sigma(x, M^2) = u(x, M^2) + d(x, M^2) + c(x, M^2) + s(x, M^2) + \bar{u}(x, M^2) + \bar{d}(x, M^2) + \bar{c}(x, M^2) + \bar{s}(x, M^2) , \quad (3.1.7)$$

$$\Delta(x, M^2) = u(x, M^2) - d(x, M^2) + c(x, M^2) - s(x, M^2) + \bar{u}(x, M^2) - \bar{d}(x, M^2) + \bar{c}(x, M^2) - \bar{s}(x, M^2) , \quad (3.1.8)$$

where u , d , s and c stand for up, down, strange and charmed quarks respectively. The same notation holds for the anti-quarks. The scale dependence of $F_i(x, Q^2)$ in (3.1.6) was observed for the first time by the SLAC-MIT group [6] and confirmed by many other experiments (for a review see [7]). Until now all these experiments were carried out in the kinematical range $0.01 < x < 0.95$, $Q^2 < 300 \text{ GeV}^2$. At HERA [8] this range will become $x \geq 10^{-4}$ and $Q^2 \leq 2 \cdot 10^4 \text{ GeV}^2$, which probably can be extended to $x \geq 10^{-5}$ and $Q^2 \leq 10^5 \text{ GeV}^2$ when the ep facility at LEP*LHC [9] is put into operation. The small- x region is of utmost interest for the current (HERA) and future (LEP*LHC) experiments. Besides the study of perturbative and non-perturbative effects [11], the extraction of the parton densities from the deep inelastic data is one of their most important goals. In particular we want to mention the gluon density which is expected to increase very steeply when x gets very small. An accurate knowledge of these densities at very small- x values is necessary in order

to make precise predictions for interesting processes like Higgs- and top production at the future pp colliders LHC and SSC.

As far as theory is concerned much progress has been made in the calculation of higher order QCD corrections to the anomalous dimensions of composite operators which determine the scale evolution of the parton densities. The inverse Mellin transforms of the coefficients in the perturbation series of the anomalous dimension represent the Altarelli-Parisi (AP) splitting functions which are known up to second order in α_s [13]–[17]. Also known is the order α_s contribution to the DIS coefficient functions appearing in (3.1.6) [18]–[20]. With the advent of HERA and the planned ep facility at LEP+LHC we are entering a new era in which the small- x region will be explored. Due to improved detection techniques we expect better statistics so that the higher order QCD corrections beyond the next-to-leading order (NLO) will become noticeable and therefore have to be calculated. This requires the computation of the three loop anomalous dimension (or the $\mathcal{O}(\alpha_s^3)$ AP splitting functions) and the order α_s^2 contributions to the DIS coefficient function. The latter will be calculated in this chapter. We will give many details of the calculation thereby stressing the procedure of mass factorization which is non-trivial in computations of QCD corrections beyond the next-to-leading order in α_s . Further we will give examples of how the existing order α_s predictions are modified by including the $\mathcal{O}(\alpha_s^2)$ corrections, where we pay attention to recent as well as current experiments.

This chapter will be organized as follows. In the next section we present some details of the calculation of the second order contribution to the DIS coefficient function $C_i(x, Q^2/M^2)$ for $i = 2, L$. In section 3.3 we discuss the effect of this $\mathcal{O}(\alpha_s^2)$ corrected quantity on the proton structure functions $F_i(x, Q^2)$ and its implication for the extraction of the parton densities. The most complicated three particle phase space integrals which occur in the calculation are presented in appendix 3A. The long expressions for the coefficient functions, not shown in section 3.2, are explicitly given for arbitrary R and M in appendix 3B.

3.2 The calculation of the coefficient functions

In this section we will give an outline of the calculation of the $\mathcal{O}(\alpha_s^2)$ corrections to the DIS coefficients in (3.1.6) including their dependence on M and R . Following the procedure given in [19, 20, 23] the hadronic structure functions $F_i(x, Q^2)$ can be

denoted in the following way

$$F_i(x, Q^2) = x \sum_k \int_x^1 \frac{dz}{z} \hat{f}_k\left(\frac{x}{z}\right) \hat{F}_{i,k}(z, Q^2, \varepsilon) \quad k = q, \bar{q}, g ; \quad i = 2, L , \quad (3.2.1)$$

where \hat{f}_k and $\hat{F}_{i,k}$ denote the bare parton density and the parton structure function corresponding to the parton k respectively. The latter describes the QCD radiative corrections to the parton subprocess

$$k + V \rightarrow 'X' . \quad (3.2.2)$$

Since the object $\hat{F}_{i,k}$ is collinearly divergent, indicated by the parameter ε , we have to perform mass factorization in order to remove the pole terms of the type $1/\varepsilon$. To that purpose it is convenient to split the parton densities and the parton structure functions into a singlet (S), non-singlet (NS) and a gluonic part. Since we limit ourselves to the one photon exchange process in 2.1 only ($V = \gamma$), equation (3.2.1) gives

$$\begin{aligned} F_i(x, Q^2) = x \int_x^1 \frac{dz}{z} \left[\frac{5}{18} \left\{ \hat{\Sigma}\left(\frac{x}{z}\right) \hat{F}_{i,q}^S(z, Q^2, \varepsilon) + \hat{G}\left(\frac{x}{z}\right) \hat{F}_{i,g}\left(\frac{x}{z}, Q^2, \varepsilon\right) \right\} \right. \\ \left. + \frac{1}{6} \hat{\Delta}\left(\frac{x}{z}\right) \hat{F}_{i,q}^{NS}(z, Q^2, \varepsilon) \right] , \end{aligned} \quad (3.2.3)$$

for an even number of flavours, where we have put $\hat{F}_{i,q} = \hat{F}_{i,\bar{q}}$ (S and NS). The gluon density \hat{g} , the singlet quark density $\hat{\Sigma}$ and the non-singlet quark density $\hat{\Delta}$ are related to \hat{f}_k (3.2.1) in the following way

$$\begin{aligned} \hat{G}(z) &= \hat{f}_g(z) , \\ \hat{\Sigma}(z) &= \sum_q (\hat{f}_q(z) + \hat{f}_{\bar{q}}(z)) , \\ \hat{\Delta}(z) &= \sum_{q=\text{up}} (\hat{f}_q(z) + \hat{f}_{\bar{q}}(z)) - \sum_{q=\text{down}} (\hat{f}_q(z) + \hat{f}_{\bar{q}}(z)) , \end{aligned} \quad (3.2.4)$$

where 'up' denotes the up, charm and top quark, and 'down' denotes the down, strange and bottom quark. The parton subprocesses contributing to the parton structure functions up to order α_s^2 are listed in table 2.1. The corresponding Feynman graphs for the γ^*q subprocesses can be found in figs. 3.1–3.7. The diagrams for the γ^*g subprocesses can be obtained from figs. 3.3, 3.5, 3.6 by interchanging a quark in the initial state with a gluon in the final state. In calculating the loop- and phase space integrals one encounters three types of divergences: ultraviolet (UV), infrared (IR) and collinear singularities. They are regularized using the technique of n -dimensional regularization with $\varepsilon = n - 4$ where ε has already been mentioned

below (3.2.2). Notice that there are no γ_5 matrices in the matrix elements since we only consider photon-quark interactions. The parton structure functions can be obtained from the parton structure tensor which is defined by

$$\widehat{W}_{\mu\nu}(\hat{p}, q) = \frac{1}{2} \frac{1}{4\pi} \sum_{k=1}^{\infty} \int dPS^{(k)} M_{\mu}(k) M_{\nu}(k)^* , \quad (3.2.5)$$

with (see appendix B of [23])

$$\int dPS^{(k)} = \left\{ \prod_{j=1}^k \int \frac{d^n \hat{p}_j}{(2\pi)^{n-1}} \delta^{(+)}(\hat{p}_j^2) \right\} (2\pi)^n \delta^{(n)}(\hat{p} + q - \prod_{i=1}^k \hat{p}_i) , \quad (3.2.6)$$

where $M_{\mu}(k)$ denotes the amplitude for the photon-parton reaction

$$\gamma^* + \hat{p} \rightarrow \hat{p}_1 + \hat{p}_2 + \dots \hat{p}_k . \quad (3.2.7)$$

Further we have averaged over all spins in the initial state. The factor $1/2$ in (3.2.5) stands for the average of the quark spin. In the case when a gluon is present in the initial state, the $1/2$ has to be replaced by $1/(n-2)$. For $V = \gamma$ (3.2.2) the parton structure tensor can be written as follows

$$\begin{aligned} \widehat{W}_{\mu\nu}(\hat{p}, q) = & \frac{1}{2} \left(g_{\mu\nu} - \frac{q_{\mu} q_{\nu}}{q^2} \right) \widehat{F}_L(z, Q^2) + \left\{ \hat{p}_{\mu} \hat{p}_{\nu} - \frac{\hat{p} \cdot q}{q^2} (\hat{p}_{\mu} q_{\nu} + \hat{p}_{\nu} q_{\mu}) \right. \\ & \left. + g_{\mu\nu} \frac{(\hat{p} \cdot q)^2}{q^2} \right\} \frac{\widehat{F}_2(z, Q^2)}{\hat{p} \cdot q} , \end{aligned} \quad (3.2.8)$$

with $z = Q^2/2\hat{p} \cdot q$ ($q^2 = -Q^2$) and $\hat{p}^2 = 0$. From (3.2.8) it follows that

$$\widehat{F}_L(z, Q^2) = - \frac{2q^2}{(\hat{p} \cdot q)^2} \widehat{p}^{\mu} \widehat{p}^{\nu} \widehat{W}_{\mu\nu} , \quad (3.2.9)$$

$$\widehat{F}_2(z, Q^2) = - \frac{2}{n-2} \left\{ \widehat{W}_{\mu}^{\mu} + (n-1) \frac{q^2}{(\hat{p} \cdot q)^2} \widehat{p}^{\mu} \widehat{p}^{\nu} \widehat{W}_{\mu\nu} \right\} . \quad (3.2.10)$$

In zeroth order in α_s we obtain the simple parton model results (fig. 3.1)

$$\widehat{F}_{L,q}^{(0)} = \widehat{F}_{L,g}^{(0)} = 0 , \quad \widehat{F}_{2,q}^{(0)} = \delta(1-z) , \quad \widehat{F}_{2,g}^{(0)} = 0 . \quad (3.2.11)$$

3.2.1 The first order results

The first order corrections, denoted by $\widehat{F}_{i,k}^{(1)}$, have also been calculated in the literature [18]–[20]. In the case of n -dimensional regularization the order α_s expressions, computed up to constant terms, can be found in [19, 20]. Since the mass factorization has to be carried out up to order α_s^2 , one also needs those terms in $\widehat{F}_{i,k}^{(1)}(z, Q^2, \epsilon)$ which are proportional to ϵ .

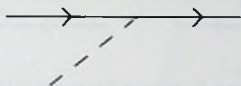


Fig. 3.1. The Born contribution to the subprocess $q(\bar{q}) + V \rightarrow q(\bar{q})$.

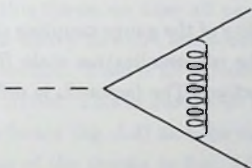


Fig. 3.2. The one loop correction to the subprocess $q(\bar{q}) + V \rightarrow q(\bar{q})$.

Therefore we have repeated the calculation of the graphs in figs. 3.2 and 3.3 and the results can be presented in the following form

$$\hat{F}_{L,q}^{(1)} = \frac{\alpha_s^u}{4\pi} S_\epsilon \left(\frac{Q^2}{\mu^2} \right)^{\epsilon/2} \left[\bar{c}_{L,q}^{(1)} + \epsilon a_{L,q}^{(1)} \right], \quad (3.2.12)$$

$$\hat{F}_{2,q}^{(1)} = \frac{\alpha_s^u}{4\pi} S_\epsilon \left(\frac{Q^2}{\mu^2} \right)^{\epsilon/2} \left[P_{qq}^{(0)} \frac{1}{\epsilon} + \bar{c}_{2,q}^{(1)} + \epsilon a_{2,q}^{(1)} \right], \quad (3.2.13)$$

$$\hat{F}_{L,g}^{(1)} = n_f \frac{\alpha_s^u}{4\pi} S_\epsilon \left(\frac{Q^2}{\mu^2} \right)^{\epsilon/2} \left[\bar{c}_{L,g}^{(1)} + \epsilon a_{L,g}^{(1)} \right], \quad (3.2.14)$$

$$\hat{F}_{2,g}^{(1)} = n_f \frac{\alpha_s^u}{4\pi} S_\epsilon \left(\frac{Q^2}{\mu^2} \right)^{\epsilon/2} \left[P_{qg}^{(0)} \frac{1}{\epsilon} + \bar{c}_{2,g}^{(1)} + \epsilon a_{2,g}^{(1)} \right], \quad (3.2.15)$$

where μ^2 and S_ϵ are artefacts of n -dimensional regularization. The mass parameter μ

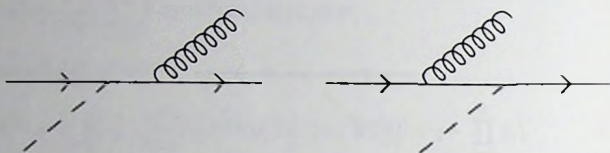


Fig. 3.3. Diagrams contributing to the subprocess $q(\bar{q}) + V \rightarrow q(\bar{q}) + g$. The graphs corresponding to the subprocess $g + V \rightarrow q + \bar{q}$ can be obtained from those presented in this figure by interchanging the incoming (anti)quark line with the outgoing gluon line.

originates from the dimensionality of the gauge coupling constant in n dimensions and should not be confused with the renormalization scale R and the mass factorization scale M defined in the introduction. The factor S_ϵ is defined by

$$S_\epsilon = \exp\left\{\frac{\epsilon}{2}(\gamma_E - \ell n 4\pi)\right\} . \quad (3.2.16)$$

Further α_s^0 denotes the bare strong coupling constant and $P_{ij}^{(0)}$ ($i, j = q, \bar{q}, g$) stands for the lowest order contribution to the Altarelli-Parisi splitting functions [12]. Using our conventions they can also be found in eqs. (2.13)–(2.16) of [33]. The coefficients $\bar{c}_{k,i}^{(1)}$ which already exist in the literature [19, 20], are presented in eqs. (3B.1), (3B.2), (3B.9), (3B.12). The coefficients $a_{k,i}^{(1)}$ are equal to

$$a_{L,q}^{(1)} = C_F [2z(\ell n(1-z) - \ell n z) - 2z] , \quad (3.2.17)$$

$$\begin{aligned} a_{2,q}^{(1)} = C_F & \left[\left(\frac{\ell n^2(1-z)}{1-z} \right)_+ - \frac{3}{2} \left(\frac{\ell n(1-z)}{1-z} \right)_+ + \left(\frac{7}{2} - 3\zeta(2) \right) \left(\frac{1}{1-z} \right)_+ \right. \\ & - \frac{1}{2}(1+z)\ell n^2(1-z) - \frac{1+z^2}{1-z}\ell n z \ell n(1-z) + \frac{1}{2} \frac{1+z^2}{1-z} \ell n^2 z \\ & + \frac{3}{2} \frac{1}{1-z} \ell n z + (3+2z)(\ell n(1-z) - \ell n z) - 6 - 4z \\ & \left. + \frac{3}{2}(1+z)\zeta(2) + \delta(1-z) \left(9 + \frac{3}{4}\zeta(2) \right) \right] , \end{aligned} \quad (3.2.18)$$

$$a_{L,g}^{(1)} = T_f [8z(1-z)(\ell n(1-z) - \ell n z - 3)] , \quad (3.2.19)$$

$$\begin{aligned}
a_{2,6}^{(1)} = & T_f \left[(1 - 2z + 2z^2) (\ell n^2(1 - z) - 2\ell n z \ell n(1 - z) + \ell n^2 z) \right. \\
& - 2(1 - 8z + 8z^2) (\ell n(1 - z) - \ell n z) - 3(1 - 2z + 2z^2) \zeta(2) \\
& \left. + 6 - 44z + 44z^2 \right] , \tag{3.2.20}
\end{aligned}$$

where the $SU(N)$ colour factors C_F and T_f are given by $C_F = (N^2 - 1)/2N$, $T_f = 1/2$ respectively.

3.2.2 Diagrams contributing at second order

The order α_s^2 contributions to $\hat{F}_{i,k}$, denoted by $\hat{F}_{i,k}^{(2)}$, are obtained as follows. The calculation of the amplitude $M_\mu(k)M_\nu^*(k)$ in (3.2.5) was performed in n dimensions using the algebraic manipulation programs REDUCE [24], SCHOONSCHIP [25] and FORM [26]. After having computed the traces, we have to integrate the matrix elements over all internal loop- and final-state momenta which is the most difficult part of the calculation. In this thesis we take all partons to be massless. The case of massive quarks (e.g. when heavy flavours are produced in the final state) will be discussed at the end of this section. Even if all partons are massless the integrals are very numerous and far from trivial. This in particular holds for the two-loop integrals appearing in the quark form factor (fig. 3.4) and the three body phase space integrals showing up in the calculation of the graphs in figs. 3.6, 3.7. Some of them have pole terms starting in $1/\epsilon^4$ so that the numerator has to be expanded up to order ϵ^4 .

The two-loop virtual contribution to $\hat{F}_{2,q}^{(0)}$, represented by the graphs in fig. 3.4, is given by the quark form factor which can be found in (2.49) of [27] (see also appendix A of [28]). The result agrees with the one quoted in [29]. Notice that the last graph in fig. 3.4 does not contribute for $V = \gamma$ because of Furry's theorem. It only plays a role in the case $V = Z$ provided one sums over all flavours in a quark family in order to cancel the anomaly arising in this type of graph.

Next we have to compute the one-loop virtual correction to the radiative process in fig. 3.3. The corresponding graphs are shown in fig. 3.5. The amplitude of those two-to-two body subprocesses is denoted by $M(2)$ and contains all one-loop integrals. The resulting two body phase space integrals (3.2.6) constitute the easiest part of the calculation. Expression (3.2.5) reads

$$\int dPS(2) |M(2)|^2 = 2^{4-2n} \frac{\pi^{1-n/2}}{\Gamma(n/2-1)} s^{n/2-2} \int_0^\pi d\theta (\sin \theta)^{n-3} |M(2)|^2 , \tag{3.2.21}$$

where $s = (p + q)^2$ is the C.M. energy of the photon-parton system and θ is the angle between the incoming parton and one of the outgoing partons. The Feynman

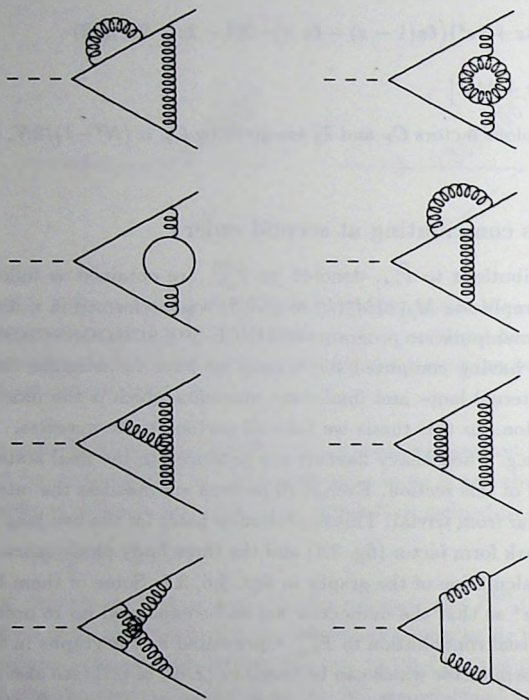


Fig. 3.4. The two loop corrections to the subprocess $q(\bar{q}) + V \rightarrow q(\bar{q})$. The ghost contribution to the gluon self energy is included but not shown in the figure.

integrals which contain loop momenta in the numerator can be reduced to scalar loop integrals using an n -dimensional extension of the reduction program in [30]. The expressions for the scalar loop integrals which are valid for all n can be found in appendix D of [28] (see also [31]). Following the procedure in [20, 23] we can split the phase space integrals emerging from (3.2.21) into a soft (singular at $s = 0$) and a hard (regular at $s = 0$) gluon part. The soft gluon integrals, which only show up in the γ^*q subprocess, have already been calculated in [28]. The hard gluon/quark

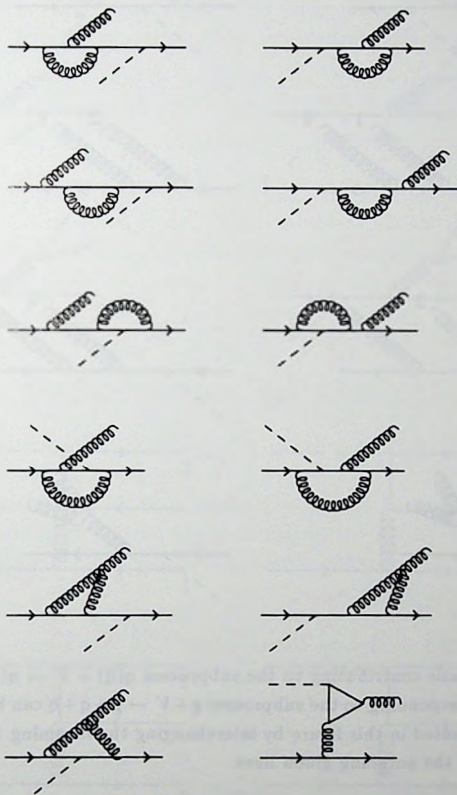


Fig. 3.5. The one loop corrections to the subprocess $q(\bar{q}) + V \rightarrow q(\bar{q}) + g$. The graphs corresponding to the subprocess $g + V \rightarrow q + \bar{q}$ can be obtained from those presented in this figure by interchanging the incoming (anti)quark line with the outgoing gluon line.

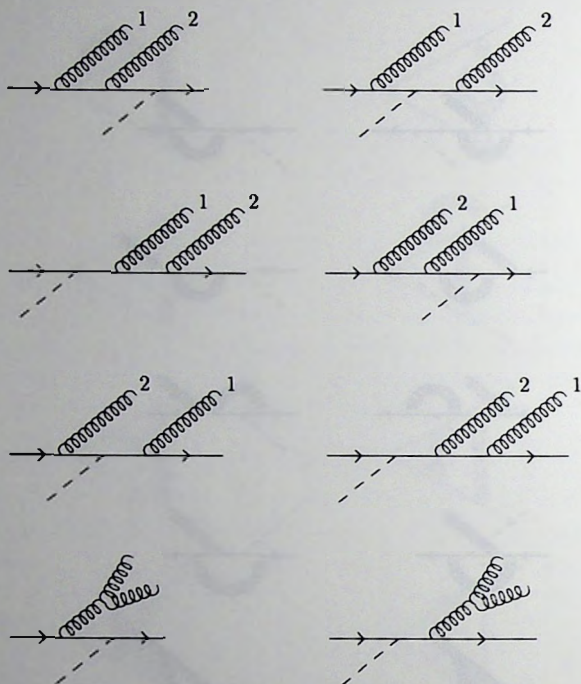


Fig. 3.6. Diagrams contributing to the subprocess $q(\bar{q}) + V \rightarrow q(\bar{q}) + g + g$. The graphs corresponding to the subprocess $g + V \rightarrow g + q + \bar{q}$ can be obtained from those presented in this figure by interchanging the incoming (anti)quark line with one of the outgoing gluon lines.

integrals which appear for γ^*q as well as for γ^*g are very numerous so that we cannot present them in this thesis. Finally the last graph in fig. 3.5 containing the triangle fermion loop does not contribute when $V = \gamma$ for the same reasons as mentioned for the last diagram in fig. 3.4. Only in the case that $V = Z$ and the quarks in the loop are massive it will give a contribution provided one sums over all members of a quark family in order to cancel the anomaly originating from the triangle fermion loop.

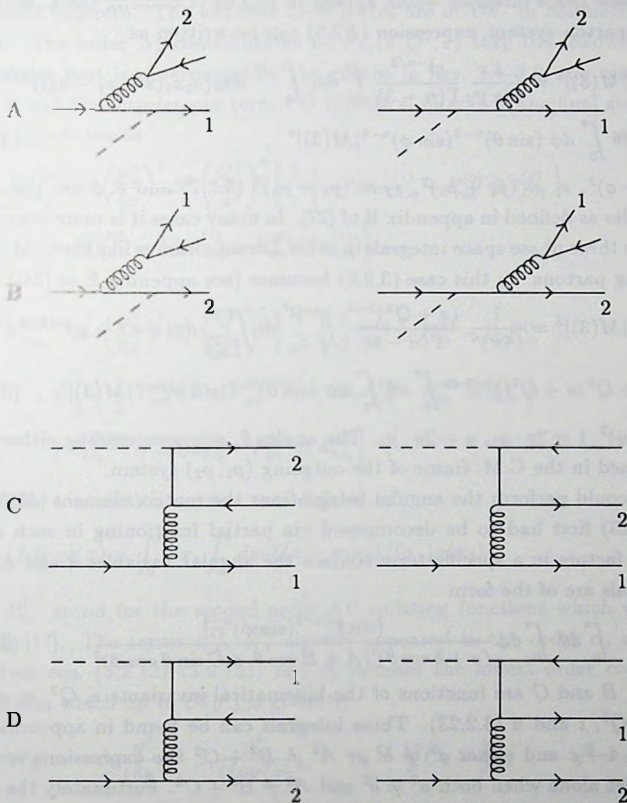


Fig. 3.7. Diagrams contributing to the subprocesses $q + V \rightarrow q(1) + q(2) + \bar{q}$ and $\bar{q} + V \rightarrow \bar{q}(1) + \bar{q}(2) + q$. If $q(1) \neq q(2)$ or $\bar{q}(1) \neq \bar{q}(2)$, only combinations A and C have to be considered. If $q(1) = q(2)$ or $\bar{q}(1) = \bar{q}(2)$, combinations B and D have to be added to A and C.

The most difficult and laborious part of the calculation can be attributed to the purely radiative two to three body subprocesses given by the diagrams in figs. 3.6, 3.7 of which the amplitude is denoted by $M(3)$. They involve the computation of the three body phase space integrals which appear in (3.2.6). Choosing the C.M. frame of the photon-parton system, expression (3.2.5) can be written as

$$\int dPS^{(3)} |M(3)|^2 = \frac{1}{(4\pi)^n} \frac{s^{1-n/2}}{\Gamma(n-3)} \int_0^s ds_1 \int_0^{s-s_1} ds_2 \{s_1 s_2 (s - s_1 - s_2)\}^{n/2-2} \int_0^\pi d\theta \int_0^\pi d\phi (\sin \theta)^{n-3} (\sin \phi)^{n-4} |M(3)|^2, \quad (3.2.22)$$

with $s = (p + q)^2$, $s_1 = (p_1 + p_3)^2$, $s_2 = (p_2 + p_3)^2$ (3.2.7) and θ, ϕ are the polar, azimuthal angles as defined in appendix B of [27]. In many cases it is more convenient to evaluate the three phase space integrals in other Lorentz frames like the C.M. frame of two outgoing partons. In this case (3.2.6) becomes (see appendix E of [28])

$$\int dPS^{(3)} |M(3)|^2 = \frac{1}{(4\pi)^n} \frac{(s + Q^2)^{3-n}}{\Gamma(n-3)} \int_0^{s+Q^2} dt \int_{\frac{-t+Q^2}{s+Q^2}}^{\frac{-t}{s+Q^2}} du (s - t - u)^{n/2-2} \int_0^\pi d\theta \int_0^\pi d\phi (\sin \theta)^{n-3} (\sin \phi)^{n-4} |M(3)|^2, \quad (3.2.23)$$

with $s = (p + q)^2$, $t = 2p \cdot p_3$, $u = 2q \cdot p_3$. The angles θ, ϕ , corresponding either to p_1 or p_2 , are defined in the C.M. frame of the outgoing (p_1, p_2) system.

Before we could perform the angular integrations the matrix element $|M(3)|^2$ in (3.2.22), (3.2.23) first had to be decomposed via partial fractioning in such a way that only two factors in a specific term contain the angular variables θ and ϕ . The angular integrals are of the form

$$I_n^{(i,j)} = \int_0^\pi d\theta \int_0^\pi d\phi \frac{(\sin \theta)^{n-3} (\sin \phi)^{n-4}}{(a + b \cos \theta)^i (A + B \cos \theta + C \sin \theta \cos \phi)^j}, \quad (3.2.24)$$

where a, b, A, B and C are functions of the kinematical invariants s, Q^2, s_1 and s_2 (3.2.22) or s, Q^2, t and u (3.2.23). These integrals can be found in appendix C of [32]. For $n = 4 + \epsilon$ and either $a^2 \neq b^2$ or $A^2 \neq B^2 + C^2$ the expressions are very cumbersome, let alone when both $a^2 \neq b^2$ and $A^2 \neq B^2 + C^2$. Fortunately the latter case can be avoided by choosing an appropriate frame. Like in the calculation of the two to two parton process mentioned below (3.2.21), the three particle phase space integrals can be split in a soft and a hard gluon part. The soft integrals only show up in the γ^*q reaction and are calculated in [28]. In this chapter we included the hard gluon/quark integrals which appear in the γ^*q as well as γ^*g subprocesses. Because of their large number we can only show the most difficult ones in appendix 3B. They belong to the class of angular integrals where either $a^2 \neq b^2$ or $A^2 \neq B^2 + C^2$.

3.2.3 Mass factorization in the $\overline{\text{MS}}$ scheme

Adding all virtual, soft and hard gluon contributions, the IR divergences cancel while computing the parton structure functions $\hat{F}_{i,k}(z, Q^2, \epsilon)$, in accordance with the Bloch-Nordsieck theorem. The left-over divergences are of UV- or collinear (initial state) origin. The order α_s^2 contributions to $\hat{F}_{2,q}(z, Q^2, \epsilon)$ take the following form. The non-singlet part is determined by the graphs in figs. 3.4–3.6, the contributions A^2 , B^2 , AB and the interference term CD (identical quarks in the final state) in fig. 3.7. It can be written as

$$\hat{F}_{2,q}^{(2),NS} = \left(\frac{\alpha_s^2}{4\pi}\right)^2 S_\epsilon^2 \left(\frac{Q^2}{\mu^2}\right)^\epsilon \left[\frac{1}{\epsilon} \left\{ -2\beta_0 \bar{c}_{L,q}^{(1)} + P_{qq}^{(0)} \otimes \bar{c}_{L,q}^{(1)} \right\} + \bar{c}_{2,q}^{(1),NS} - 2\beta_0 a_{L,q}^{(1)} + P_{qq}^{(0)} \otimes a_{L,q}^{(1)} \right] , \quad (3.2.25)$$

$$\begin{aligned} \hat{F}_{2,q}^{(2),S} = & \left(\frac{\alpha_s^2}{4\pi}\right)^2 S_\epsilon^2 \left(\frac{Q^2}{\mu^2}\right)^\epsilon \left[\frac{1}{\epsilon^2} \left\{ \frac{1}{2} P_{qq}^{(0)} \otimes P_{qq}^{(0)} - \beta_0 P_{qq}^{(0)} \right\} \right. \\ & + \frac{1}{\epsilon} \left\{ \frac{1}{2} (P_{qq}^{(1),NS} + P_{q\bar{q}}^{(1),NS}) - 2\beta_0 \bar{c}_{2,q}^{(1)} + P_{qq}^{(0)} \otimes \bar{c}_{2,q}^{(1)} \right\} \\ & \left. + \bar{c}_{2,q}^{(2),NS} - 2\beta_0 a_{2,q}^{(1)} + P_{qq}^{(0)} \otimes a_{2,q}^{(1)} \right] , \quad (3.2.26) \end{aligned}$$

where the convolution symbol \otimes is defined by

$$(f \otimes g)(x) = \int_0^1 dx_1 \int_0^1 dx_2 \delta(x - x_1 x_2) f(x_1) g(x_2) . \quad (3.2.27)$$

Here $P_{ij}^{(1)}$ stand for the second order AP splitting functions which were computed in [13]–[17]. The terms $\bar{c}_{i,k}^{(1)}$, $a_{i,k}^{(1)}$ already appeared in the order α_s contribution to $\hat{F}_{i,k}^{(1)}$ (see eqs. (3.2.12)–(3.2.15)) and β_0 denotes the lowest order coefficient in the β -function which up to $\mathcal{O}(g^5)$ is given by

$$\beta(g) = -\beta_0 \frac{g^3}{16\pi^2} - \beta_1 \frac{g^5}{(16\pi^2)^2} , \quad \beta_0 = \frac{11}{3} C_A - \frac{2}{3} n_f , \quad g^2 = 4\pi\alpha_s . \quad (3.2.28)$$

where $C_A = N$ for $SU(N)$ and n_f stands for the number of light flavours. Notice that the above and subsequent expressions are written in a shorthand notation where all arguments in the functions like z , Q^2 are suppressed. Further the non-pole terms are constructed in such a way that $\bar{c}_{i,k}^{(l)}$ denotes the order α_s^l contributions to the DIS coefficient functions $C_{i,k}$ (3.1.6) in the $\overline{\text{MS}}$ scheme. The non-singlet splitting function consists of two parts i.e. $P_{qq}^{(1),NS}$ and $P_{q\bar{q}}^{(1),NS}$. The former can be attributed to the processes in figs. 3.4–3.6, the process A in fig. 3.7 and the interference between

reactions A and C in fig. 3.7, provided the quarks in the final state are not identical. The splitting function $P_{q\bar{q}}^{(1),NS}$ is determined by the interference between reactions C and D in fig. 3.7 due to the presence of identical (anti)quarks in the final state. In a similar way we can also split the second order contribution to the coefficient function

$$c_{i,q}^{(2),NS} = c_{i,q}^{(2),NS,+} + c_{i,q}^{(2),NS,-}, \quad (3.2.29)$$

where $c_{i,q}^{(2),NS,-}$ is due to identical quarks in the final state and $c_{i,q}^{(2),NS,+}$ accounts for the remaining contributions. The singlet parton structure function $\hat{F}_{i,q}^{(2),S}$ ($i = 2, L$) equals

$$\hat{F}_{i,q}^{(2),S} = \hat{F}_{i,q}^{(2),NS} + \hat{F}_{i,q}^{(2),PS}, \quad (3.2.30)$$

where $\hat{F}_{i,q}^{(2),PS}$ denotes the pure singlet (PS) part which is determined by the process C in fig. 3.7, provided the quarks in the final state are not identical.

$$\begin{aligned} \hat{F}_{L,q}^{(2),PS} = n_f \left(\frac{\alpha_s}{4\pi} \right)^2 S_\epsilon^2 \left(\frac{Q^2}{\mu^2} \right)^\epsilon & \left[\frac{1}{\epsilon} \left\{ P_{gq}^{(0)} \otimes \bar{c}_{L,g}^{(1)} \right\} + \bar{c}_{L,q}^{(2),PS} \right. \\ & \left. + P_{gq}^{(0)} \otimes a_{L,g}^{(1)} \right], \end{aligned} \quad (3.2.31)$$

$$\begin{aligned} \hat{F}_{2,q}^{(2),PS} = n_f \left(\frac{\alpha_s}{4\pi} \right)^2 S_\epsilon^2 \left(\frac{Q^2}{\mu^2} \right)^\epsilon & \left[\frac{1}{\epsilon^2} \left\{ \frac{1}{2} P_{qg}^{(0)} \otimes P_{gq}^{(0)} \right\} + \frac{1}{\epsilon} \left\{ \frac{1}{2} P_{q\bar{q}}^{(1),PS} \right. \right. \\ & \left. \left. + P_{gq}^{(0)} \otimes \bar{c}_{2,g}^{(1)} \right\} + \bar{c}_{2,q}^{(2),PS} + P_{gq}^{(0)} \otimes a_{2,g}^{(1)} \right]. \end{aligned} \quad (3.2.32)$$

In the case the quarks in the final state are identical, we also have to include reactions B and D in fig. 3.7. However the answers for $\hat{F}_{i,q}^{(2),NS,+}$ and $\hat{F}_{i,q}^{(2),PS}$ do not differ from the ones derived for the non-identical quark case. Here $\hat{F}_{i,q}^{(2),NS,+}$ is the part of $\hat{F}_{i,q}^{(2),NS}$ (3.2.25), (3.2.26), which can be attributed to $P_{q\bar{q}}^{(1),NS}$ and $c_{i,q}^{(2),NS,+}$ (3.2.29). Finally the order α_s^2 contributions to $\hat{F}_{i,g}(z, Q^2, \epsilon)$ become

$$\begin{aligned} \hat{F}_{L,g}^{(2)} = n_f \left(\frac{\alpha_s}{4\pi} \right)^2 S_\epsilon^2 \left(\frac{Q^2}{\mu^2} \right)^\epsilon & \left[\frac{1}{\epsilon} \left\{ -2\beta_0 \bar{c}_{L,g}^{(1)} + P_{gg}^{(0)} \otimes \bar{c}_{L,g}^{(1)} + P_{qg}^{(0)} \otimes \bar{c}_{L,q}^{(1)} \right\} \right. \\ & \left. + \bar{c}_{L,g}^{(2)} - 2\beta_0 a_{L,g}^{(1)} + P_{gg}^{(0)} \otimes a_{L,g}^{(1)} + P_{qg}^{(0)} \otimes a_{L,q}^{(1)} \right], \end{aligned} \quad (3.2.33)$$

$$\begin{aligned} \hat{F}_{2,g}^{(2)} = n_f \left(\frac{\alpha_s}{4\pi} \right)^2 S_\epsilon^2 \left(\frac{Q^2}{\mu^2} \right)^\epsilon & \left[\frac{1}{\epsilon^2} \left\{ \frac{1}{2} P_{qg}^{(0)} \otimes (P_{gg}^{(0)} + P_{q\bar{q}}^{(0)}) - \beta_0 P_{qg}^{(0)} \right\} \right. \\ & + \frac{1}{\epsilon} \left\{ \frac{1}{2} P_{qg}^{(1)} - 2\beta_0 \bar{c}_{2,g}^{(1)} + P_{gg}^{(0)} \otimes \bar{c}_{2,g}^{(1)} + P_{qg}^{(0)} \otimes \bar{c}_{2,q}^{(1)} \right\} \\ & \left. + \bar{c}_{2,g}^{(2)} - 2\beta_0 a_{2,g}^{(1)} + P_{gg}^{(0)} \otimes a_{2,g}^{(1)} + P_{qg}^{(0)} \otimes a_{2,q}^{(1)} \right]. \end{aligned} \quad (3.2.34)$$

Notice that using our conventions the second order AP splitting functions $P_{ij}^{(1)}$ can also be found in eqs. (2.36)–(2.39) of [33]. Further $P_{ij}^{(k)}$ ($k \geq 1$) is always understood to be represented in the $\overline{\text{MS}}$ scheme. After having computed $\hat{\mathcal{F}}_{i,k}$ we have to perform coupling constant renormalization. Choosing the $\overline{\text{MS}}$ scheme this can be achieved by replacing the bare (unrenormalized) coupling constant α_s^u by

$$\frac{\alpha_s^u}{4\pi} = \frac{\alpha_s(R^2)}{4\pi} \left(1 + \frac{\alpha_s(R^2)}{4\pi} \frac{2\beta_0}{\epsilon} S_\epsilon \left(\frac{R^2}{\mu^2} \right)^{\epsilon/2} \right), \quad (3.2.35)$$

where R represents the renormalization scale. After having removed the UV singularities the remaining pole terms can be attributed to initial state collinear divergences only, because $\hat{\mathcal{F}}_{i,k}$ is an inclusive quantity. The latter singularities are removed by mass factorization which proceeds in the following way

$$\hat{\mathcal{F}}_{i,q}^{\text{NS}} = \Gamma_{qq}^{\text{NS}} \otimes C_{i,q}^{\text{NS}}, \quad (3.2.36)$$

$$\hat{\mathcal{F}}_{i,q}^{\text{S}} = \Gamma_{qq}^{\text{S}} \otimes C_{i,q}^{\text{S}} + \Gamma_{gq} \otimes C_{i,g}, \quad (3.2.37)$$

$$\hat{\mathcal{F}}_{i,g} = 2n_f \Gamma_{qg} \otimes C_{i,q}^{\text{S}} + \Gamma_{gg} \otimes C_{i,g}. \quad (3.2.38)$$

In all above quantities coupling constant renormalization has already been carried out. The collinear divergences are absorbed into the transition functions Γ_{ij} so that the DIS coefficient functions $C_{i,k}$ are finite. Both functions depend on the mass factorization scale M and are scheme dependent. Combining the equations (3.1.6), (3.2.3), (3.2.37), (3.2.37) and (3.2.38) the mass factorized (scale dependent) parton densities are defined by

$$\Delta = \Gamma_{qq}^{\text{NS}} \otimes \hat{\Delta}, \quad (3.2.39)$$

$$\Sigma = \Gamma_{qq}^{\text{S}} \otimes \hat{\Sigma} + 2n_f \Gamma_{qg} \otimes \hat{G}, \quad (3.2.40)$$

$$G = \Gamma_{gq} \otimes \hat{\Sigma} + \Gamma_{gg} \otimes \hat{G}. \quad (3.2.41)$$

In the literature there are two popular mass factorization schemes, i.e. the $\overline{\text{MS}}$ and the DIS scheme. Starting with the $\overline{\text{MS}}$ scheme the transition functions take the following form

$$\Gamma_{qq}^{\text{NS}} = 1 + \frac{\alpha_s^u}{4\pi} S_\epsilon \left(\frac{M^2}{\mu^2} \right)^{\epsilon/2} \left[\frac{1}{\epsilon} P_{qq}^{(0)} \right] + \left(\frac{\alpha_s^u}{4\pi} \right)^2 S_\epsilon^2 \left(\frac{M^2}{\mu^2} \right)^\epsilon \left[\frac{1}{\epsilon^2} \left\{ \frac{1}{2} P_{qq}^{(0)} \otimes P_{qq}^{(0)} - \beta_0 P_{qq}^{(0)} \right\} + \frac{1}{\epsilon} \left\{ \frac{1}{2} P_{qq}^{(1),\text{NS}} + \frac{1}{2} P_{qq}^{(1),\text{NS}} \right\} \right], \quad (3.2.42)$$

$$\Gamma_{qq}^{\text{S}} = \Gamma_{qq}^{\text{NS}} + 2n_f \Gamma_{qq}^{\text{PS}}, \quad (3.2.43)$$

$$\Gamma_{qq}^{PS} = \left(\frac{\alpha_s}{4\pi}\right)^2 S_\epsilon^2 \left(\frac{M^2}{\mu^2}\right)^\epsilon \left[\frac{1}{\epsilon^2} \left\{ \frac{1}{4} P_{qg}^{(0)} \otimes P_{gq}^{(0)} \right\} + \frac{1}{\epsilon} \left\{ \frac{1}{4} P_{qq}^{(1),PS} \right\} \right] , \quad (3.2.44)$$

$$\Gamma_{qg} = \frac{\alpha_s}{4\pi} S_\epsilon \left(\frac{M^2}{\mu^2}\right)^{\epsilon/2} \left[\frac{1}{2\epsilon} P_{qg}^{(0)} \right] + \left(\frac{\alpha_s}{4\pi}\right)^2 S_\epsilon^2 \left(\frac{M^2}{\mu^2}\right)^\epsilon \left[\frac{1}{\epsilon^2} \left\{ \frac{1}{4} P_{qg}^{(0)} \otimes (P_{gg}^{(0)} + P_{qq}^{(0)}) - \frac{1}{2} \beta_0 P_{qg}^{(0)} \right\} + \frac{1}{\epsilon} \left\{ \frac{1}{4} P_{qg}^{(1)} \right\} \right] , \quad (3.2.45)$$

$$\Gamma_{gq} = \frac{\alpha_s}{4\pi} S_\epsilon \left(\frac{M^2}{\mu^2}\right)^{\epsilon/2} \left[\frac{1}{\epsilon} P_{gq}^{(0)} \right] , \quad (3.2.46)$$

$$\Gamma_{gg} = 1 + \frac{\alpha_s}{4\pi} S_\epsilon \left(\frac{M^2}{\mu^2}\right)^{\epsilon/2} \left[\frac{1}{\epsilon} P_{gg}^{(0)} \right] . \quad (3.2.47)$$

In order to obtain short expressions we have expressed the transition functions in the bare coupling constant α_s . The 1 in (3.2.42) and (3.2.47) denotes the distribution $\delta(1-z)$. The same notation holds for the coefficient functions presented below. Further the Γ_{ij} are sufficiently expanded in order α_s to render the DIS coefficient functions finite up to order α_s^2 . After having performed coupling constant renormalization (see (3.2.35)) we substitute Γ_{ij} into (3.2.37)–(3.2.38) and obtain the DIS coefficient functions. Choosing the renormalization scale R to be equal to the mass factorization scale M they read as follows. The non-singlet coefficient function is equal to

$$\bar{C}_{L,q}^{NS} = \frac{\alpha_s}{4\pi} \left[\bar{c}_{L,q}^{(1)} \right] + \left(\frac{\alpha_s}{4\pi}\right)^2 \left[\left\{ -\beta_0 \bar{c}_{L,q}^{(1)} + \frac{1}{2} P_{qq}^{(0)} \otimes \bar{c}_{L,q}^{(1)} \right\} L_M + \bar{c}_{L,q}^{(2),NS} \right] , \quad (3.2.48)$$

$$\begin{aligned} \bar{C}_{2,q}^{NS} = & 1 + \frac{\alpha_s}{4\pi} \left[\frac{1}{2} P_{qq}^{(0)} L_M + \bar{c}_{2,q}^{(1)} \right] + \left(\frac{\alpha_s}{4\pi}\right)^2 \left[\left\{ \frac{1}{8} P_{qq}^{(0)} \otimes P_{qq}^{(0)} - \frac{1}{4} \beta_0 P_{qq}^{(0)} \right\} L_M^2 \right. \\ & \left. + \left\{ \frac{1}{2} (P_{qq}^{(1),NS} + P_{q\bar{q}}^{(1),NS}) - \beta_0 \bar{c}_{2,q}^{(1)} + \frac{1}{2} P_{qq}^{(0)} \otimes \bar{c}_{2,q}^{(1)} \right\} L_M + \bar{c}_{2,q}^{(2),NS} \right] . \end{aligned} \quad (3.2.49)$$

The singlet coefficient function is given by

$$\bar{C}_{i,q}^S = \bar{C}_{i,q}^{NS} + \bar{C}_{i,q}^{PS} , \quad (i = 2, L) , \quad (3.2.50)$$

$$\bar{C}_{L,q}^{PS} = n_f \left(\frac{\alpha_s}{4\pi}\right)^2 \left[\left\{ \frac{1}{2} P_{gq}^{(0)} \otimes \bar{c}_{L,g}^{(1)} \right\} L_M + \bar{c}_{L,q}^{(2),PS} \right] , \quad (3.2.51)$$

$$\bar{C}_{2,q}^{\text{PS}} = n_f \left(\frac{\alpha_s}{4\pi} \right)^2 \left[\left\{ \frac{1}{8} P_{qg}^{(0)} \otimes P_{gq}^{(0)} \right\} L_M^2 + \left\{ \frac{1}{2} P_{qq}^{(1),\text{PS}} + \frac{1}{2} P_{gq}^{(0)} \otimes \bar{c}_{2,g}^{(1)} \right\} L_M + \bar{c}_{2,q}^{(2),\text{PS}} \right] . \quad (3.2.52)$$

The gluon coefficient function becomes

$$\bar{C}_{L,g} = n_f \frac{\alpha_s}{4\pi} \left[\bar{c}_{L,g}^{(1)} \right] + n_f \left(\frac{\alpha_s}{4\pi} \right)^2 \left[\left\{ -\beta_0 \bar{c}_{L,g}^{(1)} + \frac{1}{2} P_{gg}^{(0)} \otimes \bar{c}_{L,g}^{(1)} + \frac{1}{2} P_{qg}^{(0)} \otimes \bar{c}_{L,q}^{(1)} \right\} L_M + \bar{c}_{L,g}^{(2)} \right] , \quad (3.2.53)$$

$$\bar{C}_{2,g} = n_f \frac{\alpha_s}{4\pi} \left[\frac{1}{2} P_{qg}^{(0)} L_M + \bar{c}_{2,g}^{(1)} \right] + n_f \left(\frac{\alpha_s}{4\pi} \right)^2 \left[\left\{ \frac{1}{8} P_{qg}^{(0)} \otimes (P_{gg}^{(0)} + P_{qq}^{(0)}) - \frac{1}{8} \beta_0 P_{qg}^{(0)} \right\} L_M^2 + \left\{ \frac{1}{2} P_{qg}^{(1)} - \beta_0 \bar{c}_{2,g}^{(1)} + \frac{1}{2} P_{gg}^{(0)} \otimes \bar{c}_{2,g}^{(1)} + \frac{1}{2} P_{qg}^{(0)} \otimes \bar{c}_{2,q}^{(1)} \right\} L_M + \bar{c}_{2,g}^{(2)} \right] , \quad (3.2.54)$$

where

$$L_M = \ell n \frac{Q^2}{M^2} , \quad \alpha_s \equiv \alpha_s(M^2) . \quad (3.2.55)$$

In the case M is different from R , the resulting coefficient functions can be very easily derived from the above expressions (3.2.48)–(3.2.54) by replacing

$$\alpha_s(M^2) = \alpha_s(R^2) \left(1 + \frac{\alpha_s(R^2)}{4\pi} \beta_0 \ell n \left(\frac{R^2}{M^2} \right) \right) . \quad (3.2.56)$$

Explicit expressions for the coefficient functions (3.2.48)–(3.2.54) can be found in appendix 3B.1.

3.2.4 Mass factorization in the DIS scheme

In the case the mass factorization is carried out in the DIS scheme the transition functions become

$$\Gamma_{qq}^{\text{NS}} = \hat{F}_{2,q}^{\text{NS}}|_{Q^2=M^2} ; \quad \Gamma_{qg}^{\text{S}} = \hat{F}_{2,q}^{\text{S}}|_{Q^2=M^2} ; \quad n_f \Gamma_{qg} = \frac{1}{2} \hat{F}_{2,g}^{\text{S}}|_{Q^2=M^2} , \quad (3.2.57)$$

where $\hat{F}_{k,l}$ are given in (3.2.26), (3.2.30) and (3.2.34). Unfortunately such a unique definition does not exist for the transition functions Γ_{gq} and Γ_{gg} because in deep inelastic scattering the gluon does not directly couple to the vector boson V . Therefore there is some freedom of choice except that all Γ 's have to satisfy the relations

$$\int_0^1 dx \, x [\Gamma_{gg} + 2n_f \Gamma_{qg}] = 1 , \quad (3.2.58)$$

$$\int_0^1 dx \, x \left[\Gamma_{qq}^S + \Gamma_{gq} \right] = 1 \quad , \quad (3.2.59)$$

which follow from the momentum conservation sum rule. Following the definition in [34] we choose

$$\Gamma_{gq} = \frac{\alpha_s}{4\pi} \left(\frac{M^2}{\mu^2} \right)^{\epsilon/2} \left[\frac{1}{\epsilon} P_{gq}^{(0)} - \bar{c}_{2,q}^{(1)} \right] \quad , \quad (3.2.60)$$

$$\Gamma_{gg} = 1 + \frac{\alpha_s}{4\pi} \left(\frac{M^2}{\mu^2} \right)^{\epsilon/2} \left[\frac{1}{\epsilon} P_{gg}^{(0)} - n_f \bar{c}_{2,g}^{(1)} \right] \quad . \quad (3.2.61)$$

After substitution of α_s^u (3.2.35) in the above expressions the coefficient functions in the DIS scheme read

$$C_{L,q}^{NS} = \frac{\alpha_s}{4\pi} \left[\bar{c}_{L,q}^{(1)} \right] + \left(\frac{\alpha_s}{4\pi} \right)^2 \left[\left\{ -\beta_0 \bar{c}_{L,q}^{(1)} + \frac{1}{2} P_{qq}^{(0)} \otimes \bar{c}_{L,q}^{(1)} \right\} L_M + \bar{c}_{L,q}^{(2),NS} - \bar{c}_{2,q}^{(1)} \otimes \bar{c}_{L,q}^{(1)} \right] \quad , \quad (3.2.62)$$

$$C_{2,q}^{NS} = 1 + \frac{\alpha_s}{4\pi} \left[\frac{1}{2} P_{qq}^{(0)} L_M \right] + \left(\frac{\alpha_s}{4\pi} \right)^2 \left[\left\{ \frac{1}{8} P_{qq}^{(0)} \otimes P_{qq}^{(0)} - \frac{1}{4} \beta_0 P_{qq}^{(0)} \right\} L_M^2 + \left\{ \frac{1}{2} (P_{qq}^{(1),NS} + P_{q\bar{q}}^{(1),NS}) - \beta_0 \bar{c}_{2,q}^{(1)} \right\} L_M \right] \quad , \quad (3.2.63)$$

$$C_{L,q}^{PS} = n_f \left(\frac{\alpha_s}{4\pi} \right)^2 \left[\left\{ \frac{1}{2} P_{gq}^{(0)} \otimes \bar{c}_{L,g}^{(1)} \right\} L_M + \bar{c}_{L,q}^{(2),PS} + \bar{c}_{2,q}^{(1)} \otimes \bar{c}_{L,g}^{(1)} \right] \quad , \quad (3.2.64)$$

$$C_{2,q}^{PS} = n_f \left(\frac{\alpha_s}{4\pi} \right)^2 \left[\left\{ \frac{1}{8} P_{q\bar{g}}^{(0)} \otimes P_{gq}^{(0)} \right\} L_M^2 + \left\{ \frac{1}{2} P_{qq}^{(1),PS} + \frac{1}{2} P_{gq}^{(0)} \otimes \bar{c}_{2,g}^{(1)} + \frac{1}{2} P_{q\bar{g}}^{(0)} \otimes \bar{c}_{2,q}^{(1)} \right\} L_M \right] \quad , \quad (3.2.65)$$

$$C_{L,g} = n_f \frac{\alpha_s}{4\pi} \left[\bar{c}_{L,g}^{(1)} \right] + n_f \left(\frac{\alpha_s}{4\pi} \right)^2 \left[\left\{ -\beta_0 \bar{c}_{L,g}^{(1)} + \frac{1}{2} P_{gg}^{(0)} \otimes \bar{c}_{L,g}^{(1)} + \frac{1}{2} P_{q\bar{g}}^{(0)} \otimes \bar{c}_{L,q}^{(1)} \right\} L_M + \bar{c}_{L,g}^{(2)} - \bar{c}_{2,g}^{(1)} \otimes (\bar{c}_{L,q}^{(1)} - n_f \bar{c}_{L,g}^{(1)}) \right] \quad , \quad (3.2.66)$$

$$C_{2,g} = n_f \frac{\alpha_s}{4\pi} \left[\frac{1}{2} P_{q\bar{g}}^{(0)} L_M \right] + n_f \left(\frac{\alpha_s}{4\pi} \right)^2 \left[\left\{ \frac{1}{8} P_{q\bar{g}}^{(0)} \otimes (P_{gg}^{(0)} + P_{qq}^{(0)}) - \frac{1}{4} \beta_0 P_{q\bar{g}}^{(0)} \right\} L_M^2 + \left\{ \frac{1}{2} P_{q\bar{g}}^{(1)} - \beta_0 \bar{c}_{2,g}^{(1)} + \frac{1}{2} P_{q\bar{g}}^{(0)} \otimes \bar{c}_{2,q}^{(1)} + \frac{1}{2} \bar{c}_{2,g}^{(1)} \otimes (P_{gg}^{(0)} - P_{qq}^{(0)} + n_f P_{q\bar{g}}^{(0)}) \right\} L_M \right] \quad . \quad (3.2.67)$$

Notice that $C_{2,q}^{NS}$, $C_{2,q}^S$ and $C_{2,g}$ vanish at $Q^2 = M^2$. Explicit expressions for the coefficient functions in the DIS scheme can be found in appendix 3B.2. The anomalous dimensions of the composite operators γ_{ij} which are related to the AP splitting functions via

$$\gamma_{ij}^{(k),n} = - \int_0^1 dx x^{n-1} P_{ij}^{(k)} , \quad (3.2.68)$$

change while going from the \overline{MS} to the DIS scheme. Consequently the AP splitting functions will undergo a similar change. In [13]–[17] they are only calculated in the \overline{MS} scheme. In the DIS scheme they can be obtained by performing a finite mass factorization, denoted by Z , which relates the transition functions $\bar{\Gamma}_{ij}$ computed in the \overline{MS} scheme (3.2.42)–(3.2.47) to the transition functions Γ_{ij} in the DIS scheme (3.2.57), (3.2.60), (3.2.61). In the singlet case Z becomes a matrix which is defined by

$$\bar{\Gamma}_{ij} = Z_{ik} \Gamma_{kj} . \quad (3.2.69)$$

For the DIS coefficient function this implies

$$C_i = (Z^{-1})_{ki} \bar{C}_k . \quad (3.2.70)$$

From the definition of the anomalous dimension

$$\gamma_{ij} = \beta(g, \varepsilon) \Gamma_{ik} \frac{d(\Gamma^{-1})_{kj}}{dg} , \quad \beta(g, \varepsilon) = \frac{\varepsilon}{2} + \beta(g) , \quad (3.2.71)$$

one can derive

$$\gamma_{ij} = Z_{il} \bar{\gamma}_{lm} (Z^{-1})_{mj} + \beta(g) Z_{il} \frac{d(Z^{-1})_{lj}}{dg} . \quad (3.2.72)$$

If we want to determine the γ_{ij} (DIS scheme) up to $\mathcal{O}(\alpha_s^2)$ it is sufficient to know Z up to $\mathcal{O}(\alpha_s)$. From the transition functions given above one infers

$$Z = \begin{pmatrix} 1 + \frac{\alpha_s}{4\pi} \bar{c}_{2,q}^{(1)} & \frac{\alpha_s}{4\pi} \bar{c}_{2,g}^{(1)} \\ -\frac{\alpha_s}{4\pi} \bar{c}_{2,q}^{(1)} & 1 - n_f \frac{\alpha_s}{4\pi} \bar{c}_{2,g}^{(1)} \end{pmatrix} . \quad (3.2.73)$$

Expanding γ and $\bar{\gamma}$ in α_s i.e.

$$\gamma_{ij} = \sum_{m=0}^{\infty} \left(\frac{\alpha_s}{4\pi} \right)^{m+1} \gamma_{ij}^{(m)} , \quad (3.2.74)$$

the singlet anomalous dimensions in the DIS scheme become

$$\gamma_{qq} = \frac{\alpha_s}{4\pi} \gamma_{qq}^{(0)} + \left(\frac{\alpha_s}{4\pi} \right)^2 \left\{ \bar{\gamma}_{qq}^{(1)} + 2\beta_0 \bar{c}_{2,q}^{(1)} + \bar{c}_{2,g}^{(1)} \bar{\gamma}_{gq}^{(0)} + \bar{c}_{2,q}^{(1)} \bar{\gamma}_{qg}^{(0)} \right\} , \quad (3.2.75)$$

$$\gamma_{qg} = \frac{\alpha_s}{4\pi} \bar{\gamma}_{qg}^{(0)} + \left(\frac{\alpha_s}{4\pi} \right)^2 \left\{ \bar{\gamma}_{qg}^{(1)} + 2\beta_0 \bar{c}_{2,g}^{(1)} + \bar{c}_{2,g}^{(1)} (\bar{\gamma}_{gg}^{(0)} - \bar{\gamma}_{qq}^{(0)}) + \bar{\gamma}_{qg}^{(0)} (\bar{c}_{2,q}^{(1)} + n_f \bar{c}_{2,g}^{(1)}) \right\} , \quad (3.2.76)$$

$$\gamma_{gq} = \frac{\alpha_s}{4\pi} \bar{\gamma}_{gq}^{(0)} + \left(\frac{\alpha_s}{4\pi} \right)^2 \left\{ \bar{\gamma}_{gq}^{(1)} - 2\beta_0 \bar{c}_{2,q}^{(1)} + \bar{c}_{2,q}^{(1)} (\bar{\gamma}_{gg}^{(0)} - \bar{\gamma}_{qq}^{(0)}) - \bar{\gamma}_{gq}^{(0)} (\bar{c}_{2,q}^{(1)} + n_f \bar{c}_{2,g}^{(1)}) \right\} , \quad (3.2.77)$$

$$\gamma_{gg} = \frac{\alpha_s}{4\pi} \bar{\gamma}_{gg}^{(0)} + \left(\frac{\alpha_s}{4\pi} \right)^2 \left\{ \bar{\gamma}_{gg}^{(1)} - 2\beta_0 n_f \bar{c}_{2,g}^{(1)} - \bar{c}_{2,g}^{(1)} \bar{\gamma}_{gq}^{(0)} - \bar{c}_{2,q}^{(1)} \bar{\gamma}_{qg}^{(0)} \right\} . \quad (3.2.78)$$

The non-singlet case is trivial since Z becomes a scalar only. Hence we get

$$\gamma_{qq}^{NS} = \frac{\alpha_s}{4\pi} \bar{\gamma}_{qq}^{(0)} + \left(\frac{\alpha_s}{4\pi} \right)^2 \left\{ \bar{\gamma}_{qq}^{(1),NS} + 2\beta_0 \bar{c}_{2,q}^{(1)} \right\} . \quad (3.2.79)$$

The anomalous dimensions γ_{qq} and γ_{qg} can also be derived from the coefficient functions, (3.2.62)–(3.2.67), which are presented in the DIS scheme, since they satisfy the Callan-Symanzik equation

$$\left[\left\{ M \frac{\partial}{\partial M} + \beta(g) \frac{\partial}{\partial g} \right\} \delta_{kj} - \gamma_{kj} \right] C_{i,k} = 0 , \quad (i = 2, L) . \quad (3.2.80)$$

3.2.5 Checks on our results

As a check on our results we computed the Mellin transform of the coefficient function $C_{i,k}$ in an analytical way. The latter is defined as follows

$$C_{i,k}^n(Q^2/M^2) = \int_0^1 dz z^{n-1} C_{i,k}(z, Q^2/M^2) , \quad i = 2, L , \quad k = q, g . \quad (3.2.81)$$

The above quantity has also been computed in the \overline{MS} scheme up to order α_s^2 in [35] for $n = 2, 4, 6, 8, 10$ by using a totally different method [36]. We found complete agreement with their results. Notice that the method in [36] only provides us with the moments up to finite n (here $n \leq 10$) without giving the full x -dependence of the coefficient function. On the other hand using the method in [36] one can compute the Mellin transform in (3.2.81) up to order α_s^3 provided n is small. Using our method this is extremely difficult because of the very complicated three-loop and four-body phase space integrals which have to be carried out. Another important check is that in both schemes $C_{2,q}^{NS,1} = 1$ up to order α_s^2 . The latter is a consequence of the Adler sum rule which leads to the identity $C_{2,q}^{NS,1} = 1$ in all orders of perturbation theory

[19]. In table 3.1 we have listed the first ten moments of $\bar{c}_{2,q}^{(2),NS}$. They appear in the perturbation expansion of the Mellin transform

$$\bar{C}_{2,q}^{NS,n}(1) = \int_0^1 dz z^{n-1} \bar{C}_{2,q}^{NS}(z, 1) = \sum_{i=0}^{\infty} \left(\frac{\alpha_s}{4\pi} \right)^i \bar{c}_{2,q}^{(i),NS,n} =$$

$$1 + \frac{\alpha_s}{4\pi} C_F B_{1,F}^n + \left(\frac{\alpha_s}{4\pi} \right)^2 \left\{ C_F^2 B_{2,F}^n + C_A C_F B_{2,A}^n + n_f C_F B_{2,f}^n \right\} + \dots, \quad (3.2.82)$$

with

$$\bar{c}_{2,q}^{(2),NS,n} = \bar{c}_{2,q}^{(2),NS,+,n} + (-1)^n \bar{c}_{2,q}^{(2),NS,-,n}, \quad (3.2.83)$$

where the lowest order coefficient $B_{1,F}^n$ can be found in [61]. Because of the cumbersome expressions we have resorted to a numerical evaluation of the moments only (five significant digits). The numbers listed in table 3.1 agree with those given in eq. 19 of [33]. The x -dependence of the order α_s^2 contribution to the longitudinal

n	$B_{2,F}^{(n)}$	$B_{2,A}^{(n)}$	$B_{2,f}^{(n)}$
1	0	0	0
2	17.908	- 3.536	- 4.000
3	22.322	8.161	- 8.344
4	31.842	21.434	- 12.741
5	43.805	35.635	- 16.980
6	58.478	49.609	- 21.010
7	74.722	63.363	- 24.827
8	92.394	76.638	- 28.444
9	110.94	89.510	- 31.878
10	130.27	101.91	- 35.146

Table 3.1. The first ten moments of $\bar{c}_{2,q}^{(2),NS}$, see (3.2.82)

coefficient function $C_{L,k}(x, 1)$ has been calculated already earlier in the literature. For $C_{L,q}^{NS}$ see [37]–[39], [42] (\overline{MS}) and [41] (DIS). The coefficient function $C_{L,q}^{PS}$ can be found in [40], [42] (\overline{MS}) and [41] (DIS). Finally $C_{L,g}$ is presented in [41] (DIS) and

[42] ($\overline{\text{MS}}$). We disagree with all results in the above literature except for $C_{L,q}^{\text{NS}}$, $C_{L,q}^{\text{PS}}$ in eqs. (8) and (9) of [42]. Concluding this comparison with the literature we note that there only exists complete agreement between our results and the ones found in [35].

3.2.6 The omission of the third order anomalous dimension

At the end of this section we want to discuss the two missing pieces in our calculation which are needed in order to make a full phenomenological analysis of the deep inelastic lepton hadron data. The first piece refers to heavy flavour contributions to the DIS coefficient functions. In our calculation we have assumed that all quarks have zero masses. This is correct for the light quarks but certainly incorrect when heavy flavours like bottom or top appear in the final state. The assumption may also be incorrect for the charmed quark. Heavy flavour contributions to deep inelastic lepton-hadron scattering, where the exchanged photon in fig. 2.1 is highly virtual, have been investigated in [43]. The second piece, which is the most complicated one, is the three loop contribution to the anomalous dimension $\gamma_{ij}^{(l)}$ ($i, j = q, \bar{q}, g$). It determines the scale evolution of the parton densities in the next-to-next-to-leading-logarithmic (NNLL) approximation. Notice that the coefficients of the perturbative expansion of the DIS hadron structure function in the running coupling constant are only scheme independent if $c_{i,k}^{(l)}$ as well as $\gamma_{ij}^{(l)}$ are known [13, 45]. This is important for the determination of the running coupling constant as well as the QCD scale Λ . The implication of omitting the three loop anomalous dimension $\gamma_{ij}^{(2)}$ in the analysis of the deep inelastic data will be discussed below. From [21, 22] we infer that at large x ($x > 0.3$) the deep inelastic structure function $F_2(x, Q^2)$ is dominated by the quark densities and the non-singlet part of the coefficient function. Taking the Mellin transform we obtain

$$\int_0^1 dx x^{n-1} F_2(x, Q^2) = A^n(M^2) C_2^{\text{NS},n}(Q^2/M^2) , \quad (3.2.84)$$

with

$$A^n(M^2) = \frac{5}{18} \Sigma^n(M^2) + \frac{1}{6} \Delta^n(M^2) . \quad (3.2.85)$$

The coefficient function $C_2^{\text{NS},n}$ is the asymptotic solution of the Callan-Symanzik equation in (3.2.80). Up to order $\alpha_s^2(Q^2)$ it is equal to

$$C_{2,q}^{\text{NS},n}(Q^2/M^2) = B^{\text{NS},n}(M^2) \left[1 + \frac{\alpha_s(Q^2)}{4\pi} \left\{ c_{2,q}^{(1)} + \frac{\gamma_{qq}^{(1),\text{NS}}}{2\beta_0} - \frac{\beta_1 \gamma_{qq}^{(0)}}{2\beta_0^2} \right\} \right]$$

$$\begin{aligned}
& + \left(\frac{\alpha_s(Q^2)}{4\pi} \right)^2 \left\{ c_{2,q}^{(2),NS} + \frac{1}{2} \left(\frac{\gamma_{qq}^{(1),NS}}{\beta_0} - \frac{\beta_1 \gamma_{qq}^{(0)}}{\beta_0^2} \right) c_{2,q}^{(1)} + \frac{1}{8} \left(\frac{\gamma_{qq}^{(1),NS}}{\beta_0} - \frac{\beta_1 \gamma_{qq}^{(0)}}{\beta_0^2} \right)^2 \right. \\
& \left. + \frac{1}{4} \left(\frac{\gamma_{qq}^{(2),NS}}{\beta_0} - \frac{\beta_1 \gamma_{qq}^{(1),NS}}{\beta_0^2} - \frac{\beta_2 \gamma_{qq}^{(0)}}{\beta_0^2} + \frac{\beta_1^2 \gamma_{qq}^{(0)}}{\beta_0^3} \right) \right\} \left[\alpha_s(Q^2) \right]^{\frac{\gamma_{qq}^{(0)}}{2\beta_0}}, \quad (3.2.86)
\end{aligned}$$

where β_i are the coefficients in the series expansion of the beta-function (3.2.28) which are known up to $i = 3$ [44]. The factor $B^n(M^2)$ is determined by putting $Q^2 = M^2$ in the above equation. As is known in the literature [13, 45] the coefficients between the curly brackets are scheme independent which, for the order $\alpha_s(Q^2)$ term, can be easily inferred from (3.2.79). Therefore the scheme dependence of $c_{2,q}^{(2),NS}$ in (3.2.86) has to be compensated by $\gamma_{qq}^{(2),NS}$ and the lowest order coefficients $c_{2,q}^{(1)}$ and $\gamma_{qq}^{(1),NS}$. Now we can argue that for the non-singlet structure function the anomalous dimension $\gamma_{qq}^{(2),NS}$ can probably be neglected with respect to $c_{2,q}^{(2),NS}$ in the region where the corrections are large provided all coefficients are calculated in the \overline{MS} scheme. An analysis of the known radiative corrections reveals that for $x > 0.5$ F_2 is dominated by the soft gluon contributions which show up as large logarithms of the type $\ln^j(1-z)/(1-z)_+$ in $\bar{c}_{2,q}^{(i),NS}(z)$ and $\bar{P}_{qq}^{(i),NS}(z)$. The calculations carried out in this chapter and the soft gluon resummation formulas presented in [46] reveal the behaviour

$$\bar{c}_{2,q}^{(i),NS}(z) \xrightarrow{z \rightarrow 1} \sum_{j=0}^{2i-1} a_j^{(i)} \left(\frac{\ln^j(1-z)}{1-z} \right)_+, \quad (3.2.87)$$

or

$$\bar{c}_{2,q}^{(i),NS,n}(z, 1) \xrightarrow{n \rightarrow \infty} \sum_{j=0}^{2i-1} \tilde{a}_j^{(i)} \frac{1}{j+1} (\ln n)^{j+1}, \quad (3.2.88)$$

Furthermore in [14] one has made the following conjecture

$$P_{qq}^{(i),NS}(z) \xrightarrow{z \rightarrow 1} a^{(i)} \left(\frac{1}{1-z} \right)_+, \quad (3.2.89)$$

or

$$\bar{\gamma}_{qq}^{(i),NS,n} \xrightarrow{n \rightarrow \infty} a^{(i)} \ln n, \quad (3.2.90)$$

which is confirmed by the existing calculations carried out for $i = 0, 1$, see [13]–[17]. This conjecture is further corroborated by a combination of the findings in refs. [46] and [47]. In the latter it is shown that there exists a relation between the coefficients of the large logarithms appearing in $\bar{c}_{2,q}^{(i),NS}$ and the coefficients of the same terms in $P_{qq}^{(i),NS}$. If we combine this result with the series expansion in α_s of the soft gluon resummation formulas in [46], one can infer that $\bar{\gamma}_{qq}^{(2),NS}$ maximally behaves as

$b^{(2)}\ell n^2(n)$ for $n \rightarrow \infty$. However nothing can be said about $b^{(2)}$. Its vanishing can only be shown by an explicit calculation. If we assume that the above asymptotic expressions hold for all i , in particular for $i = 2$, one can neglect $\bar{\gamma}_{qq}^{(2),NS}$ with respect to $\bar{c}_{2,q}^{(1),NS}$ and $\bar{c}_{2,q}^{(2),NS}$ in the second order coefficient of (3.2.86). Therefore the large corrections for $x > 0.5$ can be attributed to the coefficient functions $c_{2,q}^{(i),NS}$ only. For $x < 0.5$ the $O(\alpha_s^2)$ correction to $F_2(x, Q^2)$ due to $c_{2,q}^{(2),NS}$ turns out to be small (on the one percent level), because of a strong cancellation between the regular and singular terms in the coefficient function. Since the same type of terms also appears in $\bar{\gamma}_{qq}^{(2),NS}$, we expect that this cancellation happens here too so that the contribution to $F_2(x, Q^2)$ due to the NS anomalous dimension will be small. Summarizing the above we conclude that for corrections above the one percent level the contribution due to $\bar{\gamma}_{qq}^{(2),NS}$ can be neglected in the whole x -region.

Unfortunately the above arguments, regarding the omission of the second order anomalous dimension with respect to the coefficient function, do not apply any more to the singlet hadron structure function. At small x ($x < 0.01$) $F_2(x, Q^2)$ gets a noticeable contribution from the product of the gluon coefficient function $C_{2,g}(z, Q^2/M^2)$ and the gluon density $G(x/z, M^2)$ appearing in (3.1.6). A part of these large corrections is due to the logarithmic terms of the type $\ell n^j z/z$, which show up in the coefficient function $C_{2,g}(z)$ and the AP splitting function $P_{gq}(z)$. They also appear in $C_{2,q}^{PS}(z)$ (3.2.52) and $P_{qg}(z)$ but the latter are of minor importance because they mainly influence the contribution of the sea quarks which is always smaller than the contribution of the gluon part. The physical origin of these corrections can be traced back to soft gluon exchanges in the t -channel graphs which contribute to $\hat{F}_{2,g}^{(2)}$ (3.2.34). However there are other important contributions to $F_2^S(x, Q^2)$ which cannot be attributed to these type of logarithms only. A thorough analysis of the order α_s^2 correction reveals that at $x = 10^{-4}$ part of the order α_s^2 correction can be traced back to those terms which dominate the coefficient function $c_{2,g}^{(2)}(z)$ near $z = 1$. They are given by the logarithms $\ell n^j(1 - z)$ (see (3B.12)). This is not surprising if one looks at the integral in (3.1.6). In the limit $x \rightarrow 0$ the gluon density $G(x/z, M^2)$ in the integrand gets very large near $z = 1$. Since in this region $C_{i,g}(z, Q^2/M^2)$ is dominated by the terms $\ell n^j(1 - z)$ it is understandable that the integral in (3.1.6) gets an important contribution from the region $z \approx 1$. This does not mean that the $\ell n^j z/z$ terms are unimportant. On the contrary if the latter would be omitted the correction to $F_2(x, Q^2)$, which is negative in the small- x region, would be positive. Actually the analysis shows that the $\ell n^j z/z$ terms are compensated by the regular part in $c_{2,g}^{(2)}(z)$ which dominates the region $0 < z < 1$. Notice that the whole analysis

depends on the chosen parametrization of the gluon density $G(x/z, M^2)$. The steeper it rises at small x the more important the region near $z = 1$ becomes, because of the logarithmic behaviour of $c_{2,g}^{(2)}(z)$ which is given by $\ln^j(1-z)$, see above. Even if the $\ln^j z/z$ terms would dominate the radiative corrections there are no arguments that their power j in the AP splitting function $P_{gg}^{(n)}(z)$ would be smaller than the one appearing in $c_{2,g}^{(n)}(z)$. This is in contrast with our findings for the $\ln^j(1-z)/(1-z)_+$ corrections present in $P_{qq}^{(k),NS}(z)$ and $c_{2,q}^{(k),NS}(z)$. Actually the opposite happens as is revealed by the existing calculations. In the limit $z \rightarrow 0$ we have:

$$c_{2,g}^{(2)}(z) \xrightarrow{z \rightarrow 0} \text{regular} \quad , \quad \bar{c}_{2,g}^{(2)}(z) \xrightarrow{z \rightarrow 0} n_f C_A \left(-\frac{16}{3z} \zeta(2) + \frac{344}{27z} \right) \quad , \quad (3.2.91)$$

$$P_{gg}^{(1)}(z) \xrightarrow{z \rightarrow 0} C_A \left(\frac{8}{z} \right) \quad , \quad P_{gg}^{(1)}(z) \xrightarrow{z \rightarrow 0} C_A T_f \left(-\frac{400}{9z} \right) + C_F T_f \left(\frac{32}{3z} \right) \quad , \quad (3.2.92)$$

with $T_f = 1/2$. Here regular means that no terms show up of the type $\ln^j z/z$ ($j = 0, 1, \dots$). The Mellin transform of the above expressions can be easily calculated using

$$\int_0^1 dz \, z^{n-1} \left(\frac{1}{z} \ln^j z \right) = (-1)^j \frac{\Gamma(j+1)}{(n-1)^{j+1}} \quad . \quad (3.2.93)$$

About the higher order α_s corrections to $C_{2,g}$ and P_{gg} not much is known but we expect that the most singular behaviour of $P_{gg}^{(2)}$ is given by $\ln z/z$. This prediction is corroborated by the findings in [48] for the C_A^3 part of $P_{gg}^{(2)}$ (see (1.5) and (7.36) in [48]). About the other colour structure parts nothing is known. This implies that probably $P_{gg}^{(2)}(z)$ is more singular at $z = 0$ than $C_{2,g}^{(2)}(z)$. The Mellin transform of the renormalization group improved singlet hadron structure function is much more complicated than the non-singlet expression presented in (3.2.86). Up to order $\alpha_s(Q^2)$ its expression can be found in [18]. Because of the discussion above we cannot neglect in the order $\alpha_s^2(Q^2)$ contribution the third order anomalous dimension $\gamma_{gg}^{(2)}$ with respect to the second order coefficient function $c_{2,g}^{(2)}$. Therefore $\gamma_{gg}^{(2)}$ has to be calculated exactly which is far from trivial in view of the complications described in [49]. This implies that our ignorance about $\gamma_{gg}^{(2)}(x)$ (or $P_{gg}^{(2)}(x)$) hampers the analysis of deep inelastic data in the small- x region. In the next section we show that $\bar{c}_{2,g}^{(2)}$ is appreciable in the range $10^{-4} < x < 10^{-2}$ and it is not unlikely that the missing $P_{gg}^{(2)}$ leads to even larger corrections. Moreover we expect that in this range non-perturbative effects in the gluon density become very important. Therefore it will be very difficult to distinguish perturbative and non-perturbative contributions to the hadron structure function in the small- x region. Contrary to the situation with

$F_2(x, Q^2)$, the existing order α_s^2 corrected anomalous dimensions are sufficient to provide us with the renormalization group improved longitudinal structure function $F_L(x, Q^2)$ which is now corrected up to order $\alpha_s^2(Q^2)$. As an example we give the contribution to $F_L(x, Q^2)$ due to the quark densities and the non-singlet part of the coefficient function.

$$\int_0^1 dx x^{n-1} F_L(x, Q^2) = A^n(M^2) C_L^{NS,n}(Q^2/M^2) , \quad (3.2.94)$$

with

$$C_{L,q}^{NS,n}(Q^2/M^2) = B^{NS,n}(M^2) \left[\frac{\alpha_s(Q^2)}{4\pi} \left\{ c_{L,q}^{(1)} \right\} + \left(\frac{\alpha_s(Q^2)}{4\pi} \right)^2 \left\{ c_{L,q}^{(2),NS} \right. \right. \\ \left. \left. + \frac{1}{2} \left(\frac{\gamma_{qq}^{(1),NS}}{\beta_0} - \frac{\beta_1 \gamma_{qq}^{(0)}}{\beta_0^2} \right) c_{L,q}^{(1)} \right\} \right] [\alpha_s(Q^2)]^{\frac{\gamma_{qq}^{(0)}}{2\beta_0}} . \quad (3.2.95)$$

The more complicated singlet expressions can be inferred from [13]. Comparing the coefficient functions $C_{L,i}$ with $C_{2,i}$ ($i = q, \bar{q}, g$) we note the following. There are no soft gluon corrections present in $c_{L,q}^{(k),NS}$ ($k = 1, 2$) as shown in (3.2.87), (3.2.88). However terms of the type $\ell n^j z/z$ appear in the coefficient functions $C_{L,q}^{PS}(z)$ and $C_{L,g}(z)$ which can be attributed to soft gluon exchanges in t-channel graphs (see the discussion above (3.2.94)). They show up for the first time in the $\mathcal{O}(\alpha_s^2)$ contributions $c_{L,q}^{(2),PS}(z)$ and $c_{L,g}^{(2)}(z)$ which behave like $1/z$. Like in the case of $c_{2,g}^{(2)}(z)$ their importance depends very heavily on the chosen parton densities, in particular on the gluon density.

3.3 Results

Bearing in mind the uncertainties due to the missing third order anomalous dimension, we will study the effect of the order α_s^2 corrections to the deep inelastic proton structure functions $F_i(x, Q^2)$ ($i = 2, L$). In order to make a comparison with the already known complete order α_s renormalization group improved structure functions (3.2.84) and (3.2.94), we will use the parametrization for the parton densities as given in [50] (HMRSB) and [51] (MTB) which are based on the BCDMS data [53]¹. The MTB set contains the next-to-leading-log (NLL) parametrization in the DIS as well as \overline{MS} scheme whereas the former (HMRSB) describes the NLL parton densities in the \overline{MS} scheme only. They are all listed in table 3.2 including the corresponding QCD scale parameter Λ . This parameter also appears in the two loop corrected running

¹The parton densities in [50] and [51] are defined to be equal to $xf_l(x, M^2)$ ($l = q, \bar{q}, g$) where $f_l(x, M^2)$ stands for the parton densities appearing in $\Sigma(x, M^2)$ (3.1.7) and $\Delta(x, M^2)$, (3.1.8)

coupling constant where the number of light flavours n_f is chosen to be four. The renormalization scale R will always be put equal to the mass factorization scale M . In the discussion below we will choose the $\overline{\text{MS}}$ scheme and take $M = Q$ unless stated otherwise. The order α_s^k corrected structure function is denoted by $F_i^{(k)}(x, Q^2)$ where $k = 0, 1, 2$ for $i = 2$ and $k = 1, 2$ for $i = L$. Notice that because of the missing three loop anomalous dimension (splitting function) the next-to-next-to-leading-log (NNLL) parton densities are not available so that $F_2(x, Q^2)|_{\text{NLL}}$ does not fully represent the complete order α_s^2 renormalization improved structure function. The same holds for $F_L^{(0)}(x, Q^2)|_{\text{NLL}}$ for which the leading log (LL) approximation would be more appropriate. However in this chapter we are more interested in effects due to higher order corrections to the DIS coefficient function than in differences in $F_L^{(k)}(x, Q^2)$ between the LL and NLL parametrizations for the parton densities. In the following we will use the NLL parton densities and only comment on the LL if necessary.

In sections 3.3.1 and 3.3.2 we will treat the following topics:

1. The effect of the order α_s^2 corrections on the deep inelastic proton structure functions $F_i(x, Q^2)$ ($i = 2, L$) and the extraction of the parton densities from the data in past [7], present [54] and future [8, 9] experiments.
2. The improvement in the factorization scale- and scheme dependence of $F_i(x, Q^2)$ when higher order corrections are included.
3. The issue whether the discrepancy between the combined SLAC-BCDMS data and the NLL approximation of $F_2(x, Q^2)$ can be attributed to higher twist effects or to soft gluon corrections.
4. The modification of the relation between the gluon density and the longitudinal structure function $F_L(x, Q^2)$ due to $\mathcal{O}(\alpha_s^2)$ corrections.

In particular we focus our attention on the data obtained from the BCDMS experiment [53] ($0.1 < x < 0.75$) and the data which will be collected from HERA ($10^{-4} < x < 0.5$) very soon.

3.3.1 Results for F_2

We start with the study of the order α_s^2 corrections to $F_2(x, Q^2)$ since this is the best measured structure function from which the data are mainly extracted. To that purpose we define the quantity

$$K^{(2)}(x, Q^2) = \frac{F_2^{(2)}(x, Q^2)}{F_2^{(1)}(x, Q^2)}. \quad (3.3.1)$$

Note that the parton densities represented by $G(x, M^2)$, $\Sigma(x, M^2)$ (3.1.7) and $\Delta(x, M^2)$ (3.1.8) occurring in (3.1.6) are determined in such a way that $F_2^{(1)}(x, Q^2)$ fits the data. The deviation of $K^{(2)}$ from 1 will then indicate how the free (non-perturbative) parameters describing the x -dependence of the parton densities have to be modified in order to bring $F_2^{(2)}(x, Q^2)$ in agreement with the data.

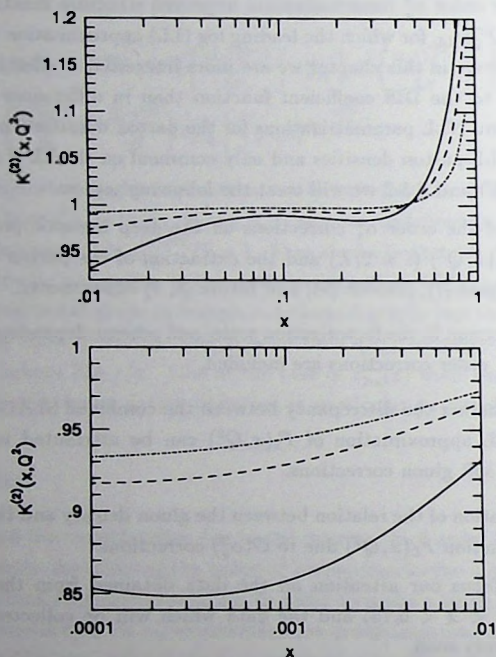


Fig. 3.8. The quantity $K^{(2)}(x, Q^2)$ (3.3.1) (MTB1MS) in the region $0.01 < x < 0.9$ for $Q^2 = 10 \text{ GeV}^2$ (solid line), $Q^2 = 100 \text{ GeV}^2$ (dashed line) and $Q^2 = 10^4 \text{ GeV}^2$ (dashed dotted line) and in the region $10^{-4} < x < 10^{-2}$ for $Q^2 = 10 \text{ GeV}^2$ (solid line), $Q^2 = 50 \text{ GeV}^2$ (dashed line) and $Q^2 = 100 \text{ GeV}^2$ (dashed dotted line).

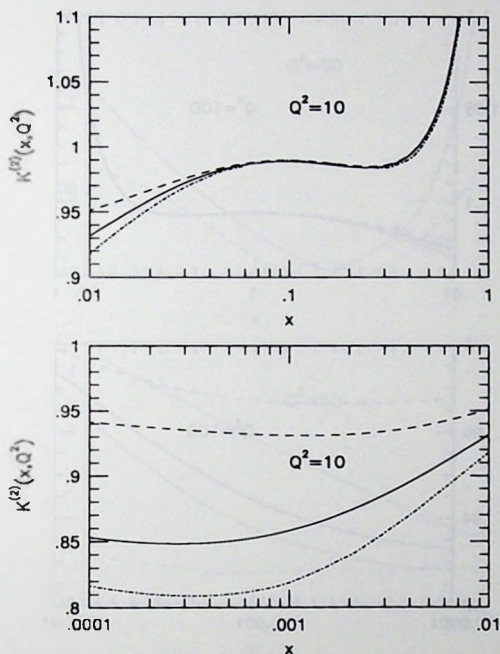


Fig. 3.9. Parton density dependence of $K^{(2)}(x, Q^2)$ at $Q^2 = 10 \text{ GeV}^2$ in the region $10^{-4} < x < 0.9$: MTB1MS (solid line), MTB2MS (dashed line), HMRSB (dashed dotted line).

In fig. 3.8 (MTB1MS set) we have plotted the ratio $K^{(2)}$ (3.3.1) for the values $Q^2 = 10, 100$ and 10^4 GeV^2 in the range $0.01 \leq x \leq 0.9$ which is accessible to current and past experiments. For future as well as current experiments we have also studied the range $10^{-4} < x < 10^{-2}$ for $Q^2 = 10, 50$ and 100 GeV^2 . Fig. 3.8 reveals large corrections in the regions $x > 0.5$ and $x < 0.01$ in particular at small Q^2 values. For $x > 0.5$ the large positive corrections are wholly due to soft gluon radiation which is represented by the logarithmic terms $\ell n^j(1-z)/(1-z)_+$ appearing in the non-singlet

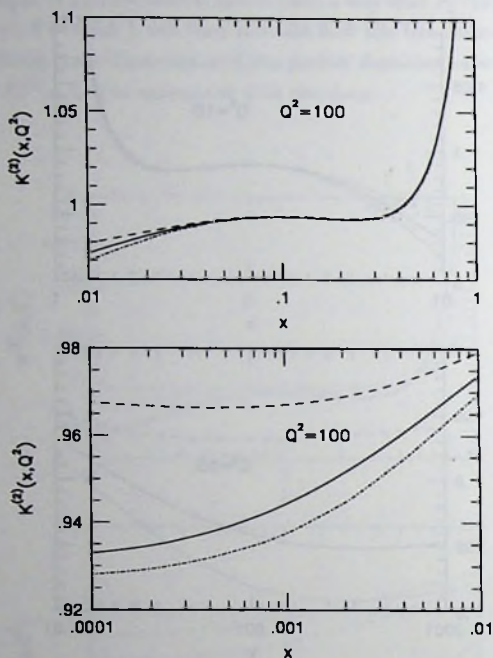


Fig. 3.10. Parton density dependence of $K^{(2)}(x, Q^2)$ at $Q^2 = 100 \text{ GeV}^2$ in the region $10^{-4} < x < 0.9$: MTB1MS (solid line), MTB2MS (dashed line), HMRSB (dashed dotted line).

part of the coefficient function. As has been discussed in the last part of the previous section, the large negative corrections to $F_2(x, Q^2)$ in the region $10^{-4} < x < 10^{-2}$ do not only originate from soft gluon exchanges in t -channel graphs, represented by the $\ln^j z/z$ terms in $\tilde{e}_{2,g}^{(2)}(z)$ near $z = x$. It turns out that the region $z > x$ is important too. Moreover the contribution of the third order anomalous dimension cannot be neglected here like in the non-singlet case. In fig. 3.9 ($Q^2 = 10 \text{ GeV}^2$) and fig. 3.10 ($Q^2 = 100 \text{ GeV}^2$) we have investigated the dependence of $K^{(2)}$ (3.3.1) on the chosen

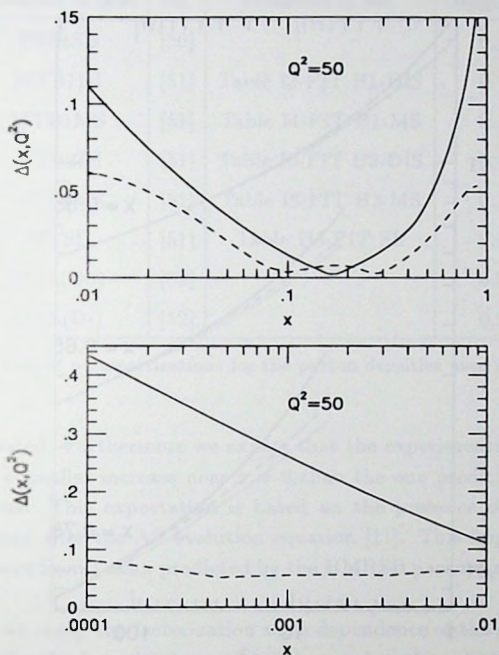


Fig. 3.11. Factorization scale dependence represented by the quantity $\Delta^{(i)}(x, Q^2)$ (3.3.2) at $Q^2 = 50$ GeV² in the region $10^{-4} < x < 0.9$. $\Delta^{(1)}(x, Q^2)$ (solid line), $\Delta^{(2)}(x, Q^2)$ (dashed line). (MTB1MS parametrization.)

parton densities. Here we have taken the MTB1MS, MTB2MS and HMRSB sets (see table 3.2). Note that the gluon density $G(z, M^2)$ in MTB2MS shows a much steeper rise near $z = 0$ than in the other two sets. Comparing fig. 3.9 with fig. 3.10 the difference between the three predictions for $K^{(2)}$ becomes less when Q^2 gets larger, which can be attributed to the decrease of the running coupling constant. The figures reveal that the parametrization with the steepest gluon behaviour provides us with the smallest correction. This feature can be traced back to the characteristics of the

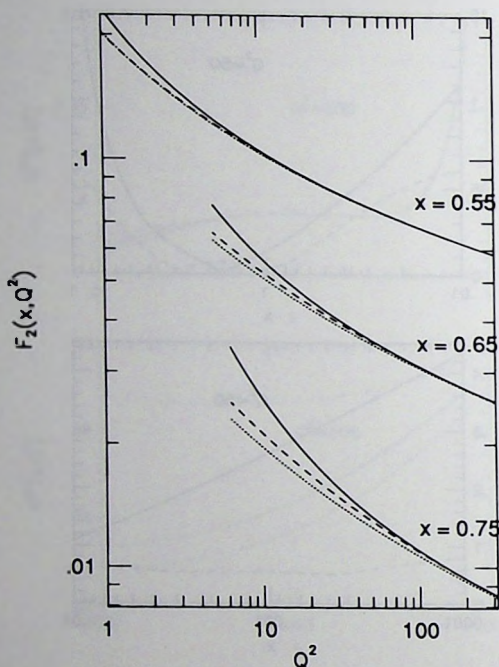


Fig. 3.12. The proton structure function $F_2(x, Q^2)$ in the large x -region:

$F_2^{NLL+HT}(x, Q^2)$: NLL + higher twist, see [55] (solid line);

$F_2^{NLL}(x, Q^2)$: NLL see [55] (dotted line);

$F_2^{AIP}(x, Q^2)$: see (3.3.3) (dashed line)

AP equation which mixes the gluon density $G(z, M^2)$ and the singlet combination of the quark densities $\Sigma(z, M^2)$, (3.2.40). Like the gluon density the latter gets very large at small x which can be wholly attributed to the contribution of the sea quarks. Now $\Sigma(z, M^2)$ already shows up at the Born level ($F_2^{(0)}$), whereas $G(z, M^2)$ only appears in $F_2^{(1)}$ and $F_2^{(2)}$. It turns out that when the gluon density gets steeper it strongly enhances $F_2^{(1)}$ via $\Sigma(z, M^2)$ so that the negative effect due to the coefficient function

Notation in text	ref.	Notation in ref.	$\Lambda_{\text{QCD}}(\text{GeV})$
HMRSB	[50]		0.190
MTB1DI	[51]	Table I3-FIT B1-DIS	0.194
MTB1MS	[51]	Table I4-FIT B1-MS	0.194
MTB2DI	[51]	Table I5-FIT B2-DIS	0.191
MTB2MS	[51]	Table I6-FIT B2-MS	0.191
MTSL	[51]	Table II3-FIT SL	0.144
WFS(D0)	[52]		0.215
WFS(D-)	[52]		0.215

Table 3.2. List of parametrizations for the parton densities used in this chapter.

$\bar{C}_{2,g}^{(2)}$ is compensated. Furthermore we expect that the experimentally observed gluon density shows a smaller increase near $z = 0$ than the one predicted by the existing parametrizations. This expectation is based on the presence of non-perturbative effects which may alter the AP evolution equation [11]. This implies that $K^{(2)}$ will deviate even more from 1 than predicted by the HMRSB parametrization in figs. 3.9, 3.10.

In fig. 3.11 we study the factorization scale dependence of the structure functions $F_2^{(1)}$ and $F_2^{(2)}$. For the factorization scale we have taken the values $M = \frac{1}{2}Q, Q, 2Q$. To investigate the M -dependence it is very convenient to define the quantity

$$\Delta^{(i)} = \frac{\max(F_2^{(i)}(\frac{1}{2}Q), F_2^{(i)}(Q), F_2^{(i)}(2Q)) - \min(F_2^{(i)}(\frac{1}{2}Q), F_2^{(i)}(Q), F_2^{(i)}(2Q))}{\text{average}(F_2^{(i)}(\frac{1}{2}Q), F_2^{(i)}(Q), F_2^{(i)}(2Q))} \quad (3.3.2)$$

Fig. 3.11 reveals that $\Delta^{(2)} < \Delta^{(1)}$, so $F_2^{(2)}$ is less sensitive to the chosen scale than $F_2^{(1)}$, except in the region $x > 0.2$ where no improvement appears. However we want to stress that this improvement in the small x -region is very sensitive to the choice of n_f (the number of light flavours) and it completely disappears when $n_f \geq 5$. This is mainly due to the gluonic coefficient function $C_{2,g}$ (3.2.54) which is proportional to n_f . For $x = 0.5$ we also studied the improvement of the factorization scale dependence by comparing $(F_2^{(0)})_{\text{LL}}, (F_2^{(0)})_{\text{NLL}}, (F_2^{(1)})_{\text{LL}}$ and $(F_2^{(1)})_{\text{NLL}}$. We did not see any difference between the LL and NLL parametrization for $F_2^{(0)}$ as well as $F_2^{(1)}$. However $F_2^{(1)}$ is considerably less sensitive to the chosen scale than $F_2^{(0)}$, showing that the coefficient

function plays a more important role in the improvement of the factorization scale dependence than the second order contribution to the anomalous dimension. Notice that the latter accounts for the difference between the LL and NLL parton densities.

In fig. 3.12 we try to improve a recent fit made in [55, 56] to the combined SLAC-BCDMS data. In this reference one has shown that in the region $x > 0.5$ the combined data cannot be fitted by the fully order α_s renormalization group improved structure function F_2^{LT} (dotted line in fig. 3.12). Here the superscript LT refers to leading twist and F_2^{LT} can be identified with the NLL structure function $F_2^{(1)}$. A better fit (solid line in fig. 3.12) was only possible when "higher twist terms" were taken into account, so that additional free parameters had to be introduced. This fit is given by the function $F_2^{HT} = F_2^{LT}(1 + C(x)/Q^2)$, where $C(x)$ represents the higher twist effect and is given in table 3.2 of [56]. The function $C(x)$ had been chosen in such a way that the best fit to the data was obtained. In our opinion the difference between the data and F_2^{LT} can be attributed to the large logarithmic terms of the type mentioned in (3.2.87) which show up in the higher order corrections to the non-singlet coefficient function. These contributions, which are due to soft gluon radiation, were not taken into account in the analysis of [55, 56]. To estimate the effect of the missing order α_s^2 part of the NS coefficient function in F_2^{LT} [55] we approximate $F_2^{(2)}(x, Q^2)$ for $x > 0.5$ by

$$F_2^{app}(x, Q^2) = x \int_x^1 \frac{dz}{z} F_2^{LT}\left(\frac{x}{z}, Q^2\right) \left\{ 1 + \left(\frac{\alpha_s(Q^2)}{4\pi} \right)^2 \bar{c}_{2,q}^{(2),NS}(z, 1) \right\} , \quad (3.3.3)$$

which is a reasonable approximation since $\bar{c}_{2,q}^{(2),PS}$ and $\bar{c}_{2,g}^{(2)}$ are negligible in this region. Expression (3.3.3) is represented by the dashed line in fig. 3.12 and we observe that the latter is closer to F_2^{HT} than F_2^{LT} . Notice that we have rescaled F_2^{app} a little bit so that $F_2^{app} = F_2^{HT}$ at $Q^2 = 316 \text{ GeV}^2$. The approximation can be improved by including soft gluon corrections beyond $\mathcal{O}(\alpha_s^2)$. In order to get a better description of the deep inelastic data taken at large x and small Q^2 one should resum these corrections using the soft gluon resummation techniques in [46].

3.3.2 Results for F_L

We now focus our attention on the effect of the order α_s^2 contribution to the longitudinal structure function $F_L(x, Q^2)$. In particular we are interested in the ratio of the longitudinal and transverse cross section defined by $R = \sigma_L/\sigma_T$. The order α_s^2

corrected $R^{(n)}$ is given by

$$R^{(n)}(x, Q^2) = \frac{F_L^{(n)}(x, Q^2)}{\left(1 + \frac{4M_p^2 x^2}{Q^2}\right) F_2^{(n-1)}(x, Q^2) - F_L^{(n)}(x, Q^2)} \quad (n = 1, 2, 3) \quad (3.3.4)$$

where M_p denotes the proton mass.

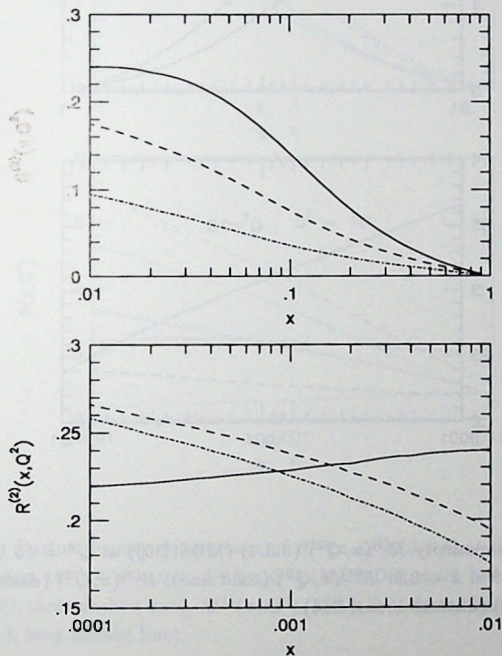


Fig. 3.13. The quantity $R^{(2)}(x, Q^2)$ (3.3.4) (MRS(D0)) in the region $0.01 < x < 0.9$ for $Q^2 = 10 \text{ GeV}^2$ (solid line), $Q^2 = 100 \text{ GeV}^2$ (dashed line) and $Q^2 = 10^4 \text{ GeV}^2$ (dashed dotted line) and in the region $10^{-4} < x < 10^{-2}$ for $Q^2 = 10 \text{ GeV}^2$ (solid line), $Q^2 = 50 \text{ GeV}^2$ (dashed line) and $Q^2 = 100 \text{ GeV}^2$ (dashed dotted line).

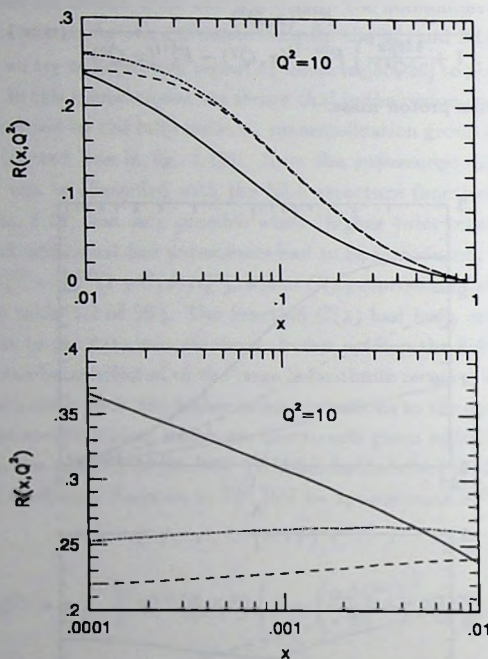


Fig. 3.14. The quantity $R^{(i)}(x, Q^2)$ (3.3.4) (MRS(D0)) at $Q^2 = 10 \text{ GeV}^2$ in the region $10^{-4} < x < 0.9$: $R^{(1)}(x, Q^2)$ (solid line), $R^{(2)}(x, Q^2)$ (dashed line) and $R^{(3)}(x, Q^2)$ (dashed dotted line).

In fig. 3.13 (MRS(D0)) we have plotted $R^{(2)}$ in the range $0.01 \leq x \leq 1$ for $Q^2 = 10, 100$ and 10^4 GeV^2 and in the region $10^{-4} < x < 10^{-2}$ for $Q^2 = 10, 50$ and 100 GeV^2 . The figure reveals that $R^{(2)}$ is very small in the large- x region ($0.1 < x < 1$). For $x < 0.1$ it increases very rapidly at decreasing x -values. Furthermore when Q^2 gets small (e.g. $Q^2 = 10 \text{ GeV}^2$) $R^{(2)}$ hardly varies in the range $10^{-4} < x < 3 \cdot 10^{-3}$. For $x > 0.1$ the non-singlet part of the coefficient function dominates the longitudinal structure function $F_L(x, Q^2)$. Here the contributions due to $\bar{c}_{L,q}^{(1),NS}$ as well as $\bar{c}_{L,q}^{(2),NS}$

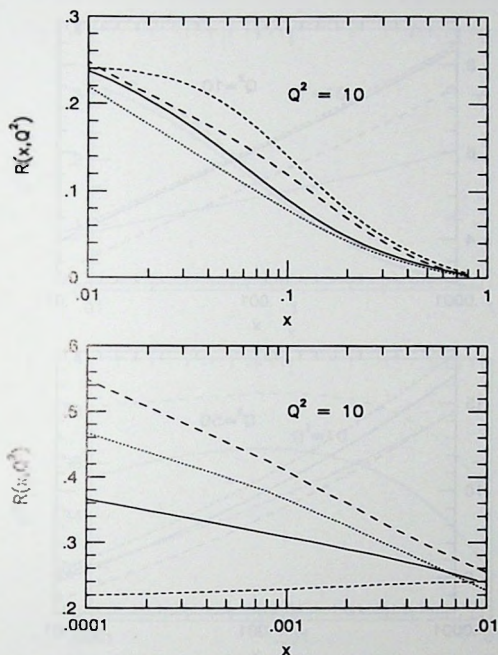


Fig. 3.15. Parton density dependence of $R^{(i)}(x, Q^2)$ (3.3.4) at $Q^2 = 10 \text{ GeV}^2$ in the region $10^{-4} < x < 0.9$: $R^{(1)}(x, Q^2)$ (MRS(D0), solid line), $R^{(2)}(x, Q^2)$ (MRS(D0), short dashed line), $R^{(1)}(x, Q^2)$ (MRS(D-), dotted line), $R^{(2)}(x, Q^2)$ (MRS(D-), long dashed line).

are positive although there are no soft gluon corrections of the type $\ln^i(1-z)/(1-z)$ present in $\bar{c}_{L,q}^{(2),NS}$. For $x < 0.1$ $F_L(x, Q^2)$ is dominated by the gluonic coefficient function although the pure singlet part is not negligible. In the large- x region $F_L^{(2)} > F_L^{(1)}$ and their difference is small. At small x ($x < 6 \cdot 10^{-3}$ for MRS(D0)) $F_L^{(1)} > F_L^{(2)}$, but here the difference between $F_L^{(1)}$ and $F_L^{(2)}$ is much larger. This difference is due to $\bar{c}_{L,g}^{(2)}$ which leads to negative contributions to $F_L(x, Q^2)$ in the small- x region. However

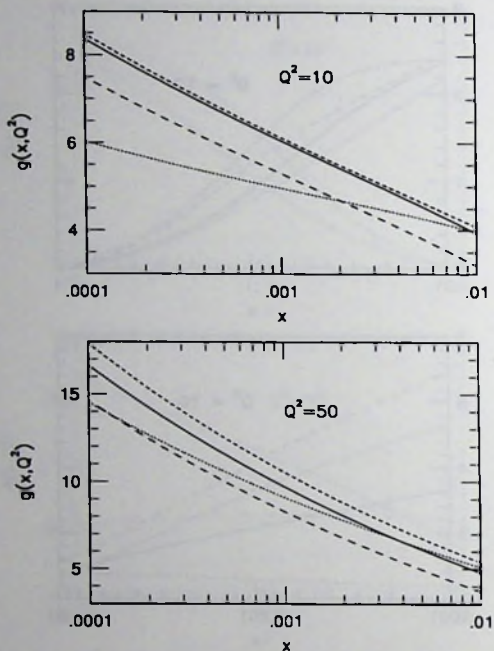


Fig. 3.16. The quantity $g(x, Q^2)$ (3.3.5) (MTB1MS) in the region $10^{-4} < x < 10^{-2}$ for $Q^2 = 10, 50 \text{ GeV}^2$: $F_L(x, Q^2) = F_L^{(1)}(x, Q^2)$ (solid line), $F_L(x, Q^2) = F_L^{(2)}(x, Q^2)$ (dotted line), $xG(x, Q^2)$ (short dashed line), $2.5xG(2.5x, Q^2)$ (long dashed line).

the sign and size of the contribution at small x wholly depends on the chosen gluon density $G(x/z, M^2)$. If the latter rises very steeply near $x = 0$, as is for instance the case in the MRS(D-) parametrization, the correction due to $\bar{\alpha}_{L,g}^{(2)}(z)$ is positive because the large z -region becomes more important.

The above findings for $F_L(x, Q^2)$ also hold for $R(x, Q^2)$ because of the relation between these functions (3.3.4). This is revealed by fig. 3.14 where we compare $R^{(1)}$

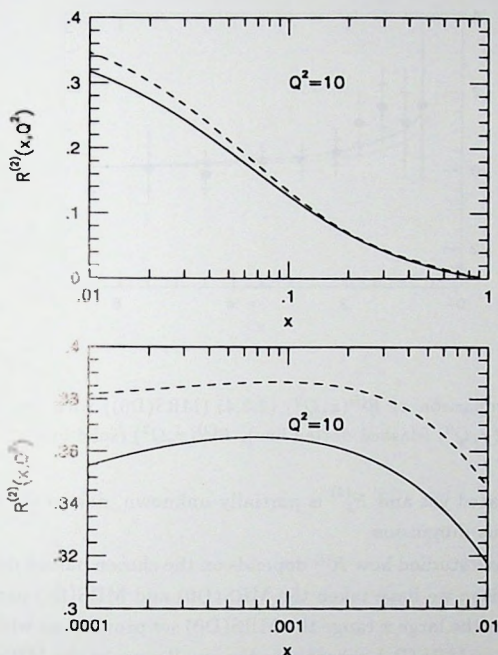


Fig. 3.17. Scheme dependence of $R^{(2)}(x, Q^2)$ (3.3.4) at $Q^2 = 10 \text{ GeV}^2$ in the region $10^{-4} < x < 0.9$: MTB1MS (\overline{MS} scheme, solid line), MTB1DI (DIS scheme, dashed line).

to $R^{(2)}$ for $Q^2 = 10 \text{ GeV}^2$. We observe that in the range $0.01 < x < 1$ $R^{(2)}$ is slightly above $R^{(1)}$, whereas for $x < 0.01$ $R^{(1)} > R^{(2)}$. Furthermore in the small- x region the difference between $R^{(2)}$ and $R^{(1)}$ is quite large and can amount to 40% of $R^{(1)}$ at $x = 10^{-4}$. In fig. 3.14 we have also plotted $R^{(3)}$, where $F_L^{(3)}$ is put equal to $F_L^{(2)}$ since nothing is known about the order α_s^3 contribution to F_L . In the range $0.01 \leq x \leq 1$ $R^{(3)} \sim R^{(2)}$ whereas for $x < 0.01$ $R^{(3)}$ is slightly larger than $R^{(2)}$. However this result has to be interpreted with caution since one should bear in mind that $F_L^{(3)}$

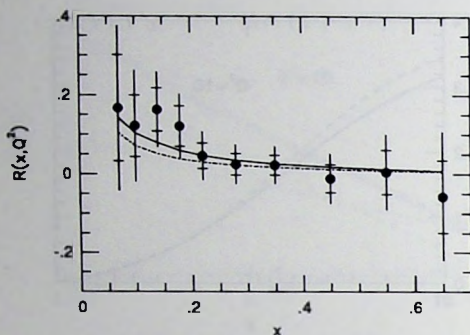


Fig. 3.18. Comparison of $R^{(i)}(x, Q^2)$ (3.3.4) (MRS(D0)) with the BCDMS data [59]: $R^{(1)}(x, Q^2)$ (dashed dotted line), $R^{(2)}(x, Q^2)$ (solid line).

has not been calculated yet and $F_2^{(2)}$ is partially unknown, due to the missing of the three-loop anomalous dimension.

In fig. 3.15 we have studied how $R^{(i)}$ depends on the chosen parton density (see also [60]). For a comparison we have taken the MRS(D0) and MRS(D-) parametrizations listed in table 3.2. In the large x range the MRS(D0) set provides us with larger values for $R^{(i)}$ ($i = 1, 2$) than MRS(D-), whereas in the small x range the MRS(D0) set leads to smaller values for $R^{(i)}$ ($i = 1, 2$) than MRS(D-). The difference is in particular striking in the small x range where $R^{(1)}$ (MRS(D-)) can become approximately 1.3 times larger than $R^{(1)}$ (MRS(D0)). This is because $F_L^{(1)}$ is much more sensitive to the gluon density than $F_2^{(0)}$. Notice that the $\mathcal{O}(\alpha_s^2)$ corrections are positive in the case of MRS(D-) and negative in the case of MRS(D0). Therefore if second order corrections are included $R^{(2)}$ (MRS(D0)) even moves further from $R^{(2)}$ (MRS(D-)) (factor of 2.5). We should remark that the picture looks different when one makes a comparison between the MTB1MS and MTB2MS parametrizations, which are considered to be the obsolete equivalents of MRS(D0) and MRS(D-), respectively. For this comparison we refer to [10]. Also striking is that when the gluon density shows a steep behaviour near $z = 0$ (The Lipatov pomeron effect included in MRS(D-)), the higher order QCD corrections get smaller than in the case of MRS(D0), where the gluon density shows a less steep behaviour. Irrespective which parton density one chooses, the

convergence of the perturbation series for R is very slow in the small- x region. As a consequence the extraction of the gluon density from the longitudinal structure function, as proposed in the literature [57, 58], will be hampered. From the lowest order approximation for F_L (i.e. $F_L^{(1)}$) one can derive the following relation which holds in the small- x region (see eq. 9 in [57]).

$$g(x, Q^2) \equiv \frac{x}{a} G\left(\frac{x}{a}, Q^2\right) = 1.77 \frac{3\pi}{2\alpha_s(Q^2)} F_L(x, Q^2) , \quad (3.3.5)$$

where a is an arbitrary parameter which for $F_L = F_L^{(1)}$ is usually chosen to be 0.4 [57, 58]. However we discovered that in the case of the MTB1 set the above approximation becomes much better when $a = 1$ and $F_L = F_L^{(1)}$. In fig. 3.16 this is checked for $10^{-4} < x < 10^{-2}$ at $Q^2 = 10$ and 50 GeV². The figure also reveals that at low Q^2 the above approximation breaks down when $F_L^{(1)}$ is replaced by $F_L^{(2)}$, which can be attributed to the large negative contribution of the second order gluonic coefficient function $\mathcal{G}_{Lg}^{(2)}$. If we assume that $F_L^{(2)}$ gives a much better description of the data than $F_L^{(1)}$ the relation (3.3.5) is not suitable any more to determine the gluon density. In the case of the MTB2 set $F_L^{(2)}$ is very close to $F_L^{(1)}$, so that the relation (3.3.5) can be used to determine the gluon density. However as explained above we expect that the measured gluon density will deviate from the one given by the MTB2 parametrization in particular in the small- x region.

We have also studied the factorization scale (M) and scheme dependence of $F_L^{(i)}$ and $R^{(i)}$. One observes a considerable improvement in the scale dependence of $F_L^{(2)}$ with respect to $F_L^{(1)}$ in particular in the region $10^{-4} < x < 10^{-2}$. The difference disappears in the large- x regime where the plots are almost the same as the ones shown for $\Delta^{(1)}$ and $\Delta^{(2)}$ in the case of $F_2^{(1)}$ and $F_2^{(2)}$ (see fig. 3.11). Further it turns out that $R^{(1)}$ and $R^{(2)}$ are much more sensitive to the choice made for M than the corresponding $F_L^{(1)}$ and $F_L^{(2)}$. This can be wholly attributed to the strong scale dependence of $F_2^{(0)}$ appearing in the denominator of $R^{(1)}$ (3.3.4) which is of course improved for $F_2^{(1)}$, but not to that extent as is exhibited by $F_L^{(2)}$. In fig. 3.17 we have also compared $R^{(2)}$ calculated in the $\overline{\text{MS}}$ scheme with $R^{(2)}$ calculated in the DIS scheme, using the parametrizations MTB1MS and MTB1DI (table 3.2) respectively. The figure reveals that a change of scheme has little effect on $R^{(2)}$ in the range $10^{-4} < x < 10^{-2}$. The difference is of the order of about 6% of $R^{(2)}$ computed in the $\overline{\text{MS}}$ scheme. Our general experience is that the above quantities are much more dependent on the factorization scale M than on the chosen scheme. Finally we have also plotted $R^{(1)}$ and $R^{(2)}$ in the range $0.05 < x < 0.65$ for which BCDMS data are available [59] (see fig. 3.18). For each data point the average value for Q^2 , i.e.

$\langle Q^2 \rangle$, can be found in table 2 of [59]. It varies from $\langle Q^2 \rangle = 15 \text{ GeV}^2$ at $x = 0.07$ to $\langle Q^2 \rangle = 50 \text{ GeV}^2$ at $x = 0.65$. As already discussed above there is not much difference between $F_L^{(1)}$ and $F_L^{(2)}$ in this region and both are in agreement with the data.

3.3.3 Conclusions

Summarizing the above we have completely calculated the second order contribution to the DIS coefficient functions including their dependence on the renormalization- and mass factorization scale. The effects on the first order renormalization group improved proton structure functions are studied. It turns out that the corrections are appreciable and positive for $F_2(x, Q^2)$ when $x > 0.5$, which can be wholly attributed to soft gluon radiation. In the small- x region the corrections to F_2 as well as F_L are negative and large in particular at small Q^2 values, which cannot be explained by multiple soft gluon exchanges in t -channel graphs only. The size and sign of the radiative corrections also depend on the chosen parton density set and the behaviour of the gluonic coefficient function $C_{i,g}(z)$ in the whole z -region. These large corrections and the still unknown three loop contribution to the anomalous dimension will seriously hamper the extraction of the gluon density from the proton structure function. Since in the small- x region also non-perturbative aspects will play an important role, the extraction of the gluon density will become difficult because of theoretical uncertainties present in perturbative as well as non-perturbative QCD.

Appendices

3A Phase space integrals

Here we list the most complicated two to three body phase space integrals which emerge after the decomposition of the matrix elements in the way described below (3.2.21). All of them contain massive denominators carrying the virtual photon momentum. Some of these massive denominators depend on the polar angle θ and the azimuthal angle ϕ (see (3.2.24)). The kinematics of the two to three body process is given by

$$p_1 + p_5 \rightarrow p_2 + p_3 + p_4, \quad (3A.1)$$

with $\sum_{i=1}^5 p_i = 0$ and p_5 denoting the photon momentum. Therefore we have $p_i^2 = 0$ ($i = 1-4$), $p_5^2 = q^2 = -Q^2$ and further we define $P_{ij} = (p_i + p_j)^2$. The above momenta

can be expressed in the angular variables θ and ϕ and the kinematical invariants indicated in (3.2.22) and (3.2.23), depending on the chosen frame (see appendices C in [27], E in [28]) and D in [31]). The most complicated integrals are ($\varepsilon = n - 4$)

$$\int dPS^{(3)} \frac{1}{P_{24}P_{25}P_{34}P_{35}} = \frac{1}{(4\pi)^{\varepsilon+3}} \frac{(s+Q^2)^{\varepsilon-3}}{\Gamma(1+\varepsilon)} (1-z)^{\varepsilon-1} \left[\frac{4}{\varepsilon^3} - \frac{4}{\varepsilon^2} \ell n z + \frac{1}{\varepsilon} \left\{ -2Li_2(1-z) + \ell n^2 z - 3\zeta(2) \right\} + 5S_{1,2}(1-z) + \frac{5}{6} \ell n^3 z + 3\zeta(2) \ell n z + 4\ell n z Li_2(1-z) + 2\ell n z Li_2(-z) + 3\zeta(3) - 4Li_3(-z) \right], \quad (3A.2)$$

$$\int dPS^{(3)} \frac{1}{P_{12}P_{34}P_{35}} = \frac{1}{(4\pi)^{\varepsilon+3}} \frac{(s+Q^2)^{\varepsilon-2}}{\Gamma(1+\varepsilon)} (1-z)^{\varepsilon-1} \left[-\frac{1}{\varepsilon^2} \ell n z + \frac{1}{\varepsilon} \left\{ \frac{3}{4} \ell n^2 z \right\} + 5S_{1,2}(1-z) - 4Li_3(-z) + \frac{5}{2} \ell n z Li_2(1-z) + 2\ell n z Li_2(-z) + \frac{3}{4} \zeta(2) \ell n z + \frac{11}{24} \ell n^3 z - 3\zeta(3) \right], \quad (3A.3)$$

$$\int dPS^{(3)} \frac{1}{P_{12}P_{13}P_{25}P_{35}} = \frac{1}{(4\pi)^{\varepsilon+3}} \frac{(s+Q^2)^{\varepsilon-3}}{\Gamma(1+\varepsilon)} \frac{(1-z)^{\varepsilon}}{1+z} \left[-\frac{8}{\varepsilon^2} \ell n z + \frac{1}{\varepsilon} \left\{ -8Li_2(1-z) - 4Li_2(-z) - 4\ell n z \ell n(1+z) - \ell n^2 z - 2\zeta(2) \right\} + 4Li_3\left(\frac{1-x}{1+z}\right) - 4Li_3\left(-\frac{1-x}{1+z}\right) - 2S_{1,2}(1-z) + 4Li_3(1-z) + 4S_{1,2}(-z) - 2Li_3(-z) - 2\ell n z Li_2(1-z) + 4\ell n(1+z) Li_2(-z) + 2\zeta(2) \ell n(1+z) + 4\zeta(2) \ell n z + 2\ell n z \ell n^2(1+z) - \ell n^2 z \ell n(1+z) + \frac{1}{6} \ell n^3 z - 2\zeta(3) \right], \quad (3A.4)$$

$$\int dPS^{(3)} \frac{1}{P_{13}P_{25}P_{35}} = \frac{1}{(4\pi)^{\varepsilon+3}} \frac{(s+Q^2)^{\varepsilon-2}}{\Gamma(1+\varepsilon)} \frac{(1-z)^{\varepsilon}}{1+z} \left[\frac{2}{\varepsilon^2} \ell n z + \frac{1}{\varepsilon} \left\{ 2Li_2(1-z) + 2Li_2(-z) + 2\ell n z \ell n(1+z) + \zeta(2) \right\} - 2Li_3\left(\frac{1-x}{1+z}\right) + 2Li_3\left(-\frac{1-x}{1+z}\right) - \frac{1}{2} \zeta(2) \ell n z - \frac{1}{6} \ell n^3 z \right], \quad (3A.5)$$

$$\int dPS^{(3)} \frac{P_{12}}{P_{14}^2 P_{25} P_{35}} = \frac{1}{(4\pi)^{\epsilon+3}} \frac{(s+Q^2)^{\epsilon-2}}{\Gamma(1+\epsilon)} (1-z)^\epsilon \left[\frac{1}{\epsilon^2} \left\{ -1 - \frac{1}{3}z + z^{-1} + \frac{1}{3}z^{-2} \right\} + \frac{1}{\epsilon} \left\{ \left(1 + \frac{1}{3}z + z^{-1} + \frac{1}{3}z^{-2}\right) \ell n z - \frac{4}{3} + \frac{2}{9}z + \frac{4}{3}z^{-1} - \frac{2}{9}z^{-2} \right\} + \left(1 + \frac{1}{3}z + z^{-1} + \frac{1}{3}z^{-2}\right) \left(Li_2(1-z) - \frac{1}{2} Li_2(-z) - \frac{1}{2} \ell n z \ell n(1+z) + \frac{1}{4} \ell n^2 z \right) + \left(\frac{7}{6} - \frac{2}{9}z + \frac{7}{6}z^{-1} - \frac{2}{9}z^{-2} \right) \ell n z + \left(\frac{3}{4} + \frac{1}{4}z - \frac{5}{4}z^{-1} - \frac{5}{12}z^{-2} \right) \zeta(2) - \frac{17}{18} + \frac{11}{27}z + \frac{17}{18}z^{-1} - \frac{11}{27}z^{-2} \right] , \quad (3A.6)$$

$$\int dPS^{(3)} \frac{1}{P_{14} P_{25} P_{35}} = \frac{1}{(4\pi)^{\epsilon+3}} \frac{(s+Q^2)^{\epsilon-2}}{\Gamma(1+\epsilon)} (1-z)^\epsilon \left[\frac{1}{\epsilon^2} \left\{ 2 - 2z^{-1} \right\} + \frac{1}{\epsilon} \left\{ -2(1+z^{-1}) \ell n z + 2 - 2z^{-1} \right\} + (1+z^{-1})(-2 Li_2(1-z) + Li_2(-z) + \ell n z \ell n(1+z) - 2 \ell n z) - \left(\frac{1}{2} + z^{-1} \right) \ell n^2 z + \left(-\frac{3}{2} + \frac{5}{2}z^{-1} \right) \zeta(2) + 2 - 2z^{-1} \right] . \quad (3A.7)$$

3B The DIS coefficient functions in the \overline{MS} and DIS scheme

In this appendix we will present the explicit expressions for the DIS coefficient functions $C_{i,k}(z, Q^2/M^2)$ ($i = 2, L, k = q, \bar{q}, g$) which are calculated in section 3.2. In order to make the presentation self-contained, we also give the order α_s contributions $c_{i,k}^{(1)}$ which have already been presented in the literature [18]–[20]. The non-singlet and pure singlet part of the longitudinal coefficient function can be found in [42]. We will refer to them where appropriate. Finally the renormalization scale in the coupling constant α_s is always taken to be equal to the factorization scale M . If one chooses R different from M , $\alpha_s(M^2)$ has to be replaced following the prescription in (3.2.56).

3B.1 Order α_s^2 corrected coefficient functions in the \overline{MS} scheme

The coefficient functions presented in (3.2.48)–(3.2.54) read as follows

$$\bar{C}_{L,q}^{NS} = \frac{\alpha_s}{4\pi} C_F \left[4z \right] + \left(\frac{\alpha_s}{4\pi} \right)^2 \left[\left\{ C_F^2 \left(8z(2\ell n(1-z) - \ell n z) + 4(2+z) \right) + C_A C_F \left(-\frac{44}{3}z \right) + n_f C_F \left(\frac{8}{3}z \right) \right\} L_M \right]$$

$$+ \bar{c}_{L,q}^{(2),NS} \Big] , \quad (3B.1)$$

where $\bar{a}_{L,q}^{(2),NS}$ is given in (8) of [42].

$$\begin{aligned} \bar{C}_{2,q}^{NS} = & 1 + \frac{\alpha_s}{4\pi} \left[C_F \left\{ 4 \left(\frac{1}{1-z} \right)_+ - 2(1+z) + 3\delta(1-z) \right\} L_M \right. \\ & + C_F \left\{ 4 \left(\frac{\ell n(1-z)}{1-z} \right)_+ - 3 \left(\frac{1}{1-z} \right)_+ - 2(1+z)\ell n(1-z) \right. \\ & \left. \left. - 2 \frac{1+z^2}{1-z} \ell n z + 6 + 4z + \delta(1-z)(-4\zeta(2) - 9) \right\} \right] \\ & + \left(\frac{\alpha_s}{4\pi} \right)^2 \left[\left\{ C_F^2 \left(16 \left(\frac{\ell n(1-z)}{1-z} \right)_+ + 12 \left(\frac{1}{1-z} \right)_+ \right. \right. \right. \\ & \left. \left. - 8(1+z)\ell n(1-z) - 4 \frac{1+z^2}{1-z} \ell n z + 2(1+z)\ell n z - 2(5+z) \right. \right. \\ & \left. \left. + \left\{ -8\zeta(2) + \frac{9}{2} \right\} \delta(1-z) \right\} \right. \\ & + C_A C_F \left(-\frac{22}{3} \left(\frac{1}{1-z} \right)_+ + \frac{11}{3}(1+z) - \frac{11}{2}\delta(1-z) \right) \\ & + n_f C_F \left(\frac{4}{3} \left(\frac{1}{1-z} \right)_+ - \frac{2}{3}(1+z) + \delta(1-z) \right) \Big\} L_M^2 \\ & + \left\{ C_F^2 \left(24 \left(\frac{\ell n^2(1-z)}{1-z} \right)_+ - 12 \left(\frac{\ell n(1-z)}{1-z} \right)_+ - (32\zeta(2) \right. \right. \\ & + 45) \left(\frac{1}{1-z} \right)_+ + \frac{1+z^2}{1-z} (4\ell n^2 z - 24\ell n z \ell n(1-z) - 6\ell n z) \\ & + \frac{1+z^2}{1+z} (4\ell n^2 z - 16Li_2(-z) - 16\ell n z \ell n(1+z) \\ & - 8\zeta(2)) + (1+z) (4Li_2(1-z) + 4\ell n z \ell n(1-z) - 12\ell n^2(1-z) \\ & - 4\ell n^2 z + 16\zeta(2)) + 8(2+3z)\ell n(1-z) - 2(3+11z)\ell n z \\ & + 2(19+14z) + \left\{ 40\zeta(3) - 12\zeta(2) - \frac{51}{2} \right\} \delta(1-z) \Big\} \\ & + C_A C_F \left(-\frac{44}{3} \left(\frac{\ell n(1-z)}{1-z} \right)_+ + \left(\frac{367}{9} - 8\zeta(2) \right) \left(\frac{1}{1-z} \right)_+ \right. \\ & + \frac{1+z^2}{1-z} \left(\frac{44}{3} \ell n z + 2\ell n^2 z \right) + \frac{1+z^2}{1+z} (8Li_2(-z) - 2\ell n^2 z \\ & + 8\ell n z \ell n(1+z) + 4\zeta(2)) + (1+z) \left(\frac{22}{3} \ell n(1-z) + 4\zeta(2) \right) \\ & \left. - \frac{1}{9}(164 + 434z) + \left(-12\zeta(3) + \frac{88}{3}\zeta(2) + \frac{215}{6} \right) \delta(1-z) \right) \end{aligned}$$

$$\begin{aligned}
& + n_f C_F \left(\frac{8}{3} \left(\frac{\ell n(1-z)}{1-z} \right)_+ - \frac{58}{9} \left(\frac{1}{1-z} \right)_+ - \frac{8}{3} \frac{1+z^2}{1-z} \ell n z \right. \\
& \left. - \frac{4}{3} (1+z) \ell n(1-z) + \frac{1}{9} (32+68z) + \left(-\frac{16}{3} \zeta(2) - \frac{19}{3} \right) \delta(1-z) \right) \} L_M \\
& + \bar{c}_{2,q}^{(2),NS,+} + \bar{c}_{2,q}^{(2),NS,-} \Big] , \tag{3B.2}
\end{aligned}$$

where C_A , C_F denote the colour factors ($C_F = (N^2 - 1)/2N$ and $C_A = N$ for $SU(N)$) and n_f stands for the number of flavours. Further $\bar{c}_{2,q}^{(2),NS,+}$ and $\bar{c}_{2,q}^{(2),NS,-}$ are respectively

$$\begin{aligned}
\bar{c}_{2,q}^{(2),NS,+} = & C_F^2 \left[\frac{1+z^2}{1-z} \left\{ 4\ell n^3(1-z) - (14\ell n z + 9)\ell n^2(1-z) - (4Li_2(1-z) - 12\ell n^2 z \right. \right. \\
& - 12\ell n z + 16\zeta(2) + \frac{27}{2})\ell n(1-z) - \frac{4}{3}\ell n^3 z - \frac{3}{2}\ell n^2 z + (-24Li_2(-z) + 24\zeta(2) \\
& + \frac{61}{2})\ell n z + 12Li_3(1-z) - 12S_{1,2}(1-z) + 48Li_3(-z) - 6Li_2(1-z) + 32\zeta(3) \\
& + 18\zeta(2) + \frac{51}{4} \Big\} + (1+z) \left\{ 2\ell n z \ell n^2(1-z) + 4(Li_2(1-z) - \ell n^2 z)\ell n(1-z) \right. \\
& - 4(Li_2(1-z) + \zeta(2))\ell n z + \frac{5}{3}\ell n^3 z - 4Li_3(1-z) \Big\} + (40 + 8z - 48z^2 - \frac{72z^3}{5} \\
& + \frac{8}{5z^2}) (Li_2(-z) + \ell n z \ell n(1+z)) + (-8 + 40z) (\ell n z Li_2(-z) + S_{1,2}(1-z) \\
& - 2Li_3(-z) - \zeta(2)\ell n(1-z)) + (5 + 9z)\ell n^2(1-z) + \frac{1}{2}(-91 + 141z)\ell n(1-z) \\
& - (28 + 44z)\ell n z \ell n(1-z) - (14 + 30z)Li_2(1-z) + (\frac{29}{2} + \frac{25}{2}z + 24z^2 \\
& + \frac{36z^3}{5})\ell n^2 z + \frac{1}{10}(13 - 407z + 144z^2 - \frac{16}{z})\ell n z + (-10 + 6z - 48z^2 \\
& - \frac{72z^3}{5})\zeta(2) + \frac{407}{20} - \frac{1917z}{20} + \frac{72z^2}{5} + \frac{8}{5z} + \{ 6\zeta(2)^2 - 78\zeta(3) + 69\zeta(2) \\
& + \frac{331}{8} \} \delta(1-z) \Big]
\end{aligned}$$

$$\begin{aligned}
& + C_A C_F \left[\frac{1+z^2}{1-z} \left\{ -\frac{11}{3} \ell n^2(1-z) + (4Li_2(1-z) + 2\ell n^2 z + \frac{44}{3} \ell n z - 4\zeta(2) \right. \right. \\
& + \frac{367}{18} \ell n(1-z) - \ell n^3 z - \frac{55}{6} \ell n^2 z + (4Li_2(1-z) + 12Li_2(-z) - \frac{239}{6}) \\
& \ell n z - 12Li_3(1-z) + 12S_{1,2}(1-z) - 24Li_3(-z) + \frac{22}{3} Li_2(1-z) + 2\zeta(3) \\
& + \frac{22}{3} \zeta(2) - \frac{3155}{108} \left. \right\} + 4(1+z) (Li_2(1-z) + \ell n z \ell n(1-z)) + (-20 - 4z + 24z^2 \\
& + \frac{36z^3}{5} - \frac{8}{3z}) (Li_2(-z) + \ell n z \ell n(1+z)) + (4-20z) (\ell n z Li_2(-z) \\
& + S_{1,2}(1-z) - 2Li_3(-z) - \zeta(2) \ell n(1-z)) + (\frac{133}{6} - \frac{1113}{18} z) \ell n(1-z) \\
& + (-2 + 2z - 12z^2 - \frac{18z^3}{5}) \ell n^2 z + \frac{1}{30} (13 + 1753z - 216z^2 + \frac{24}{z}) \ell n z + \\
& (-2 - 10z + 24z^2 + \frac{36z^3}{5}) \zeta(2) - \frac{9687}{540} + \frac{59157}{540} z - \frac{36z^2}{5} - \frac{4}{5z} \\
& + \left\{ \frac{71}{5} \zeta(2)^2 + \frac{140}{3} \zeta(3) - \frac{251}{3} \zeta(2) - \frac{5465}{72} \right\} \delta(1-z) \Big] \\
& + n_f C_F \left[\frac{1+z^2}{1-z} \left\{ \frac{2}{3} \ell n^2(1-z) - (\frac{8}{3} \ell n z + \frac{29}{9}) \ell n(1-z) - \frac{4}{3} Li_2(1-z) \right. \right. \\
& + \frac{5}{3} \ell n^2 z + \frac{19}{3} \ell n z - \frac{4}{3} \zeta(2) + \frac{247}{54} \left. \right\} + \frac{1}{3} (1 + 13z) \ell n(1-z) - \frac{1}{3} (7 + 19z) \ell n z \\
& - \frac{23}{18} - \frac{27}{2} z + \left\{ \frac{4}{3} \zeta(3) + \frac{38}{3} \zeta(2) + \frac{457}{36} \right\} \delta(1-z) \Big] , \tag{3B.3}
\end{aligned}$$

$$\bar{c}_{2,q}^{(2),NS,-} =$$

$$\begin{aligned}
& C_F \left(C_F - \frac{1}{2} C_A \right) \left[\frac{1+z^2}{1+z} \left\{ (4\ell n^2 z - 16\ell n z \ell n(1+z) - 16Li_2(-z) \right. \right. \\
& - 8\zeta(2) \ell n(1-z) - (2\ell n^2 z - 20\ell n z \ell n(1+z) + 8\ell n^2(1+z) - 8Li_2(1-z)
\end{aligned}$$

$$\begin{aligned}
& +16Li_2(-z) - 8) \ell n z - 16 \ell n(1+z) Li_2(-z) - 8\zeta(2) \ell n(1+z) - 16S_{1,2}(-z) \\
& +16Li_3\left(\frac{1-z}{1+z}\right) - 16Li_3(1-z) + 8S_{1,2}(1-z) + 8Li_3(-z) - 16Li_3\left(-\frac{1-z}{1+z}\right) \\
& + 8\zeta(3) \Big\} + (4+20z) (\ell n^2 z \ell n(1+z) - 2 \ell n z \ell n^2(1+z) - 2\zeta(2) \ell n(1+z) \\
& - 4 \ell n(1+z) Li_2(-z) + 2Li_3(-z) - 4S_{1,2}(-z) + 2\zeta(3)) + (32+32z+43z^2 \\
& - \frac{72z^3}{5} + \frac{8}{5z^2}) (Li_2(-z) + \ell n z \ell n(1+z)) + 8(1+z) (Li_2(1-z) \\
& + \ell n z \ell n(1-z)) + 16(1-z) \ell n(1-z) + (-4-16z-24z^2 + \frac{36z^3}{5}) \ell n^2 \\
& + \frac{1}{5} (-26-106z+72z^2 - \frac{8}{z}) \ell n z + (-4+20z+48z^2 - \frac{72z^3}{5}) \zeta(2) \\
& + \frac{1}{5} (-162+82z+72z^2 + \frac{8}{z}) \Big] . \tag{3B.4}
\end{aligned}$$

In the above expression the terms of the type $\ell n^i(1-z)/(1-z)$ have to be understood in the distributional sense, like in (3B.2).

In the case we have a Z instead of a photon or a W , we should also take into account the (finite) contribution of the axial part of the AC interference term, which equals

$$\begin{aligned}
\bar{C}_{2,q}^{ACaxial} = & \left(\frac{\alpha_s}{4\pi}\right)^2 C_F \Big[32(3z^3 - 3z^2 + z) Li_2(1-z) \\
& - 32\left(\frac{3}{5}z^3 + \frac{1}{3}z - \frac{1}{15}\frac{1}{z^2}\right) \{ Li_2(-z) + \ell n z \ell n(1+z) \} + 16\left(\frac{18}{5}z^3 - 3z^2 \right. \\
& + \frac{4}{3}z) \ell n^2 z + 32\left(\frac{12}{5}z^3 - 3z^2 + \frac{2}{3}z\right) \zeta(2) + 16\left(\frac{1}{15} - \frac{24}{5}z^2 + \frac{12}{5}z - \frac{2}{15}\frac{1}{z} \right. \\
& \left. + \frac{1}{1-z} - \frac{1}{1+z}\right) \ell n z - \frac{8}{5}\left(\frac{1}{3} + 48z^2 - 42z - \frac{41}{3}z\right) \Big] . \tag{3B.5}
\end{aligned}$$

Further we have

$$\begin{aligned}
\bar{C}_{L,q}^{PS} = & n_f \left(\frac{\alpha_s}{4\pi}\right)^2 \Big[C_F T_f \left\{ -32z \ell n z - \frac{32}{3}\left(3 - 2z^2 - \frac{1}{z}\right) \right\} L_M \\
& + \bar{c}_{L,q}^{(2),PS} \Big] , \tag{3B.6}
\end{aligned}$$

with $z\bar{c}_{L,q}^{(2),PS}$ in (9) of [42].

$$\begin{aligned}\bar{C}_{2,q}^{PS} = n_f \left(\frac{\alpha_s}{4\pi} \right)^2 & \left[C_F T_f \left\{ 8(1+z)\ell n z + \frac{4}{3} \left(3 - 4z^2 - 3z + \frac{4}{z} \right) \right\} L_M^2 \right. \\ & + C_F T_f \left\{ 16(1+z) \left(Li_2(1-z) + \ell n z \ell n(1-z) - \ell n^2 z \right) + 32z^2 \ell n z \right. \\ & + \frac{8}{3} \left(3 - 4z^2 - 3z + \frac{4}{z} \right) \ell n(1-z) - \frac{16}{9} \left(39 + 4z^2 - 30z - \frac{13}{z} \right) \left. \right\} L_M \\ & \left. + \bar{c}_{2,q}^{(2),PS} \right] ,\end{aligned}\quad (3B.7)$$

with

$$\begin{aligned}\bar{c}_{2,q}^{(2),PS} = 2C_F T_f & \left\{ 4\ell n z \ell n^2(1-z) - 8\ell n^2 z \ell n(1-z) + \frac{10}{3}\ell n^3 z - 8\zeta(2)\ell n z \right. \\ & - 8\ell n z Li_2(1-z) + 8\ell n(1-z) Li_2(1-z) - 8Li_3(1-z) \left. \right\} + \left(2 - 2z - \frac{8z^2}{3} \right. \\ & + \frac{8}{3z} \left. \right) \ell n^2(1-z) + \left(-\frac{104}{3} + \frac{80z}{3} - \frac{32z^2}{9} + \frac{104}{9z} \right) \ell n(1-z) + (-16 - 16z \\ & - \frac{16z^2}{3} - \frac{16}{3z}) \left(Li_2(-z) + \ell n z \ell n(1+z) \right) + \left(4 - 4z + \frac{32z^2}{3} + \frac{16}{3z} \right) Li_2(1-z) \\ & + (-1 + 15z - \frac{32z^2}{3}) \ell n^2 z + \left(56 - \frac{88z}{3} - \frac{128z^2}{9} \right) \ell n z + 16z^2 \ell n z \ell n(1-z) \\ & + \left(-4 - 12z + \frac{16z^2}{3} - \frac{32}{3z} \right) \zeta(2) + \frac{158}{9} - \frac{422z}{9} + \frac{448z^2}{27} + \frac{344}{27z} \left. \right] .\end{aligned}\quad (3B.8)$$

$$\begin{aligned}\bar{C}_{L,g} = n_f T_f \frac{\alpha_s}{4\pi} & \left[16z(1-z) \right] + n_f \left(\frac{\alpha_s}{4\pi} \right)^2 \left[\left\{ C_F T_f \left(32z \ell n z \right. \right. \right. \\ & + 16(1 - 2z^2 + z) \left. \right\} + C_A T_f \left(64z(1-z)\ell n(1-z) - 128z \ell n z \right. \\ & \left. \left. - \frac{32}{3} \left(3 - 17z^2 + 15z - \frac{1}{z} \right) \right) \right\} L_M + \bar{c}_{L,g}^{(2)} \right] ,\end{aligned}\quad (3B.9)$$

with

$$\bar{c}_{L,g}^{(2)} =$$

$$\begin{aligned}
& 2C_F T_f \left[16z \left(Li_2(1-z) + \ell n z \ell n(1-z) \right) + \left(\frac{-32z}{3} + \frac{64z^3}{5} + \frac{32}{15z^2} \right) \right. \\
& \left(Li_2(-z) + \ell n z \ell n(1+z) \right) + (8 + 24z - 32z^2) \ell n(1-z) - \left(\frac{32z}{3} + \frac{32z^3}{5} \right) \ell n^2 z \\
& + \frac{1}{15} \left(-104 - 624z + 288z^2 - \frac{32}{z} \right) \ell n z + \left(\frac{-32z}{3} + \frac{64z^3}{5} \right) \zeta(2) \\
& \left. - \frac{128}{15} - \frac{304z}{5} + \frac{336z^2}{5} + \frac{32}{15z} \right] \\
& + 2C_A T_f \left[-64z Li_2(1-z) + (32z + 32z^2) \left(Li_2(-z) + \ell n z \ell n(1+z) \right) \right. \\
& + (16z - 16z^2) \ell n^2(1-z) + (-96z + 32z^2) \ell n z \ell n(1-z) + (-16 - 14z \\
& + \frac{464z^2}{3} + \frac{16}{3z}) \ell n(1-z) + 48z \ell n^2 z + (16 + 128z - 208z^2) \ell n z + 32z^2 \zeta(2) \\
& \left. + \frac{16}{3} + \frac{272z}{3} - \frac{848z^2}{9} - \frac{16}{9z} \right] . \tag{3B.10}
\end{aligned}$$

The second moment (3.2.82) of the above expression reads ($T_f = 1/2$)

$$\bar{c}_{L,g}^{(2),2} = n_f C_F \left(-\frac{16}{5} \zeta(3) - \frac{116}{135} \right) + n_f C_A \left(\frac{173}{27} \right) , \tag{3B.11}$$

which agrees with the result presented in eq. 17 of [35]. The higher moments were checked both numerically and analytically. They also agree with the ones listed in eq. 17 of [35].

$$\begin{aligned}
\bar{C}_{2,g} = n_f T_f \frac{\alpha_s}{4\pi} & \left[4(1 - 2z + 2z^2) L_M + 4(1 - 2z + 2z^2) \left(\ell n(1-z) - \ell n z \right) \right. \\
& \left. - 4 + 32z(1-z) \right] + n_f \left(\frac{\alpha_s}{4\pi} \right)^2 \left[\left\{ C_F T_f \left(-4(1 + 4z^2 - 2z) \ell n z \right. \right. \right. \\
& + 8(1 + 2z^2 - 2z) \ell n(1-z) - 2 + 8z \left. \right) + C_A T_f \left(8(1 + 4z) \ell n z \right. \\
& + 8(1 + 2z^2 - 2z) \ell n(1-z) + \frac{4}{3} \left(3 - 31z^2 + 24z + \frac{4}{z} \right) \left. \right\} L_M^2 \\
& + \left\{ C_F T_f \left(16(1 + 2z^2 - 2z) \left(\ell n^2(1-z) - 2\zeta(2) \right) + 8(1 + 4z^2 - 2z) \ell n^2 z \right. \right. \\
& \left. \left. - 8(3 + 8z^2 - 6z) \ell n z \ell n(1-z) + 8(1 + 10z^2 - 6z) \ell n z \right. \right.
\end{aligned}$$

$$\begin{aligned}
& + 8(1 - 2z)Li_2(1 - z) - 4(7 + 20z^2 - 24z)\ell n(1 - z) + 4(9 + 4z^2 - 17z) \\
& + C_A T_f \left(32z(3 - z)\ell n z \ell n(1 - z) - 16(1 + 2z^2 + 2z)(\ell n z \ell n(1 + z) \right. \\
& + Li_2(-z)) - 16(1 + 3z)\ell n^2 z + 16(1 + 4z)Li_2(1 - z) - 16(1 + 2z^2)\zeta(2) \\
& + 8z(25z - 24)\ell n z + 8(1 + 2z^2 - 2z)\ell n^2(1 - z) - \frac{8}{3}(3 + 67z^2 \\
& - 60z - \frac{4}{z})\ell n(1 - z) - \frac{4}{9}(165 - 407z^2 + 276z - \frac{52}{z}) \left. \right) \} L_M \\
& + \frac{32}{3} \left. \right] , \tag{3B.12}
\end{aligned}$$

where $\tilde{c}_{2,g}^{(2)}$ equals

$$\begin{aligned}
\tilde{c}_{2,g}^{(2)} = & 2C_{FT} \left\{ 8(1 + z)^2 \left\{ -4S_{1,2}(-z) - 4\ell n(1 + z)Li_2(-z) - 2\zeta(2)\ell n(1 + z) \right. \right. \\
& - 2\ell n z \ell n^2(1 + z) + \ell n^2 z \ell n(1 + z) \left. \right\} + 4(1 - z)^2 \left\{ \frac{5}{6}\ell n^3(1 - z) - \left(2\ell n z \right. \right. \\
& + \frac{13}{4} \left. \right) \ell n^2(1 - z) + \left(2Li_2(1 - z) + 2\ell n^2 z + 4\ell n z + \frac{7}{2} \right) \ell n(1 - z) - \frac{5}{12}\ell n^3 z \\
& + \left(Li_2(1 - z) - 4Li_2(-z) + 3\zeta(2) \right) \ell n z - 4Li_3(1 - z) - S_{1,2}(1 - z) \\
& + 12Li_3(-z) + 13\zeta(3) + \frac{13}{2}\zeta(2) \left. \right\} + z^2 \left\{ \frac{10}{3}\ell n^3(1 - z) - 12\ell n z \ell n^2(1 - z) \right. \\
& + \left(16\ell n^2 z - 16\zeta(2) \right) \ell n(1 - z) - 5\ell n^3 z + \left(12Li_2(1 - z) + 20\zeta(2) \right) \ell n z \\
& - 8Li_3(1 - z) + 12S_{1,2}(1 - z) \left. \right\} + \left(48 + \frac{64z}{3} + \frac{96z^3}{5} + \frac{8}{15z^2} \right) \left(Li_2(-z) \right. \\
& + \ell n z \ell n(1 + z) \left. \right) + \left(14z - 23z^2 \right) \ell n^2(1 - z) + \left(-12z + 10z^2 \right) \ell n(1 - z) \\
& + \left(-24z + 56z^2 \right) \ell n z \ell n(1 - z) + 64z Li_3(-z) + \left(-10 + 24z \right) Li_2(1 - z) \\
& + \left(-\frac{3}{2} + \frac{22z}{3} - 36z^2 - \frac{48z^3}{5} \right) \ell n^2 z + \frac{1}{15} \left(-236 + 339z - 648z^2 - \frac{8}{z} \right) \ell n z
\end{aligned}$$

$$\begin{aligned}
& + (64z + 36z^2)\zeta(3) + \left(-\frac{20z}{3} + 46z^2 + \frac{96z^3}{5}\right)\zeta(2) - \frac{647}{15} + \frac{239}{5}z - \frac{36z^2}{5} \\
& + \frac{8}{15z} \Big] \\
& + 2C_A T_f \Big[4(1+z)^2 \{ S_{1,2}(1-z) - 2Li_3(-z) + 4S_{1,2}(-z) - 2\ell n z Li_2(1-z) \\
& + 4\ell n(1+z) Li_2(-z) + 2\ell n z Li_2(-z) + 2\zeta(2)\ell n(1+z) + 2\ell n z \ell n^2(1+z) \\
& + \ell n^2 z \ell n(1+z) \} + 8(1+2z+2z^2) \{ Li_3\left(\frac{1-z}{1+z}\right) - Li_3\left(-\frac{1-z}{1+z}\right) \\
& - \ell n(1-z) Li_2(-z) - \ell n z \ell n(1-z)\ell n(1+z) \} + \left(-24 + \frac{80z^2}{3} - \frac{16}{3z}\right) Li_2(-z) \\
& + \ell n z \ell n(1+z) \Big] + z^2 \Big(-4S_{1,2}(1-z) + 16Li_3(-z) + 8\ell n z Li_2(1-z) \\
& + 8\ell n^2 z \ell n(1+z) \Big) + \frac{2}{3} (1-2z+2z^2) \ell n^3(1-z) + (24z-8z^2) \ell n z \ell n^2(1-z) \\
& + \left(-2+36z-\frac{122z^2}{3}+\frac{8}{3z}\right) \ell n^2(1-z) + (-4-32z+8z^2) \ell n^2 z \ell n(1-z) \\
& + (8-144z+148z^2) \ell n z \ell n(1-z) + (4+40z-8z^2) \ell n(1-z) Li_2(1-z) \\
& - (20-24z+32z^2) \zeta(2) \ell n(1-z) - \frac{1}{9} \left(186+1362z-1570z^2-\frac{104}{z}\right) \ell n(1-z) \\
& + (-4-72z+8z^2) Li_3(1-z) + \frac{1}{3} \left(12-192z+176z^2+\frac{16}{z}\right) Li_2(1-z) \\
& + \frac{1}{3} (10+28z) \ell n^3 z + \left(-1+88z-\frac{194z^2}{3}\right) \ell n^2 z + (-48z+16z^2) \zeta(2) \ell n z \\
& + \left(58+\frac{584z}{3}-\frac{2090z^2}{9}\right) \ell n z - (10+12z+12z^2) \zeta(3) \\
& + \frac{1}{3} \left(12-240z+268z^2-\frac{32}{z}\right) \zeta(2) + \frac{239}{9} + \frac{1072z}{9} - \frac{4493z^2}{27} + \frac{344}{27z} \Big] . \quad (3B.13)
\end{aligned}$$

The second moment (see (3.2.82)) of the above expression reads ($T_f = 1/2$)

$$\bar{c}_{2,g}^{(2),2} = C_F \left(\frac{16}{5} \zeta(3) - \frac{4799}{810} \right) + C_A \left(-22\zeta(3) + \frac{115}{324} \right) , \quad (3B.14)$$

which agrees with the result presented in eq. 21 of [35].

3B.2 Order α_s^2 corrected coefficient functions in the DIS scheme

In order α_s , the longitudinal coefficients $c_{L,q}^{(1)}$, $c_{L,g}^{(1)}$ do not change while going from the $\overline{\text{MS}}$ to the DIS scheme. However the order α_s coefficients $c_{2,q}^{(1)}$ and $c_{2,g}^{(1)}$ do change. They become

$$c_{2,q}^{(1)} = 0, \quad c_{2,g}^{(1)} = 0, \quad (3B.15)$$

whereas the mass factorization parts, which are proportional to L_M , remain unaltered.

In $\mathcal{O}(\alpha_s^2)$ the leading mass factorization parts in the DIS scheme do not differ from those already presented in the $\overline{\text{MS}}$ scheme. Therefore we limit ourselves in the former scheme to the presentation of the next-to-leading mass factorization parts and the non-log coefficients present in (3.2.62)–(3.2.67). In order to avoid long expressions we only give the difference between these terms and their $\overline{\text{MS}}$ analogs. Starting with the longitudinal coefficient functions (see (3.2.29)), we have

$$c_{L,q}^{(2),\text{NS}} = \bar{c}_{L,q}^{(2),\text{NS}} + C_F^2 \left[4z \left\{ 2\ell n z \ell n(1-z) - \ell n^2 z + 4\zeta(2) - 2Li_2(1-z) - 2\ell n^2(1-z) \right\} + 4(2-z)\ell n z - 4(2-5z)\ell n(1-z) - 4(1-10z) \right], \quad (3B.16)$$

$$c_{L,q}^{(2),\text{PS}} = \bar{c}_{L,q}^{(2),\text{PS}} + C_F T_f \left[32z(1-z) \left(\ell n^2(1-z) - 2\zeta(2) - 4 \right) + 16z(1-2z) \left(\ell n^2 z - 2\ell n z \ell n(1-z) \right) - 16(1+6z^2-3z)\ell n z + 16(1+6z^2-7z)\ell n(1-z) + 32zLi_2(1-z) \right], \quad (3B.17)$$

$$c_{L,g}^{(2)} = \bar{c}_{L,g}^{(2)} + C_F T_f \left[16z \left\{ \ell n^2 z - 2Li_2(1-z) - 2\ell n z \ell n(1-z) \right\} - 16(1-2z^2+z)\ell n(1-z) + 16(1-2z^2+7z)\ell n z + 32(1-4z^2+3z) \right] \\ + n_f T_f^2 \left[64z(1+z) \left\{ 2Li_2(1-z) - \ell n^2 z + 2\ell n z \ell n(1-z) \right\} - 32(1+9z^2+18z)\ell n z + 32(1-7z^2+6z)\ell n(1-z) - 16(5-67z^2+62z) \right]. \quad (3B.18)$$

The above transition formulae agree with those in the appendix of [60]. The coefficient functions $C_{2,k}$ in the DIS scheme become

$$\begin{aligned} C_{2,q}^{NS} = & \bar{C}_{2,q}^{NS} - \frac{\alpha_s}{4\pi} \bar{c}_{2,q}^{(1)} - \left(\frac{\alpha_s}{4\pi} \right)^2 \left[C_F^2 \left\{ 24 \left(\frac{\ell n^2(1-z)}{1-z} \right)_+ - 12 \left(\frac{\ell n(1-z)}{1-z} \right)_+ \right. \right. \\ & - (32\zeta(2) + 45) \left(\frac{1}{1-z} \right)_+ + 4 \frac{1+z^2}{1-z} (\ell n^2 z - 4\ell n z \ell n(1-z)) \\ & + (1+z)(4\ell n z \ell n(1-z) - 2\ell n^2 z - 12\ell n^2(1-z) \\ & + 4Li_2(1-z) + 16\zeta(2)) - 8(1+2z)\ell n z + 8(2+3z)\ell n(1-z) \\ & \left. \left. + 6(7+4z) + \delta(1-z)(16\zeta(3) - 27) \right\} L_M + \bar{c}_{2,q}^{(2),NS} \right] , \end{aligned} \quad (3B.19)$$

where

$$\bar{c}_{2,q}^{(2),NS} = \bar{c}_{2,q}^{(2),NS,+} + \bar{c}_{2,q}^{(2),NS,-} . \quad (3B.20)$$

$$\begin{aligned} C_{2,q}^{PS} = & \bar{C}_{2,q}^{PS} - n_f \left(\frac{\alpha_s}{4\pi} \right)^2 \left[C_F T_f \left\{ -4(1+4z^2-2z)(\ell n^2 z - 2\ell n z \ell n(1-z)) \right. \right. \\ & - 8(1+2z^2-2z)(\ell n^2(1-z) - 2\zeta(2)) + 4(1-12z^2+8z)\ell n z \\ & + 4(7+12z^2-16z)\ell n(1-z) - 8(1-2z)Li_2(1-z) \\ & \left. \left. + 4(5+16z^2-12z) \right\} L_M + \bar{c}_{2,q}^{(2),PS} \right] , \end{aligned} \quad (3B.21)$$

$$\begin{aligned} C_{2,g} = & \bar{C}_{2,g} - n_f \frac{\alpha_s}{4\pi} \bar{c}_{2,g}^{(1)} - n_f \left(\frac{\alpha_s}{4\pi} \right)^2 \left[\left\{ C_F T_f \left(4(1+4z^2-2z)(\ell n^2 z \right. \right. \right. \\ & - 2Li_2(1-z)) + 16(1+2z^2-2z)(\ell n^2(1-z) - \zeta(2)) \\ & - 8(3+8z^2-6z)\ell n z \ell n(1-z) + 4(1+32z^2-16z)\ell n z \\ & - 4(5+32z^2-36z)\ell n(1-z) + 4(7-10z) \left. \right\} \\ & + n_f T_f^2 \left(8(1+4z^2+4z)(2Li_2(1-z) + 2\ell n z \ell n(1-z) - \ell n^2 z) \right. \\ & - 32(1+5z^2+8z)\ell n z + 32(1-3z^2+2z)\ell n(1-z) \\ & \left. \left. - 8(11-59z^2+48z) \right) \right\} L_M + \bar{c}_{2,g}^{(2)} \right] . \end{aligned} \quad (3B.22)$$

References

- [1] D.H. Coward et al., Phys. Rev. Lett. 20 (1968) 292;
E.D. Bloom et al., Phys. Rev. Lett. 23 (1969) 930;
H. Breidenbach et al., Phys. Rev. Lett. 23 (1969) 935.
- [2] R.P. Feynman, "Photon-Hadron Interactions", W.A. Benjamin, New York 1972.
- [3] H. Fritsch, M. Gell-Mann and H. Leutwyler, Phys. Lett. B74 (1973) 365,
W. Marciano and H. Pagels, Phys. Rep. 36C (1978) 137.
- [4] K. Wilson, Phys. Rev. D10 (1974) 2455.
- [5] D.J. Gross and F. Wilczek, Phys. Rev. Lett. 30 (1973) 1343;
H.D. Politzer, Phys. Rev. Lett. 30 (1973) 1346.
- [6] R.E. Taylor, Proceedings of the International Symposium on Lepton and Photon Interactions at High Energies, Stanford 1975.
- [7] R.G. Roberts and M.R. Whalley, J. Phys. G.; Nucl. Part. Phys. 17 (1991) D1-D151.
- [8] A.C. Bawa et al., Proceedings of the HERA Workshop, Hamburg, October 12-14, 1987, ed. R.P. Peccei, vol. 1, p. 183.
- [9] Proceedings of the large Hadron Collider Workshop, Aachen, October 4-9, 1990, eds. G. Jarlskog and D. Rein, vol. 2, p. 829.
- [10] E.B. Zijlstra and W.L. van Neerven, Nucl. Phys. B383 (1992) 525.
- [11] Proceedings of the small- x Workshop, DESY, Hamburg, eds. A. Ali and J. Bartels, May 1990, Nucl. Phys. B (Proc. Suppl.) 18C (1991).
- [12] V.N. Gribov and L.N. Lipatov, Sov.J.Nucl.Phys. 15 (1972) 438, 675;
G. Altarelli and G. Parisi, Nucl. Phys. B126 (1977) 298.
- [13] E.G. Floratos, D.A. Ross and C.T. Sachrajda, Nucl. Phys. B129 (1977) 66,
Erratum B139 (1978) 545; Nucl.Phys. B152 (1979) 493.
- [14] A. Gonzalez-Arroyo, C. Lopez and F.J. Yndurain, Nucl. Phys. B153 (1979) 161.
- [15] A. Gonzalez-Arroyo and C. Lopez, Nucl. Phys. B166 (1980) 429.

- [16] E.G. Floratos, P. Lacaze and C. Kounnas, Phys. Lett. B98 (1981) 89, 225.
- [17] G. Curci, W. Furmanski and R. Petronzio, Nucl. Phys. B175 (1980) 27;
W. Furmanski and R. Petronzio, Phys. Lett. B97 (1980) 437.
- [18] W.A. Bardeen, A.J. Buras, D.W. Duke and T. Muta, Phys.Rev. D18 (1978) 3998.
- [19] G. Altarelli, R.K. Ellis and G. Martinelli, Nucl. Phys. B143 (1978) 521, Erratum B146 (1978) 544; *ibid.* B157 (1979) 461.
- [20] B. Humpert and W.L. van Neerven, Nucl. Phys. B184 (1981) 225.
- [21] W.L. van Neerven and E.B. Zijlstra, Phys. Lett. B272 (1991) 127.
- [22] E.B. Zijlstra and W.L. van Neerven, Phys. Lett. B273 (1991) 476.
- [23] B. Humpert and W.L. van Neerven, Nucl. Phys. B178 (1981) 498.
- [24] A.C. Hearn, Reduce Users's Manual, The Rand Corporation, Santa Monica, CA, 1985.
- [25] H. Strubbe, Comput. Phys. Comm. 8 (1974) 1.
- [26] J.A.M. Vermaseren, Symbolic manipulation with FORM, published by CAN, Kruislaan 413, 1098 SJ Amsterdam (1991), ISBN 90-74116-01-9.
- [27] T. Matsuura and W.L. van Neerven, Z. Phys. C38 (1988) 623.
- [28] T. Matsuura, S.C. van der Marck and W.L. van Neerven, Nucl. Phys. B319 (1989) 570.
- [29] G. Kramer and B. Lampe, Z. Phys. C34 (1987) 497, Erratum C42 (1989) 504.
- [30] G. Passarino and M. Veltman, Nucl. Phys. B160 (1979) 151;
W.J.P. Beenakker, Ph.D. thesis, University of Leiden, The Netherlands, (1989).
- [31] T. Matsuura, Ph.D. thesis, University of Leiden, The Netherlands, (1989).
- [32] W. Beenakker, H. Kuijf, W.L. van Neerven and J. Smith, Phys. Rev. D40 (1989) 54.
- [33] R. Hamberg, W.L. van Neerven and T. Matsuura, Nucl. Phys. B359 (1991) 343.

- [34] M. Diemoz, F. Ferroni, E. Longo and G. Martinelli, Z. Phys. C39 (1988) 472.
- [35] S.A. Larin and J.A.M. Vermaseren, Z. Phys. C57 (1993) 93.
- [36] S.G. Gorishni and S.A. Larin, Nucl. Phys. B283 (1987) 452.
- [37] D.W. Duke, J.D. Kimel and G.A. Sowell, Phys. Rev. D25 (1982) 71.
- [38] S.N. Cousen and R.E. Ecclestone, Phys. Lett. 115B (1982) 415; Nucl. Phys. B211 (1983) 317.
- [39] A. Deotto, D.W. Duke, J.D. Kimel and G.A. Sowell, Phys. Rev. D30 (1984) 541.
- [40] J.L. Miramontes, J. Sanchez Guillén and E. Zas, Phys. Rev. D35 (1987) 863.
- [41] D.I. Kazakov et al., Phys. Rev. Lett. 65 (1990) 1535, Erratum 65 (1990) 1921.
- [42] J. Sanchez Guillén et al., Nucl. Phys. B353 (1991) 337.
- [43] E. Laenen, S. Riemersma, J. Smith and W.L. van Neerven, Nucl. Phys. B392 (1993) 162, 229.
- [44] O.V. Tarasov, A.A. Vladimirov and A.Yu. Zharkov, Phys. Lett. B93 (1980) 429.
- [45] A.N. Schellekens, Nuov. Cim. Lett. 24 (1979) 513.
- [46] G. Sterman, Nucl. Phys. 281 (1987) 310;
D. Appell, G. Sterman and P. Mackenzie, Nucl. Phys. B309 (1988) 259;
S. Catani and L. Trentadue, Nucl. Phys. B327 (1989) 323; *ibid.* B353 (1991) 183;
E. Laenen, J. Smith and W.L. van Neerven, Nucl. Phys. B369 (1992) 543.
- [47] W.L. van Neerven, Phys. Lett. 147B (1984) 175.
- [48] S. Catani, F. Fiorani, G. Marchesini, Nucl. Phys. B336 (1990) 18.
- [49] R. Hamberg and W.L. van Neerven, Nucl. Phys. B359 (1992) 143.
- [50] P.N. Harriman, A.D. Martin, R.G. Roberts and W.J. Stirling, Phys. Rev. D42 (1990) 798.
- [51] J.G. Morfin and Wu-Ki Tung, Z. Phys. C52 (1991) 13.
- [52] A.D. Martin, W.J. Stirling and R.G. Roberts, DTP-92-16, RAL-92-021, 1992.

- [53] A.C. Benvenuti et al. (BCDMS), Phys. Lett. B223 (1989) 485; ibid B237 (1990) 599.
- [54] P. Amaudruz et al. (NMC), Phys. Rev. Lett. 66 (1991) 73;
M.W. van der Heijden, Ph.D. Thesis, University of Amsterdam, The Netherlands, (1991).
- [55] A. Milsztajn et al., CERN-PPE/90-135.
- [56] M. Virchaux and A. Milsztajn, Phys. Lett. B274 (1992) 221.
- [57] J. Blümlein in "Proceedings of the Large Hadron Collider Workshop", Aachen, October 4-9, 1990, eds. G. Jarlskog and D. Rein, vol. 2, p. 850.
- [58] N. Magnussen and G.A. Schuler in "Proceedings of the Large Hadron Collider Workshop", Aachen, October 4-9, 1990, eds. G. Jarlskog and D. Rein, vol. 2, p. 858.
- [59] A.C. Benvenuti et al., CERN-PPE/89-06; Phys. Lett. B223 (1989) 485.
- [60] S. Keller et al., Phys. Lett. B270 (1991) 61.
- [61] G. Altarelli, Phys. Rep. 81 (1982), 1.
- [62] R. Barbieri, J.A. Mignaco and E. Remiddi, Nuov. Cim 11A (1972) 824.

Chapter 4

The Drell-Yan K-factor in the $\overline{\text{MS}}$ and DIS scheme

4.1 Introduction

Higher order QCD corrections enable us to examine the behaviour of the perturbation series for physical quantities at energies in the range of 10 to 10^4 GeV. In the past decade attempts have been made to improve the perturbation series beyond leading order in α_s (strong coupling constant).

The first interesting property of the perturbation series to study is its dependence on the chosen renormalization and/or mass factorization scale. In the so-called optimized perturbation theory one tries to control the variation of the series under changes in the renormalization and/or mass factorization scale. Examples are the method of fastest apparent convergence (FAC) [4] and the principle of minimal sensitivity (PMS) [5].

A second interesting feature is the appearance of large terms in the perturbative expansion due to some physical effects. An example is soft gluon radiation which gives rise to large corrections near the boundary of phase space [1]. In addition they may also contribute, together with the virtual gluonic corrections, to large constants in the various K -factors [2]. In the deep inelastic and Drell-Yan coefficient functions soft gluon radiation manifests itself near $x = 1$ as large logarithms of the type $\ln^i(1-x)/(1-x)$ where x denotes the Bjorken scaling variable. Another example is the small- x behaviour ($x \approx 0$) of the coefficient function which is due to soft gluon exchanges in the t -channel of the process under consideration [3]. The large corrections due to physical effects can be dealt with by using various techniques like the exponentiation of the large constants [6] and the resummation of the large logarithmic terms in the

coefficient function near $x = 1$ [7] and $x = 0$ [8].

A third feature which is more of phenomenological origin, is the sensitivity of the perturbation series to the parametrization of the input parton densities, in particular of the gluon density about which little is known at small x values. The problem of the dependence of the series on the parametrization of the parton densities can be solved when the new data from the experiments carried out at HERA [9] and the ep facility at LHC [10] become available.

At this moment only a few calculations of physical quantities are known beyond order α_s . They all bear on the pure leptonic induced process $e^+ + e^- \rightarrow "X"$ or on the semi-leptonic induced processes as deep inelastic lepton-hadron scattering $l_1 + H \rightarrow l_2 + "X"$ and massive lepton pair production $H_1 + H_2 \rightarrow (l_1, l_2) + "X"$ (Drell-Yan process). Here the symbols l_i , H_i and $"X"$ stand for the lepton, hadron and any inclusive final hadronic state respectively. Examples of higher order corrections to quantities measured in electron-positron collisions are the ratio $R = \sigma(e^+e^- \rightarrow "X")/\sigma(e^+e^- \rightarrow \mu^+\mu^-)$, known up to order α_s^3 [11] and the two jet cross-section which is computed up to order α_s^2 [12]. In deep inelastic lepton-hadron scattering order α_s^2 corrections to various sum rules have been calculated in [13] and the coefficient function in deep inelastic lepton-hadron scattering was computed up to order α_s^2 in chapter 3. The same has been done for the Drell-Yan K -factor which is known up to order α_s^2 in the $\overline{\text{MS}}$ scheme [14], [15]. Notice that the quantities in the electron-positron reactions only depend on the renormalization scale, whereas the coefficient functions in the semi-leptonic induced processes also depend on the mass factorization scale. The reason why the calculations of these higher order corrections are feasible is the relative simplicity of the above reactions. First the order α_s^2 corrections are obtained from an amplitude where the maximum number of external particles is five, i.e. a vector boson and four partons. Second in the case of the order α_s^3 term in the perturbation series, one can often find elegant tricks [13] which however are applicable to integrated quantities only. Unfortunately this situation considerably changes if one deals with hadron-hadron reactions with many partons in the final state. This can be mainly attributed to the intricate phase space integrals which show up in the calculation of the various distributions characteristic for these processes.

The Drell-Yan (DY) process is a nice example in which one can illustrate all features of the perturbation series mentioned in the beginning of this section. In [14] the cross section and the corresponding K -factor were calculated in the $\overline{\text{MS}}$ scheme up to order $\mathcal{O}(\alpha_s^2)$. Here we want to present these quantities in the DIS (deep inelastic scattering) scheme in order to study the uncertainty in the prediction due to the

choice of mass factorization scheme. For the calculations in the DIS scheme one needs to know the second order coefficient functions of deep inelastic lepton-hadron scattering, which have been calculated in chapter 3.

This chapter will be organized as follows. In section 4.2 we present the results of the complete order α_s^2 correction to the DY K -factor. Here the coupling constant renormalization is presented in the $\overline{\text{MS}}$ scheme, whereas the mass factorization is performed in the DIS scheme. In section 4.3 we study the effect of higher order corrections on heavy vector boson production at current and future large hadron colliders. A comparison will be made with earlier predictions which were obtained in the $\overline{\text{MS}}$ scheme. The long expressions for the order α_s^2 coefficient function, not presented in section 4.2, can be found in appendix 4A.

4.2 The order α_s^2 correction to the DY process

Massive lepton pair production in hadronic collisions proceeds through the following reaction:

$$H_1 + H_2 \rightarrow \begin{array}{c} V + "X" \\ \downarrow \\ \ell_1 + \ell_2 \end{array} \quad (4.2.1)$$

where V is one of the vector bosons of the standard model (γ , Z or W) which subsequently decays into a lepton pair (ℓ_1 , ℓ_2). The symbol " X " denotes any inclusive final hadronic state allowed by quantum number conservation laws. The colour-averaged inclusive cross section is given by

$$\frac{d\sigma^V}{dQ^2} = \tau \sigma_V(Q^2, M_V^2) W_V(\tau, Q^2) \quad , \quad \tau = \frac{Q^2}{S} \quad . \quad (4.2.2)$$

The quantity σ_V (see appendix A of [14]) is the vector boson production cross section where the incoming hadrons H_1 and H_2 are pointlike. The variables \sqrt{S} and $\sqrt{Q^2}$ stand for the C.M. energy of the incoming hadrons H_1 , H_2 and the invariant mass of the lepton pair respectively. The hadronic structure function is represented by $W_V(\tau, Q^2)$. According to the DY mechanism it can be written as (see also 2.4.11)

$$\begin{aligned} W_V(\tau, Q^2) = & \sum_{i,j} \int_0^1 dx_1 \int_0^1 dx_2 \int_0^1 dx \delta(\tau - xx_1x_2) P D_{ij}^V(x_1, x_2, M^2) \\ & \times \Delta_{ij}(x, \frac{Q^2}{M^2}, \alpha_s(M^2)) \quad . \end{aligned} \quad (4.2.3)$$

The functions PD_{ij}^V stand for the usual combination of parton densities which depend on the mass factorization scale M . The indices i and j refer to the type of incoming partons. Furthermore the PD_{ij}^V contain all information on the couplings of the quarks to the vector bosons, such as the quark charges, the Weinberg angle θ_W and the Cabibbo angle θ_c (the other angles and phases of the Kobayashi-Maskawa matrix are neglected). The explicit way in which the functions PD_{ij}^V combine with the DY coefficient functions Δ_{ij} is given in (A.20) of [14]. Actually the parton densities do not only depend on the mass factorization scale M but also on the renormalization scale R . This is because the anomalous dimensions, which determine the scale variation, depend on operator renormalization (= mass factorization) as well as on coupling constant renormalization. The same holds for the coefficient function term Δ_{ij} . The dependence of the parton densities and Δ_{ij} on the renormalization scale R can be very easily obtained by changing the argument M in the running coupling constant $\alpha_s(M^2)$ into the variable R . As has been mentioned in 3.2.35, in next to leading order this is achieved by the substitution

$$\alpha_s(M^2) = \alpha_s(R^2) \left(1 + \frac{\alpha_s(R^2)}{4\pi} \beta_0 \ln \left(\frac{R^2}{M^2} \right) \right), \quad (4.2.4)$$

where β_0 is the lowest order coefficient function of the β function (4.2.28). Notice that in the existing parametrizations of the parton distribution functions the two scales M and R are always set to be equal. The DY coefficient function Δ_{ij} is obtained from the DY parton structure function \widehat{W}_{ij} through mass factorization.

$$\begin{aligned} \widehat{W}_{ij}(z, \frac{Q^2}{\mu^2}, \alpha_s(M^2), \epsilon) = \sum_{k,l} \int_0^1 dx_1 \int_0^1 dx_2 \int_0^1 dx \delta(z - xx_1x_2) \\ \times \Gamma_{ki}(x_1, \frac{M^2}{\mu^2}, \alpha_s(M^2), \epsilon) \Gamma_{lj}(x_2, \frac{M^2}{\mu^2}, \alpha_s(M^2), \epsilon) \Delta_{kl}(x, \frac{Q^2}{M^2}, \alpha_s(M^2)) \end{aligned} \quad (4.2.5)$$

Here \widehat{W}_{ij} is determined by the partonic subprocess

$$i + j \rightarrow V + "X" \quad (4.2.6)$$

and Γ_{ki} represents the transition function (parton $i \rightarrow$ parton k). The Bjorken scaling variable z in (4.2.5) is defined as $z = Q^2/s$, where s stands for the C.M. energy of the incoming partons i and j in (4.2.6). In (4.2.5) we assume that coupling constant renormalization has already been performed, where R is set equal to M . If R is chosen to be different from M , one can replace $\alpha_s(M^2)$ occurring in the quantities \widehat{W} and Γ by the right hand side of (4.2.4). The collinear divergences showing up in \widehat{W} and Γ (4.2.5) are dealt with by using n -dimensional regularization. They manifest themselves as pole terms of the type $1/\epsilon$ ($\epsilon = n - 4$). The accompanying parameter μ is an artefact of n -dimensional regularization.

4.2.1 Diagrams contributing at second order

The parton subprocesses (4.2.6) contributing to the DY cross section are listed up to second order in α_s in table 2.2 (see also figs. 4.1–4.9). The corresponding coefficient functions Δ_{ij} (4.2.5) have been calculated from \widehat{W}_{ij} in $\mathcal{O}(\alpha_s^2)$ and the result is presented in appendix B of [14], where both coupling constant renormalization and mass factorization were carried out in the $\overline{\text{MS}}$ scheme.

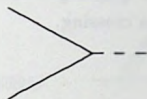


Fig. 4.1. The Born contribution to the subprocess $q + \bar{q} \rightarrow V$.

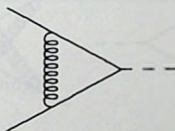


Fig. 4.2. The one loop correction to the process $q + \bar{q} \rightarrow V$.

However in this chapter the mass factorization of \widehat{W}_{ij} proceeds in the DIS scheme, whereas the coupling constant renormalization is still done in the $\overline{\text{MS}}$ scheme. To determine Δ_{ij} in the DIS scheme one needs to know the parton structure functions $\widehat{F}_{2,i}$ (for the definitions see [16], [17]) which have been calculated in chapter 3. They show up in the calculation of the hadronic structure functions of deep inelastic lepton-hadron scattering (DIS)

$$l_1 + H \rightarrow l_2 + "X" \quad (4.2.7)$$

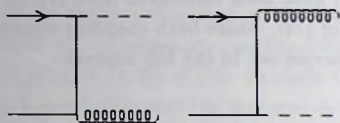


Fig. 4.3. Diagrams contributing to the subprocess $q + \bar{q} \rightarrow V + g$. The graphs corresponding to the subprocess $q(\bar{q}) + g \rightarrow V + q(\bar{q})$ can be obtained from those presented in this figure via crossing.

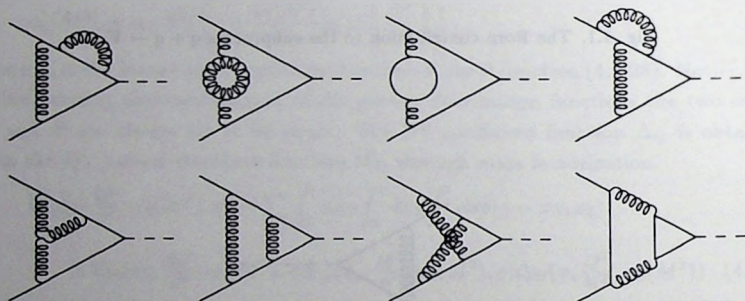


Fig. 4.4. The two loop corrections to the process $q + \bar{q} \rightarrow V$.

The parton structure functions $\hat{F}_{2,i}$ can be obtained from the parton subprocesses

$$i(p) + V(q) \rightarrow "X" , \quad (4.2.8)$$

which are listed in table 2.1. The Feynman diagrams for process (4.2.8) can be derived from the DY graphs in figs. 4.1–4.9 by interchanging the outgoing vector boson with

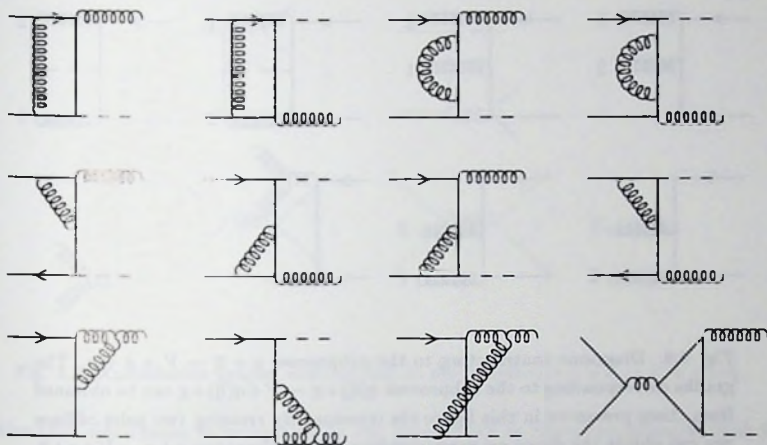


Fig. 4.5. The one loop corrections to the process $q + \bar{q} \rightarrow V + g$. The diagrams corresponding to the one loop correction to the subprocess $q(\bar{q}) + g \rightarrow V + q(\bar{q})$ can be obtained via crossing.

one of the incoming partons (crossing).

4.2.2 Mass factorization in the DIS scheme

The DIS coefficient function C_2 can be obtained via mass factorization

$$\begin{aligned} \hat{F}_{2,i}(z, \frac{Q^2}{\mu^2}, \alpha_s(M^2), \epsilon) = \sum_k \int_0^1 dx_1 \int_0^1 dx \delta(z - xx_1) \Gamma_{ki}(x, \frac{M^2}{\mu^2}, \alpha_s(M^2), \epsilon) \\ \times C_{2,k}(x_1, \frac{Q^2}{M^2}, \alpha_s(M^2)) . \end{aligned} \quad (4.2.9)$$

Here the comments regarding M and R are the same as given below (4.2.6). Note that in DIS the Bjorken scaling variable z is defined by $Q^2/2p \cdot q$ (see (4.2.8)). In the $\overline{\text{MS}}$ scheme the transition functions Γ_{ij} can be expanded in a power series of $\alpha_s(M)$ in which the residues of the pole terms $1/\epsilon$ are represented by the AP splitting functions

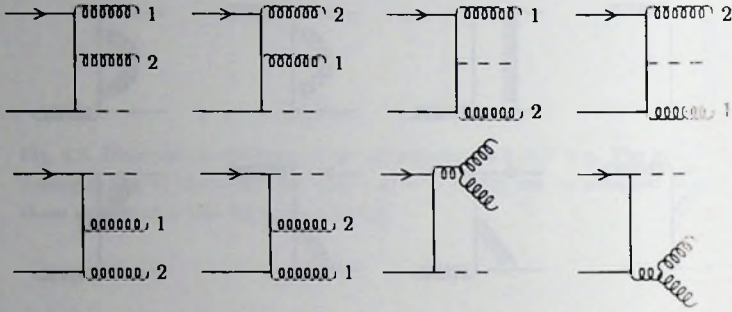


Fig. 4.6. Diagrams contributing to the subprocess $q + \bar{q} \rightarrow V + g + g$. The graphs corresponding to the subprocess $q(\bar{q}) + g \rightarrow V + q(\bar{q}) + g$ can be obtained from those presented in this figure via crossing. By crossing two pairs of lines one can obtain the diagrams corresponding to the subprocess $g + g \rightarrow V + q + \bar{q}$.

$P_{ij}^{(n)}$ [2] (explicit expressions for Γ_{ij} can be found in eqs. (2.28)–(2.34) of [14], see also [18]). The relation between the anomalous dimension $\gamma_{ij}^{(k)}$ and the splitting functions is given by

$$\gamma_{ij}^{(k),n} = - \int_0^1 dx x^{n-1} P_{ij}^{(k)} . \quad (4.2.10)$$

The transition functions connect the bare parton densities (indicated by a hat) to the mass factorized (scale dependent) parton densities in the following way

$$q_i = \Gamma_{qg} \hat{g} + \Gamma_{qq}^{NS} \hat{q}_i + \Gamma_{qq}^{NS} \hat{\bar{q}}_i + \Gamma_{qq}^{PS} \sum_l (\hat{q}_l + \hat{\bar{q}}_l) , \quad (4.2.11)$$

$$\bar{q}_i = \Gamma_{qg} \hat{g} + \Gamma_{qq}^{NS} \hat{\bar{q}}_i + \Gamma_{qq}^{NS} \hat{q}_i + \Gamma_{qq}^{PS} \sum_l (\hat{q}_l + \hat{\bar{q}}_l) , \quad (4.2.12)$$

$$g = \Gamma_{gq} \sum_l (\hat{q}_l + \hat{\bar{q}}_l) + \Gamma_{gg} \hat{g} . \quad (4.2.13)$$

Here the index i indicates the type of flavour. In the above equations we have the following identities

$$\Gamma_{qq}^{NS} = \Gamma_{q\bar{q}}^{NS} ; \quad \Gamma_{q\bar{q}}^{NS} = \Gamma_{\bar{q}q}^{NS} ; \quad \Gamma_{qq}^{PS} = \Gamma_{q\bar{q}}^{PS} = \Gamma_{\bar{q}q}^{PS} = \Gamma_{\bar{q}\bar{q}}^{PS} ; \quad (4.2.14)$$

$$\Gamma_{qg} = \Gamma_{\bar{q}g} ; \quad \Gamma_{gq} = \Gamma_{g\bar{q}} . \quad (4.2.15)$$

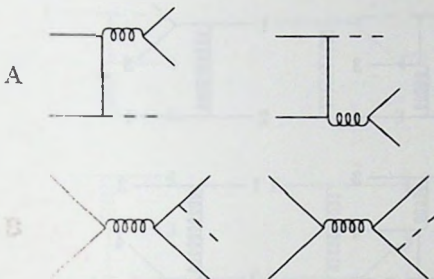


Fig. 4.7. Annihilation graphs contributing to the subprocess $q + \bar{q} \rightarrow V + q + \bar{q}$.

Notice that since mass factorization in the case of DY is more complicated than for the DIS process, our notations for the splitting functions differ a little bit from the ones used in chapter 3. Here we distinguish between Γ_{qq}^{NS} and $\Gamma_{q\bar{q}}^{NS}$. Furthermore the transition functions are flavour independent. The superscripts NS and PS stand for non-singlet and pure singlet respectively. The singlet (S) transition functions are defined by

$$\Gamma_{qq}^S = \Gamma_{qq}^{NS} + n_f \Gamma_{qq}^{PS}, \quad \Gamma_{q\bar{q}}^S = \Gamma_{q\bar{q}}^{NS} + n_f \Gamma_{q\bar{q}}^{PS}. \quad (4.2.16)$$

The lowest order contribution to the pure singlet part Γ_{qq}^{PS} , which originates from fig. 4.8 or fig. 4.9, starts in order α_s^2 and is determined by one of the combinations C^2 , D^2 , E^2 or F^2 (4A.21). The splitting function $\Gamma_{q\bar{q}}^{NS}$ also starts in $\mathcal{O}(\alpha_s^2)$ and receives contributions from the interference terms CE and DF in figs. 4.8 and 4.9. It can be attributed to identical quarks in the final state (4A.24). Since the bare and mass factorized densities have to satisfy the momentum conservation sum rules

$$\int_0^1 dx \, x \left[\sum_i \{ \hat{q}_i(x) + \hat{\bar{q}}_i(x) \} + \hat{g}(x) \right] = 1, \quad (4.2.17)$$

$$\int_0^1 dx \, x \left[\sum_i \{ q_i(x, M^2) + \bar{q}_i(x, M^2) \} + g(x, M^2) \right] = 1, \quad (4.2.18)$$

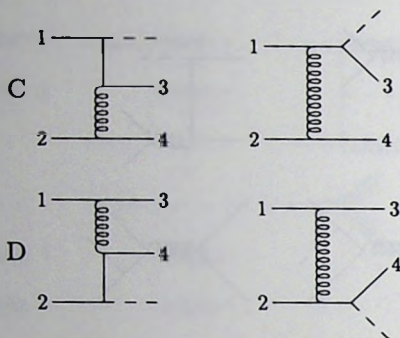


Fig. 4.8. Gluon exchange graphs contributing to the subprocesses $q + \bar{q} \rightarrow V + q + \bar{q}$ and $q + q \rightarrow V + q + q$.

one can derive the following relations

$$\int_0^1 dx \, x [\Gamma_{gg} + 2n_f \Gamma_{qg}] = 1 \quad , \quad (4.2.19)$$

$$\int_0^1 dx \, x [\Gamma_{qq}^S + \Gamma_{q\bar{q}}^S + \Gamma_{gq}] = 1 \quad , \quad (4.2.20)$$

which automatically hold when the Γ_{ij} are computed in the \overline{MS} scheme. Using the latter scheme for the coupling constant renormalization as well as the mass factorization, one can derive from (4.2.9) the deep inelastic coefficient function in lepton-hadron scattering. The non-singlet (NS) as well as singlet (S) part will be presented below up to order α_s^2 . The non-singlet coefficient function is given by

$$\begin{aligned} \bar{C}_{2,q}^{NS} = \bar{C}_{2,\bar{q}}^{NS} = & 1 + \frac{\alpha_s}{4\pi} \left[\frac{1}{2} P_{qq}^{(0)} L_M + \bar{c}_{2,q}^{(1)} \right] + \left(\frac{\alpha_s}{4\pi} \right)^2 \left[\left\{ \frac{1}{8} P_{qq}^{(0)} \otimes P_{qq}^{(0)} - \frac{1}{4} \beta_0 P_{qq}^{(0)} \right\} L_M^2 \right. \\ & \left. + \left\{ \frac{1}{2} (P_{qq}^{(1),NS} + P_{q\bar{q}}^{(1),NS}) - \beta_0 \bar{c}_{2,q}^{(1)} + \frac{1}{2} P_{qq}^{(0)} \otimes \bar{c}_{2,q}^{(1)} \right\} L_M + \bar{c}_{2,q}^{(2),NS} \right] \quad . \quad (4.2.21) \end{aligned}$$

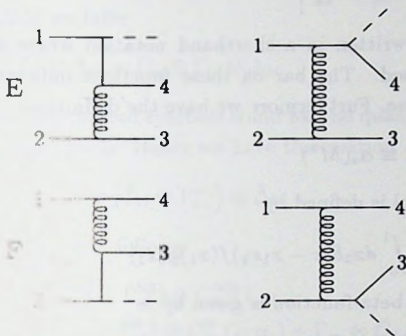


Fig. 4.9. Gluon exchange graphs contributing to the subprocess $q + q \rightarrow V + q + q$ with identical quarks in the initial and/or final state.

The $\mathcal{O}(\alpha_s^2)$ non-singlet coefficient can be split into

$$\bar{c}_{2,q}^{(2),NS} = \bar{c}_{2,q}^{(2),NS,+} + \bar{c}_{2,q}^{(2),NS,-} \quad (4.2.22)$$

In (4.2.21) and (4.2.22) $\bar{C}_{2,q}^{(2),NS,-}$ and $P_{qq}^{(1),NS}$ are due to identical quarks in the final state (CE and DF combinations in figs. 4.8, 4.9). The singlet coefficient function equals

$$\bar{C}_{2,q}^S = \bar{C}_{2,\bar{q}}^S = \bar{C}_{2,q}^{NS} + \bar{C}_{2,q}^{PS} \quad (4.2.23)$$

The function $\bar{C}_{2,q}^{PS}$, which is determined by fig. 4.8 or fig. 4.9 (see the comment below (4.2.16)) denotes the pure singlet part. It is equal to

$$\begin{aligned} \bar{C}_{2,q}^{PS} = \bar{C}_{2,\bar{q}}^{PS} = n_f \left(\frac{\alpha_s}{4\pi} \right)^2 & \left[\left\{ \frac{1}{8} P_{qg}^{(0)} \otimes P_{gq}^{(0)} \right\} L_M^2 + \left\{ \frac{1}{2} P_{qq}^{(1),PS} \right. \right. \\ & \left. \left. + \frac{1}{2} P_{gq}^{(0)} \otimes \bar{c}_{2,g}^{(1)} \right\} L_M + \bar{c}_{2,q}^{(2),PS} \right] \quad (4.2.24) \end{aligned}$$

The gluon coefficient function is given by

$$\bar{C}_{2,g} = n_f \frac{\alpha_s}{4\pi} \left[\frac{1}{2} P_{qg}^{(0)} L_M + \bar{c}_{2,g}^{(1)} \right] + n_f \left(\frac{\alpha_s}{4\pi} \right)^2 \left[\left\{ \frac{1}{8} P_{qg}^{(0)} \otimes (P_{gg}^{(0)} + P_{qq}^{(0)}) \right\} \right]$$

$$\begin{aligned}
& -\frac{1}{4}\beta_0 P_{\mathbf{qg}}^{(0)} \} L_M^2 + \left\{ \frac{1}{2} P_{\mathbf{qg}}^{(1)} - \beta_0 \bar{c}_{2,\mathbf{g}}^{(1)} + \frac{1}{2} P_{\mathbf{gg}}^{(0)} \otimes \bar{c}_{2,\mathbf{g}}^{(1)} \right. \\
& \left. + \frac{1}{2} P_{\mathbf{qg}}^{(0)} \otimes \bar{c}_{2,\mathbf{q}}^{(1)} \right\} L_M + \bar{c}_{2,\mathbf{g}}^{(2)} \Big] . \quad (4.2.25)
\end{aligned}$$

The above equations are written in a shorthand notation where all arguments in the functions are suppressed. The bar on these functions indicates that they are computed in the $\overline{\text{MS}}$ scheme. Furthermore we have the definitions

$$L_M = \ln \frac{Q^2}{M^2} , \quad \alpha_s \equiv \alpha_s(M^2) \quad (4.2.26)$$

and the convolution symbol is defined by

$$(f \otimes g)(x) = \int_0^1 dx_1 \int_0^1 dx_2 \delta(x - x_1 x_2) f(x_1) g(x_2) . \quad (4.2.27)$$

The first coefficient in the beta-function is given by

$$\beta_0 = \frac{11}{3} C_A - \frac{2}{3} n_f , \quad (4.2.28)$$

where $C_A = N$ for $SU(N)$ and n_f stands for the number of light flavours. The lowest order contributions to $\bar{C}_{2,i}$ ($i = \mathbf{q}, \mathbf{g}$), which have been computed more than ten years ago, can be found in many review papers, see e.g. [2]. The second order contributions to $\bar{C}_{2,i}$ are presented in chapter 3.

In this chapter we will perform the mass factorization in the DIS scheme, whereas the coupling constant remains determined in the $\overline{\text{MS}}$ scheme. In DIS the transition functions become

$$\Gamma_{\mathbf{qg}}^{\text{NS}} = \hat{F}_{2,\mathbf{q}}^{\text{NS}}|_{Q^2=M^2} ; \quad \Gamma_{\mathbf{qg}}^{\text{S}} = \hat{F}_{2,\mathbf{q}}^{\text{S}}|_{Q^2=M^2} ; \quad n_f \Gamma_{\mathbf{qg}} = \frac{1}{2} \hat{F}_{2,\mathbf{g}}|_{Q^2=M^2} . \quad (4.2.29)$$

Unfortunately such a unique definition does not exist for the transition functions $\Gamma_{\mathbf{gq}}$ and $\Gamma_{\mathbf{gg}}$ because in deep inelastic scattering the gluon does not directly couple to the vector boson V . Therefore there is some freedom of choice except that all Γ 's have to satisfy the relations in (4.2.19) and (4.2.20). Following the definition in [19] we choose

$$\Gamma_{\mathbf{gq}} = \frac{\alpha_s}{4\pi} \left[\frac{1}{\epsilon} P_{\mathbf{gq}}^{(0)} - \bar{c}_{2,\mathbf{q}}^{(1)} \right] , \quad (4.2.30)$$

$$\Gamma_{\mathbf{gg}} = 1 + \frac{\alpha_s}{4\pi} \left[\frac{1}{\epsilon} P_{\mathbf{gg}}^{(0)} - n_f \bar{c}_{2,\mathbf{g}}^{(1)} \right] , \quad (4.2.31)$$

which is sufficient for the calculation of the DIS- and DY coefficient functions up to $\mathcal{O}(\alpha_s^2)$. In the DIS scheme the former become

$$C_{2,\mathbf{q}}|_{Q^2=M^2} = 1 , \quad C_{2,\mathbf{g}}|_{Q^2=M^2} = 0 . \quad (4.2.32)$$

The DY coefficient function in the DIS scheme can now be obtained from (4.2.5) and (4.2.29)–(4.2.31). However there exists a shorter way if one bears in mind that a change of scheme only involves a finite mass factorization. This can be seen as follows. From (4.2.5) we infer

$$\bar{W}_{ij} = \bar{\Gamma}_{ki} \otimes \bar{\Gamma}_{lj} \otimes \bar{\Delta}_{kl} = \Gamma_{ki} \otimes \Gamma_{lj} \otimes \Delta_{kl} , \quad (4.2.33)$$

where the barred and unbarred symbols stand for the quantities calculated in the $\overline{\text{MS}}$ and DIS scheme respectively. Hence we have the relation

$$\Delta_{mn} = (\bar{\Gamma}_{ki} \otimes \bar{\Gamma}_{lj}) \otimes (\bar{\Gamma}_{ij} \otimes \Gamma_{jn}^{-1}) \otimes \bar{\Delta}_{kl} . \quad (4.2.34)$$

From (4.2.9) and (4.2.29) it follows

$$\Gamma_{qq}^{\text{NS}} + \Gamma_{q\bar{q}}^{\text{NS}} = \bar{\Gamma}_{qq}^{\text{NS}} + \bar{\Gamma}_{q\bar{q}}^{\text{NS}} \otimes \bar{C}_{2,q}^{\text{NS}}(1, \alpha_s) , \quad (4.2.35)$$

$$\Gamma_{qq}^{\text{S}} + \Gamma_{q\bar{q}}^{\text{S}} = \bar{\Gamma}_{qq}^{\text{S}} + \bar{\Gamma}_{q\bar{q}}^{\text{S}} \otimes \bar{C}_{2,q}^{\text{S}}(1, \alpha_s) + \bar{\Gamma}_{gq} \otimes \bar{C}_{2,g}(1, \alpha_s) , \quad (4.2.36)$$

$$\Gamma_{qg} = 2n_f \bar{\Gamma}_{qg} \otimes \bar{C}_{2,q}^{\text{S}}(1, \alpha_s) + \bar{\Gamma}_{gg} \otimes \bar{C}_{2,g}(1, \alpha_s) , \quad (4.2.37)$$

where q can be replaced by \bar{q} and vice versa.

Using (4.2.34)–(4.2.37) we can now obtain the expressions for the DY coefficient function in the DIS scheme. In the case of the non-singlet part this is very easy. Here we have

$$\Delta_{q\bar{q}}^{\text{NS}} = (C_{2,q}^{\text{NS}})^{-1} \otimes (C_{2,q}^{\text{NS}})^{-1} \otimes \bar{\Delta}_{q\bar{q}}^{\text{NS}} . \quad (4.2.38)$$

In the other cases the computation of Δ_{ij} involves some algebra because Γ_{ij} as well as Δ_{ij} become a matrix. After a straight forward calculation the expression for $\bar{\Delta}_{ij}$ can be cast in the following form [14]

$$\begin{aligned} \bar{\Delta}_{q\bar{q}}^{\text{NS}} = 1 + \frac{\alpha_s}{4\pi} \left[P_{q\bar{q}}^{(0)} L_M + \bar{\Delta}_{q\bar{q}}^{(1)} \right] + \left(\frac{\alpha_s}{4\pi} \right)^2 \left[\left\{ \frac{1}{2} P_{q\bar{q}}^{(0)} \otimes P_{q\bar{q}}^{(0)} - \frac{1}{2} \beta_0 P_{q\bar{q}}^{(0)} \right\} L_M^2 \right. \\ \left. + \left\{ P_{q\bar{q}}^{(1),\text{NS}} - \beta_0 \bar{\Delta}_{q\bar{q}}^{(1)} + P_{q\bar{q}}^{(0)} \otimes \bar{\Delta}_{q\bar{q}}^{(1)} \right\} L_M + \bar{\Delta}_{q\bar{q}}^{(2),\text{NS}} \right] \end{aligned} \quad (4.2.39)$$

$$\bar{\Delta}_{q\bar{q}}^{\text{NS}} = \left(\frac{\alpha_s}{4\pi} \right)^2 \left[P_{q\bar{q}}^{(1),\text{NS}} L_M + \bar{\Delta}_{q\bar{q}}^{(2),\text{NS}} \right] \quad (4.2.40)$$

$$\begin{aligned} \bar{\Delta}_{q\bar{q}}^{\text{PS}} = \bar{\Delta}_{q\bar{q}}^{\text{PS}} = \left(\frac{\alpha_s}{4\pi} \right)^2 \left[\left\{ \frac{1}{16} P_{q\bar{q}}^{(0)} \otimes P_{q\bar{q}}^{(0)} \right\} L_M^2 + \left\{ \frac{1}{4} P_{q\bar{q}}^{(1),\text{PS}} + \right. \right. \\ \left. \left. \frac{1}{2} P_{q\bar{q}}^{(0)} \otimes \bar{\Delta}_{q\bar{q}}^{(1)} \right\} L_M + \bar{\Delta}_{q\bar{q}}^{(2),\text{PS}} \right] \end{aligned} \quad (4.2.41)$$

$$\begin{aligned}\bar{\Delta}_{q\bar{q}} = & \frac{\alpha_s}{4\pi} \left[\frac{1}{4} P_{q\bar{q}}^{(0)} L_M + \bar{\Delta}_{q\bar{q}}^{(1)} \right] + \left(\frac{\alpha_s}{4\pi} \right)^2 \left[\left\{ \frac{1}{16} P_{q\bar{q}}^{(0)} \otimes (3P_{q\bar{q}}^{(0)} + P_{g\bar{g}}^{(0)}) \right. \right. \\ & - \frac{1}{8} \beta_0 P_{q\bar{q}}^{(0)} \left. \right\} L_M^2 + \left\{ \frac{1}{4} P_{q\bar{q}}^{(1)} - \beta_0 \bar{\Delta}_{q\bar{q}}^{(1)} + \frac{1}{2} \bar{\Delta}_{q\bar{q}}^{(1)} \otimes (P_{q\bar{q}}^{(0)} + P_{g\bar{g}}^{(0)}) \right. \\ & \left. \left. + \frac{1}{4} P_{q\bar{q}}^{(0)} \otimes \bar{\Delta}_{q\bar{q}}^{(1)} \right\} L_M + \bar{\Delta}_{q\bar{q}}^{(2)} \right] \quad (4.2.42)\end{aligned}$$

$$\bar{\Delta}_{g\bar{g}} = \left(\frac{\alpha_s}{4\pi} \right)^2 \left[\left\{ \frac{1}{8} P_{q\bar{q}}^{(0)} \otimes P_{q\bar{q}}^{(0)} \right\} L_M^2 + \left\{ P_{q\bar{q}}^{(0)} \otimes \bar{\Delta}_{q\bar{q}}^{(1)} \right\} L_M + \bar{\Delta}_{g\bar{g}}^{(2)} \right] \quad (4.2.43)$$

The lowest order coefficients $\bar{\Delta}_{q\bar{q}}^{(1)}$ and $\bar{\Delta}_{q\bar{q}}^{(1)}$ can be found in many places in the literature, see e.g. [2]. The $\mathcal{O}(\alpha_s^2)$ contributions $\bar{\Delta}_{ij}^{(2)}$ have been recently calculated and are presented in appendix B of [14]. The DY coefficient function in the DIS scheme can now be expressed in the $\overline{\text{MS}}$ coefficients of \bar{C}_i in (4.2.21)–(4.2.25) and $\bar{\Delta}_{ij}$ in (4.2.44)–(4.2.48) as follows

$$\begin{aligned}\Delta_{q\bar{q}}^{\text{NS}} = & \bar{\Delta}_{q\bar{q}}^{\text{NS}} - 2 \left(\frac{\alpha_s}{4\pi} \right) \bar{c}_{2,q}^{(1)} + \left(\frac{\alpha_s}{4\pi} \right)^2 \left[-2P_{q\bar{q}}^{(0)} \otimes \bar{c}_{2,q}^{(1)} L_M - 2\bar{c}_{2,q}^{(2),\text{NS},+} \right. \\ & \left. + \bar{c}_{2,q}^{(1)} \otimes (3\bar{c}_{2,q}^{(1)} - 2\bar{\Delta}_{q\bar{q}}^{(1)}) \right] \quad (4.2.44)\end{aligned}$$

$$\Delta_{q\bar{q}}^{\text{NS}} = \bar{\Delta}_{q\bar{q}}^{\text{NS}} - 2 \left(\frac{\alpha_s}{4\pi} \right)^2 \bar{c}_{2,q}^{(2),\text{NS},-} \quad (4.2.45)$$

$$\begin{aligned}\Delta_{q\bar{q}}^{\text{PS}} = & \bar{\Delta}_{q\bar{q}}^{\text{PS}} + \left(\frac{\alpha_s}{4\pi} \right)^2 \left[\frac{1}{4} P_{q\bar{q}}^{(0)} \otimes \bar{c}_{2,q}^{(1)} L_M - \bar{c}_{2,q}^{(2),\text{PS}} \right. \\ & \left. + \bar{c}_{2,q}^{(1)} \otimes (\bar{\Delta}_{q\bar{q}}^{(1)} - \frac{1}{2} \bar{c}_{2,g}^{(1)}) \right] \quad (4.2.46)\end{aligned}$$

$$\begin{aligned}\Delta_{q\bar{q}} = & \bar{\Delta}_{q\bar{q}} - \frac{1}{2} \left(\frac{\alpha_s}{4\pi} \right) \bar{c}_{2,g}^{(1)} + \left(\frac{\alpha_s}{4\pi} \right)^2 \left[\left\{ -\frac{1}{4} P_{q\bar{q}}^{(0)} \otimes (\bar{c}_{2,q}^{(1)} - \bar{c}_{2,g}^{(1)}) \right. \right. \\ & - \frac{1}{2} P_{q\bar{q}}^{(0)} \otimes \bar{c}_{2,g}^{(1)} \left. \right\} L_M - \frac{1}{2} \bar{c}_{2,g}^{(2)} + \bar{c}_{2,g}^{(1)} \otimes (\bar{\Delta}_{q\bar{q}}^{(1)} - \frac{1}{2} \bar{c}_{2,g}^{(1)} - \frac{1}{2} \bar{\Delta}_{q\bar{q}}^{(1)} + \bar{c}_{2,q}^{(1)}) \\ & \left. - \bar{c}_{2,q}^{(1)} \otimes \bar{\Delta}_{q\bar{q}}^{(1)} \right] \quad (4.2.47)\end{aligned}$$

$$\Delta_{g\bar{g}} = \bar{\Delta}_{g\bar{g}} + \left(\frac{\alpha_s}{4\pi} \right)^2 \left[-\frac{1}{2} P_{q\bar{q}}^{(0)} \otimes \bar{c}_{2,g}^{(1)} L_M - \bar{c}_{2,g}^{(1)} \otimes (2\bar{\Delta}_{q\bar{q}}^{(1)} - \frac{1}{2} \bar{c}_{2,g}^{(1)}) \right] \quad (4.2.48)$$

The expressions for Δ_{ij} are explicitly given in appendix 4A.

Summarizing this section we conclude that the DY coefficient function has now been completely calculated up to order α_s^2 in the $\overline{\text{MS}}$ as well as DIS scheme. However in order to make a full phenomenological analysis two pieces are still missing.

The first piece is the three-loop contribution to the anomalous dimension γ_{ij} which determines the scale evolution of the parton densities. Notice that the coefficients of the perturbative expansion in the running coupling constant for the DY cross section are only scheme independent if $\Delta_{ij}^{(k)}$ as well as $\gamma_{ij}^{(k)}$ are known [20]. We will estimate the error due to the missing of the third order anomalous dimension $\gamma_{ij}^{(2)}$ in the next section. Another part that has to be calculated is heavy flavour production in the DY process. It is given by the reactions $q + \bar{q} \rightarrow Q + \bar{Q} + V$ (graphs A and B in fig. 4.7) and $g + g \rightarrow Q + \bar{Q} + V$ (fig. 4.6). In this thesis we assume all heavy flavours to be massless, which is probably correct for c and b production at large hadron colliders but certainly incorrect for top-quark production. However we expect that this effect will be small. Heavy quark contributions to the triangle graphs of figs. 4.4 and 4.5 have been studied in [21]. It turns out that these corrections are smaller than one percent of the DY cross section.

4.3 Total cross sections for W- and Z-production

In this section we will show results for vector boson production and compare them with the most recent data from the UA1 [22], UA2 [23] (CERN, Sp \bar{p} S) and CDF [24] (Fermilab, Tevatron) experiments. The total inclusive cross section is given by (see (4.2.2))

$$\sigma_{\text{tot}}(S) = \int dQ^2 \tau \sigma_V(Q^2, M_V^2) W_V(\tau, Q^2) . \quad (4.3.1)$$

The pointlike hadron cross section $\sigma_V(Q^2, M_V^2)$ for $V = \gamma, Z, W$ is explicitly given in appendix A of [14]. The hadronic structure function $W_V(\tau, Q^2)$ (4.2.3) can be written as

$$W_V(\tau, Q^2) = \sum_{ij} \int_{\tau}^1 \frac{dx}{x} \Phi_{ij}(x, M^2) \Delta_{ij}\left(\frac{\tau}{x}, Q^2, M^2\right) , \quad (4.3.2)$$

where Φ_{ij} denotes the parton flux which is defined by

$$\Phi_{ij}(x, M^2) = \int_x^1 \frac{dy}{y} PD_{ij}^V\left(y, \frac{x}{y}, M^2\right) . \quad (4.3.3)$$

The explicit form for $W_V(\tau, Q^2)$ can be found in (A.20) of [14]. The DY coefficient functions Δ_{ij} are listed in appendix B of [14] ($\overline{\text{MS}}$ scheme) and in appendix 4A of this chapter (DIS scheme). At high energies the total cross section is dominated by W- and Z-production. Since the widths of these vector bosons are small compared

Notation in text	Ref.	Notation in ref.	$\Lambda_{QCD}(GeV)$
MTEDI	[25]	Table II-FIT E-DIS	0.155
MTB1DI	[25]	Table I3-FIT B1-DIS	0.194
MTB1MS	[25]	Table I4-FIT B1-MS	0.194
MTB2DI	[25]	Table I5-FIT B2-DIS	0.191
MTB2MS	[25]	Table I6-FIT B2-MS	0.191
MTSNDI	[25]	Table II1-FIT SN-DIS	0.237
MTSNMS	[25]	Table II2-FIT SN-MS	0.237
MTSL	[25]	Table II3-FIT SL	0.144
DFLM4	[19]	Set 4	0.200

Table 4.1. List of parametrizations for the parton densities used in this chapter.

to their masses, the integral in (4.3.1) can be performed using the narrow width approximation.

We will now present the DY cross section and its K -factor for both $p\bar{p}$ and pp collisions at current and future high energy colliders. The C.M. energies under consideration are $\sqrt{S} = 0.63$ TeV (Sp\bar{p}S), $\sqrt{S} = 1.8$ TeV (Tevatron), $\sqrt{S} = 16$ TeV (LHC) and $\sqrt{S} = 40$ TeV (SSC). For the electroweak parameters we take the following values : $M_Z = 91.17$ GeV, $M_W = 80.29$ GeV, $G_F = 1.166 \cdot 10^{-5}$ GeV⁻² (Fermi constant), $\sin^2 \theta_W = 0.224$ and $\sin^2 \theta_C = 0.05$. Further we assume the top-quark to be heavier than the W. The running coupling constant $\alpha_s(R^2)$ is determined up to two loop order in the \overline{MS} scheme. The number of flavours n_f is chosen to be five and the QCD scale parameter Λ in $\alpha_s(R^2)$ is the same as the one appearing in the parton densities (see table 4.1).

In this section we will make a comparison between the DY cross section calculated in the DIS and in the \overline{MS} scheme. Therefore we need parton densities parametrized in both schemes, which however are based on the same set of data. Here we have taken the parametrizations of [25], in particular the ones based on the BCDMS experiment [26]. They are listed in table 4.1. We have also included the DFLM4 set [19] of parton densities which however are only available in the DIS scheme. Unless stated otherwise, all figures are obtained using the MTB1DI parametrization. The renormalization

scale R is always taken to be equal to the mass factorization scale M (see the comment below (4.2.4)), for which we have chosen the canonical value Q . Since the total cross section is calculated in the narrow width approximation, this implies $Q = M_V$ (vector boson mass). The dependence of the cross section on M and R will be discussed at the end of this section. Since we did not observe any difference in the behaviour of Z - and W -production, all figures and almost all tables are given for the W cross section σ_W where for convenience we have taken $\sigma_W = \sigma_{W^+} + \sigma_{W^-}$. All numerical results in this chapter are produced by our Fortran program ZWPROD.

For the discussion of the various contributions to the Drell-Yan coefficient function it is convenient to introduce the K -factor. In this chapter the theoretical K -factor is defined as follows

$$K_{th} = \sum_{n=0}^{\infty} K^{(n)} \quad (4.3.4)$$

where $K^{(n)}$ is the $\mathcal{O}(\alpha_s^n)$ contribution to the K -factor. It is given by

$$K^{(n)} = \frac{W^{(n)}(\tau, Q^2)}{W^{(0)}(\tau, Q^2)} = \frac{\sigma^{(n)}}{\sigma^{(0)}} \quad (4.3.5)$$

The functions $W^{(n)}(\tau, Q^2)$ and $\sigma^{(n)}$ are the $\mathcal{O}(\alpha_s^n)$ corrections to the hadronic structure function $W_V(\tau, Q^2)$ and cross section respectively, see (4.2.2). They both originate from the $\mathcal{O}(\alpha_s)$ part of Δ_{ij} (4.2.3). To study only the effect of the corrections to Δ_{ij} , we will use the same densities in the numerator as well as denominator of (4.3.5). In principle one should take the leading log (LL) approximation for $\sigma^{(0)}$ or $W_V^{(0)}$, but, as we will show later on, in practice one obtains better results if the next to leading log (NLL) parametrization for the parton densities is used. The order α_s^i corrected K -factor is defined by

$$K_i = \sum_{l=0}^i K^{(l)} = \frac{\sigma_i}{\sigma_0} \quad (4.3.6)$$

where σ_i is the $\mathcal{O}(\alpha_s^i)$ corrected DY cross section and σ_0 the Born contribution.

In the discussion of the results we will try to answer the following questions:

1. How large is the $\mathcal{O}(\alpha_s^2)$ contribution to the K -factor ($K^{(2)}$) compared to the $\mathcal{O}(\alpha_s)$ one ($K^{(1)}$)?
2. Which of the four different subprocesses, i.e. $q\bar{q}$, qg , qq and gg , dominates the $\mathcal{O}(\alpha_s^2)$ part of the DY cross section?
3. How does the cross section depend on the various parametrizations chosen for the parton densities?

4. How does the cross section depend on the different choices made for the factorization scale M and the renormalization scale R ?
5. How do the answers on questions 1–4 depend on the chosen scheme, i.e. DIS versus $\overline{\text{MS}}$?

As was already mentioned in [14], the answers to 1 and to lesser extent to 2 and 3 very heavily depend on the scales M and R and the chosen scheme. A change of scheme at a fixed value of M and R alters the coefficients in the perturbation series for Δ_{ij} . The same happens if in a given scheme M or R is varied. It also entails a redistribution of the contributions from the various production mechanisms to the cross section. Therefore the answers on 1, 2 and 3 only make sense if scheme and scale are specified. In this section we answer questions 1–4 in the DIS scheme and compare them with the results found in [14], which were presented in the $\overline{\text{MS}}$ scheme.

4.3.1 The size of the corrections

In fig. 4.10 we show the various K -factors defined in (4.3.5) and (4.3.6) for W -production at $p\bar{p}$ colliders where $0.5 \text{ TeV} < \sqrt{S} < 50 \text{ TeV}$. The figure reveals that in particular at large \sqrt{S} the $\mathcal{O}(\alpha_s^2)$ contribution to the K -factor i.e. $K^{(2)}$ is much smaller than $K^{(1)}$ so that in this region the first order corrected cross section σ_1 is hardly modified by including higher order QCD corrections. In the $\overline{\text{MS}}$ scheme $K^{(2)}$ [14] even becomes negative (LHC and SSC energies). However this depends on the specific choice made for the parton density parametrization. The property that $K^{(2)}$ is small at very large energies can be wholly attributed to the $q\bar{q}$ subprocess. Notice that the latter gives a negative contribution to the K -factor in the whole energy range so that the positive contribution of the $q\bar{q}$ subprocess is always compensated (see fig. 4.11). Notice that the $\mathcal{O}(\alpha_s)$ part from the $q\bar{q}$ subprocess to the K -factor $K^{(1)}$ is negative too. However in this case its absolute value is always smaller than the one computed for the $q\bar{q}$ reaction at the same order of α_s (see fig. 4.11).

The separate contributions to the K -factor coming from the four subprocesses in table 2.2 are shown in fig. 4.11. The features of this figure are exactly the same as already had been shown by choosing the $\overline{\text{MS}}$ scheme. Like in the case of $\overline{\text{MS}}$, the DIS scheme shows that the K -factor is dominated by the $q\bar{q}$ and qg subprocesses, whereas the contributions from the gg and qq channels are very small. The reason why some channels are more important than other ones, depends on the interplay between Φ_{ij} and Δ_{ij} in (4.3.2), since a contribution from a specific subprocess only

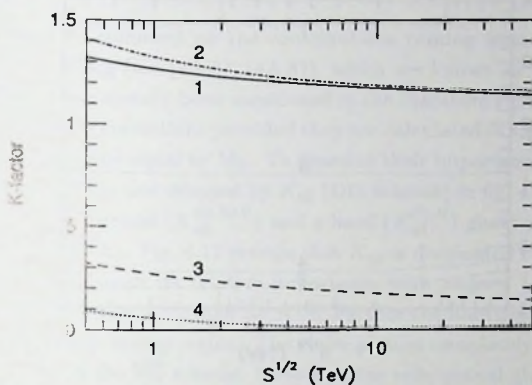


Fig. 4.10. The K -factor for $W^+ + W^-$ production at a $p\bar{p}$ collider (see eqs. (4.3.5) and (4.3.6)). 1: K_1 ; 2: K_2 ; 3: $K^{(1)}$; 4: $K^{(2)}$.

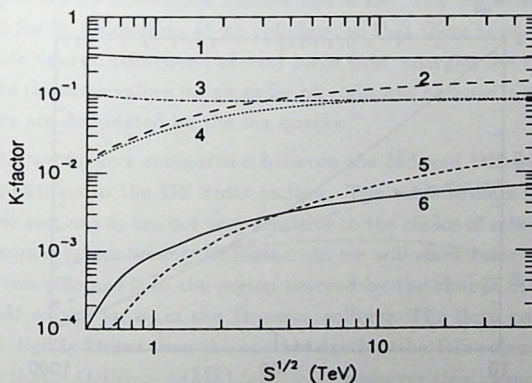


Fig. 4.11. The various contributions to the K -factor for $W^+ + W^-$ production at a $p\bar{p}$ collider (see eq. (4.3.5)). 1: $K_{q\bar{q}}^{(1)}$; 2: $-K_{q\bar{q}}^{(1)}$; 3: $K_{q\bar{q}}^{(2)}$; 4: $-K_{q\bar{q}}^{(2)}$; 5: $K_{gg}^{(2)}$; 6: $K_{q\bar{q}}^{(2)}$.

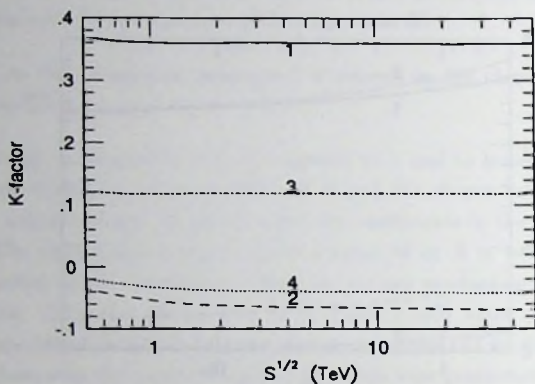


Fig. 4.12. The soft+virtual ($S + V$) and hard (H) gluon part of $K_{q\bar{q}}^{(i)}$ for $W^+ + W^-$ production at a $p\bar{p}$ collider (see eq. (4.3.5)). 1: $K_{q\bar{q}}^{(1),S+V}$; 2: $K_{q\bar{q}}^{(1),H}$; 3: $K_{q\bar{q}}^{(2),S+V}$; 4: $K_{q\bar{q}}^{(2),H}$.

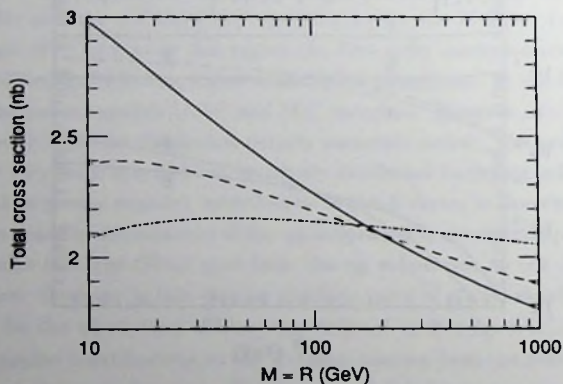


Fig. 4.13. Mass factorization scale (M) dependence of Z -production for $Sp\bar{p}S$, $\sqrt{S} = 0.63$ TeV. Solid line: $\sigma_0 + \sigma_{q\bar{q}}^{(1),S+V} + \sigma_{q\bar{q}}^{(2),S+V}$. Long-dashed line: $\sigma_{1,\text{exact}} + \sigma_{q\bar{q}}^{(2),S+V}$. Dash-dot line: $\sigma_{2,\text{exact}}$.

becomes large when the flux Φ_{ij} and the correction term Δ_{ij} get large in the same x -region.

We also want to comment on the contributions coming from the distributions \mathcal{D}_i and $\delta(1-x)$ in $\Delta_{q\bar{q}}$ (see (4A.3), (4A.8)), which are known as soft/virtual gluon contributions. As has already been mentioned in the literature ([16], [17], [27]) $\Delta_{q\bar{q}}^{(1)}$ is dominated by these corrections provided they are calculated in the DIS scheme and $M (= R)$ is chosen to be equal to M_V . To examine their importance we have plotted the corresponding K -factors denoted by $K_{q\bar{q}}$ (DIS scheme) in fig. 4.12. Here we have split $K_{q\bar{q}}^{(i)}$ into a soft/virtual ($K_{q\bar{q}}^{(i),S+V}$) and a hard ($K_{q\bar{q}}^{(i),H}$) gluon part, according to the description in (4A.2). Fig. 4.12 reveals that $K_{q\bar{q}}$ is dominated by the soft/virtual gluon correction, although its relative importance with respect to the hard gluon part is less pronounced for $K^{(2)}$ than for $K^{(1)}$. Further the hard gluon corrections are negative over the whole energy region. The above picture completely changes if the K -factor is computed in the $\overline{\text{MS}}$ scheme. Instead of the soft/virtual gluon contributions it is now the hard gluon part that dominates $K_{q\bar{q}}$ and the former is small and negative in the region $0.5 < \sqrt{S} < 50$ TeV. This observation illustrates very nicely that the answer to the question, which reaction or production mechanism is dominant, depends very much on the chosen scheme and scale. The above characteristics are also observed for W -production at pp colliders, so that there is no need to illustrate this in separate figures. Moreover, at very large C.M. energies the cross sections and K -factors take the same values for pp as for $p\bar{p}$ collisions because in this energy region both reactions are dominated by the sea quarks.

In table 4.2 we make a comparison between the $\overline{\text{MS}}$ and DIS predictions for the various contributions to the DY cross section. The table reveals that the order α_s^i corrected cross sections σ_i are not very sensitive to the choice of scheme, although the difference becomes larger when i increases. As we will show later on, the difference between the two schemes is in the region covered by the change of the mass factorization scale M except for σ_2 at the Tevatron collider. The Born cross section σ_0 for $\overline{\text{MS}}$ is always slightly larger than the one obtained in the DIS scheme. On the other hand we find that $\sigma_i(\text{DIS}) > \sigma_i(\overline{\text{MS}})$ for $i \geq 1$. However this inequality depends on the chosen parton density. Although the $\mathcal{O}(\alpha_s)$ and $\mathcal{O}(\alpha_s^2)$ contributions from the soft/virtual and hard gluon parts heavily depend on the chosen scheme, the total $q\bar{q}$ result is hardly affected by this choice. For the qg subprocess this dependence is stronger and we find both for the $\mathcal{O}(\alpha_s)$ and $\mathcal{O}(\alpha_s^2)$ contributions that the $\overline{\text{MS}}$ result is always more negative than the one obtained for DIS. Finally we observe that when the energy increases from 0.63 to 40 TeV the soft/virtual part of σ_i becomes less

$W^+ + W^-$ production (nb)								
	$S\bar{p}\bar{p}S$		Tevatron		LHC		SSC	
	\overline{MS}	DIS	\overline{MS}	DIS	\overline{MS}	DIS	\overline{MS}	DIS
Born								
$q\bar{q}$	4.91	4.87	15.9	15.6	119.	118.	262.	259.
$O(\alpha_s)$								
$q\bar{q}, S + V$	0.61	1.78	1.15	5.64	7.5	42.6	14.7	93.1
$q\bar{q}, H$	0.93	-0.21	3.40	-0.96	26.2	-7.8	58.2	-17.8
$q\bar{q}, \text{total}$	1.54	1.57	4.55	4.67	33.6	34.7	72.9	75.3
qg	-0.18	-0.10	-1.56	-0.98	-20.8	-15.4	-47.9	-37.6
$\sigma^{(1)}$	1.36	1.47	3.00	3.70	12.8	19.4	24.9	37.7
σ_1	6.26	6.34	18.9	19.3	132.	138.	287.	297.
$O(\alpha_s^2)$								
$q\bar{q}, S + V$	-0.05	0.58	-0.11	1.86	-0.8	14.0	-1.8	30.7
$q\bar{q}, H$	0.47	-0.12	1.31	-0.59	9.5	-4.8	20.3	-10.9
$q\bar{q}, \text{total}$	0.43	0.47	1.22	1.32	9.0	9.9	19.5	21.5
qg	-0.13	-0.09	-1.04	-0.79	-14.3	-10.2	-32.4	-22.3
gg	0.0022	0.0006	0.043	0.020	1.5	1.1	4.4	3.6
$q\bar{q} + q\bar{q}$	0.0020	0.0016	0.016	0.029	0.4	0.7	1.0	1.8
$\sigma^{(2)}$	0.31	0.38	0.24	0.58	-3.5	1.5	-7.5	4.6
σ_2	6.57	6.72	19.2	19.9	129.	139.	279.	302.

Table 4.2. Comparison of \overline{MS} and DIS scheme results at $S\bar{p}\bar{p}S$, Tevatron, LHC and SSC. The results were obtained using the MTB1MS (\overline{MS}) and MTB1DI (DIS) parton density parametrizations (see table 4.1).

important. Therefore at very large energies the soft gluon approximation to the total DY cross section breaks down. In this case resummation of the soft gluon terms, which entails the exponentiation of the large coefficient of the $\delta(1-x)$ function, does not make sense any more and overestimates the cross section. For $\sqrt{S} < 0.63$ TeV one can still apply resummation techniques provided one chooses a different factorization scale. An example is given for Z-production at the $S\bar{p}\bar{p}S$ ($\sqrt{S} = 0.63$ TeV) in fig. 4.13. Here we have plotted $\sigma_{2,\text{exact}}$, $\sigma_{1,\text{exact}} + \sigma_{q\bar{q}}^{(2),S+V}$ and $\sigma_0 + \sigma_{q\bar{q}}^{(1),S+V} + \sigma_{q\bar{q}}^{(2),S+V}$. This figure shows that when the hard gluon part and the other parton reactions are omitted one introduces a large scale variation in the total cross section. However if we choose $M = 148$ GeV, that is $1.6M_Z$, the cross section $\sigma_{2,\text{exact}}$ is nicely reproduced by $\sigma_{1,\text{exact}} + \sigma_{q\bar{q}}^{(2),S+V}$. This property can be used if we want to estimate the effect of

the $\mathcal{O}(\alpha_s^2)$ contributions to differential distributions like $d^2\sigma/dy dQ^2$ or $d^2\sigma/dx_F dQ^2$ in the DY process for which exact expressions do not exist. Here y and x_F denote the rapidity and longitudinal momentum fraction of the dilepton pair respectively. This estimate is only possible if one knows at least the soft/virtual gluon part of the above differential cross sections up to $\mathcal{O}(\alpha_s^2)$. Notice that besides the normalization one also gets a good approximation for the shape of the distributions, since in many processes the latter hardly change when higher order QCD corrections are taken into account. Finally the discussion of figs. 4.11, 4.12 and table 4.2 also applies to Z-production at pp and p \bar{p} colliders, so that there is no need to present separate figures or tables for this reaction.

4.3.2 Dependence on the parton density parametrization

Next we want to discuss the dependence of the DY cross section on the parametrization of the various parton densities used in this chapter. These densities are mainly extracted from data obtained in deep inelastic lepton-hadron scattering which are taken for $0.01 \leq x < 0.9$ and $2 \text{ GeV}^2 < Q^2 < 230 \text{ GeV}^2$. They depend on:

1. The specific data set obtained from different experiments like EMC [28], BCDMS [26] or CDHSW [29].
2. The parametrization of the parton densities $f_i(x, M^2)$ ($i = q, \bar{q}, g$) with respect to x at some input value for M^2 . At large energies the small- x behaviour is very important, in particular for the gluon density $G(x, M^2)$.
3. The evolution with respect to the scale M which is determined by the AP equation. It contains the AP splitting functions $P_{ij}^{(l)}$ which are known for $l = 0, 1$. Since they have not been calculated for $l > 1$, only leading log ($l = 0$) and next to leading log ($l = 0$ and $l = 1$) parametrizations for the parton densities exist.
4. The order of α_s in which the DIS coefficient function is taken into account. Since the parton densities are obtained from the DIS hadron structure function $F_j(x, Q^2)$ ($j = 2, 3$), one also needs the corresponding coefficient function up to $\mathcal{O}(\alpha_s^j)$, provided the AP splitting functions are known up to $\mathcal{O}(\alpha_s^{j+1})$.

The experiments done in the past provide us with different data sets which do not always agree. The quality of the data depends on statistical and systematical errors, detector efficiencies, luminosities etc. Often the data obtained from different

experiments have some discrepancies with respect to their mutual normalization. It is clear that these experimental uncertainties will influence the x -behaviour of the parton densities.

Although the parton densities give a reasonable fit of the current deep inelastic lepton hadron data, they are still inadequate to describe vector boson production at future high energy colliders. This process requires the knowledge of the parton densities at $x \sim M_V/\sqrt{S}$. For LHC and SSC this implies $x \sim 6 \cdot 10^{-3}$ and $x \sim 3 \cdot 10^{-3}$ respectively. A recent analysis [20] has shown that W - and Z -production at these future colliders even probes sea quarks at $x \sim 10M_V^2/S$, which is about $3 \cdot 10^{-5}$ for SSC. Therefore one has to extrapolate these densities to x -regions which were not accessible to the deep inelastic experiments carried out up to now. In the future this situation will improve when the HERA machine is put into operation. The above-mentioned uncertainty in the small- x dependence in particular affects the gluon density which is experimentally badly known. In the literature many parametrizations for this density exist, depending on the theoretical assumptions. Notice that such a change of the parametrization of the gluon density $G(x, M^2)$ at some input value for M^2 will also strongly influence the small- x behaviour of the sea quarks at higher M^2 , because the sea quarks are coupled to the gluons through the AP evolution equations. This implies that at high energies considerable differences in the size of the DY cross section can be expected, even at the Born level, if one changes the $x \rightarrow 0$ behaviour of $G(x, M^2)$ at some input value for M^2 . To incorporate this kind of uncertainties in our predictions for the W - and Z -production rates, we have taken the sets MTB1DI and MTB2DI in table 4.1, where for MTB2DI the gluon density shows a much steeper rise at $x \rightarrow 0$ than for MTB1DI.

The total cross sections for W - and Z -production are displayed for the four collider energies in tables 4.3 and 4.4 respectively. They show the same characteristics as observed in the \overline{MS} scheme [14]. For Sp \overline{p} S and Tevatron the difference between the various parametrizations is so large that one can hardly distinguish the $\mathcal{O}(\alpha_s)$ - from the $\mathcal{O}(\alpha_s^2)$ corrected cross sections. The situation becomes worse at LHC and SSC, where it even might become difficult to identify the first order corrections. This in particular holds for the MTB2DI set which yields a cross section which is roughly two times larger than the one obtained by the other parametrizations. The different predictions are mainly due to the different parametrizations of the small- x behaviour of the parton densities rather than on the data set from which the latter are derived. At the Sp \overline{p} S ($\sqrt{S} = 0.63$ TeV) the predictions obtained from the parton distributions in [25] (table 4.1) fairly agree. However the DFLM4 [19] leads to cross sections which

W ⁺ + W ⁻ production (nb)				
$\alpha_s(M_W)$	MTB1DI	DFLM4	MTB2DI	MTEDI
	0.118	0.118	0.117	0.114
Sp̄pS ($\sqrt{S} = 0.63$ TeV)				
Born	4.87	4.36	4.80	4.72
$\mathcal{O}(\alpha_s)$	6.34	5.73	6.26	6.09
$\mathcal{O}(\alpha_s^2)$	6.72	6.09	6.64	6.43
Tevatron ($\sqrt{S} = 1.8$ TeV)				
Born	15.6	16.2	16.2	14.5
$\mathcal{O}(\alpha_s)$	19.3	20.2	20.2	17.8
$\mathcal{O}(\alpha_s^2)$	19.9	20.9	21.0	18.2
LHC ($\sqrt{S} = 16$ TeV)				
Born	118.	131.	199.	102.
$\mathcal{O}(\alpha_s)$	138.	153.	238.	118.
$\mathcal{O}(\alpha_s^2)$	139.	154.	243.	119.
SSC ($\sqrt{S} = 40$ TeV)				
Born	259.	233.	576.	223.
$\mathcal{O}(\alpha_s)$	297.	263.	686.	254.
$\mathcal{O}(\alpha_s^2)$	302.	267.	701.	258.

Table 4.3. The total cross section for W-production at Sp̄pS, Tevatron, LHC and SSC.

are below the ones obtained from [25]. Unless the uncertainty originating from the use of different parametrizations for the parton densities is reduced, it will not be possible to learn much about higher order QCD corrections at future colliders by studying vector boson production.

Since the different parametrizations mainly affect the normalization of the cross sections, one gets a better impression of the size of the corrections by studying the K -factor (see (4.3.4)–(4.3.6)). Here the K -factor is defined in such a way that the same parametrization is used in the numerator as well as denominator in (4.3.5) and (4.3.6) so that the normalization effect, mainly due to the small- x behaviour, drops out. The first and second order K -factors for W- and Z-production are given in tables 4.5 and 4.6 respectively. Here one hardly sees any differences in K_1 and K_2 obtained from the various parametrizations except at very high energies. This is due to the

Z-production (nb)				
$\alpha_s(M_Z)$	MTB1DI	DFLM4	MTB2DI	MTEDI
	0.115	0.116	0.115	0.112
SppS ($\sqrt{S} = 0.63$ TeV)				
Born	1.55	1.36	1.52	1.58
$\mathcal{O}(\alpha_s)$	2.03	1.79	1.98	2.03
$\mathcal{O}(\alpha_s^2)$	2.15	1.91	2.11	2.15
Tevatron ($\sqrt{S} = 1.8$ TeV)				
Born	4.81	4.93	4.91	4.50
$\mathcal{O}(\alpha_s)$	5.96	6.17	6.13	5.52
$\mathcal{O}(\alpha_s^2)$	6.16	6.40	6.37	5.68
LHC ($\sqrt{S} = 16$. TeV)				
Born	36.1	40.0	58.8	31.0
$\mathcal{O}(\alpha_s)$	42.0	46.8	70.6	35.8
$\mathcal{O}(\alpha_s^2)$	42.5	47.4	72.2	36.2
SSC ($\sqrt{S} = 40$. TeV)				
Born	80.4	75.9	172.	69.1
$\mathcal{O}(\alpha_s)$	92.1	85.8	205.	78.6
$\mathcal{O}(\alpha_s^2)$	93.6	87.1	209.	80.0

Table 4.4. The total cross section for Z-production at SppS, Tevatron, LHC and SSC.

steeply rising gluon density in the MTB2DI set, which mainly influences the K -factor via the qg subprocess. From these tables one can also observe that the K -factors are roughly the same for W - and Z -production which implies that the ratio

$$R = \frac{\sigma_W}{\sigma_Z} \frac{B(W \rightarrow \ell \nu_\ell)}{B(Z \rightarrow \ell^+ \ell^-)} \quad (4.3.7)$$

is almost independent of QCD corrections.

4.3.3 The omission of the third order anomalous dimension

Besides the uncertainty in the small- x behaviour, which can be settled when the new HERA data become available, we also have to deal with the large scale extrapolation of the parton densities. These are extracted from measurements at scales which vary between $0.5 < Q^2 < 230 \text{ GeV}^2$ and which are about two orders of magnitude lower

W ⁺ + W ⁻ production				
$\alpha_s(M_W)$	MTB1DI	DFLM4	MTB2DI	MTEDI
	0.118	0.118	0.117	0.114
Sp̄pS ($\sqrt{S} = 0.63$ TeV)				
K_1	1.30	1.31	1.30	1.29
K_2	1.38	1.40	1.38	1.36
Tevatron ($\sqrt{S} = 1.8$ TeV)				
K_1	1.24	1.25	1.25	1.23
K_2	1.28	1.29	1.30	1.26
LHC ($\sqrt{S} = 16$ TeV)				
K_1	1.17	1.17	1.20	1.16
K_2	1.18	1.18	1.23	1.17
SSC ($\sqrt{S} = 40$ TeV)				
K_1	1.15	1.13	1.19	1.14
K_2	1.17	1.15	1.22	1.16

Table 4.5. K -factors for W-production at Sp̄pS, Tevatron, LHC and SSC.

than those characteristic for W- and Z-production where $Q^2 \sim 10^4$ GeV². Contrary to the small- x behaviour, one has a good theoretical knowledge of the extrapolation of the parton densities from low to high Q^2 values, since the scale evolution is determined by the AP equations. However in order to give an accurate determination of these densities at large scales one needs to know the higher order AP splitting functions in the evolution equation. That this is necessary one can immediately infer from table 4.7. Although the leading log (LL) and the next to leading log (NLL) approximation fit the low Q^2 data equally well, they give a different prediction for the W cross section. Here one has to compare the LL Born approximation with the fully $\mathcal{O}(\alpha_s)$ corrected NLL cross section in the DIS as well as in the $\overline{\text{MS}}$ scheme. Notice that the LL parametrization MTSL and the NLL parametrizations MTSNDI (DIS scheme) and MTSNMS ($\overline{\text{MS}}$ scheme) are based on the same data set. The discrepancy can be partially removed by including the $\mathcal{O}(\alpha_s)$ DY coefficient function in the LL approximation. In this case the error for $\sqrt{S} = 0.63, 1.8, 16$ and 40 TeV amounts to 5%, 12%, 25% and 28% of the exact $\mathcal{O}(\alpha_s)$ corrected cross section respectively, provided the correction is calculated in the DIS scheme. In the $\overline{\text{MS}}$ scheme the

Z-production				
$\alpha_s(M_Z)$	MTB1DI	DFLM4	MTB2DI	MTEDI
	0.115	0.116	0.115	0.112
Sp̄pS ($\sqrt{S} = 0.63$ TeV)				
K_1	1.31	1.32	1.30	1.28
K_2	1.39	1.40	1.38	1.36
Tevatron ($\sqrt{S} = 1.8$ TeV)				
K_1	1.24	1.25	1.25	1.23
K_2	1.28	1.30	1.30	1.26
LHC ($\sqrt{S} = 16$. TeV)				
K_1	1.17	1.17	1.20	1.15
K_2	1.18	1.19	1.23	1.17
SSC ($\sqrt{S} = 40$. TeV)				
K_1	1.15	1.13	1.19	1.14
K_2	1.16	1.15	1.21	1.16

Table 4.6. K -factors for Z-production at Sp̄pS, Tevatron, LHC and SSC.

discrepancy is larger and becomes 8%, 17%, 35% and 36%. The difference between the $\mathcal{O}(\alpha_s)$ corrected cross section in the LL and the one calculated in the NLL approximation can be wholly attributed to the missing second order splitting function $P_{ij}^{(1)}$ (4.2.10) in the former quantity. Therefore the error expressed in the percentages above is proportional to α_s . The fully $\mathcal{O}(\alpha_s^2)$ corrected cross section requires besides the $\mathcal{O}(\alpha_s^2)$ contribution to the DY coefficient function Δ_{ij} also the second order DI coefficient function $C^{(2)}$ and the third order AP splitting functions which are necessary to determine the next-to-next-to-leading log (NNLL) approximation for the parton densities. Although the coefficient functions are now known up to $\mathcal{O}(\alpha_s^2)$, the third order AP splitting functions have not been calculated yet, so that the NNLL parton densities are still not available. Therefore we have to rely on the NLL approximation in order to compute the cross section. Due to the absence of the third order splitting functions the error in the $\mathcal{O}(\alpha_s^2)$ results obtained by MTSNDI and MTSNMS in table 4.7 is of $\mathcal{O}(\alpha_s^2)$. This error can be estimated by squaring the relative errors expressed in percentages mentioned above for the $\mathcal{O}(\alpha_s)$ case. Here the discrepancies in the $\overline{\text{MS}}$ scheme will serve for guidance. Hence we quote as error for the $\mathcal{O}(\alpha_s^2)$ corrected

W ⁺ + W ⁻ production (nb)				
	DIS	\overline{MS}	DIS	\overline{MS}
	MTSL	MTSL	MTSNDI	MTSNMS
$\alpha_s(M_W)$	0.112	0.112	0.121	0.121
Sp $\overline{p}p$ S ($\sqrt{S} = 0.63$ TeV)				
Born	4.59	4.59	4.77	4.93
$\mathcal{O}(\alpha_s)$	5.92	5.78	6.26	6.36
$\mathcal{O}(\alpha_s^2)$	6.25	6.04	6.67	6.70
Tevatron ($\sqrt{S} = 1.8$ TeV)				
Born	14.4	14.4	16.0	17.1
$\mathcal{O}(\alpha_s)$	17.6	16.8	20.0	20.1
$\mathcal{O}(\alpha_s^2)$	18.1	16.9	20.1	21.1
LHC ($\sqrt{S} = 16$ TeV)				
Born	105.	105.	136.	152.
$\mathcal{O}(\alpha_s)$	119.	112.	160.	172.
$\mathcal{O}(\alpha_s^2)$	119.	107.	162.	168.
SSC ($\sqrt{S} = 40$ TeV)				
Born	233.	233.	311.	351.
$\mathcal{O}(\alpha_s)$	258.	244.	361.	391.
$\mathcal{O}(\alpha_s^2)$	258.	232.	366.	383.

Table 4.7. The total cross section for W-production at Sp $\overline{p}p$ S, Tevatron, LHC and SSC. In column 1 and 2 the DY coefficient function is determined in the DIS and \overline{MS} scheme respectively.

cross sections at $\sqrt{S} = 0.63, 1.8, 16, 40$ TeV the percentages 0.5%, 3%, 12% and 13% respectively.

Summarizing the above discussion, we have seen that the Born cross section using the LL approximation for the parton densities disagrees with the fully $\mathcal{O}(\alpha_s)$ corrected result. The difference is mainly due to the absence of the $\mathcal{O}(\alpha_s)$ DY coefficient function $\Delta_{ij}^{(1)}$ and to a lesser extent to the missing second order splitting function. Generalizing this to higher orders we expect that Δ_{ij} constitutes the bulk of the radiative corrections to the DY process, so that our $\mathcal{O}(\alpha_s^2)$ corrected cross section fairly approaches the exact $\mathcal{O}(\alpha_s^2)$ result. Here exact means including the NNLL order parton densities.

4.3.4 Scale dependence

After having discussed the uncertainties due to the choice of schemes, the set of parton densities, the small- x behaviour and large scale extrapolation, we investigate the factorization and renormalization scale dependence of the DY cross section. In [14] the variation of the cross sections was studied where the factorization scale M was put equal to the renormalization scale R . This was done because there is no distinction between these two scales in the parton densities. However in this chapter we will also study the cross section when M is varied independently of R . Using the MTB1DI parametrization we have plotted the cross section for W -production in the range $10 \text{ GeV} < M < 1000 \text{ GeV}$ with $M = R$ in figs. 4.14–4.17 for energies characteristic for the current and future colliders.

Here we show the $\mathcal{O}(\alpha_s^i)$ corrected cross sections σ_i (4.3.6) for the DIS scheme (MTB1DI set). In addition we have also plotted σ_2 in the $\overline{\text{MS}}$ scheme which is computed using the corresponding MTB1MS set. At increasing i we observe a considerable improvement in the scale dependence of σ_i , as was to be expected. In fig. 4.14 (Sp \bar{p} S) and fig. 4.15 (Tevatron) there is a maximum in σ_2 which is not present in σ_0 and σ_1 . According to the principle of minimal sensitivity (PMS) there is an optimal scale which however depends very heavily on the chosen scheme (see e.g. fig. 4.15). Notice that in fig. 4.15 the maximum in σ_2 for DIS turns into a minimum for $\overline{\text{MS}}$. Figs. 4.14, 4.15 also show that σ_0 never intersects σ_1 or σ_2 , a feature which was also observed in the $\overline{\text{MS}}$ scheme. This picture changes in fig. 4.16 (LHC) and fig. 4.17 (SSC) where the maximum in σ_2 has disappeared and $\sigma_2 = \sigma_0$ near $M = 100 \text{ GeV}$. The latter represents the optimal scale according to the principle of fastest apparent convergence (FAC). Comparing the DIS with the $\overline{\text{MS}}$ scheme we notice that in the range $10 \leq M \leq 1000 \text{ GeV}$, $(\sigma_2^{\text{DIS}})_{\text{max}} - (\sigma_2^{\text{DIS}})_{\text{min}} \leq \sigma_2^{\text{DIS}} - \sigma_2^{\overline{\text{MS}}}$ for all collider energies. We also see that σ_2^{DIS} is closer to $\sigma_2^{\overline{\text{MS}}}$ than σ_1^{DIS} to σ_2^{DIS} , except for fig. 4.15 (Tevatron). Further $\sigma_2^{\text{DIS}} > \sigma_2^{\overline{\text{MS}}}$, but this depends on the chosen parton density (here MTB1). In the case of MTSN (table 4.1) $\sigma_2^{\text{DIS}} < \sigma_2^{\overline{\text{MS}}}$ as can e.g. been seen in table 4.7. In order to study the variation of the cross sections under the change of scales and schemes more carefully, we have shown in table 4.8 the following quantities

$$S_i = \frac{(\sigma_i)_{\text{max}} - (\sigma_i)_{\text{min}}}{(\sigma_i)_{\text{av}}} \quad (4.3.8)$$

and

$$\Sigma_i = \frac{(\sigma_2^{\text{DIS}} - \sigma_2^{\overline{\text{MS}}})_{\text{max}}}{\bar{\sigma}_2}, \quad (4.3.9)$$

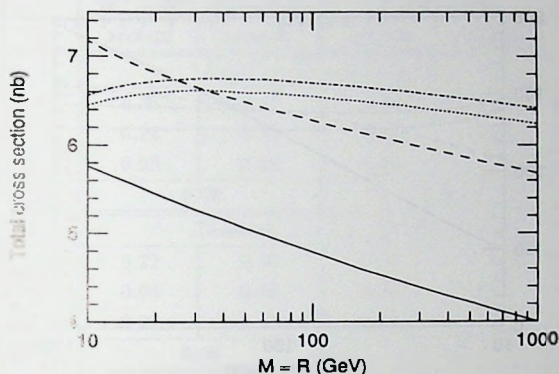


Fig. 4.14. Mass factorization scale (M) dependence of $\sigma_{W^{++}W^{-}}$ for SpPbS, $\sqrt{S} = 0.63$ TeV. Solid line: Born, DIS scheme. Long-dashed line: $\mathcal{O}(\alpha_s)$, DIS scheme. Dash-dot line: $\mathcal{O}(\alpha_s^2)$, DIS scheme. Dotted line: $\mathcal{O}(\alpha_s^2)$, $\overline{\text{MS}}$ scheme.

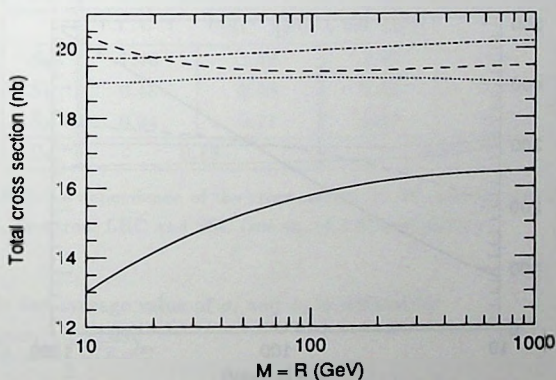


Fig. 4.15. Mass factorization scale (M) dependence of $\sigma_{W^{++}W^{-}}$ for Tevatron, $\sqrt{S} = 1.8$ TeV. Solid line: Born, DIS scheme. Long-dashed line: $\mathcal{O}(\alpha_s)$, DIS scheme. Dash-dot line: $\mathcal{O}(\alpha_s^2)$, DIS scheme. Dotted line: $\mathcal{O}(\alpha_s^2)$, $\overline{\text{MS}}$ scheme.

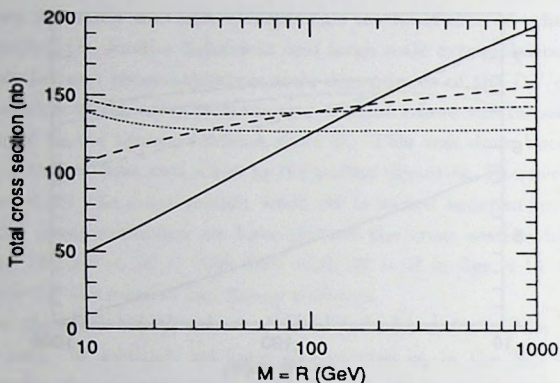


Fig. 4.16. Mass factorization scale (M) dependence of $\sigma_{W^+ + W^-}$ for LHC, $\sqrt{S} = 16$ TeV. Solid line: Born, DIS scheme. Long-dashed line: $\mathcal{O}(\alpha_s)$, DIS scheme. Dash-dot line: $\mathcal{O}(\alpha_s^2)$, DIS scheme. Dotted line: $\mathcal{O}(\alpha_s^2)$, $\overline{\text{MS}}$ scheme.

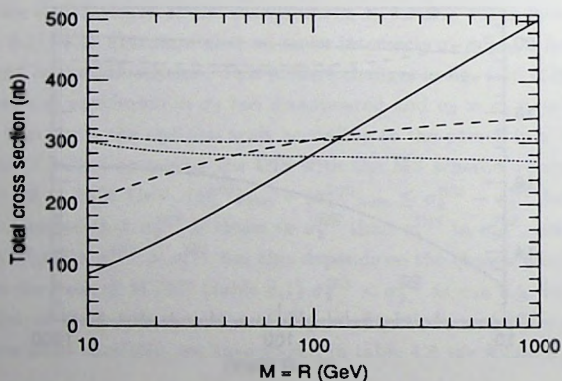


Fig. 4.17. Mass factorization scale (M) dependence of $\sigma_{W^+ + W^-}$ for SSC, $\sqrt{S} = 40$ TeV. Solid line: Born, DIS scheme. Long-dashed line: $\mathcal{O}(\alpha_s)$, DIS scheme. Dash-dot line: $\mathcal{O}(\alpha_s^2)$, DIS scheme. Dotted line: $\mathcal{O}(\alpha_s^2)$, $\overline{\text{MS}}$ scheme.

	W ⁺ + W ⁻ production		Z-production	
	MTB1DI	MTB1MS	MTB1DI	MTB1MS
	SppS ($\sqrt{S} = 0.63$ TeV)			
S_0	0.36	0.42	0.41	0.48
S_1	0.24	0.23	0.24	0.25
S_2	0.05	0.06	0.05	0.07
Σ_2	0.03		0.04	
	Tevatron ($\sqrt{S} = 1.8$ TeV)			
	0.22	0.16	0.14	0.09
	0.06	0.06	0.08	0.11
	0.02	0.01	0.02	0.02
Σ_2	0.06		0.06	
	LHC ($\sqrt{S} = 16$ TeV)			
S_0	1.18	1.18	1.13	1.06
S_1	0.36	0.33	0.33	0.23
S_2	0.06	0.09	0.09	0.14
Σ_2	0.11		0.17	
	SSC ($\sqrt{S} = 40$ TeV)			
S_0	1.46	1.46	1.41	1.35
S_1	0.48	0.43	0.45	0.36
S_2	0.04	0.11	0.07	0.17
Σ_2	0.13		0.20	

Table 4.8. Scale dependence of the cross section for W- and for Z-production at SppS, Tevatron, LHC and SSC (see eq. (4.3.8) and (4.3.9)).

where $(\sigma_i)_{av}$ is the average value of σ_i and $\bar{\sigma}_2$ is defined by

$$\bar{\sigma}_2 = \frac{(\sigma_2^{DIS})_{av} + (\sigma_2^{\overline{MS}})_{av}}{2} \quad (4.3.10)$$

From table 4.8 we infer that the scale variation in the cross sections decreases when higher order QCD corrections are taken into account. One also observes $\Sigma_2 > S_2$ except for $\sqrt{S} = 0.63$ TeV (SppS), which leads to the conclusion that a change in schemes leads to a slightly larger variation than a change in M (factorization scale). However this difference is not very significant if one realizes that the DIS parametrization in [25] is obtained from the \overline{MS} densities via a finite mass factorization where

the second order coefficient function is not taken into account. Moreover the third order splitting functions are omitted in all existing parametrizations.

In the three dimensional plots fig. 4.18 and 4.19 we show the variation of σ_2 (DIS) when M is varied independently of R and vice versa in the range $0.5M_W < M, R < 2.0M_W$. We see that the variation in M introduces more or less the same changes in σ_2 as the variation in R for $\sqrt{S} = 0.63$ TeV (fig. 4.18) as well as $\sqrt{S} = 1.8$ TeV (fig. 4.19). Notice that changes in the DY coefficient function due to a variation in M can be compensated by the parton flux (4.3.3), since the latter depends on the mass factorization scale too. However R does not appear in the parton flux so that one would expect that σ_2 is much more sensitive to the renormalization scale, which is actually not the case as one can see in figs. 4.18 and 4.19.

4.3.5 Comparison with experiment

Bearing in mind the uncertainties due to the parametrization of the parton density, the choice of scale and the choice of scheme, we can now predict the cross sections measured by the UA1 [22], UA2 [23] and CDF [24] collaborations. In particular we focus the attention on the decay channels $W \rightarrow l\nu_l$ and $Z \rightarrow l^+l^-$ for $l = e, \mu$. In this case we have to multiply the total cross sections σ_i with the branching ratios $BR(W \rightarrow l\nu_l)$ and $BR(Z \rightarrow l^+l^-)$.

Starting with the CERN collider SppS ($\sqrt{S} = 0.63$ TeV, see table 4.9), we find that the central values of the UA1 results for W- and Z-production [22], which were obtained in the μ, ν_μ channel only, are well below our second order predictions. However due to the large statistical and systematical errors, all our results are compatible with their data. In the case of UA2 [23] for Z-production the second order corrected cross sections σ_2 are in very good agreement with the experimental values, although the first order corrected ones σ_1 can accommodate the data rather well too. However like for UA1 the UA2 data for W-production lie systematically below our $\mathcal{O}(\alpha_s^2)$ predictions. For the Tevatron collider at FNAL ($\sqrt{S} = 1.8$ TeV, see table 4.10), the Born approximation as well as the higher order corrected cross section agree with the data due to the large systematic errors in the CDF experiment [24]. The predictions in tables 4.9, 4.10 are not very sensitive to the chosen scheme. They also do not depend too much on the chosen parametrizations, although the parton densities based on the EMC data (MTED1, MTEMS) lead to values for the cross sections lying below the ones derived from the BCDMS group. Since the C.M. energies are not too large, the difference between the predictions based on different parametrizations for the gluon density (MTB1 versus MTB2) does not become significant yet.

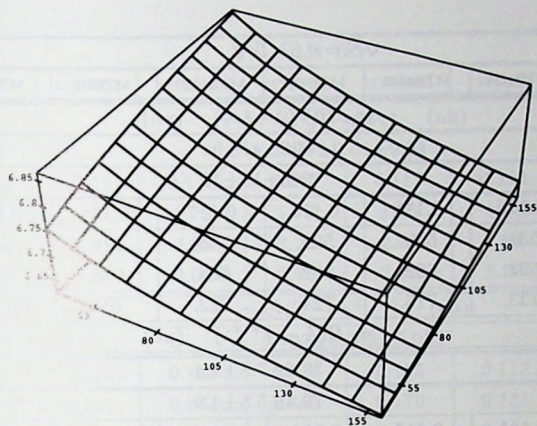


Fig. 4.18. Mass factorization scale (M) and renormalization scale (R) dependence of σ_{W++W-} (nb) for SppS, $\sqrt{S} = 0.63$ TeV. M and R are expressed in units of GeV.

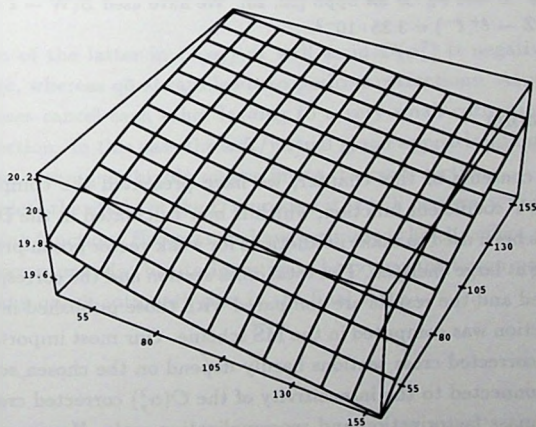


Fig. 4.19. Mass factorization scale (M) and renormalization scale (R) dependence of σ_{W++W-} (nb) for Tevatron, $\sqrt{S} = 1.8$ TeV. M and R are expressed in units of GeV.

$\sqrt{S} = 0.63 \text{ TeV}$						
	MTB1DI	MTB1MS	MTB2DI	MTB2MS	MTEDI	MTEMS
	$\sigma_W B(W \rightarrow \ell \nu_\ell) \text{ (pb)}$					
UA1	$609 \pm 41 \pm 94$					
UA2	$660 \pm 15 \pm 37$					
$\alpha_s(M_W)$	0.118	0.118	0.117	0.117	0.114	0.114
Born	531.	535.	523.	535.	514.	525.
$\mathcal{O}(\alpha_s)$	691.	682.	682.	686.	663.	685.
$\mathcal{O}(\alpha_s^2)$	733.	715.	723.	722.	701.	715.
	$\sigma_Z B(Z \rightarrow \ell^+ \ell^-) \text{ (pb)}$					
UA1	$58.6 \pm 7.8 \pm 8.4$					
UA2	$70.4 \pm 5.5 \pm 4.0$					
$\alpha_s(M_Z)$	0.115	0.115	0.115	0.115	0.112	0.112
Born	51.9	51.9	50.9	51.4	53.0	53.6
$\mathcal{O}(\alpha_s)$	68.0	66.7	66.3	66.1	68.0	67.7
$\mathcal{O}(\alpha_s^2)$	72.1	70.0	70.7	69.7	72.1	71.4

Table 4.9. $\sigma_W \cdot B$ and $\sigma_Z \cdot B$ for Sp \bar{p} S [22, 23]. We have used $B(W \rightarrow \ell \nu_\ell) = 0.109$ and $B(Z \rightarrow \ell^+ \ell^-) = 3.35 \cdot 10^{-2}$.

4.3.6 Conclusions

Summarizing the contents of this chapter, we have presented the complete $\mathcal{O}(\alpha_s^2)$ correction to the DY coefficient function, which is now calculated in the DIS scheme. This correction has been used to make predictions for weak vector boson production in $p\bar{p}$ and pp colliders at large energies. The total cross section and the corresponding K -factors are analyzed and the results are compared with those published in [14] where the coefficient function was computed in the $\overline{\text{MS}}$ scheme. Our most important finding is that the $\mathcal{O}(\alpha_s^2)$ corrected cross sections hardly depend on the chosen scheme (DIS or $\overline{\text{MS}}$). This is connected to the insensitivity of the $\mathcal{O}(\alpha_s^2)$ corrected cross sections to changes in the mass factorization and renormalization scale. However the results heavily depend on the chosen parametrizations for the parton densities. In particular we want to mention the difference between the LL and NLL approximation and the sensitivity to the small- x extrapolation of the parton densities, in particular the gluon density. The two dominant parton subprocesses are the $q\bar{q}$ - and the qg -process. The

$\sqrt{S} = 1.8 \text{ TeV}$						
	MTB1DI	MTB1MS	MTB2DI	MTB2MS	MTEDI	MTEMS
	$\sigma_W B(W \rightarrow e \nu_e) \text{ (nb)}$					
CDF	$2.06 \pm 0.04 \pm 0.34$					
$\alpha_s(M_W)$	0.118	0.118	0.117	0.117	0.114	0.114
Born	1.70	1.73	1.77	1.85	1.58	1.68
$\mathcal{O}(\alpha_s)$	2.10	2.06	2.20	2.24	1.94	1.98
$\mathcal{O}(\alpha_s^2)$	2.17	2.09	2.28	2.28	1.98	2.01
	$\sigma_Z B(Z \rightarrow e^+ e^-) \text{ (nb)}$					
CDF	$0.197 \pm 0.012 \pm 0.032$					
$\alpha_s(M_Z)$	0.115	0.115	0.115	0.115	0.112	0.112
Born	0.161	0.164	0.165	0.170	0.151	0.159
$\mathcal{O}(\alpha_s)$	0.200	0.196	0.205	0.207	0.185	0.189
$\mathcal{O}(\alpha_s^2)$	0.206	0.199	0.213	0.213	0.190	0.193

Table 4.10. $\sigma_W \cdot B$ and $\sigma_Z \cdot B$ for Tevatron [24]. We have used $B(W \rightarrow e \nu_e) = 0.109$ and $B(Z \rightarrow e^+ e^-) = 3.35 \cdot 10^{-2}$.

contribution of the latter in $\mathcal{O}(\alpha_s)$ as well as in $\mathcal{O}(\alpha_s^2)$ is negative over the whole energy range, whereas $q\bar{q}$ always leads to positive corrections. At very large energies both processes cancel each other leading to a very small correction to the K -factor and cross section. In this case the soft/virtual gluon approximation breaks down and resummation techniques highly overestimate the cross section.

To complete the study of the DY process it is still necessary to compute the third order splitting function. However we have estimated that its effect will turn out to be small. Moreover one also has to investigate heavy vector boson production together with an heavy quark-antiquark pair in the final state.

Appendix

4A Drell-Yan coefficient functions

In this appendix we will present the explicit expressions for the DY coefficient functions Δ_{ij} , the calculation of which is outlined in section 4.2. In order to make the presentation self contained we also give the $\mathcal{O}(\alpha_s)$ corrections already calculated in the literature [16, 17, 27]. We distinguish the following contributions to Δ_{ij} :

- I. quark-antiquark (non-singlet and other contributions)
- II. (anti)quark-gluon,
- III. the quark-antiquark (pure singlet) and non-identical quark-quark,
- IV. the identical quark-quark and
- V. gluon-gluon.

Before presenting the results, we want to make two remarks. Firstly, in the expressions below the scale in the running coupling constant α_s is always taken to be the renormalization scale R . Secondly, for the interference terms, we use the convention that $AC = AC^\dagger + CA^\dagger$, etc. (see figs. 4.7–4.9). The way the parton densities combine with the various Δ_{ij} is explicitly given in (A.20) of [14].

I The quark-antiquark contributions $\Delta_{q\bar{q}}^{\text{NS}}$

The lowest order contribution originating from the Born graph in fig. 4.1 is given by

$$\Delta_{q\bar{q}}^{(0)} = \delta(1-x) \quad . \quad (4A.1)$$

The $\mathcal{O}(\alpha_s)$ correction to the $q\bar{q}$ subprocess which receives contributions from the graphs in figs. 4.2 and 4.3 has been calculated in the literature [16, 17, 27]. From the numerical as well as the theoretical point of view it is convenient to split $\Delta_{q\bar{q}}^{(1)}$ into two pieces¹, viz.

$$\Delta_{q\bar{q}}^{(1)}(x) = \Delta_{q\bar{q}}^{(1),S+V}(x) + \Delta_{q\bar{q}}^{(1),H}(x) \quad , \quad (4A.2)$$

where the superscripts $S+V$ and H denote the soft/virtual and hard gluon part respectively. The soft (S) gluon part is obtained from fig. 4.3 by taking the soft

¹Note that in $\mathcal{O}(\alpha_s)$ $\Delta_{q\bar{q}}^{(1)} = \Delta_{q\bar{q}}^{\text{NS}}$.

limit $x \rightarrow 1$ in the phase space integrals. The virtual (V) part is determined by the Feynman graphs in fig. 4.2. The expression for $\Delta_{q\bar{q}}^{(1),S+V}$ equals

$$\Delta_{q\bar{q}}^{(1),S+V} = \frac{\alpha_s}{4\pi} C_F \left\{ \delta(1-x) \left[6 \ln \left(\frac{Q^2}{M^2} \right) + 16\zeta(2) + 2 \right] + 8\mathcal{D}_0 \ln \left(\frac{Q^2}{M^2} \right) + 8\mathcal{D}_1 + 6\mathcal{D}_0 \right\} . \quad (4A.3)$$

The distribution \mathcal{D}_i which is defined by

$$\mathcal{D}_i = \delta(1-x) \frac{\ln^{i+1} \delta}{(i+1)} + \theta(1-\delta-x) \frac{\ln^i(1-x)}{1-x} , \quad (4A.4)$$

originates from soft gluons only, whereas the coefficient of the function $\delta(1-x)$ receives contributions from the soft as well as virtual gluon corrections. The parameter δ [17], [27] is introduced in order to distinguish between the soft ($x \geq 1-\delta$) and hard ($x \leq 1-\delta$) gluon regions in the phase space integrals, showing up in the calculation of the graphs in fig. 4.3. The $\ln \delta$ terms arise when the factor $(1-x)^{-1+\epsilon}$ appearing in these integrals is replaced by the distribution

$$(1-x)^{-1+\epsilon} \rightarrow \frac{1}{\epsilon} \delta^\epsilon \delta(1-x) + (1-x)^{-1+\epsilon} \theta(1-x-\delta) . \quad (4A.5)$$

In the literature the $\ln \delta$ terms are often omitted and the distributions \mathcal{D}_i are then denoted by $(\ln^i(1-x)/(1-x))_+$, see e.g. [2], [16]. The hard gluon part which originates from the region $x \leq 1-\delta$ in the phase space integrals is given by

$$\Delta_{q\bar{q}}^{(1),H} = \frac{\alpha_s}{4\pi} C_F \left\{ -4(1+x) \ln \left(\frac{(1-x)Q^2}{M^2} \right) - 8x - 12 \right\} , \quad (4A.6)$$

with $C_F = (N^2 - 1)/2N$ for $SU(N)$.

The $\mathcal{O}(\alpha_s^2)$ contribution to $\Delta_{q\bar{q}}$ is determined by the diagrams in figs. 4.4–4.7. It also includes the interference between the quark-antiquark annihilation graphs in fig. 4.7. and the gluon exchange graphs in fig. 4.8. It can be split into two parts. The first part originates from the graphs in figs. 4.4–4.6 and the combinations in figs. 4.7 and 4.8 represented by A², AC and AD. Since the corresponding renormalized parton structure function $\widehat{W}_{q\bar{q}}$ has collinear divergences we have to perform mass factorization. Therefore this first part does not depend on the produced vector boson V, so that it shows up in the DY hadronic structure function $W_V(\tau, Q^2)$ in (2.3) for V = γ , Z and W. The second part of $\Delta_{q\bar{q}}^{(2)}$ consists of the contributions $\Delta_{q\bar{q},B^2}^{(2)}$, $\Delta_{q\bar{q},BC}^{(2)} = \Delta_{q\bar{q},BD}^{(2)}$, $\Delta_{q\bar{q},AC}^{(2),V}$ and $\Delta_{q\bar{q},AC}^{(2),A}$ ², see figs. 4.7 and 4.8. The appearance of

²Here V and A refer to vector-vector and axial vector-axial vector interference terms.

this part in $W_V(\tau, Q^2)$ depends on the specific type of vector boson under consideration, which implies that the corresponding $W_{q\bar{q}}$ from which $\Delta_{q\bar{q}}$ is derived has to be collinearly finite. The total resulting coefficient function is denoted by (see also (2.39))

$$\begin{aligned}\Delta_{q\bar{q}}^{(2),NS} = & \Delta_{q\bar{q}}^{(2),S+V} + \Delta_{q\bar{q}}^{(2),C_A} + \Delta_{q\bar{q}}^{(2),C_F} + \Delta_{q\bar{q}}^{(2),A^2} \quad (\text{first part}) \\ & + \Delta_{q\bar{q},B^2}^{(2)} + \Delta_{q\bar{q},BC}^{(2)} + \Delta_{q\bar{q},AC}^{(2),V} + \Delta_{q\bar{q},AC}^{(2),A} \quad (\text{second part}) \\ & + \frac{\alpha_s}{4\pi} \beta_0 \Delta_{q\bar{q}}^{(1)} \ln \left(\frac{R^2}{M^2} \right)\end{aligned}\quad (4A.7)$$

where β_0 represents the lowest order coefficient of the β -function (2.25) which originates from coupling constant renormalization and $\Delta_{q\bar{q}}^{(1)}$ is given in (4A.2). The symbols M and R stand for the mass factorization and renormalization scale respectively.

Let us first discuss the contributions of the first part to $\Delta_{q\bar{q}}^{(2),NS}$ (4A.7). Like (4A.2) it can be split into a soft/virtual ($S+V$) part and a hard (H) gluon part. The former is determined by the two loop graphs in fig. 4.4, the soft gluon radiative corrections coming from figs. 4.5, 4.6 and the collinear quark-antiquark pairs originating from the combinations A^2 in fig. 4.7 and AC, AD in figs. 4.7 and 4.8. The expression for the $S+V$ part is equal to

$$\begin{aligned}\Delta_{q\bar{q}}^{(2),S+V} = & \left(\frac{\alpha_s}{4\pi} \right)^2 \delta(1-x) \left\{ C_A C_F \left[-11 \ln^2 \left(\frac{Q^2}{M^2} \right) \right. \right. \\ & + \left[\frac{193}{3} - 24\zeta(3) \right] \ln \left(\frac{Q^2}{M^2} \right) - \frac{154}{5} \zeta(2)^2 + \frac{2098}{9} \zeta(2) - \frac{196}{3} \zeta(3) + \frac{215}{9} \left. \right] \\ & + C_F^2 \left[\left[18 - 32\zeta(2) \right] \ln^2 \left(\frac{Q^2}{M^2} \right) + \left[24\zeta(2) + 112\zeta(3) + 15 \right] \ln \left(\frac{Q^2}{M^2} \right) \right. \\ & + \frac{548}{5} \zeta(2)^2 - 3\zeta(2) + 120\zeta(3) \left. \right] + n_f C_F \left[2 \ln^2 \left(\frac{Q^2}{M^2} \right) \right. \\ & - \frac{34}{3} \ln \left(\frac{Q^2}{M^2} \right) + \frac{16}{3} \zeta(3) - \frac{340}{9} \zeta(2) - \frac{38}{9} \left. \right] \left. \right\} \\ & + C_A C_F \left[-\frac{44}{3} \mathcal{D}_0 \ln^2 \left(\frac{Q^2}{M^2} \right) + \left[\left(\frac{536}{9} - 16\zeta(2) \right) \mathcal{D}_0 \right. \right. \\ & - \frac{176}{3} \mathcal{D}_1 \left. \right] \ln \left(\frac{Q^2}{M^2} \right) - 44 \mathcal{D}_2 + \left[\frac{338}{9} - 16\zeta(2) \right] \mathcal{D}_1 - \left[24\zeta(3) \right. \\ & - \frac{88}{3} \zeta(2) - 57 \left. \right] \mathcal{D}_0 \left. \right] + C_F^2 \left[\left[64 \mathcal{D}_1 + 48 \mathcal{D}_0 \right] \ln^2 \left(\frac{Q^2}{M^2} \right) \right. \\ & + \left[96 \mathcal{D}_2 + 144 \mathcal{D}_1 + (52 + 64\zeta(2)) \mathcal{D}_0 \right] \ln \left(\frac{Q^2}{M^2} \right) \end{aligned}$$

$$\begin{aligned}
& + 32\mathcal{D}_3 + 72\mathcal{D}_2 + (52 + 64\zeta(2))\mathcal{D}_1 + (112\zeta(3) + 24\zeta(2) + 15)\mathcal{D}_0 \Big] \\
& + n_f C_F \left[\frac{8}{3} \mathcal{D}_0 \ln^2 \left(\frac{Q^2}{M^2} \right) + \left[\frac{32}{3} \mathcal{D}_1 - \frac{80}{9} \mathcal{D}_0 \right] \ln \left(\frac{Q^2}{M^2} \right) \right. \\
& \left. + 8\mathcal{D}_2 - \frac{44}{9} \mathcal{D}_1 - (10 + \frac{16}{3}\zeta(2))\mathcal{D}_0 \right] \quad (4A.8)
\end{aligned}$$

Adding the hard gluon contribution from figs. 4.5 and 4.6 to the interference terms corresponding to the combinations AC and AD in figs. 4.7 and 4.8 yields $\Delta_{q\bar{q}}^{(2),C_A}$ and $\Delta_{q\bar{q}}^{(2),C_F}$, where the superscripts $C_A = N$ and $C_F = (N^2 - 1)/2N$ refer to the two colour structures. The expressions for these quantities are

$$\begin{aligned}
\Delta_{q\bar{q}}^{(2),C_A} = & \left(\frac{N^2-1}{N} \right)^2 C_A C_F \left\{ \frac{22}{3} (1+x) \ln^2 \left(\frac{Q^2}{M^2} \right) \right. \\
& + \left[\frac{1+x^2}{1-x} \left[-16 \text{Li}_2(1-x) - 4 \ln^2 x + \frac{52}{3} \ln x \right] \right. \\
& + (1+x) \left[8\zeta(2) + \frac{88}{3} \ln(1-x) - \frac{60}{3} \ln x \right] \\
& - \frac{4}{9} (91 + 61x) \left. \right] \ln \left(\frac{Q^2}{M^2} \right) + \frac{1+x^2}{1-x} \left[8 S_{1,2}(1-x) - 4 \text{Li}_3(1-x) \right. \\
& - \frac{22}{3} \text{Li}_2(1-x) + 12 \text{Li}_2(1-x) \ln x - \frac{2}{3} \ln^3 x + 8\zeta(2) \ln x \\
& + 4 \ln^2 x \ln(1-x) + 48 \text{Li}_3(-x) - 24 \text{Li}_2(-x) \ln x - \frac{11}{3} \ln^2 x \\
& + 36\zeta(3) + \frac{88}{3} \ln x \ln(1-x) + 33 \ln x \left. \right] + (1+x) \left[-4 \text{Li}_3(1-x) \right. \\
& + 12\zeta(3) + 8 \text{Li}_2(1-x) \ln(1-x) - 4 \text{Li}_2(1-x) \ln x - \frac{2}{3} \ln^3 x \\
& + 22 \ln^2(1-x) \left. \right] + 4(10x-2) \left[\text{Li}_2(-x) \ln x - 2 \text{Li}_3(-x) \right] \\
& - \frac{8}{5} (9x^3 + 30x^2 - 5x - 25 - \frac{1}{x^2}) \left[\text{Li}_2(-x) + \ln x \ln(1+x) \right] \\
& + 8(1+7x) S_{1,2}(1-x) + 16(1-2x) \ln(1-x) \zeta(2) + \frac{2}{3} (25x+13) \text{Li}_2(1-x) \\
& - 4 \left(\frac{18}{5} x^3 + 12x^2 - \frac{1}{3} x + \frac{5}{3} \right) \zeta(2) + \left(\frac{36}{5} x^3 + 24x^2 - \frac{59}{3} x - \frac{11}{3} \right) \ln^2 x \\
& + 8(3x+1) \ln x \ln(1-x) + \frac{1}{5} (72x^2 - \frac{913}{3} x - 311 - \frac{8}{x}) \ln x \\
& \left. + \frac{4}{9} (5x+98) \ln(1-x) + \frac{2}{5} (36x^2 - \frac{2591}{9} x - \frac{998}{3} + \frac{4}{x}) \right\} \quad (4A.9)
\end{aligned}$$

and

$$\begin{aligned}
\Delta_{q\bar{q}}^{(2),CF} = & \left(\frac{\alpha_s}{4\pi}\right)^2 C_F^2 \left\{ \left[-16 \frac{1+x^2}{1-x} \ln x + 8(1+x) \left[\ln x - 4 \ln(1-x) \right] \right. \right. \\
& - 8(5+x) \left. \right] \ln^2 \left(\frac{Q^2}{M^2} \right) + \left[\frac{1+x^2}{1-x} \left[16 \text{Li}_2(1-x) + 8 \ln^2 x - 24 \ln x \right. \right. \\
& - 48 \ln x \ln(1-x) \left. \right] + (1+x) \left[16 \text{Li}_2(1-x) - 32\zeta(2) - 4 \ln^2 x \right. \\
& + 16 \ln x \ln(1-x) - 48 \ln^2(1-x) \left. \right] - 16(3+5x) + 16(4+x) \ln x \\
& - 16(11+5x) \ln(1-x) \left. \right] \ln \left(\frac{Q^2}{M^2} \right) \\
& + \frac{1+x^2}{1-x} \left[-64 S_{1,2}(1-x) - 40 \text{Li}_2(1-x) \ln x - \frac{8}{3} \ln^3 x \right. \\
& - 96 \text{Li}_3(-x) + 24\zeta(2) \ln x + 8 \ln^2 x \ln(1-x) - 32 \ln^2(1-x) \ln x \\
& + 12 \ln^2 x - 48 \ln x \ln(1-x) + 48 \ln x \text{Li}_2(-x) - \frac{45}{2} \ln x \left. \right] \\
& + (1+x) \left[2 \ln^3 x - 16 \ln^3(1-x) - 8 \text{Li}_3(1-x) - 4\zeta(2) \ln x \right. \\
& - 56\zeta(3) - 4 \ln^2 x \ln(1-x) + 8 \ln^2(1-x) \ln x \\
& + 20 \text{Li}_2(1-x) \ln x \left. \right] - 48(1-x) \ln(1-x) \zeta(2) \\
& + 16(1-5x) \left[S_{1,2}(1-x) - 2 \text{Li}_3(-x) + \ln x \text{Li}_2(-x) \right] \\
& + \frac{16}{5} (9x^3 + 30x^2 - 5x - 25 - \frac{1}{x^2}) \left[\text{Li}_2(-x) + \ln x \ln(1+x) \right] \\
& - \frac{2}{5} (36x^3 + 120x^2 - 25x + 65) \ln^2 x + 16(7+x) \ln x \ln(1-x) \\
& - 8(11+5x) \ln^2(1-x) + 4(19+13x) \text{Li}_2(1-x) \\
& + 4 \left(\frac{36}{5} x^3 + 24x^2 - 37 - 37x \right) \zeta(2) - \frac{1}{10} (288x^2 - 1079x - 399 - \frac{32}{x}) \ln x \\
& - 4(15+43x) \ln(1-x) - \frac{2}{5} (72x^2 + 107x - 82 + \frac{8}{x}) \left. \right\} \quad (4A.10)
\end{aligned}$$

The functions $\text{Li}_n(x)$ and $S_{n,p}(x)$ denote the polylogarithms and can be found in [33]. The hard part of quark pair production due to the diagrams A in fig. 4.7 is equal to

$$\Delta_{q\bar{q},\Lambda^2}^{(2)} = \left(\frac{\alpha_s}{4\pi}\right)^2 n_f C_F \left\{ -\frac{4}{3} (1+x) \ln^2 \left(\frac{Q^2}{M^2} \right) + \left[-\frac{16}{3} \frac{1+x^2}{1-x} \ln x \right. \right.$$

$$\begin{aligned}
& -\frac{16}{3}(1+x)\ln(1-x) - \frac{8}{9}(1-11x) \Big] \ln\left(\frac{Q^2}{M^2}\right) + \frac{1+x^2}{1-x} \left[\frac{2}{3} \ln^2 x \right. \\
& + \frac{4}{3} \text{Li}_2(1-x) - 6 \ln x - \frac{16}{3} \ln x \ln(1-x) \Big] + (1+x) \left[\frac{4}{3} \text{Li}_2(1-x) \right. \\
& + \frac{8}{3} \zeta(2) - 4 \ln^2(1-x) + \frac{2}{3} \ln^2 x \Big] + \frac{2}{3} (15+7x) \ln x \\
& \left. - \frac{40}{9} (2-x) \ln(1-x) + \frac{4}{9} (42+47x) \right\} . \quad (4A.11)
\end{aligned}$$

where n_f denotes the number of light flavours.

The second part of (4A.7) could be obtained without performing mass factorization, which implies that it is scheme and scale independent. The contributions originating from the diagrams B in fig. 4.7 and the interference terms BC and BD (see figs. 4.7 and 4.8) are

$$\begin{aligned}
\Delta_{q\bar{q},B}^{(2)} = \left(\frac{\alpha_s}{4\pi}\right)^2 \Big\{ (1+x)^2 \left[-\frac{32}{3} \text{Li}_2(-x) - \frac{16}{3} \zeta(2) + \frac{8}{3} \ln^2 x \right. \right. \\
\left. \left. - \frac{32}{3} \ln x \ln(1+x) \right] + \frac{8}{3} (3+3x^2+4x) \ln x + \frac{40}{3} (1-x^2) \right\} \quad (4A.12)
\end{aligned}$$

and

$$\begin{aligned}
\Delta_{q\bar{q},BC}^{(2)} = \Delta_{q\bar{q},BD}^{(2)} = \left(\frac{\alpha_s}{4\pi}\right)^2 C_F \left(C_F - \frac{C_A}{2}\right) \Big\{ (1+x^2+3x) \left[32 S_{1,2}(1-x) \right. \right. \\
+ 16 \text{Li}_2(1-x) \ln x \Big] + (1+x)^2 \left[-48 S_{1,2}(-x) - 8 \text{Li}_3(-x) + 24 \text{Li}_2(-x) \right. \\
+ 24 \text{Li}_2(-x) \ln x - 48 \text{Li}_2(-x) \ln(1+x) + 12 \zeta(2) - 24 \zeta(2) \ln(1+x) \\
+ 8 \zeta(2) \ln x + 20 \ln^2 x \ln(1+x) - 24 \ln^2(1+x) \ln x + 24 \ln x \ln(1+x) \Big] \\
+ 36(1-x^2) \text{Li}_2(1-x) + \frac{4}{3} (1+x^2+4x) \ln^3 x + 4(9+11x) \ln x \\
\left. \left. - 2(-6+15x^2+8x) \ln^2 x - 2(-27+13x^2+14x) \right] \right\} . \quad (4A.13)
\end{aligned}$$

The matrix element corresponding to the interference term AB (fig. 4.7) involves the product of two fermion traces, each containing a vertex of the form $\gamma_\mu(v + a\gamma_5)$. Therefore we have to distinguish between the vector-vector (V) and axial vector-axial vector parts, which we will denote by $\Delta_{q\bar{q},AB}^{(2),V}$ and $\Delta_{q\bar{q},AB}^{(2),A}$ respectively. The first part is zero due to Furry's theorem

$$\Delta_{q\bar{q},AB}^{(2),V} = 0 \quad (4A.14)$$

whereas the axial vector-axial vector contribution is given by

$$\Delta_{q\bar{q},AB}^{(2),A} = \left(\frac{\alpha_s}{4\pi}\right)^2 C_F \left\{ 16 \frac{1+x^2}{1-x} \ln x + 32x \ln x + 16(3-x) \right\} \quad (4A.15)$$

The above term does not show up for $V = \gamma$, since the axial vector part is absent in the vertex. It does not contribute to W-production either, because the quarks in the final state of A and B in fig. 4.7 are different, so that the interference term AB vanishes. For Z-production the contribution from (4A.15) disappears when the up as well as the down quark are taken into account.

With the coefficient functions mentioned above we have exhausted all contributions to $\Delta_{q\bar{q}}$ except those belonging to the singlet part. Since the latter are equal to the corrections Δ_{qq} calculated for the non-identical quark-quark scattering process, we will present them there.

II The (anti)quark-gluon contribution Δ_{qg}

At $\mathcal{O}(\alpha_s)$ the qg subprocess shows up for the first time. The Drell-Yan coefficient function for this reaction has been calculated in refs. [16, 17, 27] and it is given by

$$\Delta_{qg}^{(1)} = \frac{\alpha_s}{4\pi} T_f \left\{ 2(1+2x^2-2x) \ln \left(\frac{(1-x)Q^2}{M^2} \right) + 3 + 9x^2 - 10x \right\} \quad (4A.16)$$

with $T_f = \frac{1}{2}$.

The second order contribution to Δ_{qg} can be written as

$$\Delta_{qg}^{(2)} = \Delta_{qg}^{(2)} = \Delta_{qg}^{(2),CA} + \Delta_{qg}^{(2),CF} + \Delta_{qg}^{(2),Tf} + \frac{\alpha_s}{4\pi} \beta_0 \Delta_{qg}^{(1)} \ln \left(\frac{R^2}{M^2} \right) \quad (4A.17)$$

The calculation of $\Delta_{qg}^{(2)}$ requires both mass factorization and renormalization. The latter gives rise to the β_0 term in (4A.17). Notice that the expressions given below depend on the choice made for Γ_{gg} in (2.31). The two parts $\Delta_{qg}^{(2),CA}$ and $\Delta_{qg}^{(2),CF}$ are equal to

$$\begin{aligned} \Delta_{qg}^{(2),CA} = & \left(\frac{\alpha_s}{4\pi}\right)^2 C_A T_f \left\{ \left[4(1+4x) \ln x + 4(1+2x^2-2x) \ln(1-x) \right. \right. \\ & + \frac{2}{3}(3-31x^2+24x+\frac{4}{x}) \left. \right] \ln^2 \left(\frac{Q^2}{M^2} \right) + \left[(1+2x^2+2x) \left[-8 \text{Li}_2(-x) \right. \right. \\ & - 8 \ln x \ln(1+x) \left. \right] - 8(1+3x) \ln^2 x + 8(3+2x^2+6x) \text{Li}_2(1-x) \\ & \left. \left. - 16(1+2x^2-x) \zeta(2) + 8(1-2x^2+10x) \ln x \ln(1-x) \right] \right\} \end{aligned}$$

$$\begin{aligned}
& + 12(1 + 2x^2 - 2x) \ln^2(1 - x) + \frac{4}{3}(9 - 71x^2 + 54x + \frac{8}{x}) \ln(1 - x) \\
& + 4(3 + 28x^2 - 2x) \ln x - \frac{58}{3} + \frac{146}{9}x^2 - \frac{8}{3}x + \frac{88}{9x} \Big] \ln \left(\frac{Q^2}{M^2} \right) \\
& + 8(1 + 2x^2 + 2x) \left[\text{Li}_3 \left(\frac{1+x}{1-x} \right) - \text{Li}_3 \left(-\frac{1+x}{1-x} \right) - \text{Li}_2(-x) \ln(1 - x) \right. \\
& \left. - \ln x \ln(1 - x) \ln(1 + x) \right] - 8(1 + x^2 + 2x) \left[\ln x \ln^2(1 + x) \right. \\
& \left. + 2 \ln(1 + x) \text{Li}_2(-x) + \zeta(2) \ln(1 + x) + 2 \text{S}_{1,2}(-x) \right] \\
& + \frac{8}{3} (3x^2 - 15x + 12 + \frac{2}{x}) \left[\text{Li}_2(-x) + \ln x \ln(1 + x) \right] \\
& + \frac{4}{3} (3x^2 + 3x) \ln^3 x - 8(1 + 3x) \ln^2 x \ln(1 - x) \\
& + 4(3 + 3x^2 + 4x) \ln^2 x \ln(1 + x) + 4(1 - 4x^2 + 16x) \ln x \ln^2(1 - x) \\
& + 16x(x - 2) \zeta(2) \ln x + 8(1 - 2x^2 + 9x) \ln x \text{Li}_2(1 - x) \\
& + 8(1 + 3x^2 + 2x) \ln x \text{Li}_2(-x) + 8(1 + 2x^2 - 2x) \ln^3(1 - x) \\
& - 4(3 + 8x^2 - 2x) \zeta(2) \ln(1 - x) + 4(13 + 12x^2 + 10x) \ln(1 - x) \text{Li}_2(1 - x) \\
& + 2(3 + 2x^2 - 2x) \zeta(3) - 8(7 + 7x^2 + 8x) \text{Li}_3(1 - x) \\
& + 4(17 + 8x^2 + 30x) \text{S}_{1,2}(1 - x) - 24x^2 \text{Li}_3(-x) \\
& - 4(1 + \frac{38}{3}x^2 + 22x) \ln^2 x + 4(3 + 28x^2 + 26x) \ln x \ln(1 - x) \\
& + 16(1 + \frac{10}{3}x^2 - 2x) \zeta(2) + 4(10 + 46x + \frac{4}{x}) \text{Li}_2(1 - x) \\
& + 2(5 - 31x^2 + 24x + \frac{4}{x}) \ln^2(1 - x) + \frac{2}{3}(31 + 196x^2 - 296x) \ln x \\
& - 2(13 + 79x^2 - 84x - \frac{4}{x}) \ln(1 - x) \\
& + \frac{2}{9}(150 + 1055x^2 - 1149x - \frac{38}{x}) \Big\} \quad (4A.18)
\end{aligned}$$

and

$$\Delta_{\text{qg}}^{(2), C_F} = \left(\frac{\alpha_s}{4\pi} \right)^2 C_F T_f \left\{ \left[12(1 + 2x^2 - 2x) \ln(1 - x) - 6(1 + 4x^2 - 2x) \ln x \right. \right.$$

$$\begin{aligned}
& -3(1-4x) \Big] \ln^2 \left(\frac{Q^2}{M^2} \right) + \Big[16(1+2x^2-2x) \Big[\zeta(2) + \ln^2(1-x) \Big] \\
& + 4(1-4x^2-2x) \text{Li}_2(1-x) + 2(1+4x^2-2x) \Big[\ln^2 x - 6 \ln x \ln(1-x) \Big] \\
& + 4(2-15x^2) \ln x + 2(1+30x^2-20x) \ln(1-x) \\
& + 2(3+27x^2-26x) \Big] \ln \left(\frac{Q^2}{M^2} \right) \\
& + 8(1+x^2+2x) \Big[2 \ln x \ln^2(1+x) - \ln^2 x \ln(1+x) + 4 \ln(1+x) \text{Li}_2(-x) \\
& + 2 \ln(1+x) \zeta(2) + 4 \text{S}_{1,2}(-x) \Big] + (1+4x^2-2x) \Big[4 \text{Li}_3(1-x) \\
& - 6 \ln x \ln^2(1-x) \Big] + 4(5+12x^2-10x) \Big[\ln x \zeta(2) - \frac{1}{6} \ln^3 x \Big] \\
& - \frac{8}{15} (36x^3 + 90x^2 + 100x + 60 + \frac{1}{x^2}) \Big[\text{Li}_2(-x) + \ln x \ln(1+x) \Big] \\
& + 2(3+8x^2-6x) \ln^2 x \ln(1-x) + 4(1-4x^2-2x) \ln x \text{Li}_2(1-x) \\
& - 16x^2 \Big[\ln x \text{Li}_2(-x) - \ln(1-x) \zeta(2) \Big] + 4(1+2x^2-2x) \ln^3(1-x) \\
& - 4(3+8x^2-6x) \ln(1-x) \text{Li}_2(1-x) + 16(1+3x^2-6x) \zeta(3) \\
& - 4(7+24x^2-14x) \text{S}_{1,2}(1-x) - 16(1-x^2+2x) \text{Li}_3(-x) \\
& + 2(\frac{24}{5}x^3 + 30x^2 + \frac{4}{3}x - 7) \ln^2 x + 4(4-27x^2+4x) \ln x \ln(1-x) \\
& + (5+36x^2-36x) \ln^2(1-x) - 2(\frac{48}{5}x^3 - 30x^2 + \frac{128}{3}x + 1) \zeta(2) \\
& + 24(1-3x^2-x) \text{Li}_2(1-x) + 4(11+32x^2-42x) \ln(1-x) \\
& - (\frac{589}{15} + \frac{374}{5}x^2 - \frac{522}{5}x - \frac{8}{15}\frac{1}{x}) \ln x \\
& + (\frac{109}{30} - \frac{403}{10}x^2 + \frac{166}{5}x - \frac{8}{15}\frac{1}{x}) \Big\} \tag{4A.19}
\end{aligned}$$

and

$$\begin{aligned}
\Delta_{\text{qs}}^{(2),T_f} = & \left(\frac{\alpha_s}{4\pi} \right)^2 T_f^2 n_f \Big\{ \Big[4(1+4x^2+4x) \Big[\ln^2 x \\
& - 2 \ln x \ln(1-x) - 2 \text{Li}_2(1-x) \Big] + 16(1+5x^2+8x) \ln x
\end{aligned}$$

$$\begin{aligned}
& -16(1-3x^2+2x)\ln(1-x)+4(11-59x^2+48x)\left]\ln\left(\frac{Q^2}{M^2}\right)+4(1+4x^2+4x)\left[\ln^2x\ln(1-x)-2\ln x\ln^2(1-x)-4\ln(1-x)\text{Li}_2(1-x)\right.\right. \\
& \left.-2S_{1,2}(1-x)+4\text{Li}_3(1-x)+2\zeta(2)\ln x\right]+16(1-3x^2+2x)\left[\zeta(2)-\ln^2(1-x)\right]+6(1+8x^2+8x)\ln^2x+4(1-4x^2+8x)\ln x\ln(1-x) \\
& -4(3-8x^2)\text{Li}_2(1-x)+2(15+141x^2+180x)\ln x \\
& \left.+2(7-27x^2+60x)\ln(1-x)+3(23-149x^2+126x)\right\}. \quad (4A.20)
\end{aligned}$$

Notice the absence of the functions $\delta(1-x)$ and $\mathcal{D}_i(x)$ in $\Delta_{q\bar{q}}$, which were present in the expression for $\Delta_{q\bar{q}}$. Although the second order contribution corresponds to graphs with a gluon in the final state these singular functions do not show up since the lowest order term $\Delta_{q\bar{q}}^{(1)}$ is integrable in $x=1$.

III The non-identical quark-quark contributions $\Delta_{q\bar{q}}^{\text{PS}}$

The reaction represented by the diagrams in fig. 4.8 describes quark-antiquark as well as quark-quark scattering, where the quarks in the final state are not identical [34], [35]. The contribution to the DY coefficient function can be split into two parts. The first part, represented by the combinations C^2 and D^2 , needs mass factorization, which depends on the prescription for Γ_{gq} in (2.30). In this case the contributions for $q\bar{q}$, qq and $\bar{q}q$ are all equal and are given by

$$\begin{aligned}
\Delta_{q\bar{q}, C^2}^{(2)} &= \Delta_{q\bar{q}, D^2}^{(2)} = \Delta_{qq, C^2}^{(2)} = \Delta_{qq, D^2}^{(2)} = \Delta_{\bar{q}q, C^2}^{(2)} = \Delta_{\bar{q}q, D^2}^{(2)} = \\
& \left(\frac{\alpha_s}{4\pi}\right)^2 C_F T_f \left\{ \left[4(1+x)\ln x + \frac{2}{3}(3-4x^2-3x+\frac{4}{x}) \right] \ln^2\left(\frac{Q^2}{M^2}\right) \right. \\
& + \left[2(4x^2-6x-3) \left[\ln^2x - 2\ln x\ln(1-x) \right] + 2(4x+10)\text{Li}_2(1-x) \right. \\
& + 4(2x^2-2x+1) \left[\ln^2(1-x) - 2\zeta(2) \right] + 2(20x^2+4x+5)\ln x \\
& - \frac{2}{3}(52x^2-36x+9-\frac{16}{x})\ln(1-x) \\
& \left. - \frac{2}{9}(188x^2-186x+123-\frac{44}{x}) \right] \ln\left(\frac{Q^2}{M^2}\right) \\
& \left. + 8(1+x) \left[\frac{1}{3}\ln^3x + 2\ln x\text{Li}_2(1-x) \right] - 4(4x^2-5x-2)\ln x\ln^2(1-x) \right\}
\end{aligned}$$

$$\begin{aligned}
& + 2(4x^2 - 6x - 3) \ln^2 x \ln(1-x) + \left(\frac{46}{3}x^2 - 48x - 1\right) \ln^2 x \\
& + 8(x+4) \left[\ln(1-x) \text{Li}_2(1-x) - \text{Li}_3(1-x) \right] \\
& + 4(2x^2 - 2x + 1) \left[\ln^3(1-x) + 2\zeta(3) - 4\ln(1-x)\zeta(2) \right] \\
& + 4(10x + 13) S_{1,2}(1-x) + \frac{16}{3}(x^2 + 3x + 3 + \frac{1}{x}) \left[\ln x \ln(1+x) \right. \\
& + \text{Li}_2(-x) \left. \right] + 4(x^2 + 12x + 4) \ln x \ln(1-x) + 4(4x^2 - 4x - 1)\zeta(2) \ln x \\
& - 2(7x^2 - 3x + 1 - \frac{4}{x}) \ln^2(1-x) - 2(\frac{10}{3}x^2 - 14x + 1)\zeta(2) \\
& + 2(8x + 19 + \frac{8}{x}) \text{Li}_2(1-x) + \frac{2}{3}(94x^2 + 7x + 31) \ln x \\
& - 2(46x^2 - 47x + 17 - \frac{4}{x}) \ln(1-x) \\
& - \frac{2}{9}(358x^2 - 192x - 123 + \frac{38}{x}) \left. \right\} . \tag{A.21}
\end{aligned}$$

The second part originates from the interference between the graphs C and D in fig. 4.8. Here we have to distinguish between the vector-vector (V) and the axialvector-axialvector (A) terms, denoted by $\Delta_{q\bar{q},CD}^{(2),V}$ and $\Delta_{q\bar{q},CD}^{(2),A}$ respectively, since they are not equal to each other. The expressions for the V -part equals

$$\begin{aligned}
\Delta_{q\bar{q},CD}^{(2),V} = -\Delta_{q\bar{q},CD}^{(2),V} = -\Delta_{q\bar{q},CD}^{(2),V} = \left(\frac{\alpha_s}{4\pi}\right)^2 C_F T_f \left\{ (2+x+\frac{2}{x}) \left[32 S_{1,2}(1-x) \right. \right. \\
- 96 S_{1,2}(-x) - 48 \ln^2(1+x) \ln x - 48 \zeta(2) \ln(1+x) + 40 \ln^2 x \ln(1+x) \\
- 96 \text{Li}_2(-x) \ln(1+x) \left. \right] + (1+x) \left[80 \text{Li}_2(-x) + 80 \ln x \ln(1+x) \right. \\
+ 40 \zeta(2) \left. \right] + 8(-6 + 3x + \frac{4}{x}) \text{Li}_3(1-x) - 16(-10 + 3x + \frac{10}{x}) \text{Li}_3(-x) \\
- 24(-6 + x + \frac{4}{x}) \zeta(3) + 8(10-x) \text{Li}_2(1-x) \ln x - \frac{16}{3} x \ln^3 x \\
+ 32(2x + \frac{5}{x}) \text{Li}_2(-x) \ln x + 8(10+x) \zeta(2) \ln x + 8(5-4x) \text{Li}_2(1-x) \\
- 52x \ln^2 x - 16(5+4x) \ln x - 160(1-x) \left. \right\} . \tag{A.22}
\end{aligned}$$

Notice that there is a relative minus sign between the expressions for the $q\bar{q}$ and the $q\bar{q}(\bar{q}\bar{q})$ processes. The A -part is given by

$$\Delta_{q\bar{q},CD}^{(2),A} = \Delta_{q\bar{q},CD}^{(2),A} = \Delta_{q\bar{q},CD}^{(2),A} = \left(\frac{\alpha_s}{4\pi}\right)^2 C_F T_f \left\{ (2+x) \left[32 S_{1,2}(1-x) \right. \right.$$

$$\begin{aligned}
& -96 S_{1,2}(-x) - 48 \ln^2(1+x) - 48 \zeta(2) \ln(1+x) + 40 \ln^2 x \ln(1+x) \\
& - 96 \text{Li}_2(-x) \ln(1+x) \ln x \Big] + (1+x) \Big[16 \text{Li}_2(-x) + 16 \ln x \ln(1+x) \\
& + 8 \zeta(2) \Big] + 8(2-x) \text{Li}_3(1-x) - 16(6-5x) \text{Li}_3(-x) - 24(2-3x) \zeta(3) \\
& + 8 \text{Li}_2(1-x) + 8(2+3x) \text{Li}_2(1-x) \ln x + 8(2+5x) \zeta(2) \ln x \\
& + 12 \text{Li}_3(-x) \ln x - \frac{16}{3} x \ln^3 x - 4x \ln^2 x - 16 \ln x - 32(1-x) \Big\} \quad (4A.23)
\end{aligned}$$

Finally we want to remark that in case of W-production only one of the two sets of diagrams contributes (C or D, depending on the quark flavours in the initial and final state). This implies that for W-production there is no contribution from the interference term CD.

IV The identical (anti)quark-(anti)quark contributions Δ_{qq}^{NS}

In case there are identical quarks in the initial and/or final state, we have in addition to the graphs in fig. 4.8 also the ones in fig. 4.9. As the results for E^2 , F^2 and EF are equal to those for C^2 , D^2 and CD (of course one has to implement the right statistical factors), we will not discuss them here (see the section on non-identical quark-quark scattering). The new contributions come from the interference terms CE , CF , DE and DF . Before giving the results let us explain in some detail how we have taken care of the statistical factors in our calculations.

In case of $V = \gamma$ or Z all four sets of diagrams C , D , E and F contribute and we have a statistical factor $\frac{1}{2}$. However, in the case of $V = W$ we have to distinguish between two cases (for W-production the diagrams C and D cannot contribute simultaneously).

- Identical quarks in the initial state. In this case the contribution comes from either the graphs C and F or D and E and there is no statistical factor.
- Identical quarks in the final state. Now only the combinations C and E or D and F give contributions. Moreover, in this case there is a statistical factor $\frac{1}{2}$.

For the expression of the hadronic structure function (2.3) (see A.20 of [14]) it turned out to be convenient to use the statistical factors of the W-production case. Therefore a statistical factor $\frac{1}{2}$ is included in the results for CE and DF , but this is not the case for CF and DE .

Apart from the statistical factors there is another difference between CE (DF) and CF (DE). The first contains collinear divergences and needs mass factorization, whereas the latter is free of mass singularities.

The correction corresponding to the interferences CE and DF is equal to [35, 36]

$$\begin{aligned}
 \Delta_{\text{qq,CE}}^{(2)} = \Delta_{\text{qq,DF}}^{(2)} = \Delta_{\text{qq,CE}}^{(2)} = \Delta_{\text{qq,DF}}^{(2)} = \\
 \left(\frac{\alpha_s}{4\pi} \right)^2 C_F \left(C_F - \frac{C_A}{2} \right) \left\{ \left[\frac{1+x^2}{1+x} \left[4 \ln^2 x - 8\zeta(2) \right. \right. \right. \\
 - 16 \text{Li}_2(-x) - 16 \ln x \ln(1+x) \left. \left. \right] + 8(1+x) \ln x + 16(1-x) \right] \ln \left(\frac{Q^2}{M^2} \right) \right. \\
 + \frac{1+x^2}{1+x} \left[24 S_{1,2}(1-x) - 16 \text{Li}_3(1-x) - 16 \text{Li}_3(-x) \right. \\
 + 16 \text{Li}_3 \left(\frac{1+x}{1-x} \right) - 16 \text{Li}_3 \left(-\frac{1+x}{1-x} \right) - 12\zeta(3) + 16 \text{Li}_2(1-x) \ln \\
 + 16 \text{Li}_2(-x) \ln x - 16 \text{Li}_2(-x) \ln(1-x) + 12\zeta(2) \ln x \\
 - 8\zeta(2) \ln(1-x) - \frac{2}{3} \ln^3 x + 4 \ln^2 x \ln(1-x) \\
 + 8 \ln^2 x \ln(1+x) - 16 \ln x \ln(1-x) \ln(1+x) + 8 \ln x \left. \right] \\
 + (1-x) \left[4\zeta(2) \ln x - \frac{2}{3} \ln^3 x + 16 \ln(1-x) \right] + 8(1+x) \ln x \ln(1-x) \\
 + 24x \left[4 S_{1,2}(-x) - 2 \text{Li}_3(-x) - 2\zeta(3) + 4 \ln(1+x) \text{Li}_2(-x) \right. \\
 + 2\zeta(2) \ln(1+x) + 2 \ln x \ln^2(1+x) - \ln^2 x \ln(1+x) \left. \right] \\
 + \frac{8}{5} (9x^3 - 30x^2 - 15x - 15 - \frac{1}{x^2}) \left[\text{Li}_2(-x) + \ln x \ln(1+x) \right] \\
 + 16 \text{Li}_2(1-x) + 8 \left(\frac{9}{5} x^3 - 6x^2 - 2x + 1 \right) \zeta(2) \\
 - 4 \left(\frac{9}{5} x^3 - 6x^2 - x \right) \ln^2 x - \frac{8}{5} (9x^2 - 22x + 8 - \frac{1}{x}) \ln x \\
 \left. - \frac{8}{5} (9x^2 - 11x + 1 + \frac{1}{x}) \right\}. \quad (4A.24)
 \end{aligned}$$

The expression for the interference terms CF and DE is

$$\begin{aligned}
 \Delta_{\text{qq,CF}}^{(2)} = \Delta_{\text{qq,DE}}^{(2)} = \Delta_{\text{qq,CF}}^{(2)} = \Delta_{\text{qq,DE}}^{(2)} = \\
 \left(\frac{\alpha_s}{4\pi} \right)^2 C_F \left(C_F - \frac{C_A}{2} \right) \left\{ (1-x)^2 \left[-16 S_{1,2}(1-x) \right. \right.
 \end{aligned}$$

$$+ 16 \text{Li}_3(1-x) - 24 \text{Li}_2(1-x) - 16 \text{Li}_2(1-x) \ln x - \frac{8}{3} \ln^3 x - 12 \ln^2 x \Big] \\ - 4(7 - 6x) \ln x - 2(15 + 13x^2 - 28x) \Big\} . \quad (4A.25)$$

Notice that the above expression is scheme and scale independent.

V The gluon-gluon contribution Δ_{gg}

The diagrams for the gluon-gluon subprocess can be obtained from the quark-antiquark annihilation graphs in fig. 4.6 via crossing. This subprocess shows up for the first time at $\mathcal{O}(\alpha_s^2)$ [27]. We have divided its Drell-Yan coefficient function into two parts, viz.

$$\Delta_{gg}^{(2)} = \Delta_{gg}^{(2),C_A} + \Delta_{gg}^{(2),C_F} . \quad (4A.26)$$

The C_A contribution to \widehat{W}_{gg} is collinearly finite and is therefore scheme and scale independent. The corresponding coefficient function equals

$$\Delta_{gg}^{(2),C_A} = \left(\frac{\alpha_s}{4\pi}\right)^2 \frac{N^2}{N^2-1} \left\{ (1+x)^2 \left[16 S_{1,2}(-x) + 24 \text{Li}_3(-x) + 16\zeta(3) \right. \right. \\ + \frac{16}{3} \text{Li}_2(-x) - 24 \text{Li}_2(-x) \ln x + 16 \text{Li}_2(-x) \ln(1+x) + 8\zeta(2) \ln(1+x) \\ + \frac{8}{3} \zeta(2) - 12 \ln^2 x \ln(1+x) + 8 \ln^2(1+x) \ln x + \frac{16}{3} \ln x \ln(1+x) \Big] \\ - 8(1-x)^2 S_{1,2}(1-x) + \frac{2}{3} (-2 + 25x^2 + 2x) \ln^2 x \\ \left. - \frac{2}{3} (6 + 75x^2 + 38x) \ln x - \frac{47}{3} + \frac{191}{3} x^2 - 48x \right\} . \quad (4A.27)$$

The C_F contribution to \widehat{W}_{gg} contains collinear singularities. After mass factorization we find

$$\Delta_{gg}^{(2),C_F} = \left(\frac{\alpha_s}{4\pi}\right)^2 T_f^2 \left\{ \left[-8(1+4x^2+4x) \ln x - 16(1-3x^2+2x) \right] \ln^2 \left(\frac{Q^2}{M^2} \right) \right. \\ + \left[-16(1+4x^2+4x) \left[\text{Li}_2(1-x) + \ln x \ln(1-x) \right] \right. \\ - 24(1+8x^2+8x) \ln x - 32(1-3x^2+2x) \ln(1-x) \\ \left. - 12(5-17x^2+12x) \right] \ln \left(\frac{Q^2}{M^2} \right) \\ \left. + 16(1+x)^2 \left[3 \ln^2 x \ln(1+x) - 2 \ln x \ln^2(1+x) - 2 \ln(1+x) \zeta(2) \right] \right\}$$

$$\begin{aligned}
& -4 \ln(1+x) \text{Li}_2(-x) - 4 \text{S}_{1,2}(-x) \Big] + 8(1+4x^2+4x) \Big[2 \text{Li}_3(1-x) \\
& - \ln x \ln^2(1-x) - 3 \ln x \text{Li}_2(1-x) - 2 \ln(1-x) \text{Li}_2(1-x) \Big] \\
& - \frac{4}{3}(5+12x^2+12x) \ln^3 x + 8(3+8x^2+8x) \zeta(2) \ln x - 32(1-x^2 \\
& + 2x) \text{Li}_3(-x) + 32(2+x^2+4x) \ln x \text{Li}_2(-x) - 16(1-2x^2+2x) \zeta(3) \\
& - 16(1+10x^2+16x) \text{S}_{1,2}(1-x) + 32(1+x) \Big[\text{Li}_2(-x) + \ln x \ln(1+x) \Big] \\
& - 24(3+2x^2+12x) \text{Li}_2(1-x) + 16(2-3x^2+3x) \zeta(2) \\
& - 16(1-3x^2+2x) \ln^2(1-x) - 24(1+8x^2+8x) \ln x \ln(1-x) \\
& - 4(7+6x^2+10x) \ln^2 x - 12(5-17x^2+12x) \ln(1-x) \\
& - 8(12+13x^2+48x) \ln x - 2(73-83x^2+10x) \Big\} . \tag{4A.28}
\end{aligned}$$

References

- [1] D. Amati, A. Basetto, M. Ciafaloni, G. Marchesini and G. Veneziano, Nucl. Phys. **B173** (1980) 429;
W.L. van Neerven, Phys. Lett. **B147** (1984) 175.
- [2] G. Altarelli, Phys. Rep. **81** (1982) 1; Ann. Rev. Nucl. Part. Sci. **39** (1989) 357.
- [3] S. Catani, F. Fiorani, G. Marchesini, G. Oriani, Nucl. Phys. **B361** (1991) 645.
- [4] G. Grunberg, Phys. Lett. **B95** (1980) 70, Erratum: **B110** (1982) 501; Phys. Rev. **D29** (1984) 2315.
- [5] P.M. Stevenson, Phys. Rev. **D23** (1981) 2916; Nucl. Phys. **B203** (1982) 472.
- [6] G. Parisi, Phys. Lett. **B90** (1980) 295; G. Sterman, Nucl. Phys. **281** (1987) 310.
- [7] D. Appel, P. Mackenzie and G. Sterman, Nucl. Phys. **B309** (1988) 259;
S. Catani and L. Trentadue, Nucl. Phys. **B327** (1989) 323; *ibid.* **B353** (1991) 183;
E. Laenen, J. Smith and W.L. van Neerven, Nucl. Phys. **B369** (1992) 543.

- [8] S. Catani, F. Fiorani, G. Marchesini, Nucl. Phys. B336 (1990) 18.
- [9] A.C. Bawa et al., Proceedings of the HERA Workshop, Hamburg, October 12-14, 1987, ed. R.P. Peccei, vol. 1, p. 183.
- [10] Proceedings of the Large Hadron Collider Workshop, Aachen, October 4-9, 1990, eds. G. Jarlskog and D. Rein, vol. 2, p. 829.
- [11] S.G. Gorishni, A.L. Kataev and S.A. Larin, Phys. Lett. **259** (1991) 144;
L.R. Surguladze and M.A. Samuel, Phys. Rev. Lett. **66** (1991) 560.
- [12] G. Kramer and H. Lampe, Z. Phys. **C34** (1987) 497, Erratum **C42** (1989) 504.
- [13] S.A. Larin, F.V. Tkachov and J.A.M. Vermaseren, Phys. Lett. **B272** (1991) 121
and references therein.
- [14] R. Hamberg, W.L. van Neerven and T. Matsuura, Nucl. Phys. **B359** (1991) 343.
- [15] R. Hamberg, thesis Leiden University 1991.
- [16] G. Altarelli, R.K. Ellis and G. Martinelli, Nucl. Phys. **B157** (1979) 461.
- [17] B. Humpert and W.L. van Neerven, Phys. Lett. **B184** (1981) 225.
- [18] W. Furmanski and R. Petronzio, Phys. Lett. **B97** (1980) 437;
E.G. Floratos, P. Lacaze and C. Kounnas, Phys. Lett. **B98** (1981) 89.
- [19] M. Diemoz, F. Ferroni, E. Longo and G. Martinelli, Z. Phys. **C39** (1988) 472.
- [20] E.G. Floratos, D.A. Ross and C.T. Sachrajda, Nucl. Phys. **B129** (1977) 66,
Erratum **B139** (1978) 545;
A.N. Schellekens, Nuovo Cim. Lett. **24** (1979) 513.
- [21] D.A. Dicus and S.C. Willenbrock, Phys. Rev. **D34** (1986) 148.
- [22] C. Albajar et al., UA1 Collaboration, Phys. Lett. **B253** (1991) 503.
- [23] J. Alitti et al., UA2 Collaboration, Z. Phys. **C47** (1990) 11; L. Fayard, LAL
90-48.
- [24] F. Abe et al., CDF Collaboration, Phys. Rev. Lett. **64** (1990) 152; P.F. Derwent,
CDF Collaboration, "Production properties of W, Z bosons", talk presented at
the 25th Rencontres de Moriond, Les Arcs, Savoie - France, March 1990.

- [25] J.G. Morfin and Wu-Ki Tung, Z. Phys. **C52** (1991) 13.
- [26] A.C. Benvenuti et al. (BCDMS), Phys. Lett. **B223** (1989) 485; *ibid* **B237** (1990) 599.
- [27] J. Kubar-André and F.E. Paige, Phys. Rev. **D19** (1979) 221.
- [28] I.J. Aubert et al. (EMC), Nucl. Phys. **B293** (1987) 740.
- [29] J.P. Berge et al. (CDHSW), Z. Phys. **C49** (1990) 187.
- [30] A.D. Martin and W.J. Stirling, Phys. Lett. **B248** (1990) 443.
- [31] T. Matsuura, S.C. van der Marck and W.L. van Neerven, Phys. Lett. **B211** (1988) 171; Nucl. Phys. **B319** (1989) 570.
- [32] T. Matsuura, thesis Leiden University 1989.
- [33] L. Lewin, Polylogarithms and Associated Functions, North Holland 1983;
R. Barbieri, J.A. Mignaco and E. Remiddi, Nuovo Cim. **11A** (1972) 824;
A. Devoto and D.W. Duke, Riv. Nuovo Cim. **7**, No. 6 (1984) 1.
- [34] A.P. Contogouris and J. Kripfganz, Phys. Rev. **D20** (1979) 2295;
A.N. Schellekens and W.L. van Neerven, Phys. Rev. **D21** (1980) 2619.
- [35] A.N. Schellekens, thesis Nijmegen University 1981.
- [36] A.N. Schellekens and W.L. van Neerven, Phys. Rev. **D22** (1980) 1623.
- [37] T. Matsuura, R. Hamberg and W.L. van Neerven, Nucl. Phys. **B345** (1990) 331.

Chapter 5

The structure function F_3

5.1 Introduction

In chapter 3 we calculated the order α_s^2 contributions to the singlet and non-singlet coefficient functions belonging to the deep inelastic structure functions $F_i(x, Q^2)$ ($i = 1, 2, L$). These structure functions appear in the neutral current process $\ell + H \rightarrow \ell + \text{"anything"}$, where in chapter 3 we have limited ourselves to the one photon exchange mechanism only. Summarizing our findings in chapter 3, we found that the order α_s^2 corrections to $F_2(x, Q^2)$ are appreciable in the large- x ($0.5 < x < 1.0$) as well as in the small- x region ($10^{-4} < x < 10^{-3}$). Here they can amount to 10% ($x \leq 1$) and -20% ($x \approx 10^{-4}$). The same observation has been made for F_L in the small- x region where the correction even can become -50%. Notice that the corrections at small x heavily depend on the set of parton densities in particular on the gluon distribution function. The large corrections near the boundary of phase space ($x \rightarrow 1$) which show up in $F_2(x, Q^2)$ can be wholly attributed to the non-singlet coefficient function and they originate from soft gluon bremsstrahlung. Notice that these effects due to soft gluon bremsstrahlung do not appear in the longitudinal coefficient function which explains why the corrections to $F_L(x, Q^2)$ are small in the large- x region.

Having finished the calculation of the coefficient functions mentioned above, we should also compute the coefficient function belonging to the structure function $F_3(x, Q^2)$. The latter shows up in the charged current reaction $\nu_\ell + H \rightarrow \ell + \text{"anything"}$ and the aforementioned neutral current process, where now the Z -boson exchange mechanism is also taken into account. This structure function is of much experimental as well as theoretical interest since it provides us with a beautiful test of perturbative QCD. One of the reasons is that it only receives contributions from the non-singlet part of the coefficient function and the valence quark densities which

are very well known. It is not marred by the presence of the sea quark- and gluon densities about which we have very poor information in particular in the small- x region. The other reason is that at this moment we have an abundance of data obtained in various experiments. For the most recent ones see [1] (CDHSW) and [2] (CCFR). Furthermore one also intends to measure $F_3(x, Q^2)$ at HERA [3] and the ep facility at LEP [4].

5.2 The calculation of the second order coefficient function

The unpolarized deep inelastic cross sections of the processes mentioned above are determined by the structure functions $F_i(x, Q^2)$ ($i = 1, 2, 3$), which are defined via the hadronic tensor

$$\begin{aligned} W_{\mu\nu}(p, q) &= \frac{1}{4\pi} \int d^4y e^{iqy} \langle p | [J_\mu^\dagger(y), J_\nu(0)] | p \rangle \\ &= \left(-g_{\mu\nu} + \frac{q_\mu q_\nu}{q^2} \right) F_1(x, q^2) + \left(p_\mu - \frac{p \cdot q}{q^2} q_\mu \right) \left(p_\nu - \frac{p \cdot q}{q^2} q_\nu \right) \frac{1}{p \cdot q} F_2(x, q^2) \\ &\quad - i \frac{1}{2} \epsilon_{\mu\nu\alpha\beta} p^\alpha q^\beta \frac{1}{p \cdot q} F_3(x, q^2) , \end{aligned} \quad (5.2.1)$$

where J_μ is the electroweak current and $|p\rangle$ is the unpolarized hadronic state. The Bjorken scaling variable x is defined as $x = Q^2/2p \cdot q$, where $Q^2 = -q^2$. The same definition also holds for the partonic tensor where now $|p\rangle$ stands for the struck parton and $F_i(x, Q^2)$ is replaced by the partonic structure function $\hat{F}_i(z, Q^2)$ with $z = Q^2/2p \cdot q$ (for notations see (3.2.5)–(3.2.10)). Notice that the parton structure functions contain the collinear divergences which have to be rendered finite by mass factorization in order to obtain the coefficient functions denoted by $C_{i,k}$. In addition to the structure functions above, we also have the longitudinal structure function which however depends on F_1 and F_2 via the relation

$$F_L(x, Q^2) = F_2(x, Q^2) - 2x F_1(x, Q^2) . \quad (5.2.2)$$

In the case of the charged current interaction where the target H is an isoscalar the structure functions are given by (see e.g. [5])

$$\begin{aligned} F_i(x, Q^2) &= x \int_x^1 \frac{dz}{z} \left[\Sigma(x/z, M^2) C_{i,q}^S(z, Q^2/M^2) + G(x/z, M^2) C_{i,g}(z, Q^2/M^2) \right] \\ (i = 2, L) , \end{aligned} \quad (5.2.3)$$

$$F_3(x, Q^2) = x \int_x^1 \frac{dz}{z} V(x/z, M^2) C_{3,q}^{\text{NS}}(z, Q^2/M^2) . \quad (5.2.4)$$

Here $G(x, M^2)$ denotes the gluon density and $\Sigma(x, M^2)$ and $V(x, M^2)$ stand for the singlet (S) and valence quark combination of the quark densities, respectively. The same notation also applies to the coefficient function $C_{i,\ell}(z, Q^2/M^2)$ ($\ell = q, \bar{q}, g$) where M^2 denotes the factorization scale, which we have put equal to the renormalization scale. The expressions for $C_{i,q}^{NS}$, $C_{i,q}^S$ and $C_{i,g}$ up to order α_s^2 ($i = 1, 2, L$) are the same as those derived for the one photon exchange mechanism (chapter 3), provided all partons are massless and one sums over an even number of flavours in the internal fermion loops. For massive quark contributions see [6].

The first order correction to $C_{3,q}^{NS}$ is already known in the literature (see [7]–[9]). The second order contribution which will be presented below receives contributions from the following parton subprocesses. First we have the two loop corrections to the Born reaction

$$V + q \rightarrow q \quad (5.2.5)$$

where V stands for the intermediate vector boson W or Z . Second one has to include the one loop correction to the process

$$V + q \rightarrow q + g \quad (5.2.6)$$

Finally we have to compute the following $2 \rightarrow 3$ body reactions

$$V + q \rightarrow q + g + g \quad (5.2.7)$$

$$V + q \rightarrow q + q + \bar{q} \quad (5.2.8)$$

In the latter reaction only the non-singlet part contributes after integration over the whole final state whereas the singlet part vanishes. The contributions due to processes with a gluon in the initial state are equal to zero. The vanishing of the above contributions follows from charge conjugation arguments from which one can derive the relation $\sigma_a = -\sigma_{\bar{a}}$ for the parton cross sections, where a and \bar{a} denote the parton and anti-parton, respectively. If a is an eigenstate of the charge conjugation operator then $\sigma_a = 0$.

5.2.1 The regularization of γ_5 in n dimensions

The computation of the parton cross sections proceeds in the same way as has been done for the coefficient functions $C_{i,\ell}$ ($i = 1, 2, L$), see chapter 3. The ultraviolet, infrared and collinear divergences which show up during the calculation are regularized

by using the technique of n -dimensional regularization. This means that the matrix elements as well as the phase space and the loop integrals have to be computed in n dimensions. An important difference between the calculation of $C_{3,q}$ and $C_{4,\ell}$ ($i = 1, 2, L$) is the appearance of the γ_5 matrix in the matrix elements contributing to $C_{3,q}$. Since the γ_5 matrix is only well defined in four dimensions, we have to find an appropriate extension into n dimensions. We have adopted the prescription in [10], which is also used in [11]. They make the following substitution for the axial current.

$$A_\mu = \bar{\psi} \gamma_\mu \gamma_5 \psi = \frac{i}{6} \varepsilon_{\mu\rho\sigma\tau} \bar{\psi} \gamma^\rho \gamma^\sigma \gamma^\tau \psi \quad (5.2.9)$$

Furthermore the sum over dummy Lorentz indices which appear in the trace has to be performed in n dimensions. We will explain this in more detail later. One can show [10, 11] that this prescription is equivalent to the one given by 't Hooft and Veltman [12] or Breitenlohner and Maison [13]. For reaction (5.2.8) we checked that before integration the prescription in (5.2.9) leads to the same matrix element as the method proposed by the authors of [12, 13]. However prescription (5.2.9) is more convenient if one has to compute long traces which e.g. show up in the calculation of processes (5.2.6) and (5.2.7). The only drawback of the above γ_5 prescriptions is that the axial vector current in (5.2.9) gets renormalized. In order to undo this renormalization one has to multiply the parton cross section by the renormalization constant given in eqs. (8), (11) of [11]. It is equal to

$$Z_A = 1 - \frac{\alpha_s}{4\pi} C_F (4 - 5\varepsilon) + \left(\frac{\alpha_s}{4\pi}\right)^2 \left[C_F^2 (22) + C_A C_F \left(-\frac{44}{3\varepsilon} - \frac{107}{9}\right) + n_f C_F \left(\frac{8}{3\varepsilon} + \frac{2}{9}\right) \right] \quad (5.2.10)$$

where $\varepsilon = n - 4$ and n_f stands for the number of flavours. The colour factors for $SU(N)$ are given by $C_F = (N^2 - 1)/2N$ and $C_A = N$. The integration of the matrix element can be done in two different ways. The tensor integrals containing the internal momenta can be reduced to scalar integrals. However this method is only feasible for the $n_f C_F$ part of process (5.2.8). Therefore we prefer another method which was also used in the calculation of the coefficient functions corresponding to the structure functions F_1 and F_2 in (5.2.1) (see chapter 3). The parton structure function \hat{F}_3 , corresponding to F_3 in (5.2.1), is obtained by projecting out the Levi-Civita tensor $\varepsilon_{\mu\nu\alpha\beta}$ which appears in (5.2.1) as well as in the matrix element (because of (5.2.9)). This is achieved by multiplying (5.2.1) and the matrix element by $\varepsilon^{\mu\nu\kappa\lambda} p_\kappa q_\lambda$. It leads

to products of two Levi-Civita tensors which in four dimensions has the usual form

$$\epsilon^{\mu\nu\kappa\lambda}\epsilon_{\alpha\beta\sigma\tau} = - \begin{vmatrix} \delta_{\alpha}^{\mu} & \delta_{\beta}^{\mu} & \delta_{\sigma}^{\mu} & \delta_{\tau}^{\mu} \\ \delta_{\alpha}^{\nu} & \delta_{\beta}^{\nu} & \delta_{\sigma}^{\nu} & \delta_{\tau}^{\nu} \\ \delta_{\alpha}^{\kappa} & \delta_{\beta}^{\kappa} & \delta_{\sigma}^{\kappa} & \delta_{\tau}^{\kappa} \\ \delta_{\alpha}^{\lambda} & \delta_{\beta}^{\lambda} & \delta_{\sigma}^{\lambda} & \delta_{\tau}^{\lambda} \end{vmatrix} \quad (5.2.11)$$

The projection entails a sum over dummy Lorentz indices appearing in the product of the Levi-Civita tensors. For instance in the projection of \hat{F}_3 we find $\epsilon^{\mu\nu\kappa\lambda}\epsilon_{\mu\nu\alpha\beta}$ (two dummy indices) whereas in the projection of the matrix element one also encounters combinations like $\epsilon^{\mu\nu\kappa\lambda}\epsilon_{\mu\nu\kappa\beta}$ (three dummy indices). One is now faced with the problem how to perform the sum over dummy indices: in n or in 4 dimensions. Since the determinant on the right-hand side of (5.2.11) is derived from a 4-dimensional object, one might think that the projection can be done in 4 dimensions. However this is wrong as will be explained below.

Suppose it would be allowed to project out \hat{F}_3 (5.2.1) in 4 dimensions. In principle one could then also apply the same procedure to \hat{F}_1 and \hat{F}_2 which are the partonic equivalents of F_1 and F_2 in (5.2.1). However we explicitly checked that this will lead to the wrong result for \hat{F}_1 and \hat{F}_2 . This is obvious because the internal momenta appearing in the n -dimensional phase space and loop integrals are taken in n dimensions whereas the external momenta p and q in (5.2.1) are now 4-dimensional objects. This will violate Lorentz covariance which becomes apparent if we reduce a tensor integral into scalar integrals like

$$\begin{aligned} \int d^n k \int d^n \ell \, k_{\alpha} \ell_{\beta} f(k\ell, k \cdot p, k \cdot q, \ell \cdot p, \ell \cdot q) &= g_{\alpha\beta} I_1(p \cdot q, q^2) + p_{\alpha} q_{\beta} I_2(p \cdot q, q^2) \\ &+ q_{\alpha} p_{\beta} I_3(p \cdot q, q^2) + p_{\alpha} p_{\beta} I_4(p \cdot q, q^2) + q_{\alpha} q_{\beta} I_5(p \cdot q, q^2) \quad (5.2.12) \end{aligned}$$

It is clear that p and q are n -dimensional objects. The projection in 4 dimensions leads to expressions for \hat{F}_i ($i = 1, 2$) which cannot be rendered finite by mass factorization. The residues of the collinear divergences appearing in \hat{F}_i do not correspond to the usual Altarelli-Parisi splitting functions so that mass factorization breaks down. The same happens with \hat{F}_3 if the sum over the Lorentz indices on the right-hand side of (5.2.11) is carried out in 4 dimensions. Here we discovered that in two loop order the C_F^2 part of \hat{F}_3 could not be made finite via mass factorization using the Altarelli-Parisi splitting functions. Moreover the $n_f C_F$ part of the coefficient function due to process (5.2.8) disagrees with the result obtained from the on-shell regularization method discussed below. Finally it is also in disagreement with the $n_f C_F$ part if it

is calculated using the tensor integral reduction into scalar integrals as indicated in (5.2.12). Notice that in this case the projection method can be avoided. If we now forget about the left-hand side in (5.2.11) and treat the Kronecker delta functions as n -dimensional objects the summation over dummy indices can be carried out in n dimensions. In this way the contractions $\varepsilon^{\mu\nu\kappa\lambda}\varepsilon_{\mu\nu\alpha\beta}$ and $\varepsilon^{\mu\nu\kappa\lambda}\varepsilon_{\mu\nu\kappa\beta}$ which appear in the matrix elements get a different n -dependence. Since only $\varepsilon^{\mu\nu\kappa\lambda}\varepsilon_{\mu\nu\alpha\beta}$ shows up in front of \hat{F}_3 (5.2.1), this structure function and the contracted matrix element have no common n -dependent overall factor anymore, which could otherwise be divided out. This explains why the 4 dimensional projection differs from the n -dimensional one. Only if the projection is carried out in n dimensions does the calculated \hat{F}_3 satisfy all the desired properties like mass factorization and the agreement with the on-shell regularization method which can be applied in 4 dimensions.

As a check we calculated the difference between the parton structure functions \hat{F}_3 and \hat{F}_2 for the $n_f C_F$ part of process (5.2.8). Here the ultraviolet divergences are regulated by an ultraviolet cut-off and the collinear divergences are regulated by giving the quarks a mass. Since we work in four dimensions there is no ambiguity in the definition of γ_5 or the Levi-Civita tensor. After renormalization and mass factorization the results obtained by the on-shell- and n -dimensional regularization only agree if in the latter case the contraction of Levi-Civita tensors is performed in n dimensions. This check also shows that the γ_5 -prescriptions given in [10]–[13] are correct. Another indication for the correctness of our procedure is that the parton cross sections for the singlet part of (5.2.8) and the processes with a gluon in the initial state all vanish, as is to be expected on theoretical grounds (see the statement below (5.2.8)).

5.2.2 Results for the coefficient functions

After we have computed the parton cross sections (parton structure functions), we have to perform coupling constant renormalization and mass factorization in order to remove the remaining ultraviolet singularities and collinear divergences. For both procedures we have chosen the $\overline{\text{MS}}$ scheme. The coefficients $C_{i,q}^{(q)}$ appearing in the perturbative expansion of the coefficient function $C_{i,q}$ are defined by

$$C_{i,q}(z, Q^2/M^2) = \sum \left(\frac{\alpha_s}{4\pi}\right)^\ell C_{i,q}^{(\ell)}(z, Q^2/M^2) \quad , \quad (5.2.13)$$

where $\alpha_s \equiv \alpha_s(M^2)$. If we want to choose the renormalization scale R different from the factorization scale M , one can perform a simple transformation, see (3.2.56). The

second order non-singlet coefficient function can be split in two parts

$$C_{i,q}^{(2),NS}(z, Q^2/M^2) = C_{i,q}^{(2),+}(z, Q^2/M^2) \pm C_{i,q}^{(2),-}(z, Q^2/M^2) , \quad (5.2.14)$$

where the plus sign holds for $C_{2,q}^{(2),NS}$ occurring in $C_{2,q}^S$ of (5.2.3) and the minus sign for $C_{3,q}^{(2),NS}$ occurring in $C_{3,q}^{NS}$ in (5.2.4). The coefficient function $C_{i,q}^{(2),-}$ is only due to contributions from identical quarks in the final state of process (5.2.8). The expression for $C_{3,q}^{(2),NS}$ is the same as that for the second order correction to the non-singlet polarized coefficient function, which will be given in appendix 6A (6A.1). We have also computed $C_{2,q}^{(2),-}$ where now the mass factorization is performed in the DIS scheme. The transition from the \overline{MS} scheme to the DIS scheme (denoted by omitting the bar above the expression) is given by

$$\begin{aligned} C_{3,q}^{(2),NS}(z, Q^2/M^2) &= \bar{C}_{3,q}^{(2),NS}(z, Q^2/M^2) \\ &+ C_{2,q}^{(2),NS}(z, Q^2/M^2) - \bar{C}_{2,q}^{(2),NS}(z, Q^2/M^2) + C_F^2 \left[2(1+z) \left(2Li_2(1-z) \right. \right. \\ &- 2\ell n z \ell n(1-z) + 2\ell n^2(1-z) - 3\ell n(1-z) + \ell n^2 z - 4\zeta(2) \left. \right) \\ &- 2(z+5)\ell n z - 28z - 8 \left. \right] , \end{aligned} \quad (5.2.15)$$

where $C_{2,q}^{(2),NS}(z, Q^2/M^2) - \bar{C}_{2,q}^{(2),NS}(z, Q^2/M^2)$ can be found in (3B.19). The explicit expressions for $C_{3,q}^{(2),NS}$ can be found in our computer programs and are available on request.

As a final check on our result we computed the sum rule

$$\begin{aligned} \int_0^1 dz C_{3,q}(z, Q^2/M^2) &= 1 - \frac{\alpha_s}{4\pi} \{ 3C_F \} + \left(\frac{\alpha_s}{4\pi} \right)^2 \left\{ \frac{21}{2} C_F^2 - 23C_A C_F \right. \\ &+ 4n_f C_F \left. \right\} , \end{aligned} \quad (5.2.16)$$

which agrees with the result in eq. (13) of [11], see also eq. (5.14c) in [14]. Notice that in these references the authors computed the above sum rule by using a completely different method. Their method only allows for the computation of the lowest moments of the coefficient function. However it can be extended to include the order α_s^3 correction. In our case this would be very difficult because of the very cumbersome three loop and four body phase space integrals that would have to be performed. The advantage of our expression is that the full z dependence is given which makes it more amenable for phenomenological applications.

5.3 Results for F_3

We will now study the effect of the order α_s^2 corrections on the deep inelastic structure functions $F_2(x, Q^2)$ (5.2.3) and $F_3(x, Q^2)$ (5.2.4). Here one has to bear in mind that for a complete next-to-next-to-leading order analysis one also needs the three loop contributions to the Altarelli–Parisi (AP) splitting functions P_{ij} which are not known yet. Nevertheless we can make an estimate of the order α_s^2 corrections in particular in the large- x region where the structure functions are dominated by the logarithmic terms of the type $\ln^k(1-z)/(1-z)$ which appear in the non-singlet part of the coefficient function as well as in the AP splitting function. These terms can be attributed to soft gluon radiation. In the $\overline{\text{MS}}$ scheme one can argue (see the discussion in chapter 3) that $k=0$ for the AP splitting function P_{qq}^{NS} in all orders of perturbation theory. On the other hand $k_{\text{max}} = 2\ell - 1$ for the order α_s^ℓ contribution to the coefficient function $C_{i,q}^{\text{NS}}$ ($i=2,3$). Hence the large logarithmic terms in P_{qq}^{NS} are suppressed compared to those appearing in $C_{i,q}^{\text{NS}}$ ($i=2,3$) so that in the large- x region the whole correction to $F_i(x, Q^2)$ ($i=2,3$) can be attributed to the non-singlet coefficient function. For our plots we have chosen the parton densities in [15] which are represented in the DIS scheme ([15], table I3, FIT-B1) (MTB1DI) as well as $\overline{\text{MS}}$ scheme ([15], table I4, FIT-B1) (MTB1MS) and [16] (MRS(D0)). Further we have taken the two loop corrected running coupling constant ($\Lambda = 194$ MeV) with four active flavours ($n_f = 4$).

In fig. 5.1 we have compared the order α_s corrected structure function $F_3^{(1)}(x, Q^2)$ with the order α_s^2 corrected structure function $F_3^{(2)}(x, Q^2)$, using MRS(D0). The plots are made for three representative x -values of the CCFR experiment [2], i.e. $x = 0.045$, $x = 0.275$ and $x = 0.65$. In addition we have chosen three different factorization scales, namely $M = \frac{1}{2}Q$, Q , $2Q$. It turns out that for the three chosen x -values $F_3^{(2)}(x, Q^2)$ lies within the range given by the mass factorization scale variation of $F_3^{(1)}(x, Q^2)$ and therefore the second order corrections are not noticeable. However, this depends on the chosen parton density parametrization. Fig. 1 of [17], where the MTB1MS parametrization was used, reveals that the order α_s^2 corrections are very small for $x = 0.045$ and $x = 0.275$ but become noticeable for $x = 0.65$. The reason why at larger x -values the corrections become noticeable can be attributed to the soft gluon bremsstrahlung mechanism, as discussed above.

In fig. 5.2 we have compared the order α_s^2 corrected structure function $F_3^{(2)}(x, Q^2)$ in the $\overline{\text{MS}}$ and DIS scheme. The figure reveals hardly any difference between $F_3^{(2),\text{MS}}(x, Q^2)$ and $F_3^{(2),\text{DIS}}(x, Q^2)$. Hence the order α_s^2 corrections are almost the same in the

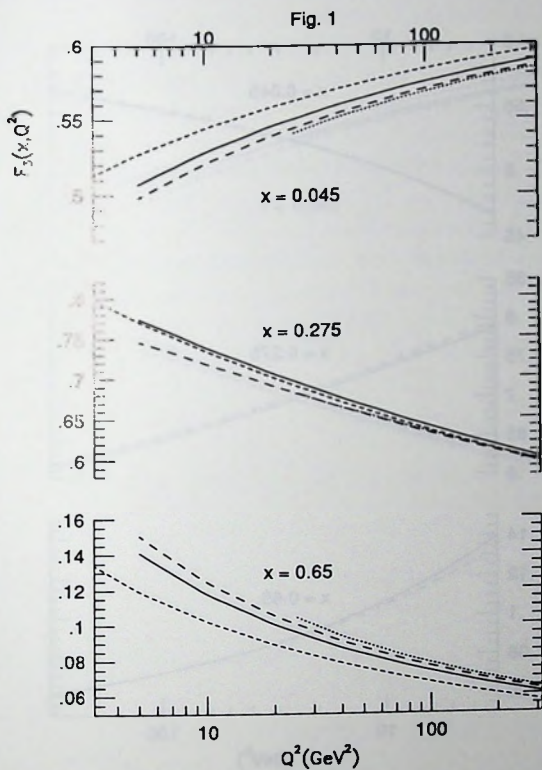


Fig. 5.1. Factorization scale dependence of $F_3^{(1)}(x, Q^2)$ and comparison with $F_3^{(2)}(x, Q^2)$, MRS(D0) parametrization.

Dotted line: $F_3^{(1)}(x, Q^2)$, $M = \frac{1}{2}Q$. Solid line: $F_3^{(1)}(x, Q^2)$, $M = Q$. Short-dashed line: $F_3^{(1)}(x, Q^2)$, $M = 2Q$. Long-dashed line: $F_3^{(2)}(x, Q^2)$, $M = Q$.

two schemes. We expect that figs. 5.1 and 5.2 will not be seriously altered when the three loop splitting function $P_{qq}^{(2),NS}$ is taken into account. For $x < 0.5$ the corrections due to the contribution from $P_{qq}^{(2),NS}$ will be of the same order of magnitude as those

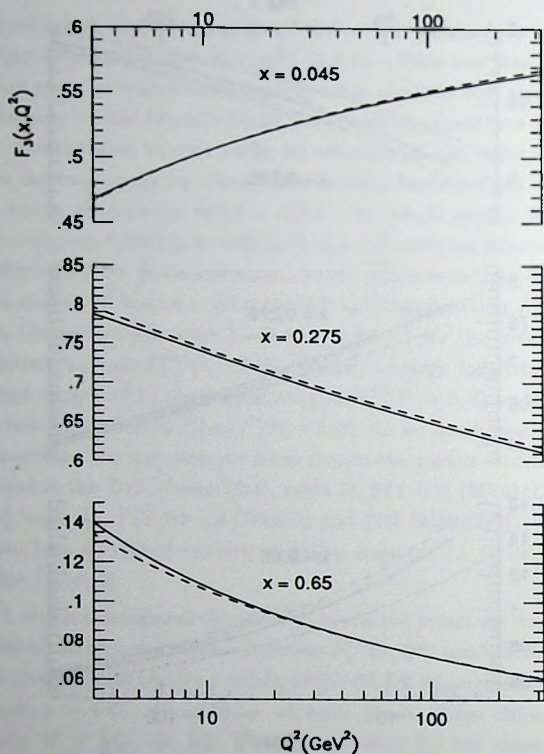


Fig. 5.2. Scheme dependence of $F_3^{(2)}(x, Q^2)$. Solid line: $F_3^{(2)}(x, Q^2)$ in the $\overline{\text{MS}}$ scheme (MTB1MS). Long-dashed line: $F_3^{(2)}(x, Q^2)$ in the DIS scheme (MTB1DI).

obtained for $C_{3,q}^{(2),\text{NS}}$ and are therefore small too. At large x ($x > 0.5$) the corrections to the structure function can be wholly attributed to $C_{3,q}^{(2),\text{NS}}$ as has been explained above.

In fig. 5.3 we have repeated the analysis for the structure function $F_2(x, Q^2)$. Here

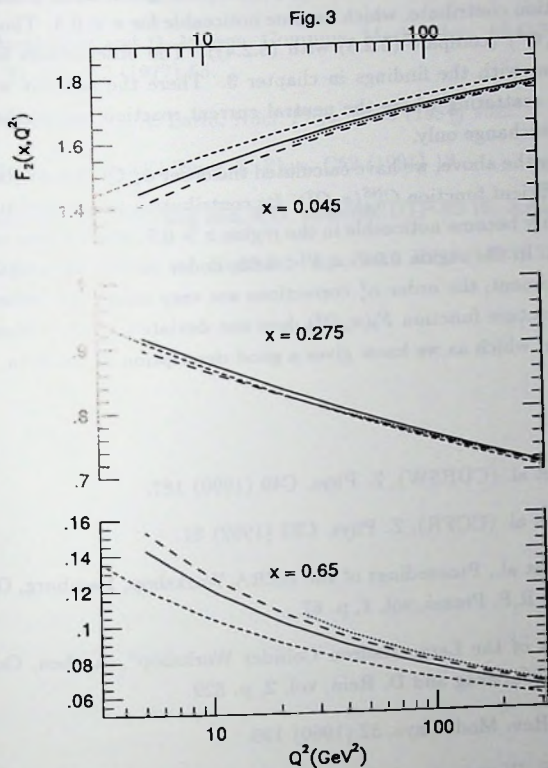


Fig. 5.3. Factorization scale dependence of $F_2^{(1)}(x, Q^2)$ and comparison with $F_2^{(2)}(x, Q^2)$, MRS(D0) parametrization.

Dotted line: $F_2^{(1)}(x, Q^2)$, $M = \frac{1}{2}Q$. Solid line: $F_2^{(1)}(x, Q^2)$, $M = Q$. Short-dashed line: $F_2^{(1)}(x, Q^2)$, $M = 2Q$. Long-dashed line: $F_2^{(2)}(x, Q^2)$, $M = Q$.

we observe the same features as is shown for $F_3(x, Q^2)$ in fig. 5.1. The corrections are small for the three chosen x -values. In [17] we saw that when the MTB1MS parametrization is used, the corrections are small for $x < 0.5$ and increase when

$x > 0.5$. Notice that in the case of $F_2(x, Q^2)$ also the gluon density and the gluon coefficient function contribute, which become noticeable for $x < 0.3$. Those terms are absent in $F_3(x, Q^2)$ (compare (5.2.3) with (5.2.4)). The observations for $F_2(x, Q^2)$ are in agreement with the findings in chapter 3. There the analysis was done for electron-proton scattering where the neutral current reaction was mediated by one virtual photon exchange only.

Summarizing the above, we have calculated the order α_s^2 QCD contribution to the non-singlet coefficient function $C_{3,q}^{NS}(z, Q^2)$. Its contribution to the structure function $F_3(x, Q^2)$ can only become noticeable in the region $x > 0.5$, which is due to soft gluon bremsstrahlung. In the region $0.045 < x < 0.65$, under current investigation by the CCFR [2] experiment, the order α_s^2 corrections are very small. Therefore the order α_s^2 corrected structure function $F_3(x, Q^2)$ does not deviate too much from the order α_s corrected one, which as we know gives a good description of the data.

References

- [1] J.P. Berge et al. (CDHSW), Z. Phys. C49 (1990) 187.
- [2] E. Oltman et al. (CCFR), Z. Phys. C53 (1992) 51.
- [3] J. Blümlein et al., Proceedings of the HERA Workshop, Hamburg, October 12-14, 1987, ed. R.P. Peccei, vol. 1, p. 67.
- [4] "Proceedings of the Large Hadron Collider Workshop", Aachen, October 4-9, 1990, eds. G. Jarlskog and D. Rein, vol. 2, p. 829.
- [5] A.J. Buras, Rev. Mod. Phys. 52 (1980) 199.
- [6] E. Laenen, S. Riemersma, J. Smith and W.L. van Neerven, Nucl. Phys. B392 (1993) 162, 229, Phys. Lett. B291 (1992) 325.
- [7] W.A. Bardeen, A.J. Buras, D.W. Duke and T. Muta, Phys.Rev. D18 (1978) 3998.
- [8] G. Altarelli, R.K. Ellis and G. Martinelli, Nucl.Phys. B157 (1979) 461.
- [9] B. Humpert and W.L. van Neerven, Nucl. Phys. B184 (1981) 225.
- [10] D. Akyeampong and R. Delbourgo, Nuov. Cim. 17A (1973) 578.
- [11] S.A. Larin and J.A.M. Vermaseren, Phys. Lett. B259 (1991) 345.

- [12] G. 't Hooft and M. Veltman, Nucl. Phys. B44 (1972) 189.
- [13] F. Breitenlohner and D. Maison, Commun. Math. Phys. 52 (1977) 11, *ibid.* 52 (1977) 39, *ibid.* 52 (1977) 55.
- [14] S.G. Gorishni and S.A. Larin, Nucl. Phys. B283 (1987) 452.
- [15] J.G. Morfin and Wu-Ki Tung, Z. Phys. C52 (1991) 13.
- [16] A.D. Martin, W.J. Stirling and R.G. Roberts, DTP-92-16, RAL-92-021, 1992.
- [17] E.B. Zijlstra and W.L. van Neerven, Phys. Lett. B297 (1993) 377.

Chapter 6

The polarized structure function G_1

6.1 Introduction

The disagreement between the theoretical prediction for the first moment of the polarized structure function $g_1(x, Q^2)$, which is given by the Ellis-Jaffe sum rule [1], and the combined SLAC-EMC data [2, 3, 4] has attracted much theoretical interest during the past years. This discrepancy between theory and experiment came as a great surprise because one expected that sum rules corresponding to conserved quantities, which are derived in the context of the constituent quark model at low energy scales, would also be valid at large energy scales characteristic for the current (parton) quark regime. Notice that sum rules which correspond to conserved quantities do not show scaling violating effects due to QCD corrections. This principle, which seems to work for unpolarized quantities, is apparently violated in the polarized case.

Many theorists have tried to explain the above discrepancy, for reviews see [5, 6, 7, 8]. One of the issues was the question whether the experimental result for the Ellis-Jaffe sum rule, which turns out to be much smaller than expected, can either be explained by a large positive polarized gluon density or by a large negative polarized sea quark density inside the proton. A combination of both is also possible. In this chapter we adopt the point of view advocated in [8, 9] that the above parton densities which were used to explain the measured size of the sum rule depend on the mass factorization scheme chosen for the Altarelli-Parisi (AP) splitting functions and the polarized coefficient functions. However one has to be careful with this explanation because the first moment of the structure function $g_1(x, Q^2)$ also depends on the x -behaviour of the parton densities. The latter is of a non-perturbative origin and cannot be determined within the framework of perturbative QCD. In the literature the x -dependence of the polarized parton densities is determined in such a way that

the experimentally observed first moment of the structure function $g_1(x, Q^2)$ is reproduced at $Q^2 = Q_0^2 = 10 \text{ GeV}^2$. However as we will show in this chapter, this is not sufficient to predict the x -behaviour of the parton densities at scales different from Q_0^2 . It will turn out that the polarized structure function $g_1(x, Q^2)$ for $Q^2 \neq Q_0^2$ considerably depends on the two extreme choices made for the sea-quark and the gluon density at $Q^2 = Q_0^2$. Since the large negative sea-quark density and the large positive gluon density are related to different schemes, one would get the impression that $g_1(x, Q^2)$ is scheme dependent which is not acceptable. This seeming scheme dependence can be resolved when parton densities are fitted to $g_1(x, Q^2)$ measured for a wide range of x and Q^2 -values. At the moment this procedure can only be applied to the unpolarized structure function $F_2(x, Q^2)$ where we have an abundance of data collected in current [11] and past [12] experiments. However the data obtained for polarized electron-proton scattering are still too poor to determine the x -dependence of $g_1(x, Q^2)$ at different Q^2 -values. Future experiments as will be carried out by SMC [13] or HERMES [14] will certainly improve upon this situation. Only if this procedure is carried out and the perturbative quantities are calculated in sufficiently high order in α_s in different schemes, the scheme dependence of the structure function will disappear. In this way one is able to determine the full x -dependence of the parton densities in the different schemes with a much higher accuracy as could be done in the past.

In this chapter we want to determine the Q^2 -evolution of $g_1(x, Q^2)$ and to investigate its dependence on the input parton densities in particular the sea-quark and gluon density. For that purpose we have calculated the order α_s^2 corrections to the singlet and non-singlet coefficient functions contributing to the structure function $g_1(x, Q^2)$. From the mass factorization of the corresponding parton cross sections we also infer the order α_s^2 contribution to the polarized AP splitting functions P_{qq}^S and P_{qg} . These corrections are included in the analysis of $g_1(x, Q^2)$. We will show that the Q^2 -variation of the latter considerably depends on the two extreme choices for the polarized parton densities made in the literature.

This chapter will be organized as follows. In section 6.2 we introduce our notations and some useful formulae. The calculation of the order α_s^2 contributions to the polarized coefficient functions is presented in section 6.3. In section 6.4 we discuss the effect of the order α_s and order α_s^2 QCD corrections to the structure function $g_1(x, Q^2)$. We also investigate the dependence of the latter on the input polarized parton densities. The long expressions for the second order corrected coefficient functions can be found in the appendix.

6.2 Kinematics

Deep inelastic lepton-proton scattering is given by the reaction

$$l_1(k_1) + H(p) \rightarrow l_2(k_2) + "X" , \quad (6.2.1)$$

where l_1, l_2 denote the in- and outgoing leptons respectively and H stands for the proton. The symbol " X " denotes any inclusive hadronic final state allowed by quantum number conservation laws. In lowest order of the electro-weak coupling constant the reaction proceeds via the exchange of one of the intermediate vector bosons V of the standard model, i.e. $V = \gamma, Z, W^\pm$. The above process is inclusive with respect to the outgoing hadrons denoted by " X ", because only the outgoing lepton is detected. In this chapter we will limit ourselves to process (6.2.1), where the exchanged vector boson V is given by the virtual photon γ .

When the incoming lepton and the target proton are polarized, the corresponding lepton-proton cross-sections can be written as

$$\frac{d^2\sigma^-}{dx dy} - \frac{d^2\sigma^+}{dx dy} = \frac{8\pi\alpha^2}{q^2} \left[\left\{ 2 - y - \frac{Mxy}{E} \right\} g_1(x, Q^2) - \frac{2Mx}{E} g_2(x, Q^2) \right] , \quad (6.2.2)$$

$$\begin{aligned} \frac{d^2\sigma^\perp}{dx dy} - \frac{d^2\sigma^\parallel}{dx dy} &= \frac{8\pi\alpha^2}{q^2} \left(\frac{2Mx(1-y)}{yE} \right)^{1/2} \left(1 - \frac{Mxy}{2(1-y)E} \right)^{1/2} \\ &\times [yg_1(x, Q^2) + 2g_2(x, Q^2)] , \end{aligned} \quad (6.2.3)$$

where the energy of the incoming lepton is represented by E and M denotes the mass of the proton. The variables x and y are defined by

$$x = \frac{Q^2}{2p \cdot q} \quad (0 < x \leq 1) , \quad y = \frac{p \cdot q}{p \cdot k_1} \quad (0 < y \leq 1) \quad (6.2.4)$$

and q denotes the momentum of the virtual vector boson V (in this case the photon) which is given by

$$q = k_1 - k_2 , \quad Q^2 = -q^2 > 0 . \quad (6.2.5)$$

The lower arrow above σ in (6.2.2) and (6.2.3) indicates the polarization of the incoming lepton in the direction of its momentum. The upper arrow on σ in (6.2.2) stands for a polarization of the proton which is parallel or anti-parallel to the polarization of the incoming lepton. The vertical arrows in (6.2.3) also belong to the proton which is now polarized perpendicular (transverse) to the polarization of the lepton in either

the up or down direction. The polarized structure functions appearing in (6.2.2) and (6.2.3) are represented by $g_1(x, Q^2)$ (longitudinal spin) and $g_2(x, Q^2)$ (transverse spin).

In this chapter we will only discuss the $\mathcal{O}(\alpha_s)$ and $\mathcal{O}(\alpha_s^2)$ corrections to the structure function $g_1(x, Q^2)$. In the QCD improved parton model it can be expressed for an even number of flavours in the following way

$$g_1(x, Q^2) = \frac{1}{2} \int_x^1 \frac{dz}{z} \left[\frac{5}{18} \left\{ \Sigma\left(\frac{x}{z}, M^2\right) C_q^S(z, Q^2/M^2) + G\left(\frac{x}{z}, M^2\right) C_g(z, Q^2/M^2) \right\} + \frac{1}{6} \Delta\left(\frac{x}{z}, M^2\right) C_q^{NS}(z, Q^2/M^2) \right], \quad (6.2.6)$$

which is analogous to (3.2.3). Here $G(x, M^2)$ denotes the polarized gluon density and $\Sigma(x, M^2)$, $\Delta(x, M^2)$ stand for the singlet (S) and non-singlet (NS) combinations of the polarized quark densities respectively. The same nomenclature also applies to the polarized deep inelastic scattering (DIS) coefficient functions $C_i(x, Q^2/M^2)$. All quantities defined above depend both on the mass factorization scale M and on the renormalization scale R . However in (6.2.6) these scales are chosen to be equal.

6.3 The calculation of the order α_s^2 corrections

In this section we will give an outline of the calculation of the $\mathcal{O}(\alpha_s)$ and $\mathcal{O}(\alpha_s^2)$ corrections to the polarized coefficient functions in (6.2.6) including their dependence on M and R .

The coefficient functions receive contributions from the parton subprocesses listed in table 2.1. The corresponding Feynman diagrams can be found in figs. 3.1–3.7 of chapter 3. Apart from some small differences in the details, which will be given below, the calculations of the polarized parton cross sections will be analogous to the ones performed for the unpolarized structure functions $F_k(x, Q^2)$ ($k = 1, 2, 3, L$) in chapter 3 and 5.

The reactions in table 2.1 are described by the parton structure tensor $\widehat{W}_{\mu\nu}$, defined as in (3.2.5). For $V = \gamma$ in table 2.1 the parton structure tensor can be written as follows

$$\widehat{W}^{\mu\nu}(p, q, s) = \widehat{W}_S^{\mu\nu}(p, q) + i \widehat{W}_A^{\mu\nu}(p, q, s), \quad (6.3.1)$$

with the symmetric part given by

$$\widehat{W}_S^{\mu\nu}(p, q) = \frac{1}{2} \left(g^{\mu\nu} - \frac{q^\mu q^\nu}{q^2} \right) \widehat{F}_L(z, Q^2) + \left\{ p^\mu p^\nu - \frac{p \cdot q}{q^2} (p^\mu q^\nu + p^\nu q^\mu) \right\}$$

$$+ g^{\mu\nu} \frac{(p \cdot q)^2}{q^2} \} \frac{\hat{F}_2(z, Q^2)}{p \cdot q} \quad (6.3.2)$$

and the antisymmetric part is equal to

$$\widehat{W}_A^{\mu\nu}(p, q, s) = -\frac{m}{2p \cdot q} \epsilon^{\mu\nu\alpha\beta} q_\alpha \left[s_\beta \hat{g}_1(z, Q^2) + \left(s_\beta - \frac{sq}{p \cdot q} p_\beta \right) \hat{g}_2(z, Q^2) \right] \quad (6.3.3)$$

Here q denotes the virtual photon momentum. Further p and s are the momentum and spin of the incoming parton respectively, with $s \cdot p = 0$, $s^2 = 1$ and $\tau = Q^2/2p \cdot q$. The structure functions defined in (6.3.2) and (6.3.3) are the partonic analogs of the hadronic structure functions. Therefore we will call them parton structure functions¹ (indicated by a hat) since they correspond to the parton subprocesses in (5.2.1) and table 2.1. The unpolarized quantities \hat{F}_2 and \hat{F}_L have been calculated up to $\mathcal{O}(\alpha_s^2)$ in chapter 3. The calculation of \hat{g}_1 proceeds as follows.

Starting with the subprocesses in table 2.1 with a quark in the initial state we follow the procedure in [15] and write the partonic tensor as

$$\widehat{W}^{\mu\nu}(p, q, s) = \frac{1}{2} \text{Tr}(1 + \gamma_5 \not{s})(\not{p} + m) G^{\mu\nu}(p, q) \quad (6.3.4)$$

Here $G^{\mu\nu}(p, q)$ is the amplitude where the external quark lines with momentum p are amputated. For the calculation it is essential that terms linear in the quark mass m are kept in $G^{\mu\nu}(p, q)$ even if one employs n -dimensional regularization in which case such terms are usually put equal to zero. One can now write $G^{\mu\nu}(p, q)$ as follows

$$G^{\mu\nu}(p, q) = G_0^{\mu\nu}(p, q) + m G_1^{\mu\nu}(p, q) \quad , \quad (6.3.5)$$

where $G_0^{\mu\nu}(p, q)$ and $G_1^{\mu\nu}(p, q)$ satisfy the properties (in 4 dimensions!).

$$\{\gamma_5, G_0^{\mu\nu}(p, q)\} = 0 \quad , \quad [\gamma_5, G_1^{\mu\nu}(p, q)] = 0 \quad . \quad (6.3.6)$$

The antisymmetric part $\widehat{W}_A^{\mu\nu}$ in (6.3.3) can now be split into two parts.

$$\begin{aligned} \widehat{W}_A^{\mu\nu}(p, q, s) &= \frac{1}{2} \text{Tr} \{ \gamma_5 \not{s} (\not{p} + m) G^{\mu\nu}(p, q) \} \\ &= \widehat{W}_{A,0}^{\mu\nu}(p, q, s) + \widehat{W}_{A,1}^{\mu\nu}(p, q, s) \quad , \end{aligned} \quad (6.3.7)$$

with

$$\begin{aligned} \widehat{W}_{A,0}^{\mu\nu}(p, q, s) &= \frac{1}{2} m \text{Tr} \{ \gamma_5 \not{s} G_0^{\mu\nu}(p, q) \} = T_1^{\mu\nu} \hat{g}_{1,0}(x, Q^2) + T_2^{\mu\nu} \hat{g}_{2,0}(x, Q^2) \\ &\quad + T_3^{\mu\nu} \hat{v}(x, Q^2) \quad , \end{aligned} \quad (6.3.8)$$

¹Do not confuse them with the earlier defined parton densities $f_i(x, M^2)$.

$$\widehat{W}_{A,1}^{\mu\nu}(p, q, s) = \frac{1}{2} m \text{Tr} \{ \gamma_5 \not{p} G_1^{\mu\nu}(p, q) \} = T_1^{\mu\nu} \widehat{g}_{1,1}(x, Q^2) + T_2^{\mu\nu} \widehat{g}_{2,1}(x, Q^2) - T_3^{\mu\nu} \widehat{v}(x, Q^2) \quad (6.3.9)$$

and the tensors $T_i^{\mu\nu}$ are given by

$$T_1^{\mu\nu} = -\frac{m}{2p \cdot q} \epsilon^{\mu\nu\gamma\beta} q_\alpha s_\beta, \quad (6.3.10)$$

$$T_2^{\mu\nu} = -\frac{m}{2p \cdot q} \epsilon^{\mu\nu\gamma\beta} q_\alpha \left(s_\beta - \frac{sq}{p \cdot q} p_\beta \right), \quad (6.3.11)$$

$$T_3^{\mu\nu} = -\frac{m}{2p \cdot q} \epsilon^{\mu\nu\gamma\beta} p_\alpha s_\beta. \quad (6.3.12)$$

The mass m which appears on the left as well as on the right hand side of (6.3.8) and (6.3.9) will be divided out so that in the case of n -dimensional regularization it can be put equal to zero. Notice that the last term in (6.3.8) and (6.3.9), which is proportional to the structure function \widehat{v} , violates current conservation which means that $\widehat{W}_{A,0}^{\mu\nu}$ and $\widehat{W}_{A,1}^{\mu\nu}$ have to be added (see also the remark below eqs. (19a,b) in [15]). The above expressions simplify if one is only interested in \widehat{g}_1 . In this case one can put $s_\alpha = p_\alpha/m$ so that $T_2^{\mu\nu} = T_3^{\mu\nu} = 0$. Furthermore if one puts $m = 0$, $\widehat{g}_{1,0}$ in (6.3.9) becomes equal to zero too and we are only left with $\widehat{g}_{1,0} \equiv \widehat{g}_1$ in (6.3.8). The calculation of \widehat{g}_1 is then the same as that carried out for \widehat{F}_3 in chapter 5. Here \widehat{F}_3 is the partonic structure function which appears in the parity violating part of the structure tensor for deep inelastic neutrino-parton scattering.

For the parton subprocesses in table 2.1 where a gluon appears in the initial state we follow the procedure in [16] (see eq. (3.11) of [16]). If we do not contract the amplitude squared in the integrand (3.2.5) with the external gluon polarizations the antisymmetric part can be written as

$$\widehat{W}_{\tau\rho}^{\mu\nu}(p, q) = \frac{2}{p \cdot q} \left[\epsilon^{\mu\nu\lambda\sigma} \epsilon_{\tau\rho\alpha\beta} q_\lambda p^\beta (\widehat{g}_1(z, Q^2) + \widehat{g}_2(z, Q^2)) - \frac{1}{p \cdot q} \epsilon^{\mu\nu\lambda\sigma} \epsilon_{\tau\rho\alpha\beta} q_\lambda p^\sigma q^\alpha p^\beta \widehat{g}_2(z, Q^2) \right]. \quad (6.3.13)$$

The Lorentz indices μ, ν and λ, σ refer to the electromagnetic current and the external gluon respectively. To compute the difference between the cross sections due to left and right handed polarized gluons one has to contract (6.3.13) with $\frac{1}{8\pi} \epsilon^{\tau\rho\alpha\beta} s_\alpha q_\beta$. The result is given by $\frac{1}{m} \widehat{W}_A^{\mu\nu}$ (6.3.3) provided $p^2 = 0$ and $s \cdot p = 0$ (p is the gluon momentum). Setting $s = p$ the structure function \widehat{g}_2 drops out and only \widehat{g}_1 remains, so that we are in the same situation as in the case when there is a quark in the

initial state. The structure function \hat{g}_1 can now be obtained in the same way as in the case of \hat{F}_3 for neutrino-parton scattering by contracting $\widehat{W}_A^{\mu\nu}$ with $\varepsilon_{\mu\nu\lambda\sigma}p^\lambda q^\sigma$. However this contraction depends on the method one uses to regularize the three different types of divergences which show up while calculating \hat{g}_1 . These divergences are represented by the ultraviolet (UV), infrared (IR) and collinear (C) singularities. In order to regularize these singularities we choose the method of n -dimensional regularization. This method turns out to be the most convenient one in particular if one wants to compute QCD corrections beyond $\mathcal{O}(\alpha_s)$. However the use of this method requires that one finds a suitable n -dimensional prescription for the γ_5 -matrix which appears in the matrix element (6.3.4) for processes with a quark in the initial state. We encountered the same problem in chapter 5 and we will use the prescription explained in section 5.2.1. Following this prescription the projection of $\widehat{W}_A^{\mu\nu}$ on \hat{g}_1 reads as follows.

$$\hat{g}_1(z, Q^2) = \frac{2}{(n-2)(n-3)} \frac{1}{p \cdot q} \varepsilon_{\mu\nu\lambda\sigma} p^\lambda q^\sigma \widehat{W}_A^{\mu\nu}(p, q, p/m) . \quad (6.3.14)$$

For our algebraic computations of the traces, the partial fractioning of the matrix elements and the analytical evaluation of the integrals we have used the algebraic manipulation program FORM [22].

We will now present the results of the calculation of \hat{g}_1 up to $\mathcal{O}(\alpha_s^2)$. Using our convention in (3.2.3) and (6.3.3) the zeroth order result is given by

$$\hat{g}_{1,q}^{(0)} = \delta(1-z) . \quad (6.3.15)$$

The first order corrections, denoted by $\hat{g}_{1,i}^{(1)}$ ($i = q, g$), have already been calculated in the literature [9, 15, 16, 23, 24] by using different regularization schemes. In the case of n -dimensional regularization the results for $\hat{g}_{1,q}^{(1)}$ ($= \hat{F}_3$) can be found in [25, 26] while for $\hat{g}_{1,g}^{(1)}$ they have been calculated in [9, 24]. Since the mass factorization has to be carried out up to order α_s^2 , one needs to know those terms in $\hat{g}_{1,i}^{(1)}(z, Q^2, \varepsilon)$ which are proportional to $\varepsilon \equiv n-4$. Therefore we had to repeat the first order calculations and the results can be presented in the same form as (3.2.13) and (3.2.15). The lowest order contributions to the polarized Altarelli-Parisi splitting functions $P_{ij}^{(0)}$ ($i, j = q, \bar{q}, g$) [26] are given by (using our conventions)

$$P_{qq}^{(0)} = 4C_F \left[\left(\frac{2}{1-z} \right)_+ - 1 - z + \frac{3}{2} \delta(1-z) \right] , \quad (6.3.16)$$

$$P_{gq}^{(0)} = 4C_F [2-z] , \quad (6.3.17)$$

$$P_{qg}^{(0)} = 8T_f [2z-1] , \quad (6.3.18)$$

$$P_{gg}^{(0)} = 8C_A \left[\frac{1}{1-z} + 1 - 2z + \frac{11}{12} \delta(1-z) \right] - \frac{4}{3} n_f \delta(1-z) , \quad (6.3.19)$$

where the $SU(N)$ colour factors are given by $C_F = (N^2 - 1)/2N$, $C_A = N$, $T_f = 1/2$ and n_f denotes the number of light flavours. The coefficients $a_i^{(1)}$ ($i = q, g$) of the first order polarized coefficient functions read

$$a_q^{(1)} = C_F \left[\left(\frac{\ell n^2(1-z)}{1-z} \right)_+ - \frac{3}{2} \left(\frac{\ell n(1-z)}{1-z} \right)_+ + \left(\frac{7}{2} - 3\zeta(2) \right) \left(\frac{1}{1-z} \right)_+ \right. \\ \left. - \frac{1}{2}(1+z)\ell n^2(1-z) - \frac{1+z^2}{1-z}\ell n z \ell n(1-z) + \frac{1}{2}\frac{1+z^2}{1-z}\ell n^2 z \right. \\ \left. + \frac{3}{2}\frac{1}{1-z}\ell n z + (2+z)(\ell n(1-z) - \ell n z - 2) + \frac{3}{2}(1+z)\zeta(2) \right. \\ \left. + \delta(1-z)\left(9 - \frac{3}{4}\zeta(2)\right) \right], \quad (6.3.20)$$

$$a_g^{(1)} = T_f \left[(2z-1)(\ell n^2(1-z) - 2\ell n z \ell n(1-z) + \ell n^2 z) \right. \\ \left. + (6-8z)(\ell n(1-z) - \ell n z) - 3(2z-1)\zeta(2) - 12 + 16z \right]. \quad (6.3.21)$$

The calculation of the $\mathcal{O}(\alpha_s^2)$ correction proceeds in the same way as in the case of the unpolarized structure functions. The procedure is extensively explained in section 3.2, so we do not repeat it here. The phase space integrals appearing in the $2 \rightarrow 2$ and $2 \rightarrow 3$ body processes can also be taken over from chapter 3, except that we had to compute some new $2 \rightarrow 3$ body phase space integrals for the process $\gamma^* + g \rightarrow q + \bar{q} + g$. It is important to note that the expressions for the second order contributions $\hat{g}_{1,i}^{(2)}$ ($i = q, g$) to the polarized parton structure function have exactly the same structure as those given for \hat{F}_2 in section 3.2, therefore we do not repeat them here. The collinear divergences in $\hat{g}_{1,i}$ ($i = q, g$) are removed by mass factorization which proceeds in the standard way characteristic of quantities which only receive contributions from twist two operators. The procedure is the same as for the unpolarized parton structure functions calculated in section 3.2.

The results for the coefficient functions are given in appendix 6A. The $\mathcal{O}(\alpha_s^2)$ non-singlet polarized AP splitting functions $P_{qq}^{(1),NS}$ and $P_{q\bar{q}}^{(1),NS}$ are also equal to the unpolarized ones and can be found in [28, 29] (in our notation see also eq. (2.36) of ([30])). Contrary to the unpolarized AP splitting functions, the second order contributions to the polarized AP splitting functions are not known yet. However we can derive them because we need them in our mass factorization procedure in which all other occurring quantities have been calculated. The polarized AP splitting functions are given by (for the definition of PS (pure singlet) see 3.2.30)

$$P_{qq}^{(1),PS} = 8C_F T_f \left[-2(1+z)\ell n^2 z - 2(1-3z)\ell n z + 2(1-z) \right], \quad (6.3.22)$$

$$\begin{aligned}
P_{qg}^{(1)} = & 4C_F T_f \left[2(1-2z) \left(-2\ell n^2(1-z) + 4\ell n z \ell n(1-z) - \ell n^2 z \right. \right. \\
& + 4\zeta(2) \left. \right) + 16(1-z)\ell n(1-z) - 2(17+16z)\ell n z - 92 + 102z \left. \right] \\
& + 4C_A T_f \left[4(1-2z) \left(\ell n^2(1-z) - \ell n^2 z - 2\ell n z \ell n(1+z) \right. \right. \\
& - 2Li_2(-z) \left. \right) - 8\zeta(2) + 4(1+8z)\ell n z - 16(1-z)\ell n(1-z) \\
& + 4(12-11z) \left. \right] .
\end{aligned} \tag{6.3.23}$$

Since the polarized splitting functions $P_{qq}^{(1),NS}$ and $P_{q\bar{q}}^{(1),NS}$ are already known, we can compute the singlet AP splitting function which is given by

$$P_{qq}^{(1),S} = P_{qq}^{(1),NS} + P_{q\bar{q}}^{(1),NS} + P_{q\bar{q}}^{(1),PS} . \tag{6.3.24}$$

Unfortunately we could not obtain the other two second order polarized splitting functions $P_{gq}^{(1)}$ and $P_{gg}^{(1)}$, since they will only show up in the third order contribution to \hat{g}_1 . This is because the gluon does not interact directly with the virtual photon as the quark does.

Before finishing this section we want to comment on the polarized coefficient functions and AP splitting functions mentioned above. They are all regular in the limit $z \rightarrow 0$, which is in contrast to the behaviour of the unpolarized quantities $C_q^{PS}(z)$, $C_g(z)$, $P_{gq}(z)$, $P_{gg}(z)$. The latter behave like $\ell n^k z/z$ as $z \rightarrow 0$. This behaviour originates from multiple gluon exchanges in the t-channel processes like $\gamma^* + q \rightarrow q + q + \bar{q}$ or $\gamma^* + g \rightarrow g + q + \bar{q}$. However this can only happen if the incoming gluon or quark helicity is not flipped. In the case of polarized scattering the helicity has to flip and the above singular contributions decouple. The above phenomenon is the same as observed in Regge theory where the pomeron can only contribute to unpolarized structure functions but it decouples in $g_1(x, Q^2)$. Another feature is the appearance of the large logarithmic terms $(\ell n^k(1-z)/(1-z))_+$ which show up in the non-singlet coefficient function \bar{C}_q^{NS} . These corrections can be attributed to soft gluon radiation, which however also appears in the unpolarized coefficient function (see chapter 3).

6.4 Results

In this section we will discuss the effect of the $\mathcal{O}(\alpha_s)$ and $\mathcal{O}(\alpha_s^2)$ QCD corrections on the hadronic structure function $g_1(x, Q^2)$ and its first moment which is given by

the Ellis-Jaffe sum rule [1]. In particular we will investigate how the Q^2 -evolution of $g_1(x, Q^2)$ depends on the chosen parton densities of the sea quark and the gluon at some input value $Q^2 = Q_0^2$.

6.4.1 Preliminaries

The n^{th} moment of the polarized structure function $g_1(x, Q^2)$ is defined by the Mellin transformation of (6.2.6).

$$g_1^n(Q^2) = \int_0^1 dx x^{n-1} g_1(x, Q^2) = \frac{1}{2} \left[\frac{5}{18} \left\{ \Sigma^n(M^2) C_q^{S,n}(Q^2/M^2) + G^n(M^2) C_q^{NS,n}(Q^2/M^2) \right\} + \frac{1}{6} \Delta^n(M^2) C_q^{NS,n}(Q^2/M^2) \right], \quad (6.4.1)$$

where the n^{th} moment of the coefficient functions C_i ($i = q, g$) is given by

$$C_i^n(Q^2/M^2) = \int_0^1 dz z^{n-1} C_i(z, Q^2/M^2), \quad (6.4.2)$$

with a similar definition for the moments of the parton densities. For the case of the $\overline{\text{MS}}$ scheme the first ten moments of the coefficient functions \bar{C}_q^{NS} (6A.1), \bar{C}_q^{PS} (6A.4) and \bar{C}_g (6A.5) are presented in tables (6.4.1), (6.4.1) and (6.4.1) respectively.

Analytically they could be expressed in rational numbers and the Riemann zeta function $\zeta(m)$ ($m = 2, 3$). However in order to shorten the expressions, we present the moments numerically, up to seven digits in the tables. Notice that up to finite n , C_i^n can also be calculated by using an alternative method (see [17, 32] and references therein), which provides us with an independent check of our calculation.

The first moments of the coefficient functions and the parton densities determine the size and the Q^2 -evolution of the Ellis-Jaffe sum rule. Starting with the coefficient functions, the first moment of the non-singlet quark coefficient function presented in the $\overline{\text{MS}}$ scheme is equal to

$$\bar{C}_q^{\text{NS},1}(Q^2/M^2) = \int_0^1 dz \bar{C}_q^{\text{NS}}(z, Q^2/M^2) = 1 - \frac{\alpha_s}{4\pi} \{3C_F\} + \left(\frac{\alpha_s}{4\pi}\right)^2 \left\{ \frac{21}{2} C_F^2 + (11L_M - 23)C_A C_F + (-2L_M + 4)n_f C_F \right\}. \quad (6.4.3)$$

Although the first moment of $\bar{C}_q^{\text{NS},1}$ is factorization scheme independent, it still depends on the renormalization choice made for $\alpha_s(\equiv \alpha_s(M^2))$. This is revealed by the logarithmic term $L_M \equiv \ln(Q^2/M^2)$ which carries a factor proportional to β_0 (3.2.28). Notice that we have put the renormalization scale R equal to the mass factorization scale M . Up to $\mathcal{O}(\alpha_s^2)$, $\bar{C}_q^{\text{NS},1}$ equals the first moment of the coefficient

n	C_F^2	$C_A C_F$	$n_f C_f$
1	10.5000	-23.0000	4.0000
2	12.5432	-17.3440	-0.0741
3	15.8800	-3.4943	-5.0567
4	24.5188	11.6410	-9.9443
5	36.1052	27.2034	-14.5485
6	50.7538	42.1577	-18.8566
7	66.9620	56.7369	-22.8925
8	84.7833	70.6212	-26.6862
9	103.4109	84.0411	-30.2660
10	122.9214	96.8539	-33.6563

Table 6.1. The first ten moments of the $\mathcal{O}(\alpha_s^2)$ contributions to the non-singlet polarized coefficient function \bar{C}_q^{NS} (6A.1). The numbers in the table are the coefficients of the $(\alpha_s/4\pi)^2$ terms at $M^2 = Q^2$ ($L_M = 0$).

function $\bar{C}_{3,q}^{\text{NS}}$ in deep inelastic neutrino-hadron scattering, see (5.2.16) in chapter 5 and eq. (13) in [17]. In $\mathcal{O}(\alpha_s^3)$ the coefficient functions \bar{C}_q^{NS} and $\bar{C}_{3,q}^{\text{NS}}$ start to deviate from each other due to the contributions of fermion loops which are proportional to n_f (see the difference between eq. (13) and eq. (19) in [17]). The first moment of the pure singlet coefficient function which is factorization scheme dependent is given by

$$\bar{C}_q^{\text{PS},1}(Q^2/M^2) = \int_0^1 dz \bar{C}_q^{\text{PS}}(z, Q^2/M^2) = n_f C_F T_f \left(\frac{\alpha_s}{4\pi}\right)^2 \left[-12L_M + 16\zeta(3) + \frac{11}{3} \right]. \quad (6.4.4)$$

Contrary to the first moment of the non-singlet coefficient function in (6.4.1) the singlet one receives a scaling-violating part which is due to $\bar{C}_q^{\text{PS},1}$ (6.4.4). It turns out (see the discussion later on) that contrary to the non-log part in (6.4.4), the coefficient of L_M is scheme independent.

Up to $\mathcal{O}(\alpha_s^2)$ the first moment of the gluonic coefficient function is equal to

$$\bar{C}_g^1(Q^2/M^2) = \int_0^1 dz \bar{C}_g(z, Q^2/M^2) = 0 \quad (6.4.5)$$

The vanishing of the first moment of the gluonic coefficient function in the $\overline{\text{MS}}$ scheme has as an important consequence that the first moment of the polarized structure

n	$C_F T_f n_f$
1	22.8996
2	7.7322
3	4.4927
4	3.0901
5	2.2976
6	1.7915
7	1.4441
8	1.1934
9	1.0058
10	0.8612

Table 6.2. The first ten moments of the $\mathcal{O}(\alpha_s^2)$ contributions to the pure singlet polarized coefficient function \bar{C}_q^{PS} (6A.4). The numbers in the table are the coefficients of the $(\alpha_s/4\pi)^2$ terms at $M^2 = Q^2$ ($L_M = 0$).

function does not receive any contribution from the gluon density. Before discussing this let us first present the first moments of the anomalous dimensions of the twist two operators contributing to g_1 . The anomalous dimensions are obtained from the AP splitting functions as follows

$$\gamma_{ij}^n = \sum_{k=0}^{\infty} \left(\frac{\alpha_s}{4\pi} \right)^{k+1} \gamma_{ij}^{(k),n}, \quad (6.4.6a)$$

$$\gamma_{ij}^{(k),n} = - \int_0^1 dz z^{n-1} P_{ij}^{(k)}(z), \quad (6.4.6b)$$

with the results (see (6.3.16)–(6.3.19) and (6.3.22), (6.3.23))

$$\gamma_{qq}^{(0),NS,1} = \gamma_{qq}^{(1),NS,1} = 0, \quad (6.4.7)$$

$$\gamma_{qq}^{(0),S,1} = 0, \quad \gamma_{qq}^{(1),S,1} = 24 C_F T_f, \quad (6.4.8)$$

$$\gamma_{gq}^{(0),1} = -6 C_F, \quad (6.4.9)$$

$$\gamma_{qg}^{(0),1} = \gamma_{qg}^{(1),1} = 0, \quad (6.4.10)$$

$$\gamma_{gg}^{(0),1} = -2\beta_0 = -\left(\frac{22}{3} C_A - \frac{4}{3} n_f \right) \quad (6.4.11)$$

The value of the singlet anomalous dimension $\gamma_{qq}^{(1),S,1}$ was already calculated in [16]. It is due to the axial anomaly which contributes via the triangular fermion loop to

n	$C_F T_f$	$C_A T_f$
1	0.0000	0.0000
2	7.0840	-13.5982
3	2.7478	-15.1280
4	-1.8179	-15.4209
5	-5.4281	-15.3327
6	-8.1651	-15.0791
7	-10.2363	-14.7508
8	-11.8152	-14.3923
9	-13.0291	-14.0267
10	-13.9692	-13.6659

Table 6.3. The first ten moments of the $\mathcal{O}(\alpha_s^2)$ contributions to the *glaue* polarized coefficient function \bar{C}_g (6A.5). The numbers in the table are the coefficients of the $(\alpha_s/4\pi)^2$ terms at $M^2 = Q^2$ ($L_M = 0$).

$\gamma_{qq}^{(1),S,1}$ in second order perturbation theory. The vanishing of $\gamma_{qg}^{(1),1}$ was shown on general grounds in [33], see also [31]. From the last reference we infer (see eq. (22)) that $\gamma_{gg}^{(1),1} = -2\beta_1$ (\overline{MS} scheme, two loop level), although we do not know $\gamma_{gg}^{(1),n}$ for general n yet. Here β_1 stands for the second order coefficient in the β -function, see (3.2.28). The non-vanishing of $\gamma_{qq}^{(1),S,1}$ in the \overline{MS} scheme implies that the conservation of the singlet quark helicity is broken at the two-loop level. The vanishing of \bar{C}_g^1 (see (6.4.5)) has as a consequence that the Ellis-Jaffe sum rule can only be reconciled with experiment by assuming a large negative sea-quark density at a scale $Q_0^2 \sim 10 \text{ GeV}^2$ although this density is supposed to vanish at very small scales according to the constituent quark model. For this reason one prefers a scheme (see e.g. [33, 34]), where the first moment of C_g is negative and $\gamma_{qq}^{(1),S,1} = 0$ which allows for a large positive gluon density and a small sea quark density. In order to increase the use of this chapter we will therefore adopt another scheme which satisfies the properties that $C_g^{(1)} < 0$ and $\gamma_{qq}^{(1),S,1} = 0$. To that purpose we alter Γ_{qg} , which otherwise would be defined according to (3.2.45), in the following way

$$\Gamma_{qg} = \frac{\alpha_s^u}{4\pi} S_\epsilon \left(\frac{M^2}{\mu^2} \right)^{\epsilon/2} \left[\frac{1}{2\epsilon} P_{qg}^{(0)} + \frac{1}{2} f_g^{(1)} \right] + \left(\frac{\alpha_s^u}{4\pi} \right)^2 S_\epsilon^2 \left(\frac{M^2}{\mu^2} \right)^\epsilon \left[\frac{1}{\epsilon^2} \left\{ \frac{1}{4} P_{qg}^{(0)} \right. \right.$$

$$\otimes (P_{gg}^{(0)} + P_{qq}^{(0)}) - \frac{1}{2}\beta_0 P_{qg}^{(0)} \left\} + \frac{1}{\varepsilon} \left\{ \frac{1}{4} P_{qg}^{(1)} + \frac{1}{2} f_g^{(2)} \right\} \right] \quad (6.4.12)$$

The above transition function can be substituted in the mass factorization formulae for $\hat{g}_{1,i}$, $i = q, g$ (which are similar to (3.2.37)-(3.2.38)). This implies that the following coefficient functions are altered with respect to the ones presented in the \overline{MS} scheme in the last section.

$$C_q^{PS} = n_f \left(\frac{\alpha_s}{4\pi} \right)^2 \left[\left\{ \frac{1}{4} P_{qg}^{(0)} \otimes P_{gq}^{(0)} \right\} L_M^2 + \left\{ \frac{1}{2} P_{qq}^{(1),PS} + \frac{1}{2} P_{gq}^{(0)} \otimes (\bar{c}_g^{(1)} - f_g^{(1)}) \right\} L_M + \bar{c}_q^{(2),PS} \right] \quad (6.4.13)$$

$$C_g' = n_f \frac{c_s}{4\pi} \left[\frac{1}{2} P_{qg}^{(0)} L_M + \bar{c}_g^{(1)} - f_g^{(1)} \right] + n_f \left(\frac{\alpha_s}{4\pi} \right)^2 \left[\left\{ \frac{1}{8} P_{qg}^{(0)} \otimes (P_{gg}^{(0)} + P_{qq}^{(0)}) - \frac{1}{4} \beta_0 P_{qg}^{(0)} \right\} L_M^2 + \left\{ \frac{1}{2} P_{qg}^{(1)} - \beta_0 (\bar{c}_g^{(1)} - f_g^{(1)}) + \frac{1}{2} P_{gg}^{(0)} \otimes (\bar{c}_g^{(1)} - f_g^{(1)}) + \frac{1}{2} P_{qg}^{(0)} \otimes \bar{c}_q^{(1)} - \frac{1}{2} P_{qq}^{(0)} \otimes f_g^{(1)} \right\} L_M + \bar{c}_g^{(2)} - \bar{c}_q^{(1)} \otimes f_g^{(1)} \right] \quad (6.4.14)$$

where $P_{ij}^{(1)'} denote the AP splitting functions in the primed scheme. Because the parton structure functions $\hat{g}_{1,i}$ ($i = q, g$) are scheme independent, we have the additional constraints that $f_g^{(2)}$ in (6.4.12) has to be equal to$

$$f_g^{(2)} = P_{gg}^{(0)} \otimes f_g^{(1)} \quad (6.4.15)$$

and the transition function Γ_{qq}^{PS} in (3.2.44) has to be equal to

$$\Gamma_{qq}^{PS} = \left(\frac{\alpha_s}{4\pi} \right)^2 S_\epsilon^2 \left(\frac{M^2}{\mu^2} \right)^\epsilon \left[\frac{1}{\varepsilon^2} \left\{ \frac{1}{4} P_{qg}^{(0)} \otimes P_{gq}^{(0)} \right\} + \frac{1}{\varepsilon} \left\{ \frac{1}{4} P_{qq}^{(1),PS} + \frac{1}{2} P_{gq}^{(0)} \otimes f_g^{(1)} \right\} \right] \quad (6.4.16)$$

The new splitting functions in the primed scheme become

$$P_{qq}^{(1),PS} = P_{qq}^{(1),PS} + P_{gq}^{(0)} \otimes f_g^{(1)} \quad (6.4.17)$$

$$P_{qg}^{(1)} = P_{qg}^{(1)} - 2\beta_0 f_g^{(1)} + P_{gg}^{(0)} \otimes f_g^{(1)} \quad (6.4.18)$$

Taking the first moment the anomalous dimensions read

$$\gamma_{qq}^{(1),S,1} = 24C_F T_f - 6C_F f_g^{(1),1} \quad (6.4.19)$$

$$\gamma_{qg}^{(1),1} = 0 \quad (6.4.20)$$

The singlet anomalous dimension in (6.4.19) vanishes when

$$f_g^{(1),1} = 4T_f \quad (6.4.21)$$

and the one in (6.4.20) remains zero irrespective of the scheme chosen. Substituting the splitting function in (6.4.17) and (6.4.18) into expressions (6.4.13) and (6.4.14) we obtain

$$C_q^{\text{PS}} = \bar{C}_q^{\text{PS}} , \quad (6.4.22)$$

$$C_g' = \bar{C}_g - n_f \frac{\alpha_s}{4\pi} \left[f_g^{(1)} \right] - n_f \left(\frac{\alpha_s}{4\pi} \right)^2 \left[\left\{ \frac{1}{2} P_{qq}^{(0)} \otimes f_g^{(1)} \right\} L_M + \bar{c}_q^{(1)} \otimes f_g^{(1)} \right] . \quad (6.4.23)$$

We see that C_q^{PS} is the same in the $\overline{\text{MS}}$ and the primed scheme. This does not mean that C_q^{PS} is scheme independent. One can show that another choice for the non-pole part of the transition function Γ_{gq} in (3.2.46) will lead to a different expression for C_q^{PS} . However if one takes the first moment it turns out that the coefficient of L_M which equals $-12n_f C_F T_f$ (6.4.4) is scheme independent. The gluonic coefficient function changes in such a way that one gets a negative contribution to the Ellis-Jaffe sum rule (6.4.1), provided the first moment of the polarized gluon density is positive. Taking the first moment of C_g' and imposing the condition (6.4.21) we get with $\bar{c}_q^{(1),1} = -3C_F$ (see (6A.1) and $T_f = 1/2$).

$$C_g'^{1,1}(Q^2/M^2) = -n_f \frac{\alpha_s}{4\pi} [2] + n_f C_F \left(\frac{\alpha_s}{4\pi} \right)^2 [6C_F] . \quad (6.4.24)$$

At $M^2 = Q^2 = 10 \text{ GeV}^2$, the $\mathcal{O}(\alpha_s^2)$ correction in (6.4.24) changes the lowest order value for $C_g'^1$ by about 14%, which means that in the case of a positive gluon density the Ellis-Jaffe sum rule will be slightly modified by including higher order corrections. Summarizing the above, we have seen that in a scheme where $f_g^{(1),1} \neq 1$ (6.4.12), the first moment of the gluonic coefficient function C_g gets a non-zero contribution and the singlet anomalous dimension γ_{qq}^S changes with respect to the one presented in the $\overline{\text{MS}}$ scheme. Furthermore it appears that the coefficient of L_M in the first moment of C_q^{PS} (6.4.13) is scheme independent. The non-vanishing of $C_g'^1$ allows for the contribution of a large positive polarized gluon density to the Ellis-Jaffe sum rule. In the special case that $f_g^{(1),1} = 4T_f$ (6.4.21) the singlet anomalous dimension $\gamma_{qq}^{S,(1)} = 0$, so that up to two-loop level the singlet quark helicity is conserved. Here we want to emphasize that a non-zero contribution to C_g' (6.4.23) and the vanishing of $\gamma_{qq}^{1,(1),S,1}$ (6.4.19) are unrelated. One can still choose a scheme where the first moments of γ_{qq}^S and C_g are both non-vanishing.

As has already been mentioned above, a different choice of scheme for the coefficient functions leads to a different parametrization of the parton densities. For

instance in the $\overline{\text{MS}}$ scheme where $C_g^1 = 0$ one has to choose a large negative sea-quark density to reconcile the first moment of g_1 with the data. On the other hand if one chooses a scheme where $C_g^1 \neq 0$, one can allow for a large positive gluon density. In the literature the x -dependence of the parton densities is determined in such a way that the first moment of g_1 agrees with the data at an average value for $Q^2 = Q_0^2 = 10 \text{ GeV}^2$. A large negative sea quark density as well as a large positive gluon density give an equally good description of the first moment of $g_1(x, Q^2)$ at $Q^2 = Q_0^2 = 10 \text{ GeV}^2$ depending on the chosen scheme. However the above findings do not imply that these parton densities lead to the same result for the higher moments of the structure function or that the Q^2 -evolution of $g_1(x, Q^2)$ does not depend on them. On the contrary, as we will illustrate below, the negative sea quark and positive gluon densities which are proposed in the literature lead to a different Q^2 -evolution of the polarized structure function, which is of course unsatisfactory. Only when more accurate data become available, which allows us to distinguish between $g_1(x, Q^2)$ taken at different Q^2 values, we are able to determine the shape of the parton densities with much higher accuracy at different scales and x -values.

6.4.2 Plots of $G_1(x, Q^2)$

Before presenting our results we would like to emphasize that a complete next-to-next-to-leading (NNLO) order analysis is not possible, since the three loop contributions to the polarized AP splitting functions have not been calculated yet. Even the two loop contributions $P_{qq}^{(1)}$ and $P_{gg}^{(1)}$ are not known and $P_{qq}^{(1), \text{PS}}$ (6.3.22), $P_{gg}^{(1)}$ (6.3.23) are presented in this chapter for the first time. In the literature the parton densities satisfying the Ellis-Jaffe sum rule are scale independent and supposed to hold for $M^2 = 10 \text{ GeV}^2$. This value is chosen because it represents the average Q^2 at which the SLAC-EMC data are taken. If the scale variation is not too large, we can compute $g_1(x, Q^2)$ in (6.2.6) for values of Q^2 which do not deviate too much from $M^2 = 10 \text{ GeV}^2$. In this case M^2 is kept fixed at 10 GeV^2 , while the Q^2 dependence is only carried by the coefficient functions C_i ($i = q, g$) and not by the parton densities as is usually the case when $M^2 = Q^2$. This fixed order perturbation theory is correct as long as $\alpha_s(M^2) \ln(Q^2/M^2) \ll 1$. This condition is satisfied if $Q^2/M^2 < 100 \text{ GeV}^2$. When $Q^2 \gg M^2$ the logarithmic terms have to be resummed via renormalization group methods. We have tested this approach for the unpolarized structure function $F_2(x, Q^2)$ for which at least the next-to-leading order (NLO) result is completely known. Since we want to compare the Q^2 -evolution of $F_2(x, Q^2)$ with that of $g_1(x, Q^2)$, it is important to note that $F_2(x, Q^2)$ is given by an expression which has the same

form as the one presented for $g_1(x, Q^2)$ in (6.2.6), except that the coefficient functions and the parton densities take their unpolarized representation. In the plots discussed below, the unpolarized and polarized structure functions are computed using the two-loop corrected running coupling constant with four active flavours ($n_f = 4$). The same n_f is also chosen in the coefficient functions. Furthermore for the unpolarized structure function $F_2(x, Q^2)$ we have chosen the set of parton densities in [35] which are parametrized in the $\overline{\text{MS}}$ scheme. The set of the polarized parton densities will be presented after we have discussed fixed order perturbation theory for $F_2(x, Q^2)$.

In fig. 6.1 we have compared $F_2^{(1)}(x, Q^2)$ for $M^2 = 10, 50, 100$ GeV² with $F_2^{(1)}(x, Q^2)$ for $M^2 = Q^2 = 10, 50, 100$ GeV². Here $F_2^{(1)}(x, Q^2)$ is computed by using the $\mathcal{O}(\alpha_s)$ corrected coefficient functions $\bar{C}_{2,i}$ ($\overline{\text{MS}}$ scheme, $i = q, g$) and the leading log (LL) parametrization of the parton densities in [35] ($\Lambda = 0.144$ GeV, $n_f = 4$, table II3-FIT-SL). The $\mathcal{O}(\alpha_s)$ corrected coefficients $\bar{C}_{2,i}$ contain the logarithmic term $L_M \equiv \ln(Q^2/M^2)$ and the non-log term $\bar{c}_{2,i}^{(1)}$ (the same as in (3.2.49) and (3.2.54)). In the case $M^2 = Q^2$ the L_M appearing in $\bar{C}_{2,i}$ equals zero and the Q^2 -evolution of $F_2^{(1)}(x, Q^2)$ proceeds via the parton densities where all leading logs are resummed. In fixed order perturbation theory, where M^2 is kept fixed, the Q^2 -evolution of $F_2^{(1)}(x, Q^2)$ proceeds via the term L_M which appears in the coefficient function $\bar{C}_{2,i}$. Fig. 6.1 reveals that the difference between these two evolutions is quite small as long as $Q^2 \leq 100$ GeV².

In fig. 6.2 we have made the same comparison for $F_2^{(2)}(x, Q^2)$, where now we have combined the $\mathcal{O}(\alpha_s^2)$ corrected coefficient function $\bar{C}_{2,i}$ ($\overline{\text{MS}}$ scheme, $i = q, g$, see chapter 3) with the next-to-leading log (NLL) parton densities given by the MTB1 set [35] ($\Lambda = 0.194$ GeV, $n_f = 4$, table I4-FIT-B1-MS). In the case M^2 is fixed, the Q^2 -evolution proceeds via the terms L_M occurring in $\bar{C}_{2,i}$, which is an improvement with respect to the single logarithmic approximation presented above. When we get $M^2 = Q^2$, the L_M -terms occurring in the coefficient functions vanishes and the Q^2 -evolution is taken over by the NLL parton densities where now the leading as well as the next-to-leading logs are resummed in all orders of perturbation theory. We see that fig. 6.2 shows a slight improvement with respect to fig. 6.1 in particular for $Q^2 = 100$ GeV². The curves for $M^2 = Q^2$ lie always above the ones obtained from fixed order perturbation theory. However the differences are so small ($< 1.5\%$) that they cannot be observed in view of the accuracy reached in experiments on unpolarized as well as polarized lepton-hadron scattering.

After having discussed the validity of fixed order perturbation theory we will present our results for the polarized structure function $g_1(x, Q^2)$. The polarized

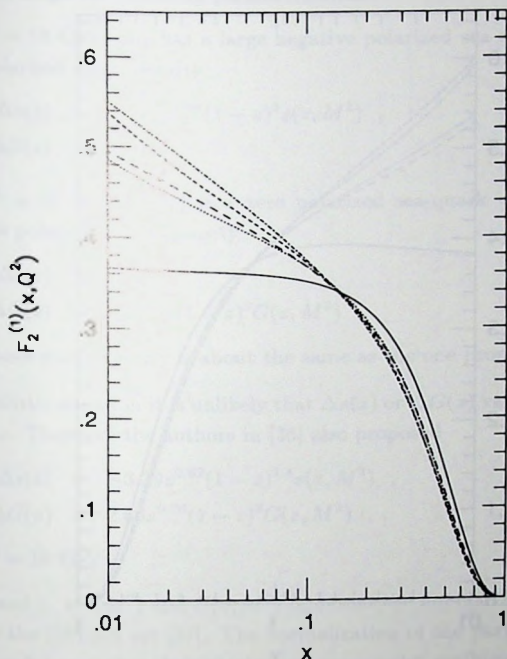


Fig. 6.1. The unpolarized structure function $F_2^{(1)}(x, Q^2)$. The LL parametrization is chosen for the parton densities and the coefficient functions are corrected up to $\mathcal{O}(\alpha_s)$.

Solid line: $M^2 = Q^2 = 10 \text{ GeV}^2$; dotted line: $M^2 = Q^2 = 50 \text{ GeV}^2$; long-dashed line: $M^2 = 10 \text{ GeV}^2$, $Q^2 = 50 \text{ GeV}^2$; short-dashed line: $M^2 = Q^2 = 100 \text{ GeV}^2$; dashed dotted line: $M^2 = 10 \text{ GeV}^2$, $Q^2 = 100 \text{ GeV}^2$.

parton densities are taken from [36]. These densities are given by

$$\Delta u_V(z) = \alpha(z) u_V(z, M^2) \quad , \quad \Delta d_V(z) = \beta(z) d_V(z, M^2) \quad , \quad (6.4.25)$$

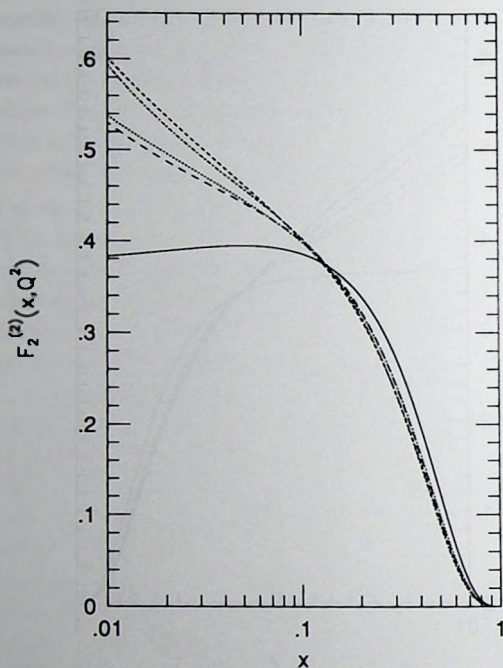


Fig. 6.2. The unpolarized structure function $F_2^{(2)}(x, Q^2)$. The NLL parametrization is chosen for the parton densities and the coefficient functions are corrected up to $\mathcal{O}(\alpha_s^2)$. The meaning of the curves is the same as in fig. 6.1.

with

$$\alpha(z) = z^{0.287}, \quad \beta(z) = \left(\frac{z - z_0}{1 - z_0} \right) z^p, \quad (6.4.26)$$

where we have chosen $z_0 = 0.75$ and $p = 0.76$. The $u_V(z, M^2)$ and $d_V(z, M^2)$ are the unpolarized parton densities given by the DFLM4 set ($\Lambda = 0.2$ GeV) at $M^2 = 10$ GeV² [37]. The sea and gluon parton densities are chosen in such a way that the

experimental result for the Ellis-Jaffe sum rule is reproduced up to $\mathcal{O}(\alpha_s)$. According to [36] we can adopt the following parametrizations

- a. At $M^2 = 10 \text{ GeV}^2$ one has a large negative polarized sea-quark density and a zero polarized gluon density

$$\Delta s(z) = -11.8z^{0.94}(1-z)^5 s(z, M^2), \quad (6.4.27)$$

$$\Delta G(z) = 0, \quad (6.4.28)$$

- b. At $M^2 = 10 \text{ GeV}^2$ one has a zero polarized sea-quark density and a large positive polarized gluon density

$$\Delta s(z) = 0, \quad (6.4.29)$$

$$\Delta G(z) = 6.0z^{0.76}(1-z)^3 G(z, M^2). \quad (6.4.30)$$

The above gluon density is about the same as the one proposed in [38].

- c. In a realistic situation it is unlikely that $\Delta s(z)$ or $\Delta G(z)$ vanishes at some scale for all z . Therefore the authors in [36] also proposed

$$\Delta s(z) = -3.39z^{0.62}(1-z)^{1.4} s(z, M^2), \quad (6.4.31)$$

$$\Delta G(z) = 2.69z^{0.76}(1-z)^3 G(z, M^2), \quad (6.4.32)$$

for $M^2 = 10 \text{ GeV}^2$

In a., b. and c. $s(z, M^2)$ and $G(z, M^2)$ represent the unpolarized parton densities belonging to the DFLM4 set [37]. The normalization of the parton densities above is chosen in such a way that their singlet and non-singlet combinations in (6.2.6) are equal to

$$\Sigma(z) = \Delta u_V(z) + \Delta d_V(z) + 3\Delta s(z), \quad (6.4.33)$$

$$\Delta(z) = \Delta u_V(z) - \Delta d_V(z) - \Delta s(z), \quad (6.4.34)$$

Notice that the charm density has been neglected although we assume that (massless) charm quarks are produced in the final state so that n_f in the running coupling constant and the coefficient functions is put equal to 4. In case a. the value of the gluon coefficient function is irrelevant since it is multiplied by a zero parton density. However in b. and c. we have to choose a gluon coefficient function of which the first moment is non-vanishing. We adopt the factorization scheme in eq. (2) of [36] which is equivalent to the following choice of $f_g^{(1)}$ in (6.4.12)

$$f_g^{(1)}(z) = 4T_f [(2z-1)(a-1) + 2(1-z)], \quad (6.4.35)$$

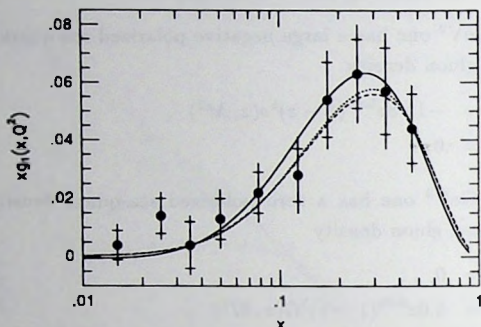


Fig. 6.3. The $\mathcal{O}(\alpha_s^k)$ corrected polarized structure function denoted by $xg_1^{(k)}(x, Q^2)$. Parton densities given by set a (6.4.27), (6.4.28). $M^2 = Q^2 = 10 \text{ GeV}^2$.

Solid line: $xg_1^{(0)}(x, Q^2)$; dotted line $xg_1^{(1)}(x, Q^2)$; short-dashed line: $xg_1^{(2)}(x, Q^2)$.

where a can be arbitrarily chosen. Here we will take $a = 2$ (see [36]). The above choice leads to the results presented in (6.4.19) and (6.4.20), which are independent of a . From $P_{qq}^{(0)}$ (6.3.16) and $\bar{e}_q^{(1)}$ (6A.1) we infer the $\mathcal{O}(\alpha_s^2)$ coefficients of C'_g in (6.4.23).

$$\begin{aligned} \frac{1}{2} P_{qq}^{(0)} \otimes f_g^{(1)} = & 8C_F T_f \left[(a-1) \left\{ (2z-1) (2\ell n(1-z) - \ell n z) + \frac{3}{2} \right\} \right. \\ & \left. + (1-z) (4\ell n(1-z) - 2\ell n z - 1) \right], \end{aligned} \quad (6.4.36)$$

and

$$\begin{aligned} \bar{e}_q^{(1)} \otimes f_g^{(1)} = & 4C_F T_f \left[(a-1) \left\{ (2z-1) (2Li_2(1-z) - 4\zeta(2) - 2\ell n z \ell n(1-z) \right. \right. \\ & + 2\ell n^2(1-z) + \ell n^2 z) + 3(3-4z)\ell n(1-z) - (3-8z)\ell n z + 5 - 14z \} \\ & + (1-z) (4Li_2(1-z) - 8\zeta(2) - 4\ell n z \ell n(1-z) + 4\ell n^2(1-z) + 2\ell n^2 z \\ & \left. \left. - 14\ell n(1-z) - 12) + (2-10z)\ell n z \right\} \right]. \end{aligned} \quad (6.4.37)$$

Using the above parton densities one can now determine $g_1(x, Q^2)$ in (6.2.6) by using

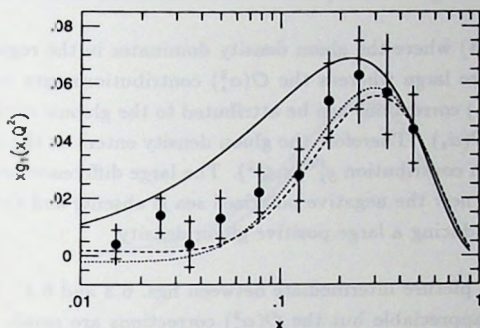


Fig. 6.4. The same as in fig. 6.3, but now for set b (6.4.29), (6.4.30).

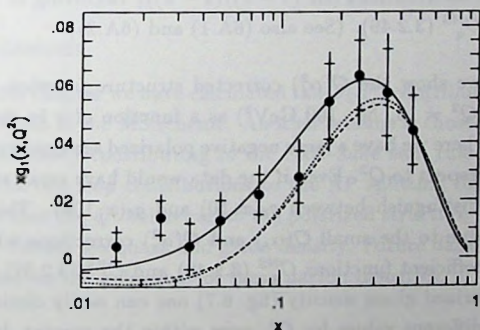


Fig. 6.5. The same as in fig. 6.3, but now for set c (6.4.31), (6.4.32).

fixed order perturbation theory. In figs. 6.3, 6.4, 6.5 we present $g_1(x, Q^2)$ by giving $xg_1^{(k)}(x, Q^2)$ for $Q^2 = M^2 = 10 \text{ GeV}^2$ and $0.01 < x < 1$. Here $g_1^{(k)}(x, Q^2)$ stands for the $\mathcal{O}(\alpha_s^k)$ corrected structure function which means that the coefficient functions are included up to $\mathcal{O}(\alpha_s^k)$.

In case a (fig. 6.3) we observe that the $\mathcal{O}(\alpha_s)$ corrections are small and the $\mathcal{O}(\alpha_s^2)$

contributions are unobservable. Therefore the large negative polarized sea quark density already gives a good description of the data on the Born level.

In case b (fig. 6.4) where the gluon density dominates in the region $x < 0.2$, the $\mathcal{O}(\alpha_s)$ corrections are large whereas the $\mathcal{O}(\alpha_s^2)$ contributions turn out to be small. The size of the $\mathcal{O}(\alpha_s)$ corrections can be attributed to the gluonic coefficient function C_g which starts at $\mathcal{O}(\alpha_s)$. Therefore the gluon density enters on the $\mathcal{O}(\alpha_s)$ level and is absent in the Born contribution $g_1^{(0)}(x, Q^2)$. The large difference between the Born contribution (where now the negative polarized sea is absent) and the data can only be removed by introducing a large positive gluon density.

Fig. 6.5 shows a picture intermediate between figs. 6.3 and 6.4. The $\mathcal{O}(\alpha_s)$ contributions are still appreciable but the $\mathcal{O}(\alpha_s^2)$ corrections are small. Notice that in all figures for $x > 0.2$ the structure function is dominated by the valence quarks, whereas at small x ($x < 0.2$) either the sea- (fig. 6.3) or the gluon (fig. 6.4) contribution dominates. In the small x -regions all corrections are negative whereas at large x ($x \leq 1$) the corrections are positive which is due to soft gluon radiation. The latter reveals itself via the distributions $(\ell n^k(1-z)/(1-z))_+$ occurring in the non-singlet coefficient function C_q^{NS} (3.2.49). (See also (6A.1) and (6A.2)).

In figs. 6.6–6.8 we show the $\mathcal{O}(\alpha_s^2)$ corrected structure function $xg_1^{(2)}(x, Q^2)$ at three values of Q^2 ($Q^2 = 10, 50, 100 \text{ GeV}^2$) as a function of x in the range $0.01 < x < 1.0$. In fig. 6.6 where we have a large negative polarized sea density there is hardly any variation with respect to Q^2 . Even if the data would have small statistical errors there is no way to distinguish between $g_1(x, 10)$ and $g_1(x, 100)$. This is, as we can infer from fig. 6.3, due to the small $\mathcal{O}(\alpha_s)$ and $\mathcal{O}(\alpha_s^2)$ corrections which are wholly due to the quark coefficient functions C_q^{NS} (3.2.49) and C_q^{PS} (3.2.52). In the case of a large positive polarized gluon density (fig. 6.7) one can easily distinguish between $g_1(x, Q^2)$ taken at different values for Q^2 , even within the current data. Besides to the gluon density this effect can also be attributed to the gluonic coefficient function C_g (3.2.54), which gives a noticeable contribution in particular in $\mathcal{O}(\alpha_s)$. From the above we can conclude that using the parametrization for the parton densities presented in [36], the Q^2 -dependence of $g_1(x, Q^2)$ is much more sensitive to the gluon density than to the sea-quark density. Therefore in order to get the same result for $g_1(x, Q^2)$ at $Q^2 > 10 \text{ GeV}^2$ one has to modify these parton densities in such a way that the scheme independence of the polarized structure function will be ensured. This program can only be carried out when more accurate data become available.

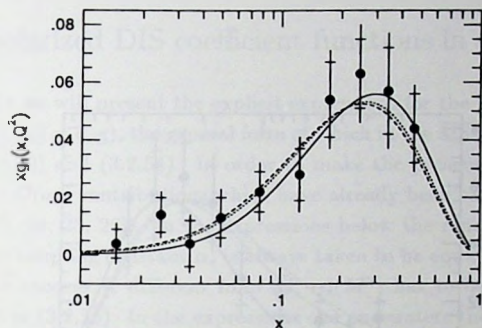


Fig. 6.6. The Q^2 dependence of the $\mathcal{O}(\alpha_s^2)$ corrected polarized structure function denoted by $xg_1^{(2)}(x, Q^2)$. Parton densities given by set a (6.4.27), (6.4.28). $M^2 = 10 \text{ GeV}^2$.

Solid line: $Q^2 = 10 \text{ GeV}^2$; dotted line: $Q^2 = 50 \text{ GeV}^2$; short-dashed line: $Q^2 = 100 \text{ GeV}^2$. The data are obtained from [3].

6.4.3 Conclusions

Summarizing this chapter we have calculated the $\mathcal{O}(\alpha_s^2)$ contributions to the polarized coefficient functions in the $\overline{\text{MS}}$ scheme. Another scheme is chosen to allow for a large polarized gluon density contributing to the Ellis-Jaffe sum rule. As a byproduct we also obtained the two loop contributions to the AP splitting functions P_{qq}^S and P_{qg} . We have shown that the Q^2 behaviour of the polarized structure function appreciably depends on the chosen sea quark and gluon density. Future data will provide us with more information on the behaviour of these parton densities.

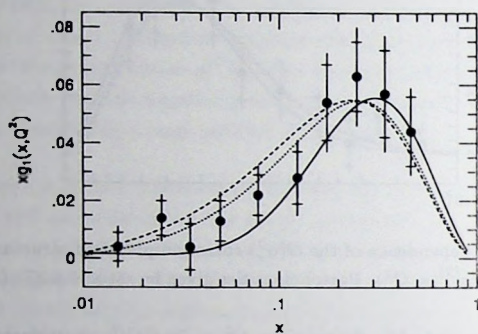


Fig. 6.7. The same as in fig. 6.5, but now for set b (6.4.29), (6.4.30).

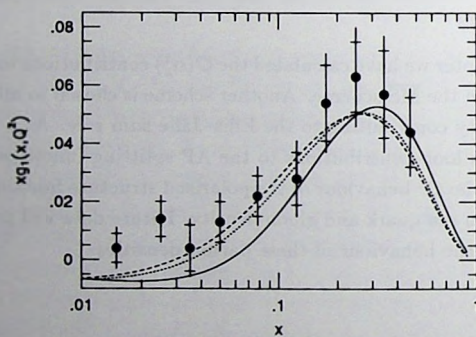


Fig. 6.8. The same as in fig. 6.5, but now for set c (6.4.31), (6.4.32).

Appendix

6A The polarized DIS coefficient functions in the $\overline{\text{MS}}$ scheme

In this appendix we will present the explicit expressions for the polarized DIS coefficient functions \bar{C}_i ($i = q, g$), the general form of which in the $\overline{\text{MS}}$ scheme can be found in (3.2.49), (3.2.52) and (3.2.54). In order to make the presentation self-contained we also give the $\mathcal{O}(\alpha_s)$ contributions which have already been calculated in the literature [see 19, 23, 24, 25, 26]). In the expressions below the renormalization scale R appearing in the coupling constant α_s is always taken to be equal to the factorization scale M . If one chooses R different from M , $\alpha_s(M^2)$ has to be replaced following the prescription in (3.2.56). In the expressions one encounters the mass factorization parts represented by $L_M = \ell n(Q^2/M^2)$ and the polylogarithms $Li_n(z)$, $S_{n,p}(z)$ [39] characteristic for higher order radiative corrections.

Up to $\mathcal{O}(\alpha_s^2)$ the non-singlet coefficient function is given by

$$\begin{aligned}
 C_q^{\text{NS}} = & \delta(1-z) + \frac{\alpha_s}{4\pi} \left[C_F \left\{ 4 \left(\frac{1}{1-z} \right)_+ - 2(1+z) + 3\delta(1-z) \right\} L_M \right. \\
 & + C_F \left\{ 4 \left(\frac{\ell n(1-z)}{1-z} \right)_+ - 3 \left(\frac{1}{1-z} \right)_+ - 2(1+z)\ell n(1-z) \right. \\
 & \left. \left. - 2 \frac{1+z^2}{1-z} \ell n z + 4 + 2z + \delta(1-z)(-4\zeta(2) - 9) \right\} \right] \\
 & + \left(\frac{\alpha_s}{4\pi} \right)^2 \left[\left\{ C_F^2 \left(16 \left(\frac{\ell n(1-z)}{1-z} \right)_+ + 12 \left(\frac{1}{1-z} \right)_+ \right. \right. \right. \\
 & \left. \left. - 8(1+z)\ell n(1-z) - 4 \frac{1+z^2}{1-z} \ell n z + 2(1+z)\ell n z - 2(5+z) \right. \right. \\
 & \left. \left. + \left\{ -8\zeta(2) + \frac{9}{2} \right\} \delta(1-z) \right\} \right. \\
 & + C_A C_F \left(-\frac{22}{3} \left(\frac{1}{1-z} \right)_+ + \frac{11}{3}(1+z) - \frac{11}{2}\delta(1-z) \right) \\
 & + n_f C_F \left(\frac{4}{3} \left(\frac{1}{1-z} \right)_+ - \frac{2}{3}(1+z) + \delta(1-z) \right) \left. \right\} L_M^2 \\
 & + \left\{ C_F^2 \left(24 \left(\frac{\ell n^2(1-z)}{1-z} \right)_+ - 12 \left(\frac{\ell n(1-z)}{1-z} \right)_+ - (32\zeta(2) \right. \right. \\
 & \left. \left. + 45) \left(\frac{1}{1-z} \right)_+ + \frac{1+z^2}{1-z} (4\ell n^2 z - 24\ell n z \ell n(1-z) - 6\ell n z) \right. \right. \\
 & \left. \left. + \frac{1+z^2}{1+z} (4\ell n^2 z - 16Li_2(-z) - 16\ell n z \ell n(1+z)) \right. \right.
 \end{aligned}$$

$$\begin{aligned}
& -8\zeta(2)) + (1+z) \left(4Li_2(1-z) + 4\ell n \, z \ell n(1-z) - 12\ell n^2(1-z) \right. \\
& - 4\ell n^2 z + 16\zeta(2)) + 8(1+2z)\ell n(1-z) - 2(1+9z)\ell n \, z \\
& + 2(16+11z) + \left\{ 40\zeta(3) - 12\zeta(2) - \frac{51}{2} \right\} \delta(1-z) \Big) \\
& + C_A C_F \left(-\frac{44}{3} \left(\frac{\ell n(1-z)}{1-z} \right)_+ + \left(\frac{367}{9} - 8\zeta(2) \right) \left(\frac{1}{1-z} \right)_+ \right. \\
& + \frac{1+z^2}{1-z} \left(\frac{44}{3} \ell n \, z + 2\ell n^2 z \right) + \frac{1+z^2}{1+z} \left(8Li_2(-z) - 2\ell n^2 z \right. \\
& + 8\ell n \, z \ell n(1+z) + 4\zeta(2)) + (1+z) \left(\frac{22}{3} \ell n(1-z) + 4\zeta(2) \right) \\
& - \frac{1}{9} (98 + 368z) + \left(-12\zeta(3) + \frac{88}{3} \zeta(2) + \frac{215}{6} \right) \delta(1-z) \Big) \\
& + n_f C_F \left(\frac{8}{3} \left(\frac{\ell n(1-z)}{1-z} \right)_+ - \frac{58}{9} \left(\frac{1}{1-z} \right)_+ - \frac{8}{3} \frac{1+z^2}{1-z} \ell r_5 \right. \\
& - \frac{4}{3} (1+z)\ell n(1-z) + \frac{1}{9} (20 + 56z) + \left(-\frac{16}{3} \zeta(2) - \frac{19}{3} \right) \delta(1-z) \Big) \Big\} L_M \\
& + \left[\bar{c}_q^{(2),NS,+} + \bar{c}_q^{(2),NS,-} \right] , \tag{6A.1}
\end{aligned}$$

where

$$\begin{aligned}
\bar{c}_q^{(2),NS,+} = & C_F^2 \left[8 \left(\frac{\ell n^3(1-z)}{1-z} \right)_+ - 18 \left(\frac{\ell n^2(1-z)}{1-z} \right)_+ \right. \\
& - (32\zeta(2) + 27) \left(\frac{\ell n(1-z)}{1-z} \right)_+ + \left(-8\zeta(3) + 36\zeta(2) + \frac{51}{2} \right) \left(\frac{1}{1-z} \right)_+ \\
& + \frac{1+z^2}{1-z} \left(-12S_{1,2}(1-z) + 12Li_3(1-z) + 48Li_3(-z) + 36\zeta(3) \right. \\
& - 6Li_2(1-z) - 24\ell n \, z \, Li_2(-z) + 24\zeta(2)\ell n \, z - 4\ell n(1-z)Li_2(1-z) \\
& + 12\ell n^2 z \ell n(1-z) - 14\ell n z \ell n^2(1-z) - \frac{4}{3} \ell n^3 z - \frac{3}{2} \ell n^2 z \\
& + 12\ell n \, z \ell n(1-z) + \frac{61}{2} \ell n \, z) + (1+z) \left(-4Li_3(1-z) \right. \\
& + 4\ell n(1-z)Li_2(1-z) - 4\ell n^3(1-z) - 4\ell n \, z \, Li_2(1-z) - 4\zeta(2)\ell n \, z \\
& + 2\ell n \, z \ell n^2(1-z) - 4\ell n^2 z \ell n(1-z) + \frac{5}{3} \ell n^3 z + 4\zeta(3)) + (1-z) \left(\right. \\
& \left. 8S_{1,2}(1-z) - 16Li_3(-z) + 8\ell n \, z \, Li_2(-z) \right) - 8(1+z+z^2+z^{-1}) \left(Li_2(-z) \right.
\end{aligned}$$

$$\begin{aligned}
& + \ell n z \ell n(1+z)) - 2(5+13z)Li_2(1-z) - 4(7+2z^2+7z)\zeta(2) \\
& + 2(5+7z)\ell n^2(1-z) + 8(1+3z)\zeta(2)\ell n(1-z) + 2(5+3z)\ell n(1-z) \\
& + \left(\frac{29}{2} + 4z^2 + \frac{41}{2}z \right) \ell n^2 z - 16(1+2z)\ell n z \ell n(1-z) + \frac{3}{2}(3-z)\ell n z \\
& - 41 - 10z + \delta(1-z) \left(6\zeta(2)^2 - 78\zeta(3) + 69\zeta(2) + \frac{331}{8} \right) \Big] \\
& + C_A C_F \left[-\frac{22}{3} \left(\frac{\ell n^2(1-z)}{1-z} \right)_+ + (-8\zeta(2) + \frac{367}{9}) \left(\frac{\ell n(1-z)}{1-z} \right)_+ \right. \\
& + \left(40\zeta(3) + \frac{44}{3}\zeta(2) - \frac{3155}{54} \right) \left(\frac{1}{1-z} \right)_+ + \frac{1+z^2}{1-z} (12S_{1,2}(1-z) \\
& - 12Li_3(1-z) - 24Li_3(-z) - 18\zeta(3) + \frac{22}{3}Li_2(1-z) + 12\ell n z Li_2(-z) \\
& + 4\ell n(1-z)Li_2(1-z) + 4\ell n z Li_2(1-z) + 2\ell n^2 z \ell n(1-z) \\
& + \frac{44}{3}\ell n z \ell n(1-z) - \ell n^3 z - \frac{55}{6}\ell n^2 z - \frac{239}{6}\ell n z) + (1+z)(4Li_2(1-z) \\
& + \frac{11}{3}\ell n^2(1-z) + 4\ell n z \ell n(1-z) - 20\zeta(3)) + (1-z)(-4S_{1,2}(1-z) \\
& + 8Li_3(-z) - 4\ell n z Li_2(-z)) + \left(8\zeta(2) - \frac{134}{9} - \frac{314}{9}z \right) \ell n(1-z) \\
& + 4(1+z+z^2+z^{-1})(Li_2(-z) + \ell n z \ell n(1+z)) + \frac{4}{3}\zeta(2)(3z^2-4z-4) \\
& - 2(2+z^2+2z)\ell n^2 z + \frac{1}{6}(157z-47)\ell n z + \frac{5}{27}(145+364z) \\
& + \delta(1-z) \left(\frac{71}{5}\zeta(2)^2 + \frac{140}{3}\zeta(3) - \frac{251}{3}\zeta(2) - 5465/72 \right) \Big] \\
& + n_f C_F \left[\frac{4}{3} \left(\frac{\ell n^2(1-z)}{1-z} \right)_+ - \frac{58}{9} \left(\frac{\ell n(1-z)}{1-z} \right)_+ \right. \\
& + \left(-\frac{8}{3}\zeta(2) + \frac{247}{27} \right) \left(\frac{1}{1-z} \right)_+ + \frac{1+z^2}{1-z} \left(-\frac{4}{3}Li_2(1-z) - \frac{8}{3}\ell n z \ell n(1-z) \right. \\
& + \frac{5}{3}\ell n^2 z + \frac{19}{3}\ell n z) + (1+z) \left(\frac{4}{3}\zeta(2) - \frac{2}{3}\ell n^2(1-z) \right) + \frac{4}{9}(5+14z)\ell n(1-z) \\
& + \frac{1}{3}(1+11z)\ell n z - \frac{2}{27}(58+151z) + \delta(1-z) \left(\frac{4}{3}\zeta(3) + \frac{38}{3}\zeta(2) \right. \\
& \left. \left. + \frac{457}{36} \right) \right] , \tag{6A.2}
\end{aligned}$$

and

$$\begin{aligned}
\bar{c}_q^{(2),NS,-} = & (C_F^2 - C_A C_F / 2) \left[\frac{1+z^2}{1+z} \left(16Li_3\left(\frac{1-z}{1+z}\right) - 16Li_3\left(-\frac{1-z}{1+z}\right) \right. \right. \\
& + 8S_{1,2}(1-z) - 16Li_3(1-z) - 16S_{1,2}(-z) + 8Li_3(-z) \\
& - 16\ell n(1-z)Li_2(-z) - 16\ell n(1+z)Li_2(-z) + 8\ell n z Li_2(1-z) \\
& + 16\ell n z Li_2(-z) - 16\ell n z \ell n(1+z)\ell n(1-z) + 20\ell n^2 z \ell n(1+z) \\
& + 4\ell n^2 z \ell n(1-z) - 8\ell n z \ell n^2(1+z) - 8\zeta(2)\ell n(1-z) - 8\zeta(2)\ell n(1+z) \\
& - 2\ell n^3 z - 8\ell n z + 8\zeta(3) \Big) + (1+z) \Big(16S_{1,2}(-z) - 8Li_3(-z) \\
& + 16\ell n(1+z)Li_2(-z) + 8\zeta(2)\ell n(1+z) + 8\ell n z \ell n^2(1+z) \\
& - 4\ell n^2 z \ell n(1+z) + 8Li_2(1-z) + 8\ell n z \ell n(1-z) - 8\zeta(3) \Big) \\
& + (1-z) \Big(16\ell n(1-z) + 30 \Big) + 8(z^2 + z^{-1}) \Big(Li_2(-z) + \ell n z \ell n(1+z) \Big) \\
& \left. - 4(2 + z^2 + z)\ell n^2 z + 4(1 + 2z^2 - z)\zeta(2) + (6 + 38z)\ell n z \right] . \quad (6A.3)
\end{aligned}$$

For the origin of $\bar{c}_q^{(2),NS,+}$ (6A.2) and $\bar{c}_q^{(2),NS,-}$ (6A.3), see the discussion below (5.2.14).

The singlet coefficient function is equal to the sum of the non-singlet and the pure singlet one (see (3.2.52)). The latter is given by

$$\begin{aligned}
\bar{C}_q^{PS} = & \left(\frac{\alpha_s}{4\pi} \right)^2 n_f C_F T_f \left[\left\{ 20(1-z) + 8(1+z)\ell n z \right\} L_M^2 \right. \\
& + \left\{ 16(1+z) \left(Li_2(1-z) + \ell n z \ell n(1-z) - \ell n^2 z \right) + 8(1-z)(5\ell n(1-z) \right. \\
& \left. - 11) - 32(2-z)\ell n z \right\} L_M + (1+z) \left(-16Li_3(1-z) + 16\ell n(1-z) \right. \\
& \times Li_2(1-z) - 16\ell n z Li_2(1-z) - 16\zeta(2)\ell n z + 8\ell n z \ell n^2(1-z) \\
& - 16\ell n^2 z \ell n(1-z) + \frac{20}{3}\ell n^3 z \Big) + (1-z) \left(20\ell n^2(1-z) - 88\ell n(1-z) \right. \\
& \left. + \frac{808}{3} \right) - 32 \left(1 + \frac{1}{3}z^2 + z + \frac{1}{3}z^{-1} \right) \left(Li_2(-z) + \ell n z \ell n(1+z) \right) \\
& + (58 + \frac{16}{3}z^2 - 6z)\ell n^2 z - 32(2-z)\ell n z \ell n(1-z) + \frac{4}{3}(137 - 19z)\ell n z \\
& \left. - \left(72 + \frac{32}{3}z^2 - 40z \right) \zeta(2) - 8(3+z)Li_2(1-z) \right] . \quad (6A.4)
\end{aligned}$$

The gluon coefficient function (3.2.54) equals

$$\begin{aligned}
\bar{C}_g = & \frac{\alpha_s}{4\pi} n_f T_f \left[4(2z-1)L_M + 4(2z-1)(\ell n(1-z) - \ell n z) + 4(3-4z) \right] \\
& + n_f \left(\frac{\alpha_s}{4\pi} \right)^2 \left[C_F T_f \left(\left\{ 4(1-2z)(-2\ell n(1-z) + \ell n z) + 6 \right\} L_M^2 \right. \right. \\
& + \left\{ 8(1-2z)(-Li_2(1-z) - 2\ell n^2(1-z) + 3\ell n z \ell n(1-z) - \ell n^2 z \right. \\
& - \zeta(2)) + 4(17-20z)\ell n(1-z) - 4(20+8z)\ell n z - 164 + 148z \left. \right\} L_M \\
& + (1-2z)(32Li_3(1-z) - 16\ell n(1-z)Li_2(1-z) - 8\ell n z Li_2(1-z) \\
& - 24\zeta(2)\ell n z - \frac{20}{3}\ell n^3(1-z) + 16\ell n z \ell n^2(1-z) - 16\ell n^2 z \ell n(1-z) \\
& + \frac{10}{3}\ell n^3 z) - 16(1+z^2+2z)(4S_{1,2}(-z) + 4\ell n(1+z)Li_2(-z) \\
& + 2\ell n z \ell n^2(1+z) - \ell n^2 z \ell n(1+z) + 2\zeta(2)\ell n(1+z)) - 32(1+z^2-6z) \\
& \times Li_3(-z) + 8(1+4z^2-2z)S_{1,2}(1-z) + \frac{16}{3}(13z^2+12z+4z^{-1})(Li_2(-z) \\
& + \ell n z \ell n(1+z)) - 4(3+28z)Li_2(1-z) + 32(1+z^2-2z)\ell n z Li_2(-z) \\
& + \frac{1}{3}(171-104z^2+48z)\ell n^2 z - (120-32z)\ell n z \ell n(1-z) \\
& + 6(9-12z)\ell n^2(1-z) - 32\zeta(2)z^2\ell n(1-z) - 4(55-4z^2-50z)\ell n(1-z) \\
& + \frac{1}{3}(800-48z^2-82z)\ell n z - 8(5-4z^2-26z)\zeta(3) \\
& - \frac{4}{3}(81-52z^2-108z)\zeta(2) + \frac{2}{3}(641-647z) \left. \right) \\
& + C_A T_f \left(\left\{ -8(1-2z)\ell n(1-z) + 16(1+z)\ell n z + 48(1-z) \right\} L_M^2 \right. \\
& + \left\{ -16(1+2z)(Li_2(-z) + \ell n z \ell n(1+z)) + 32(1+z)Li_2(1-z) \right. \\
& + 48\ell n z \ell n(1-z) - 32z\zeta(2) - 8(1-2z)\ell n^2(1-z) + 16(7-8z)\ell n(1-z) \\
& - 8(3+4z)\ell n^2 z - 24(5-4z)\ell n z - 8(20-21z) \left. \right\} L_M + 16(1+2z)(Li_3 \\
& \left. \left(\frac{1-z}{1+z} \right) - Li_3\left(-\frac{1-z}{1+z}\right) - \ell n(1-z)Li_2(-z) - \ell n z Li_2(1-z) \right)
\end{aligned}$$

$$\begin{aligned}
& -\ell n z \ell n(1-z) \ell n(1+z)) + 16(1+z^2+2z)(2S_{1,2}(-z) \\
& + \ell n z \ell n^2(1+z) + 2\ell n(1+z)Li_2(-z) + \zeta(2)\ell n(1+z)) + 8(1-2z^2 \\
& + 2z)S_{1,2}(1-z) - 8(9+2z)Li_3(1-z) - 8(1-z^2+2z)(2Li_3(-z) \\
& - \ell n z^2 \ell n(1+z) - 2\ell n z Li_2(-z)) - 16(2+z)\ell n^2 z \ell n(1-z) \\
& + 24(\ell n z \ell n^2(1-z) - 2\zeta(2)\ell n z - Li_2(1-z)) - \frac{16}{3}(6+11z^2+12z \\
& + 2z^{-1})(Li_2(-z) + \ell n z \ell n(1+z)) - \frac{4}{3}(1-2z)\ell n^3(1-z) \\
& + 8(6-7z)\ell n^2(1-z) + 8(3+2z^2-10z)\zeta(2)\ell n(1-z) + \frac{4}{3}(1+10z)\ell n^3 z \\
& + \frac{2}{3}(135+44z^2-48z)\ell n^2 z - 8(17-16z)\ell n z \ell n(1-z) + \frac{8}{3}(11z+3z^2 \\
& - 26z)\ell n z - 4(44+2z^2-53z)\ell n(1-z) - 4(3+4z^2+10z)\zeta(3) \\
& - \frac{16}{3}(27+11z^2-24z)\zeta(2) + 8(5+2z)\ell n(1-z)Li_2(1-z) \\
& + \frac{4}{3}(355-367z) \Big] . \tag{6A.5}
\end{aligned}$$

References

- [1] J. Ellis and R. Jaffe, Phys. Rev. D9 (1974) 1444; *ibid.* D10 (1974) 1669.
- [2] M.J. Alguard et al. (SLAC), Phys. Rev. Lett. 37 (1978) 1262; *ibid.* 41 (1978) 70.
- [3] J. Ashman et al. (EMC), Phys. Lett. B206 (1988) 364, Nucl. Phys. B328 (1989) 1.
- [4] B. Adeva et al. (SMC), Phys. Lett. B302 (1993) 533.
- [5] R. Jaffe, Commun. Nucl. Part. Phys. 19 (1990) 239.
- [6] E. Reya, Proceedings of the Joint International Lepton-Photon symposium and Europhysics Conference on High Energy Physics, Geneva, Switzerland, 25 July - 1 August 1991, eds. S. Hegarty, K. Potter, E. Quercigh, World Scientific, vol. 1, p. 168, DO-TH 92/17.

- [7] G. Altarelli, Polarized Structure Functions at HERA, Introduction and Overview, Proceedings of the workshop: Physics at HERA, Hamburg, October 29-30, 1991, eds. W. Buchmüller and G. Ingelman, vol. 1, p. 379.
- [8] J. Kunz, P.J. Mulders, S. Pollock, Phys. Lett. B222 (1989) 481.
- [9] G.T. Bodwin and J. Qiu, Phys. Rev. D41 (1990) 2755.
- [10] A.V. Manohar, preprint UCSD/PTH 90-28;
R.D. Carlitz and A.V. Manohar, preprint UCSD/ITH 90-32.
- [11] Proceedings of the workshop: Physics at HERA, Hamburg, October 29-30, 1991, eds. W. Buchmüller and G. Ingelman, vols. 1, 2, 3.
- [12] R.G. Roberts and M.R. Whalley, J. Phys. G. Nucl. Part. Phys. 17 (1991) D1-D151;
A.C. Benvenuti et al. (BCDMS), Phys. Lett. B223 (1989) 485; ibid. B237 (1990) 599;
P. Amaudruz et al. (NMC), Phys. Rev. Lett. 66 (1991) 73;
E. Oltman et al. (CCFR), Z. Phys. C53 (1992) 51.
- [13] J. Beaufays et al. (SMC), CERN/SPSC 88-47, SPSC/P242 (1988).
- [14] M. Düren and K. Rith, Polarized Electron-Nucleon Scattering at HERA. The HERMES Experiment. Proceedings of the workshop: Physics at HERA, Hamburg, October 29-30, 1991, eds. W. Buchmüller and G. Ingelman, vol. 1, p. 427.
- [15] J. Antoniadis and C. Kounnas, Phys. Rev. D24 (1981) 305.
- [16] J. Kodaira, Nucl. Phys. B165 (1980) 129.
- [17] S.A. Larin and J.A.M. Vermaseren, Phys. Lett. B259 (1991) 345.
- [18] S.A. Larin, Phys. Lett. B303 (1993) 113.
- [19] D. Akyeampong and R. Delbourgo, Nuov. Cim. 17A (1973) 578; 18A (1973) 94; 19A (1974) 219.
- [20] G. 't Hooft and M. Veltman, Nucl. Phys. B44 (1972) 189.
- [21] F. Breitenlohner and D. Maison, Commun. Math. Phys. 52 (1977) 11, ibid. 52 (1977) 39, ibid. 52 (1977) 55.

- [22] J.A.M. Vermaseren, Symbolic manipulation with FORM, published by CAN, Kruislaan 413, 1098 SJ Amsterdam (1991), ISBN 90-74116-01-9.
- [23] J. Kodaira, S. Matsuda, K. Susaki and T. Kematsu, Nucl. Phys. B159 (1979) 99;
J. Kodaira, S. Matsuda, T. Muta, K. Susaki and T. Kematsu, Phys. Rev. D20 (1979) 627.
- [24] W. Vogelsang, Z. Phys. C50 (1991) 275.
- [25] G. Altarelli, R.K. Ellis and G. Martinelli, Nucl. Phys. B157 (1979) 461.
- [26] B. Humpert and W.L. van Neerven, Nucl. Phys. B184 (1981) 225.
- [27] G. Altarelli and G. Parisi, Nucl. Phys. B126 (1977) 298.
- [28] E.G. Floratos, P. Lacaze and C. Kounnas, Phys. Lett. B98 (1982) 49.
- [29] G. Curci, W. Furmanski and R. Petronzio, Nucl. Phys. B175 (1980) 27.
- [30] R. Hamberg, W.L. van Neerven and T. Matsuura, Nucl. Phys. B359 (1991) 343.
- [31] G. Altarelli and B. Lampe, Z. Phys. C47 (1990) 315.
- [32] S.A. Larin, J.A.M. Vermaseren, Z. Phys. C57 (1993) 93.
- [33] G. Altarelli and G.G. Ross, Phys.Lett. B212 (1988) 391.
- [34] R.D. Carlitz, J.C. Collins and A.H. Mueller, Phys.Lett. B214 (1988) 229.
- [35] J.G. Morfin and Wu-Ki Tung, Z. Phys. C52 (1991) 13.
- [36] Hai-Yang Cheng and C.F. Wai, Phys. Rev. D46 (1992) 125.
- [37] M. Diemmoz, F. Ferroni, E. Longo and G. Martinelli, Z. Phys. C39 (1988) 472.
- [38] G. Altarelli and W.J. Stirling, Particle World 1 (1989) 40.
- [39] L. Lewin, Polylogarithms and Associated Functions, North Holland 1983;
R. Barbieri, J.A. Mignaco and E. Remiddi, Nuovo Cim. 11A (1972) 824;
A. Devoto and D.W. Duke, Riv. Nuovo Cim. 7, No. 6 (1984) 1.

Samenvatting

Tweede orde QCD correcties op zeer inelastische processen

Het gedrag van hadronen in hoog-energetische botsingen met leptonen of met andere hadronen wordt bepaald door de sterke wisselwerkingskracht die werkzaam is tussen de quarks waaruit hadronen zijn opgebouwd. De veldentheorie die de sterke wisselwerking probeert te beschrijven is Quantum Chromo Dynamica (QCD). Volgens QCD vertonen quarks onderlinge interacties door de overdracht van gluonen. De quark-gluon koppeling wordt gegeven door de sterke koppelingsconstante α_S . De grootte daarvan neemt af naarmate de energieschaal waarop het sterke wisselwerkingsproces plaatsvindt, toeneemt. Dit betekent dat bij zeer inelastische verstrooiingsprocessen α_S dermate klein wordt dat we een storingsreeks in α_S rondom de vrije-quark-theorie mogen maken. Op het moment is dit de beste manier om in QCD voorspellingen te kunnen doen die met de experimentele resultaten vergeleken kunnen worden.

Een voorbeeld van een proces waarin de sterke wisselwerking een rol speelt, is zeer inelastische electron-proton verstrooiing. Dit proces verloopt in twee fasen. De eerste fase bestaat uit de uitzending van een foton door het electron. Omdat het electron als een puntdeeltje (zonder structuur) beschouwd wordt, is dit deel van het proces gemakkelijk uit te rekenen. De tweede fase bestaat uit de daaropvolgende foton-proton verstrooiing. Om dat deel te berekenen moet het feit dat het proton structuur heeft tot uitdrukking gebracht worden in de werkzame doorsnede. Dit gebeurt door middel van een parametrisatie in termen van zogenaamde structuurfuncties. Als gevolg van de hogere orde QCD correcties worden de structuurfuncties afhankelijk van de energieschaal waarop het proces plaatsvindt. De oneindigheden die ontstaan door de manier waarop deze correcties worden uitgerekend, kunnen verwijderd worden door ze te absorberen in een onfysische grootte, de ongerenormaliseerde partondichtheid¹ van het proton. Deze renormalisatieprocedure wordt massafactorisatie genoemd. Na renormalisatie wordt de partondichtheid verondersteld wel fysisch te zijn. Ze dient

¹“Partonen” is de verzamelnaam voor quarks en gluonen.

onafhankelijk te zijn van het proces waarbij het proton betrokken is. Dit legt restricties op aan de residuen van de oneindigheden die ontstaan bij de berekeningen van hogere orde QCD correcties op andere processen.

Het hoofdonderwerp van dit proefschrift is de berekening van de tweede orde QCD correcties op alle relevante structuurfuncties van zeer inelastische electron-proton verstrooiing. De eerste orde correcties zijn reeds 15 jaar geleden uitgerekend. Onder andere door de ontwikkelingen op het gebied van computers is het nu mogelijk om ook de tweede orde correcties uit te rekenen. Een van de redenen om deze berekeningen te doen was de vooruitgang in de experimentele hoge-energiefysica. Deeltjesversnellers leveren een toenemend aantal hoge-precisie metingen in een groot aantal verschillende sterke wisselwerkingsprocessen. Daardoor ontstaat ook de behoefte aan accuratere theoretische voorspellingen om de data mee te kunnen vergelijken.

In hoofdstuk 3 berekenen we de structuurfunctie F_2 en de longitudinale structuurfunctie F_L . Deze worden gemeten in electron-proton botsingen door experimentele groepen bij HERA (Hamburg) en SLAC (Stanford) en in muon-proton botsingen bij NMC (Genève). Onze berekeningen laten zien dat de tweede orde correcties groot zijn, ze variëren van -20% tot $+10\%$ van de eerste orde gecorrigeerde resultaten. Dit zou voor een deel kunnen verklaren waarom het niet mogelijk is gebleken om de SLAC-BCDMS metingen te beschrijven met behulp van slechts de eerste orde correcties.

Met behulp van de resultaten van hoofdstuk 3 kunnen nu ook de tweede orde correcties op vectorbosonproductie in proton-(anti)proton botsingen uitgerekend worden in het DIS massafactorisatieschema. Dit doen we in hoofdstuk 4. Er blijkt weinig verschil te zijn met de eerder gepresenteerde resultaten in het $\overline{\text{MS}}$ massafactorisatieschema. Net als in dat schema zien we dat de tweede orde correcties weliswaar klein zijn, maar de ongewenste afhankelijkheid van de berekende totale werkzame doorsnede van de massafactorisatieschaal vrijwel geheel doen verdwijnen. Deze afhankelijkheid was op eerste orde nog aanzienlijk. Ze ontstaat doordat de berekening niet exact is, d.w.z. slechts tot op eindige orde uitgevoerd wordt. De massafactorisatieschaal- en -schema-onafhankelijkheid van het tweede orde resultaat geeft aan dat dit de exacte werkzame doorsnede al goed benaderd en is een indicatie voor de convergentie van de storingsreeks. Onze resultaten liggen binnen de foutengrenzen van de metingen gedaan bij de proton-antiproton versnellers van Sp $\bar{\text{p}}$ S (Genève) en Tevatron (Fermilab). Verder doen we ook voorspellingen voor de werkzame doorsnedes zoals die gemeten zouden worden bij de in de toekomst misschien te bouwen proton-proton versnellers van LHC (Genève) en SSC (Texas).

Hoofdstuk 5 is gewijd aan de berekening van de structuurfunctie F_3 die gemeten wordt in neutrino-proton verstrooiingsexperimenten, welke bijvoorbeeld door de CCFR-groep gedaan worden. In het kinematische gebied dat door dit experiment bestreken wordt, is het tweede orde gecorrigeerde resultaat nauwelijks te onderscheiden van het eerste orde resultaat, waarvan al bekend was dat het de data goed kon beschrijven. Buiten dit gebied zou de tweede orde correctie wel merkbaar kunnen zijn. Bij de berekening van F_3 is het nodig om de Diracmatrix γ_5 naar n dimensies uit te breiden, een onderwerp waarover in de literatuur veel discussie is geweest. Onze berekening is een niet-triviale manier om de uitbreidingsmethode te toetsen. Het door ons gebruikte voorschrift blijkt consistente resultaten op te leveren.

Ditzelfde γ_5 -voorschrift hebben we ook nodig in hoofdstuk 6 bij de berekening van de gepolariseerde structuurfunctie g_1 die door SLAC en EMC gemeten is in botsingen tussen gepolariseerde electronen en protonen en in de toekomst door SMC (Genève) nauwkeuriger bepaald zal worden. Als belangrijkste resultaat vinden we dat g_1 sterk afhangt van de keuze die men maakt voor de gepolariseerde zee-quark-gluondichtheden. Toekomstige metingen zullen kunnen uitwijzen welke keuze de juiste is.

Samenvattend mogen we zeggen dat de tweede orde QCD berekeningen in dit proefschrift laten zien dat bij de huidige nauwkeurigheid van de experimenten de tweede orde QCD voorspellingen in goede overeenstemming zijn met de metingen van diverse zeer inelastische verstrooiingsprocessen. Dit is een versteviging van de status van QCD als theorie voor de sterke wisselwerking. Op het moment wordt de onzekerheid in de theoretische voorspellingen voornamelijk bepaald door de vrijheid in de keuze van de partondichtheidsparametrisaties. Deze keuzevrijheid zal hopelijk grotendeels verdwijnen door de experimentele resultaten die in de nabije toekomst verwacht kunnen worden.

Curriculum vitae

Op 30 oktober 1967 ben ik geboren te Assen. Na aldaar in 1985 aan de Christelijke Scholengemeenschap het eindexamen Atheneum te hebben behaald, begon ik aan de studie Natuurkunde bij de Rijksuniversiteit Groningen. Het propaedeutisch examen volgde in augustus 1986. Het onderwerp van mijn afstudeerscriptie was de constructie van hogere orde correcties op de Lagrangianen van off-shell en on-shell supergravitatie. Dit onderzoek vond plaats onder leiding van dr. M. de Roo. Ik heb in februari 1990 het doctoraal examen Natuurkunde afgelegd.

Per 1 mei 1990 trad ik in dienst van de Rijksuniversiteit Leiden om bij prof. dr. F.A. Berends en dr. W.L.G.A.M. van Neerven op het Instituut-Lorentz aan een promotieonderzoek te beginnen op het gebied van storingstheoretische Quantum Chromo Dynamica. Ik heb gedurende twee cursusjaren werkcolleges bij het vak Quantumtheorie II verzorgd. Tijdens mijn promotieperiode werden de volgende hogenergiefysica scholen bezocht: de herfstschool "LEP results and HERA physics" in Maria Laach (Duitsland), de AIO-winterschool in Enschede, de zomerschool "Particles in the Nineties" in Les Houches (Frankrijk) en de zomerschool "QCD Analysis & Phenomenology" op Mackinac Island (Michigan). Verder heb ik werkbezoeken afgelegd aan de volgende instituten: Fermi National Accelerator Laboratory, Batavia (Illinois); State University of Wisconsin, Madison (Wisconsin); State University of New York, Stony Brook (New York); Brookhaven National Laboratory, Upton (New York); University of Durham (Engeland); Universität Bern (Zwitserland) en de Universität Mainz (Duitsland).

Sinds 16 augustus 1993 ben ik werkzaam bij het Koninklijke/Shell Exploratie en Productie Laboratorium in Rijswijk.

STELLINGEN

1. Voor een nauwkeurige QCD-analyse van de data van diepinelastische verstrooiing en het Drell-Yan proces zal het nodig zijn de tweede-ordecorrecties op de coëfficiëntfuncties mee te nemen in de berekeningen.

Dit proefschrift, hoofdstuk 3 en 4.

2. De benaming "hogere twist effect" die gebruikt wordt om de kloof tussen de gecombineerde BCDMS-SLAC-data van de structuurfunctie F_2 en de eerste-orde QCD beschrijving daarvan aan te duiden is misleidend, aangezien er aanwijzingen zijn dat ook andere niet-perturbatieve effecten een rol spelen.

M. Virchaux and A. Milsztajn, Phys. Lett. B274 (1992) 221.

Dit proefschrift, hoofdstuk 3.

3. Als de scalaire hulpvelden een rol spelen bij de koppeling van zogenaamde oude minimale supergravitatie aan een of ander systeem, kan men aantonen dat de koppeling van datzelfde systeem aan nieuwe minimale supergravitatie de lokale chirale invariantie breekt.
4. In [1] wordt vermoed dat wanneer men in nieuwe minimale supergravitatie een propagerende compensator invoert om de chirale anomalie te verwijderen en vervolgens de Wess-Zumino ijking kiest, men dan oude minimale supergravitatie krijgt. Dit vermoeden is juist.

1. Y. Shamir, Nucl.Phys. B389 (1993) 323.

5. Een programma om bestanden te vergelijken dat gebaseerd is op invoegen en schrappen werkt sneller dan een vergelijkingsprogramma dat gebaseerd is op kopiëren en achteraan toevoegen, zoals bijvoorbeeld *diff* in het besturingssysteem Unix.

W. Miller – A Software Tool Sampler.

W. Miller, E.W. Myers – Software, Practice and Experience (1985) 1025.

6. Het is mogelijk zowel on-shell als off-shell $R + \alpha R^2$ -acties te construeren, die lokaal supersymmetrisch zijn tot op $\mathcal{O}(\alpha^2)$, waarbij R de Riemann-tensor is en α een constante die omgekeerd evenredig is aan het kwadraat van de Planckmassa.

M. de Roo, A. Wiedemann, E. Zijlstra – Class.Quant.Grav.7 (1990) 1181.

7. Arnolds katafbeelding algoritme [2] geeft, ondanks het feit dat het aan de top staat van de hiërarchie van de klassieke chaos [3], een erg slechte random number generator. Dit is een illustratie van het feit dat chaotisch gedrag iets anders is dan random gedrag. Men kan echter een goede random number generator verkrijgen door de resultaten van twee katafbeeldingen met lengte vier af te wisselen.

2. V.I. Arnold and A. Avez – *Ergodic problems of Classical Mechanics* (1968)

3. H.G. Schuster – *Deterministic chaos, an introduction*, 2nd Ed. (1988).

8. Een goede definitie van de bovengrens van het meetbereik van een Pirani-vacuümmeter, gebaseerd op het principe dat bij lage druk de warmtegeleiding van gas lineair evenredig is met de druk, wordt gegeven door:

$$p_{\text{grens}} = \frac{C \sigma \alpha}{T \Lambda_0} ,$$

waarbij C een constante is die alleen afhangt van de gebruikte vacuümmeter (C is omgekeerd evenredig aan de diameter van de draad). Hierbij:

σ = de botsingsdoorsnede van het gas,

α = de energie-accommodatiecoëfficiënt van het gas,

Λ_0 = de moleculaire warmtegeleidingscoëfficiënt van het gas,

T = de gastemperatuur.

9. Wanneer aan een grootheid in de quantumveldentheorie uitsluitend “zero modes” bijdragen, kan men bij de berekeningen het ruimtelijke deel naar nul laten gaan, waardoor het probleem gereduceerd wordt tot een quantummechanisch probleem.

L. Alvarez-Gaumé, E. Witten – *Nucl.Phys. B234* (1983) 269.

10. De conjugatie-operatie zoals besproken in [4] is een speciaal geval van een quantumdeformatie.

4. E. Witten – *Nucl.Phys. B202* (1982) 253.

11. Zij gegeven de Fibonaccigetallen F_k ($k > 0$, $k \in \mathbb{N}$)

$$F_1 = 1 ; \quad F_2 = 1 ; \quad F_k = F_{k-1} + F_{k-2} \quad \text{voor } k > 2$$

en de functie

$$g_{\pm}(F_k) = \frac{1}{5} \left\{ 5F_k^2 - 6F_k F_{k+1} + 2F_{k+1}^2 \pm 2F_{k+1} \right\} ,$$

dan geldt voor $k = 4 + 10\ell$ ($\ell \in \mathbb{N}$)

$$\{F_{2k} + g_{\pm}(F_k)\}^2 + \{F_{2k-1} - 2g_{\pm}(F_k)\}^2 = F_{k+1}^4 \quad \wedge \quad g_{\pm}(F_k) \in \mathbb{N} .$$

12. De opmerking "Sinds ik met pensioen ben gegaan, heb ik het drukker dan ooit" is typisch calvinistisch.
13. Ondanks de grote technologische vooruitgang blijven bepaalde zaken tamelijk primitief, zoals bijvoorbeeld het fietsverlichtingsmechanisme dat veel te gemakkelijk kapot kan gaan en het trage zoekstelsel van Teletekst.
14. Het zou zinvol zijn om in plaats van het verplichte onderdeel Wetenschap en Samenleving in de natuurkundestudie een verplichte cursus mondelinge en schriftelijke uitdrukingsvaardigheid in te voeren.
15. In natuurkunde-opgaven zijn altijd alle gegevens relevant. Het zou realistischer zijn om ook niet-relevante gegevens te verwerken in natuurkunde-opgaven. Dit bereidt de student beter voor op het doen van onderzoek.
16. Personeelsadvertenties en contactadvertenties gaan qua bewoording steeds meer op elkaar lijken.

Ellen Zijlstra,
8 september 1993.